

AD719306

Technical Report

September 1970

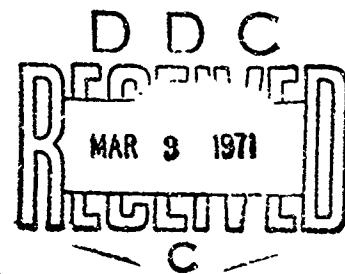
EXISTING STRUCTURES EVALUATION
Part IV: Two-Way Action Walls

Prepared for:

OFFICE OF CIVIL DEFENSE
OFFICE OF THE SECRETARY OF THE ARMY
WASHINGTON, D.C. 20310

CONTRACT DAHC20-67-C-0136
OCD Work Unit 1154F

Approved for public release, distribution unlimited



STANFORD RESEARCH INSTITUTE
Menlo Park, California 94025 · U.S.A.

Reproduced by
**NATIONAL TECHNICAL
INFORMATION SERVICE**
Springfield, Va. 22151

256

Technical Report
Detachable Summary

September 1970

EXISTING STRUCTURES EVALUATION

Part IV: Two-Way Action Walls

By: C. K. WIEHLE
J. L. BOCKHOLT
Facilities and Housing Research

Prepared for:

OFFICE OF CIVIL DEFENSE
OFFICE OF THE SECRETARY OF THE ARMY
WASHINGTON, D.C. 20310

CONTRACT DAHC20-67-C-0136
OCD Work Unit 1154F

SRI Project 6300

Approved for public release, distribution unlimited.

OCD REVIEW NOTICE

This report has been reviewed in the Office of Civil Defense and approved for publication. Approval does not signify that the contents necessarily reflect the views and policies of the Office of Civil Defense.

SUMMARY

Introduction

The objective of this investigation was to develop an evaluation procedure applicable to existing NFSS-type structures and private homes for determining the blast protection afforded and the cost of structure modifications to improve the blast protection. The approach adopted was to formulate a procedure that would permit examining the response of a structure over a range of incident overpressure levels to determine the pressure at which failure of the various elements occurs. The procedure consists of (1) a method for determining the air blast loading on the structure and structural elements, (2) a method for determining the dynamic structural response, and (3) a method for establishing the failure criterion for each structural member of interest.

Background

Past efforts in this program have been concerned with examining exterior walls, window glass, and steel frame connections. The work presented in this report extended the exterior wall response models previously developed to include exterior walls with two-way structural action and window openings.

Discussion

Approach

The procedure adopted in this study was to establish the resistance function for each wall element of interest by considering the approximate response mode and by assuming that the wall was subjected to a uniformly

distributed static load. The member was then transformed into an equivalent single-degree-of-freedom dynamic system by the use of transformation factors for the load, resistance, and mass. The equation of motion was solved on a computer using numerical integration procedures. Relatively simplified analytical models have been used for wall element analysis to prevent the overall evaluation procedure for a structure from becoming unwieldy as a result of excessive computational effort.

The effort in this phase of the work was directed primarily toward the further development and modification of the evaluation procedure previously developed. Resistance functions have been formulated that include two-way structural action and window openings in three types of exterior walls, i.e., unreinforced concrete or masonry unit walls without arching, unreinforced concrete or masonry unit walls with arching, and reinforced concrete walls. In addition, the load functions used in the initial study have been extended to include the exterior loading on the wall of a building with windows and the interior room pressure build-up caused by an air blast entering the building.

A primary difference between the current and the previous effort has been the introduction of a probability distribution in the analysis of wall elements. Although the intention since the inception of this program has been to carry along certain statistical yardsticks in the analysis of each building element, it became apparent during this phase that a combined deterministic and probabilistic approach would be needed for the realistic evaluation of existing structures subjected to nuclear air blast.

Findings

In the development of any analytical procedure, an important consideration is the comparison of the analytical predictions with experimental

information. Although the available test data for dynamically loaded walls are not extensive, it was possible during this program to compare analytical predictions with experimental data obtained from a wall tested in a laboratory shock tunnel and with test walls and houses included in nuclear field tests. A brief summary of this correlation follows.

Laboratory Wall Test. The dynamic response data from a test of a 12-in. thick, 8-ft high by 12-ft wide, brick wall were obtained from URS Research Company for comparison with the theoretically predicted response. The most useful test information was the velocity-time data measured at the horizontal centerline of the wall. The experimental and theoretical velocity-time data are reproduced on Figure S-1, together with the pertinent wall and load parameters. During the early times, e.g., at 20 msec, there is a difference of about 100 percent between the experimental and predicted velocity. However, at 90 msec, the predicted velocity is only about 15 percent higher than the measured. Possible reasons for the rather large difference during the early times are discussed in the report.

Field Test Wall Panels. The most comprehensive data available for correlation with the analytical prediction method developed in this study, were the results from wall panels included in nuclear field tests. The wall panels were located in test structures that resembled long, low, narrow buildings and that were constructed to permit failure of individual test wall panels without interference with adjacent panels.

The test results for eight types of concrete block or brick masonry walls with arching were used for comparison with the analytical prediction of the probability of occurrence of the incipient collapse overpressure. A summary of the results of the analyses of the eight walls is given in

WALL PARAMETERS

Simple One-Way Support

$L_v = 8$ ft

$t_w = 12$ in.

$f_r = 200$ psi

$E_m = 0.5 \times 10^6$ psi

$\gamma = 120$ pcf

LOAD PARAMETERS

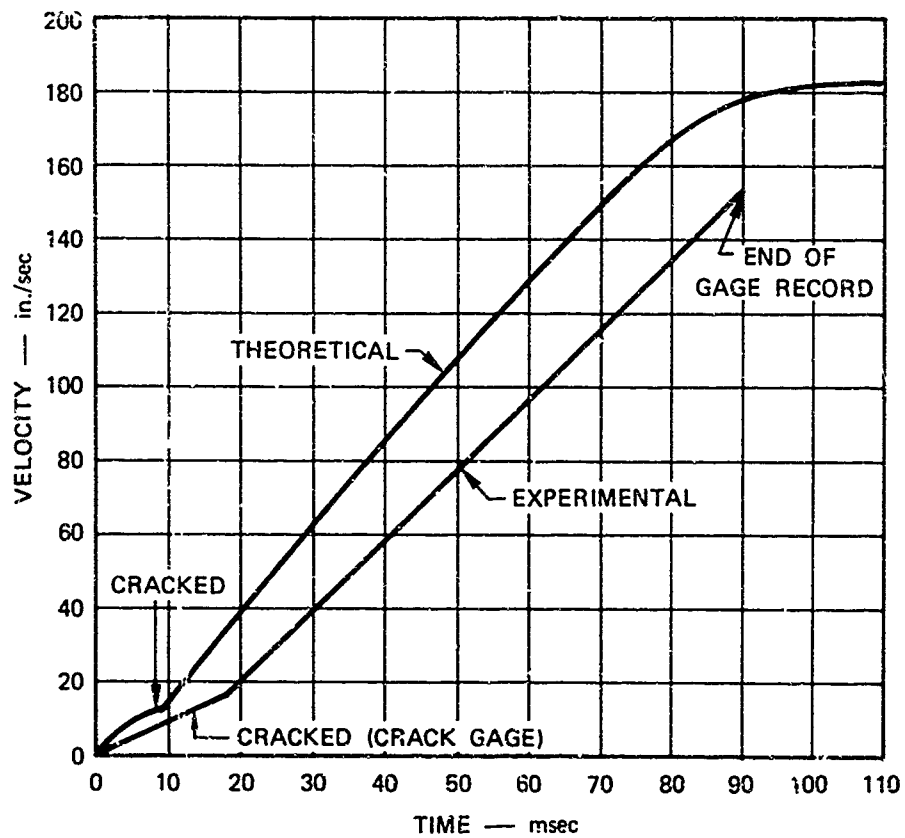
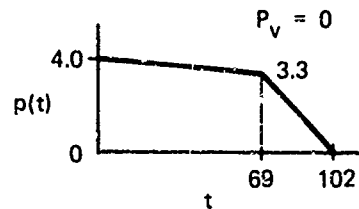


FIGURE S-1 VELOCITY VERSUS TIME FOR ONE-WAY SIMPLY SUPPORTED BRICK WALL

Table S-1. Although there were some discrepancies, in general there was good agreement between the statistical prediction of the incipient collapse pressure and the test results.

Field Test Brick Houses. The results of nuclear field tests of two types of brick load-bearing wall houses were available for comparison with the predictions from the analytical two-way action models developed for unreinforced masonry walls without arching. The first type was a two-story house tested during Operating GREENHOUSE and represented typical European construction. The second type was a two-story house tested during Operation TEAPOT and represented typical U.S. construction. The differences in the construction of the two types of houses resulted in the European house being significantly stronger than its U.S. counterpart.

In Operation GREENHOUSE, one house located at the 3.4 psi overpressure level suffered no damage to the exterior walls, although the roof collapsed, while another house at 8.7 psi was about 40 percent damaged.* In Operation TEAPOT, one house located at 1.7 psi suffered no apparent damage to the exterior masonry walls, while another house at 5.1 psi was demolished beyond repair. All houses were placed with their front wall facing toward the detonation.

A statistical analysis was made of each house type, and the incipient collapse overpressures are given in the tabulation below for comparison with the test results.

<u>Brick House (GREENHOUSE)</u>		<u>Brick House (TEAPOT)</u>	
Mean	6.36 psi	Mean	2.50 psi
Standard Deviation	0.36 psi	Standard Deviation	0.18 psi
10% Probability Value	5.90 psi	10% Probability Value	2.27 psi
90% Probability Value	6.82 psi	90% Probability Value	1.73 psi

* The description of percent building damage cited in Ref. 22 is for damage assessment purposes and is not necessarily related to the probability of survival for civil defense purposes.

Table S-1
SUMMARY OF STATISTICAL ANALYSES OF ARCHING WALLS
(Overpressure, psi)

Wall Type	Description	Mean		Standard Deviation		10 Percent Probability Value		90 Percent Probability Value		Remarks
		Value	95 Percent Confidence Interval	Value	95 Percent Confidence Interval	Value	Confidence* Interval	Value	Confidence* Interval	
1	8 in. brick (105 in. x 165 in.)	12.91	12.30 13.52	3.07	2.70 3.57	8.93	8.53 9.45	16.85	16.37 17.49	0 of 1 failed at 1.2 and 7.5 psi, 1 of 1 failed at 12 psi
2	8 in. brick (120 in. x 192 in.)	9.84	8.93 10.75	2.16	1.69 3.01	7.07	5.98 7.67	12.61	12.00 13.69	0 of 1 failed at 1.5 psi; 1 of 1 failed at 8.1 psi
3	12 in. brick	24.20	21.91 26.48	6.01	4.79 8.08	16.19	13.83 18.06	31.91	30.31 31.56	0 of 1 failed at 4.5 psi; 1 of 1 failed at 8.1 psi
4	8 in. concrete block	4.37	3.96 4.77	0.96	0.75 1.84	3.13	2.65 3.10	5.60	5.33 6.09	1 of 1 failed at 4.5 psi
5	12 in. concrete block	8.88	8.05 9.71	1.97	1.51 2.71	6.35	5.36 6.90	11.10	10.85 12.39	3 of 1 failed at 4.5 psi
6	4 in. concrete block --4 in. brick	3.97	3.60 4.35	0.99	0.79 1.33	2.70	2.26 2.96	5.25	1.99 5.68	2 of 2 failed at 4.5 psi
7	8 in. concrete block --4 in. brick	9.30	8.38 10.23	1.92	1.46 2.81	6.81	5.71 7.13	11.77	11.18 12.90	0 of 3 failed at 1.5 psi; 3 of 3 failed at 8.1 psi
8	8 in. concrete block --4 in. brick (One-way) (Two-way)	13.57 18.81	13.11 14.03 17.69 19.94	1.59 2.35	1.40 1.85 1.78 3.43	11.53 15.81	11.20 11.42	15.61 21.82	15.36 21.76	0 of 12 failed at 4.5 psi; 0 of 12 failed at 8.1 psi

* Confidence limits for the 10 and 90 percent probability values are somewhat less than 95 percent.

Recommendations

This investigation has emphasized the need for a balanced analytical and experimental program to develop an evaluation procedure for existing structures that meets the requirements of OCD. From the standpoint of predicting the collapse of exterior walls, it is recommended that the following research be conducted in the next phase of the effort:

- A sensitivity analysis should be conducted to investigate the effect on the incipient collapse overpressure of varying the probability distribution of the important load and wall parameters. In this study, sensitivity analyses have been used to assist in identifying the wall and load parameters that have an important influence on the incipient collapse overpressure of specific walls. In addition, since the evaluation of actual structures includes physical parameters that cannot readily be measured or determined precisely, the analytical procedure was modified to include a probability distribution for the important parameters rather than a single value. This, of course, lessens the requirement for preciseness in some or all of the parameters. However, some parameters may have such a large effect on the predicted collapse of a specific wall that their degree of uncertainty may mask the uncertainty in any or all of the other unknown parameters. A sensitivity study will indicate the parameters that must be determined accurately and also will provide guidance in selecting the more important areas for experimental research.
- A literature search should be conducted to gather basic information on material properties for use in this project. The analyses of wall elements in this study emphasized the need for readily available statistical data on the material properties of exterior walls, and information should be obtained for all materials needed in the evaluation of existing structures.
- Static and dynamic tests of typical exterior walls should be conducted to permit an examination of the validity of the mathematical models presented in this report or to establish the basis for additional or substitute procedures. As noted in the report, the establishment of resistance functions for two-way action walls with windows required that various assumptions be made in addition to those made in the initial effort. To support the analytical work, the specific areas for which

Experimental information is needed include the resistance function for various types of walls and support conditions; the effect of two-way action for walls with and without windows; the effect of shear and connections on wall failure; the reaction of walls throughout their response history, including collapse; and the effect of vertical in-plane forces on the resistance of wall elements. The emphasis in any test program should be to establish the primary collapse mechanism of two-way action walls with and without windows, and to determine the effect of variation of the important parameters on the incipient collapse overpressure of walls.

- Air blast interaction studies should be continued to establish more definitive blast load prediction techniques than are now available. In the report, a method is presented for calculating the net load-time function resulting from the interaction of an air blast wave with a structure with openings. The method evolved from the available schemes for determining the blast loading on the exterior surface of a building with openings and the interior pressure build-up caused by a blast wave entering a room. However, since the net load-time function is an important factor in predicting the collapse of walls in actual buildings, better information is needed to develop a more accurate procedure than used in this study. Although a number of parameters influence the blast wave interaction process, the primary areas where information is needed for determining the collapse of exterior walls are the clearing time of the reflected overpressure on the front face of any wall in a building with openings, the effect of window openings on the back-face loading of an exterior wall, and the adequacy of using the average room pressure (calculated from the room-filling procedure) as the loading on the interior surface of exterior walls located on any side of a building.



STANFORD RESEARCH INSTITUTE
Menlo Park, California 94025 U.S.A.

Technical Report

September 1970

EXISTING STRUCTURES EVALUATION

Part IV: Two-Way Action Walls

By: C. K. WIEHLE
J. L. BOCKHOLT
Facilities and Housing Research

Prepared for:

OFFICE OF CIVIL DEFENSE
OFFICE OF THE SECRETARY OF THE ARMY
WASHINGTON, D.C. 20310

CONTRACT DAHC20-67-C-0136
OCD Work Unit 1154F

SRI Project 6300

Approved for public release, distribution unlimited.

OCD REVIEW NOTICE

This report has been reviewed in the Office of Civil Defense and approved for publication. Approval does not signify that the contents necessarily reflect the views and policies of the Office of Civil Defense.

FOREWORD

This report is one of a series covering research of a continuing nature under a project for blast resistance evaluation of existing structures in the National Fallout Shelter Survey (NFSS) inventory of the U.S. Office of Civil Defense (OCD).

The objective is to develop an evaluation method for estimating blast resistance and the cost of structure modifications to improve blast protection.

The evaluation method differs from vulnerability analysis techniques by carrying along significant statistical yardsticks (e.g. on strengths of materials) in the calculations sufficient to meet the needs of shelter operations research or war-gaming. It differs from protective design/analysis by aiming at a 50% probability basis, rather than the 90%-99% probability basis intended in design/analysis methods.

The results expected of the evaluation method will provide inputs for systems analyses related to performance of structures and effects on shelterees.

The approach used for the continuing research was to develop an evaluation method for each of several structural elements (e.g., window glass, walls, and slabs), including reaction load-time history, and then for structural frames.

The research includes applications to specific buildings, such as those selected in a statistically adequate sample of NFSS structures under another OCD project, thereby making possible various extrapolations to the overall NFSS structures picture.

ABSTRACT

The objective of this investigation was to develop an evaluation procedure applicable to existing NFSS-type structures and private homes for determining the blast protection afforded and the cost of structure modifications to improve the blast protection. The approach adopted was to formulate a procedure that would permit examining the response of a structure over a range of incident overpressure levels to determine the pressure at which failure of the various elements occurs.

Past efforts in this program have been concerned with examining exterior walls, window glass, and steel frame connections. The phase of the work presented in this report extended the exterior wall response models previously developed by including exterior walls with two-way action and window openings. The evaluation procedure was also extended to include a probability distribution for each of the various "unknown" wall and load parameters. Using the wall evaluation procedure, a limited sensitivity analysis was performed and a comparison was made of the available experimental information on dynamically loaded wall elements with theoretical predictions.

CONTENTS

SUMMARY	S-1
FOREWORD	iii
ABSTRACT	v
I INTRODUCTION	1
Background	1
Approach	2
Structure Evaluation	2
Wall Element Evaluation	3
Report Organization	5
Acknowledgment	5
II AIR BLAST LOADING	7
Introduction	7
Front Face Loading	9
Interior Loading	13
Net Wall Loading	14
III RESISTANCE FUNCTIONS	17
Introduction	17
Unreinforced Concrete or Masonry Unit Wall (Without Arching)	18
Resistance Function	23
Elastic Phase - Wall Without Vertical Axial Load	23
Elastic Phase - With Vertical Load	29
Decaying Phase	34
Unreinforced Concrete or Masonry Unit Wall (With Arching)	45
Resistance Function	46
Reinforced Concrete Wall	53
Resistance Function	55
Wall Without Vertical Axial Load	60
Wall With Vertical Axial Load	67
Failure Criteria	75
Window Openings	76

CONTENTS

IV	PROBABILITY CONSIDERATIONS	87
	Introduction	87
	Statistical Analysis	92
	Monte Carlo	92
	Sampling Distribution of the Mean and Variance	95
	10 Percent and 90 Percent Probability Values	100
V	WALL REACTIONS	103
	Introduction	103
	Dynamic Reactions	103
	Support Case 1	110
	Support Case 2	112
	Support Case 3	113
	Support Case 4	114
VI	DISCUSSION	119
	Introduction	119
	Variation of Parameters	119
	Unreinforced Concrete or Masonry Unit Wall (Without Arching)	121
	Unreinforced Concrete or Masonry Unit Wall (With Arching)	125
	Reinforced Concrete Wall	125
	Experimental Correlation	125
	Laboratory Wall Test	132
	Field Test Wall Panels	135
	Field Test Brick Houses	144
	Brick House (GREENHOUSE)	145
	Test Results	148
	Analysis	148
	Brick House (TEAPOT)	158
	Test Results	161
	Analysis	162
	Summary	166
	Statistical Analysis	166

CONTENTS

VII	SUMMARY AND RECOMMENDATIONS	171
	Summary	171
	Recommendations	172
APPENDIXES		
A	TRANSFORMATION FACTORS	A-1
B	COLLAPSE MODE "b" FOR REINFORCED CONCRETE WALLS	B-1
C	STATISTICAL STUDY OF MASONRY WALLS WITH ARCHING	C-1
D	COMPUTER PROGRAMS	D-1
	REFERENCES	R-1
	NOMENCLATURE	N-1

ILLUSTRATIONS

1	Conventional Scheme for the Front Face Loading on a Closed Rectangular Block	8
2	Front Elevation of Large Multistory Building Without Openings	11
3	Calculated Pressure-Time on Front Wall of Brick House (TEAPOT)	16
4	Wall Element Assumed for Analysis	19
5	Support Cases	20
6	Resistance Function for Two-Way Action Unreinforced Concrete or Masonry Unit Wall Without Arching Support Case 1	21
7	Resistance Function for Two-Way Action Unreinforced Concrete or Masonry Unit Wall Without Arching Support Cases 2, 3, & 4	22
8	Coefficients for Maximum Elastic Moment in Two-Way Action Walls Without Vertical Load	24
9	Coefficients for Center Elastic Deflection of Two-Way Action Walls Without Vertical Load	27
10	Coefficients for Maximum Elastic Moment in Two-Way Action Walls with Vertical Load Support Case 1	31
11	Coefficients for Center Elastic Deflection of Two-Way Action Walls with Vertical Load Support Case 1	33
12	Crack Pattern Assumed for Analysis of Two-Way Action Wall	36
13	Assumed Vertical Forces on Segments of Two-Way Action Unreinforced Wall	
	(a) Lower Segment	39
	(b) Upper Segment	39

ILLUSTRATIONS (Continued)

14	Resisting Moment for One-Way Arching of Unreinforced Masonry Walls with Rigid Supports	
	(a) Solid Unreinforced Masonry Wall	48
	(b) Hollow Unreinforced Masonry Wall	48
15	Typical Resistance Function for Unreinforced Masonry Wall with Two-Way Arching	54
16	Wall and Moment Keyline Notation	56
17	Resistance Function for a Two-Way Action Reinforced Concrete Wall Support Case 1	58
18	Resistance Function for a Two-Way Action Reinforced Concrete Wall Support Cases 2, 3, and 4	59
19	ACI Moment Coefficients for Two-Way Action Walls	63
20	Assumed Collapse Modes (Yield Lines) for Reinforced Concrete Wall	
	(a) Collapse Mode "a"	66
	(b) Collapse Mode "b"	66
21	Yield-Line Patterns for Square Wall Panel with Isotropic Reinforcement	
	(a) Wall Without Window	78
	(b) Wall with Square Window	78
	(c) Wall with Long Rectangular Window	78
22	Yield-Line Patterns for Rectangular Wall Panel with Isotropic Reinforcement	
	(a) Wall Without Window	79
	(b) Typical Yield Line for Wall with Window	79
	(c) Yield Line for Wall with Wide Window	79
23	Wall with Yield-Line Pattern Intersecting Vertical Edge of Window	81
24	Wall with Yield-Line Pattern Intersecting at Common Point and Window Edge	83

ILLUSTRATIONS (Continued)

25 Peak Incident Overpressure at Incipient Collapse Versus Ultimate Compressive Strength 90

26 Peak Incident Overpressure at Incipient Collapse Versus Modulus of Elasticity 90

27 Peak Incident Overpressure at Incipient Collapse Versus Ultimate Compressive Strength and Modulus of Elasticity 91

28 Peak Incident Overpressure at Incipient Collapse Versus Clearing Distance 91

29 Probability of Occurrence of Peak Incident Overpressure at Incipient Collapse 93

30 Dynamic Forces Acting on Segment A 105

31 Dynamic Forces Acting on Segment C 107

32 Peak Incident Overpressure at Incipient Collapse Versus L_H/L_V Ratio 122

33 Peak Incident Overpressure at Incipient Collapse Versus Percent Window Opening 123

34 Peak Incident Overpressure at Incipient Collapse Versus Room Volume 124

35 Peak Incident Overpressure at Incipient Collapse Versus L_H/L_V Ratio 126

36 Peak Incident Overpressure at Incipient Collapse Versus Percent Window Opening 127

37 Peak Incident Overpressure at Incipient Collapse Versus Room Volume 128

38 Peak Incident Overpressure at Incipient Collapse Versus L_H/L_V Ratio 129

39 Peak Incident Overpressure at Incipient Collapse Versus Percent Window Opening 130

40 Peak Incident Overpressure at Incipient Collapse Versus Room Volume 131

ILLUSTRATIONS (Continued)

41	Velocity Versus Time for One-Way Simply Supported Brick Wall	134
42	View of Arching Wall Panel Test Structures	136
43	Statistical Analysis of Incipient Collapse Overpressure for Arching Walls	139
44	Picture of 12 in. Brick Wall Panel Test	141
45	Front Elevation of Two-Story Brick House (GREENHOUSE) . . .	146
46	Plan View of Two-Story Brick House (GREENHOUSE)	147
47	Post-Shot Picture of Front of Brick House Located at 8.7 psi Overpressure (GREENHOUSE)	149
48	Post-Shot Picture of Left Side of Brick House Located at 8.7 psi Overpressure (GREENHOUSE)	150
49	Calculated Load-Time on Side Wall of Brick House (GREENHOUSE) Room Volume = 1660 cu ft	155
50	Calculated Load-Time on Side Wall of Brick House (GREENHOUSE) Room Volume = 3320 cu ft	156
51	Front View of Two-Story Brick House (TEAPOT)	159
52	Plan View of Two-Story Brick house (TEAPOT)	160
53	Calculated Load-Time on Rear wall of Brick House (TEAPOT)	165
A-1	Assumed Crack, or Yield-Line Pattern for Two-Way Action Wall	A-5
B-1	Collapse Mode "b" for Reinforced Concrete Wall	B-4
C-1	Incipient Collapse Overpressure of 8 in. Brick Wall Panel on Normal Probability Paper (n = 100)	C-7
-2	Incipient Collapse Overpressure of 8 in. Brick Wall Panel on Normal Probability Paper (n = 25)	-8
-3	Statistical Analysis of Incipient Collapse Overpressure for Arching Walls	-10

ILLUSTRATIONS (Concluded)

D-1	Overall Organization of Computer Programs	D-5
-2	Flow Chart of Main Routine	-6
-3	Flow Chart of Subroutine RESIST Two-Way Unreinforced Wall Without Arching	-8
-4	Flow Chart of Subroutine RESIST Two-Way Unreinforced Wall With Arching	-10
-5	Flow Chart of Subroutine RESIST Two-Way Reinforced Concrete Wall	-12
-6	Flow Chart of Subroutine TRANS	-14
-7	Flow Chart of Subroutine LOAD	-15
-8	Flow Chart of Subroutine FILL	-17

TABLES

1	Dynamic Reactions for Two-Way Unreinforced Concrete or Masonry Unit Walls	116
2	Dynamic Reactions for Two-Way Reinforced Concrete Walls (Collapse Mode "a")	117
3	Physical Properties of Test Walls	137
4	Summary of Statistical Analyses of Arching Walls	138
A-1	Transformation Factors for Two-Way Unreinforced Concrete or Masonry Unit Walls	A-16
A-2	Transformation Factors for Two-Way Reinforced Concrete Walls (Collapse Mode "a")	-17
B-1	Dynamic Reactions for Two-Way Reinforced Concrete Walls (Collapse Mode "b")	B-9
C-1	Summary of Statistical Analysis of 8 in. Brick Wall	C-5
C-2	Physical Properties of Test Walls	-9
C-3	Summary of Statistical Analyses of Arching Walls	-12

I INTRODUCTION

Under contract to the Office of Civil Defense, Stanford Research Institute is developing a procedure for the evaluation of existing structures subjected to nuclear air blast. The objective of the overall program is to develop an evaluation procedure applicable to existing NFSS-type structures and private homes for determining the blast protection afforded and the estimated cost of structure modifications to improve the blast protection. The purpose of this phase of the work was to extend the applicability of the evaluation procedure for exterior wall elements presented in Ref. 1.

Background

Past efforts in this program have been concerned with examining exterior walls (Ref. 1), window glass (Ref. 2), and steel frame connections (Ref. 3). The work presented in this report was undertaken to extend the exterior wall response models presented in Ref. 1 by including exterior walls with two-way structural action and window openings. Another report to be published will present criteria on the effect of blast overpressure on the protection afforded by various building classes.

The evaluation of existing structures is exceedingly complex and includes many unknown aspects of both the nuclear air blast loading on, and the failure mechanisms of, structures. Past damage prediction schemes have generally been developed for physical vulnerability studies; they have limited application to the examination of the behavior of an individual structure. Although comprehensive analytical studies and experimental data provided the basis for these methods, averaging and statistical

technicians were employed to obtain the probability of a specified level of damage to a selected class of structures for various weapon yields and ranges. The work in this program, therefore, has been directed toward providing a procedure adapted to the specific requirements of the Office of Civil Defense.

Approach

Structure Evaluation

A structure evaluation procedure that can be applied to the following types of OCD problems would be desirable:

- Casualty and injury predictions.
- Debris prediction.
- Damage assessment.
- Selection of existing structures that provide the best protection.
- Selection of existing structures that have a potential for modification for upgrading to provide blast shelters.

At the present time, there unfortunately is no procedure or combination of procedures that can be used to satisfy the above requirements. A procedure is needed that is sufficiently flexible to provide the detail necessary for assessing individual structure damage, without requiring a detailed analysis of every structure in an entire city. The overall approach adopted in this study for the evaluation of existing structures to resist nuclear air blast has been the formulation of a procedure for examining the response of a structure over a range of incident overpressure levels to determine the pressure at which collapse of the various elements will occur.

Because of the complexity of both the air blast loading and the structural response calculations, the evaluation procedure employs a computer to perform the numerical computations. The program is designed with sufficient flexibility to permit subsequent modification as more complete information becomes available from current studies by various organizations. Basically, the procedure consists of (1) a method for determining the air blast loading on the structure and structural elements, (2) a method for determining the dynamic structural response up to collapse, and (3) a method for establishing the failure criterion for each structural member of interest. An iterative process is employed in which the structural response can be examined for various levels of incident overpressure and compared with a failure criterion to predict the overpressure level at which collapse of each member will occur.

Wall Element Evaluation

The method used in this study was to establish the resistance function for each wall element of interest by considering the approximate response mode and by assuming that the wall was subjected to a uniformly distributed static load. The member was then transformed into an equivalent single-degree-of-freedom dynamic system by the use of transformation factors for the load, resistance, and mass. The equation of motion was then solved on a computer using the numerical integration procedure described in Ref. 4. Although the approach has been to use established analytical procedures wherever possible (as noted in the main body of the report), it has been necessary to modify and adapt current procedures for specific use. Relatively simplified analytical models have been used for wall element analysis to prevent the overall evaluation procedure of a structure from becoming unwieldy as a result of excessive computational effort.

The effort covered in this report was directed primarily toward the further development of the evaluation procedure previously developed to determine the collapse of dynamically loaded exterior wall elements. Resistance functions have been formulated that include two-way structural action and window openings in three types of exterior walls, i.e., unreinforced concrete or masonry unit walls without arching, unreinforced concrete or masonry unit walls with arching, and reinforced concrete walls.

To apply the wall response models to actual structures, it is necessary to calculate the load-time function on both the exterior and interior surfaces of the wall. Therefore, the load functions presented in Ref. 1 have been extended to include the exterior loading on the wall of a building with windows and the interior room pressure build-up resulting from an air blast entering the building.

A primary difference between the current and the previous effort has been the introduction of a probability distribution in the analysis of wall elements. Although the intention since the inception of this program has been to carry along certain statistical yardsticks in the analysis of each building element, it became apparent during this phase of the effort that a combined deterministic and probabilistic approach would be necessary for the realistic evaluation of existing structures subjected to nuclear air blast. This is necessary because the analysis of actual building elements requires the assumption of values for the physical properties of the structure that are unknown and cannot be measured in the field without an unwarranted amount of effort.

Report Organization

Section II contains a discussion of the method adopted for calculating the net load-time function used in the evaluation of exterior walls of an actual building, and Section III concerns the extension of the resistance functions to include two-way structural action walls with and without windows. The method used to introduce probability into the wall analysis is given in Section IV, and the reactions of two-way action walls are considered in Section V. Section VI contains a discussion of a limited sensitivity analysis of two-way action walls and a comparison of the available experimental information on dynamically loaded wall elements and the theoretical predictions. Section VII presents the report conclusions and recommendations for further study.

Appendixes were included to supplement the main body of the report where needed. Appendix A presents the method used to calculate the transformation factors for two-way action walls, and Appendix B discusses an alternative crack pattern that may form in a wall under certain conditions. A detailed statistical analysis of a masonry wall with arching is given in Appendix C to demonstrate the statistical method used in the analysis. Appendix D is a discussion of the computer programs developed for the dynamic analysis of the various two-way action wall elements.

Acknowledgment

The authors gratefully acknowledge the assistance and guidance of George N. Sisson and N. A. Meador of the Office of Civil Defense during the conduct of this program.

II AIR BLAST LOADING

Introduction

As noted in the initial wall study in Ref. 1, the load-time history is an important factor in the prediction of the collapse of structural elements. In that study, four basic types of loadings were selected for an analysis of the response and collapse of exterior walls. These loadings consisted, first, of the conventional load scheme for the interaction of an air blast wave at normal incidence with the front face of a closed rectangular structure, as shown on Figure 1. This loading was included in the study since it represents the type of front face loading scheme generally used in the design and analysis of structures subjected to nuclear weapon effects. The second loading case considered was a triangular load pulse, and the third was rectangular. These load cases were included primarily because of their value in variation of parameter studies. The fourth type of load function was a step pulse to a uniform pressure followed by a linear decay to zero pressure, which was used to permit comparison of the theoretical predictions with the experimental results from the URS Shock Tunnel Facility (Ref. 5).

These four load types were considered to be adequate for studying the collapse of specific walls and for performing sensitivity analyses. However, for the correlation of the prediction methods with nuclear field test data and for the evaluation of actual structures, it is necessary to describe more definitely the net load-time history on the wall element of interest. This requires a method for calculating both the front and back face loadings. Therefore, for the current study, it was necessary to establish a procedure for determining the front and back face load-time

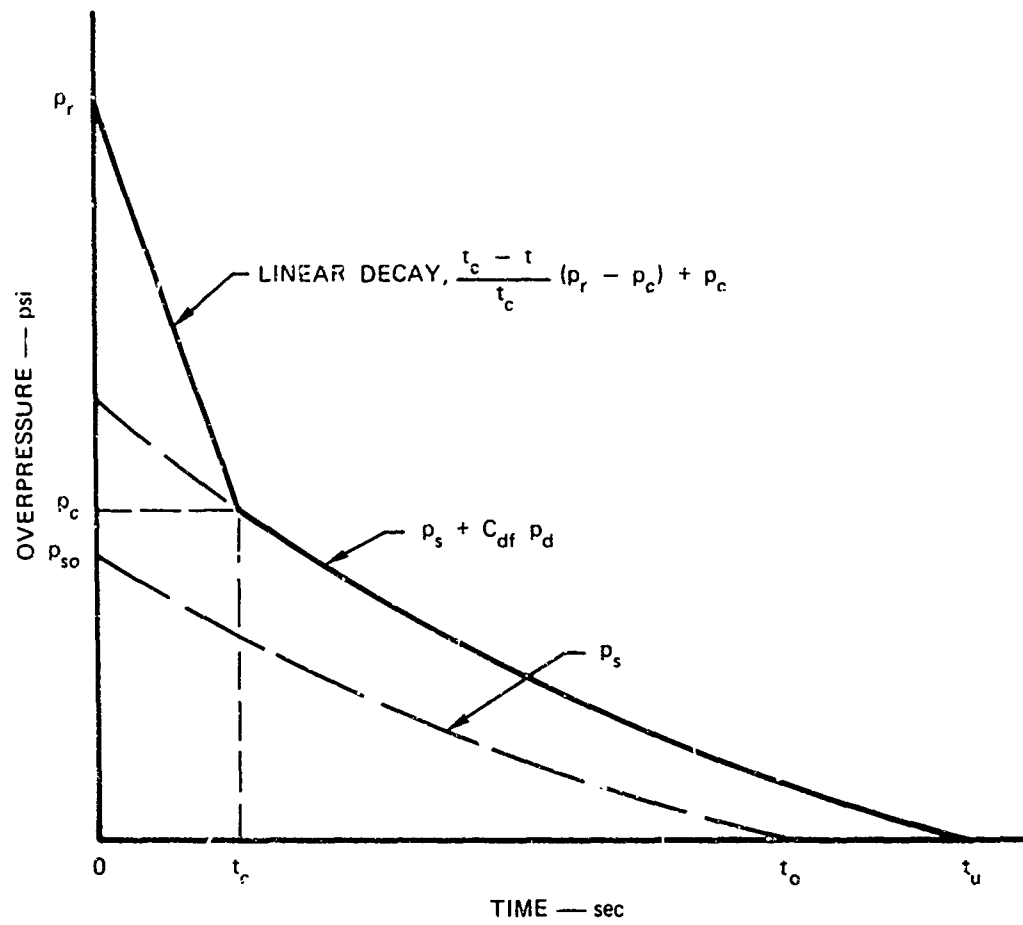


FIGURE 1 CONVENTIONAL SCHEME FOR THE FRONT FACE LOADING ON A CLOSED RECTANGULAR BLOCK

history for any wall in an actual structure. This information was used to construct a net load-time history for evaluating the collapse overpressure for the wall. For convenience of presentation, the method of load determination is discussed in three subsections. The front face and interior wall loadings are discussed briefly, followed by a general description and example of the method used to calculate the net load-time history on the exterior front wall.

Front Face Loading

The determination of the load-time function at any point on the front face of the exterior wall of a large building is an exceedingly complex problem for which no satisfactory prediction procedure is available for evaluating existing structures. For the design of structures, the conventional air blast loading scheme shown in Figure 1 was developed primarily from empirical data. To calculate the average load-time history on the front face of a closed rectangular block with this method, the reflected overpressure, p_r , is first determined. After reflection of the shock front at normal incidence, it is assumed that the clearing of the reflected overpressure is initiated at zero time and that it decays linearly to the stagnation pressure in a time, $t_c = 3 S/U$, where S is the clearing distance and U the shock front velocity. The stagnation pressure decays directly with the static and dynamic overpressures to zero pressure at time t_u . For design purposes, the load calculated in this manner is applied as a uniform pressure to the entire front face of a building.

For the evaluation of structures, the conventional load prediction method just described is inadequate for two primary reasons. First, for the front wall of a large structure, it is assumed in the conventional method that the load-time history is identical for each point on the

front wall. For example, wall panels I and II on Figure 2 would be designed to resist the same average dynamic loading, without consideration of their location. To predict the collapse of these panels, however, it would be necessary to provide a more definitive load-time history than can be determined by the conventional scheme. This can be illustrated by examining the relief of the reflected overpressure on the 10-ft square panels I and II of the 50-ft high by 130-ft long building in Figure 2. The conventional air blast prediction scheme would indicate that the clearing time of the reflected pulse from a 5 psi incident blast wave would occur in 3 S/U, or about 117 msec for both panels. However, for an actual building, panel I would be swept by rarefaction waves from both the roof and left building edges within the first 10 msec following reflection. Therefore, the average load on panel I would start to decay at about zero time, and the rate of decay would be much faster than that indicated by the 117-msec average clearing time calculated by the conventional loading method. On the other hand, the relief of the reflected overpressure on panel II would not be initiated until the rarefaction wave from the roof reached the panel in about 40 or 50 msec. Until this time, the clearing would be delayed and the load on panel II would be maintained at the value of the reflected overpressure, which decays at a relatively slow rate.* It is apparent from this brief description that the loading on panels I and II of a windowless building would be considerably different during the early diffraction period. Although this difference is not accounted for in the conventional load prediction method used for the design of structures, it is important since it can be a controlling factor in the determination of the collapse of exterior wall panels subjected to nuclear blast loading.

* For example, for a 5-Mt weapon yield, the reflected overpressure from a 5 psi shock wave, at normal incidence to a large surface, would decay from 11.39 to 11.16 psi in the first 50 msec.

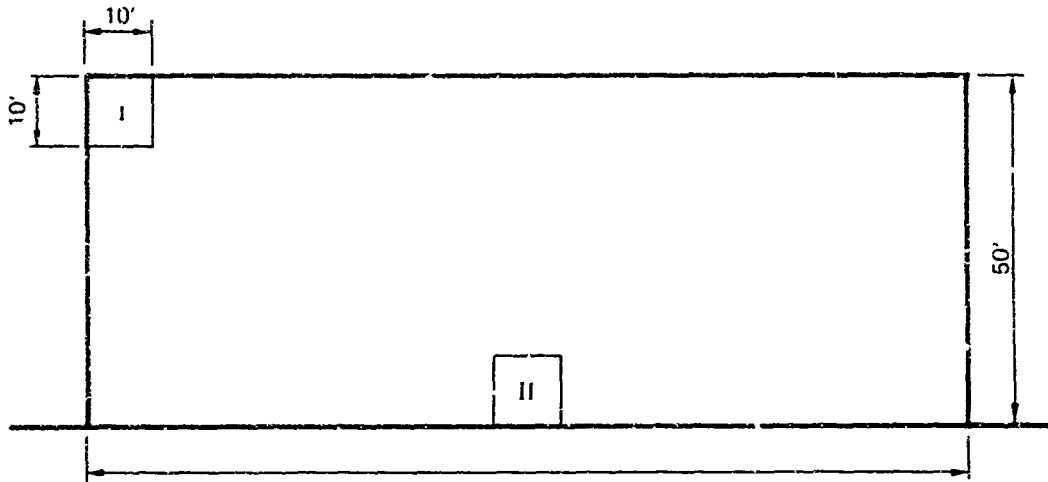


FIGURE 2 FRONT ELEVATION OF LARGE MULTISTORY BUILDING WITHOUT OPENINGS

The second reason that the conventional type of load prediction scheme is inadequate for the evaluation of structures is that it was developed for closed structures, and there is no provision for including the effect of window or door openings on the load-time history. The primary influence of wall openings on the load calculated by the conventional technique is two-fold. The first effect is a marked reduction in the clearing time of the reflected pulse, since the opening provides an additional mechanism for relief. The second effect is a reduction of the net load on the wall as a result of the loading on the back face of the front wall caused by the shock diffraction and air flow into the room through the window.

Although there are no generally accepted conventional procedures available for estimating the clearing time of the reflected overpressure on a structure with openings, Ref. 6 provides a systematic method for determining a weighted average for the clearing distance. To calculate the clearing distance with this procedure, the front face of a building is first subdivided into rectangular areas bounded by the window and door edges and the building edges. Each area is then weighted according to the number and location of the sides of the area from which clearing of the reflected overpressure can occur. The weighted average clearing distance for the front face is then determined by the summation

$$S' = \sum \frac{\delta_p h_n A_n}{A_f} \leq S \quad (1)$$

The weighted clearing distance, S' , is then used in the same manner as the clearing distance, S , to determine the clearing time, t_c . The accuracy or physical basis for the procedure could not be analytically evaluated in this study, but the values of S' determined for the cases

examined were believed to be on the low side. Also, if an analysis is made to determine the sensitivity of the weighted average clearing distance to the percentage of window openings, an anomaly will be found to exist between the procedure to calculate S' and the conventional procedure to calculate S for a closed structure. That is, as the percentage of window openings approaches zero, S' is found to be much less than S . However, as discussed in the subsection on net loading, because of the treatment of the clearing distance as a random variable for predicting the collapse of wall elements, a precise definition of the distance may not be too important.

Interior Loading

When an air blast wave strikes a building surface at or near normal incidence, the wave front reflects from the exterior wall, enters the window openings, and diffracts around the sides and roof of the building. The high pressure reservoir on the exterior face creates a flow into the building through the openings. As noted in Ref. 7, if the fraction of the opening on the exposed wall is greater than about 50 percent, the shock front will pass into the building only slightly weakened and the problem is primarily one of shock propagation. If the fraction of opening is less than 10 percent, the shock diffraction is of minor importance and the interior loading is primarily a room-filling process resulting from an expansion of the high exterior pressure into the building. Although most actual structural configurations fall between these two extremes, there is no simplified procedure available for determining the loading on interior surfaces from both the shock diffraction and the high velocity air flow. It is conceivable that a satisfactory solution to the interior loading problem could be obtained by superimposing the early shock front loading on the average pressure-time function obtained

from the room-filling techniques. However, as shown in Ref. 8, the calculation of the strength of the shock front in space and time is a tedious process requiring two-dimensional hydrodynamic computer codes and is much too involved for a simplified approach. On the other hand, for many cases of practical interest, it is expected that the primary interior load will result from the room filling caused by the air flow and not from the expansion and reflection of the weakened shock front within the room. Therefore, in this study, the interior wall loading was determined by room-filling techniques, and the contribution of the shock front to the interior loading was neglected.

Net Wall Loading

To determine the wall loading it was assumed that the blast wave before interacting with the structure was an ideal Mach waveform propagating radially outward over an ideal reflecting surface. This is an oversimplification, since in any actual situation, the blast waveform is influenced by many physical factors, e.g., terrain, surface type, blast shielding in city complexes, and airborne dust and debris. However, since there is no rational procedure available that accounts for these factors, they were not considered further in this study. It was also assumed that the duration of the positive phase of the dynamic overpressure was equal to that of the side-on overpressure and that the negative phase could be neglected for structural response calculations.

The weighted clearing distance method discussed under Front Face Loading was used to calculate the exterior pressure-time history for a wall of a building with window openings. However, since precise values are not known for many of the parameters that influence the collapse of actual structures, the wall behavior was predicted by using a deterministic approach modified by treating the important variables as random

processes. For a normally distributed function, this requires the determination of a mean value and standard deviation. Although no formal procedure was developed for applying this to the clearing time of the reflected overpressure, in general, it was accomplished as described below. For wall panels located near the edge of the front face of a building with windows, the maximum clearing distance was assumed to be equal to the greatest distance from any point on the panel to the nearest edge of the building where clearing of the reflected pulse could occur. Since this value of S was considered as a maximum, its probability of occurrence was assumed to be equal to 0.90 to 0.95. The weighted average clearing distance, S' , was then determined for the specific panel by Eq. 1. Since S' was considered as a minimum, it was assigned a probability of occurrence of 0.05 to 0.10. From these values of the clearing distance, the mean value and standard deviation could be calculated for a normal distribution function.

Although there are a number of room-filling procedures available (e.g., Refs. 9, 10, and 11), the method outlined in Ref. 7 was adopted for determining the interior pressure-time history. All current procedures provide an average pressure build-up within a room, but do not provide definitive load-time information for each interior wall surface. For each specific problem in this study, the net wall loading was obtained by a simple summation of the exterior and interior pressure-time histories. An example of the net loading on the upper portion of the front wall of the two story brick house discussed in Section VI is shown in Figure 3.

The method used to determine the net load-time function on a side or rear wall of a building was first to calculate the average load on the exterior surface of the wall by the method presented in Ref. 12 and then to subtract the interior pressure as determined in the previous subsection.

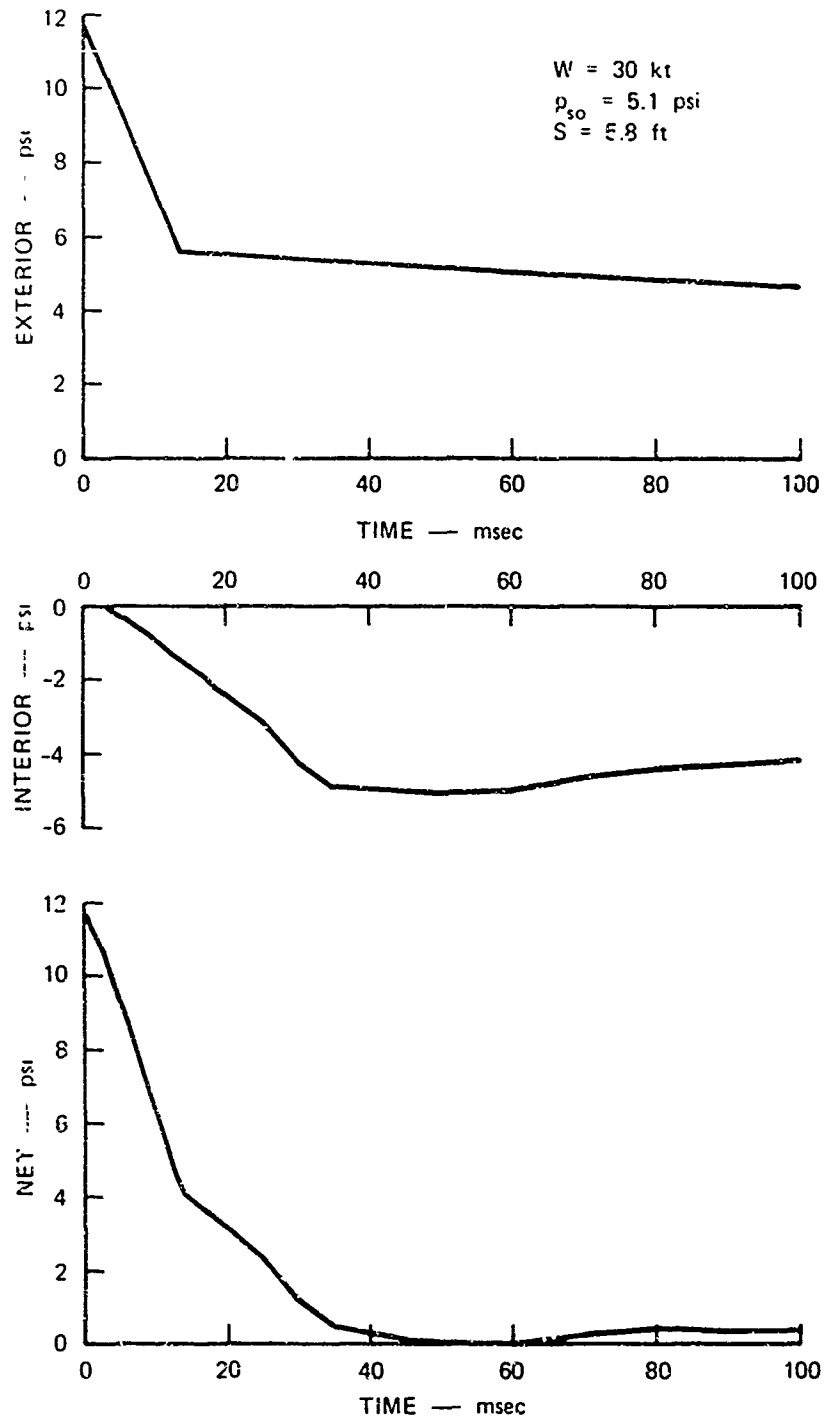


FIGURE 3 CALCULATED LOAD-TIME ON FRONT WALL OF BRICK HOUSE (TEAPOT)

III RESISTANCE FUNCTIONS

Introduction

The method used in this study to predict the behavior of exterior walls was the same as that previously developed in Ref. 1. This method required the development of a resistance function for each wall type of interest. In Ref. 1, procedures were presented for determining the resistance function for one-way structural action of three types of walls: unreinforced concrete or masonry unit walls without arching, unreinforced concrete or masonry unit walls with arching, and reinforced concrete walls. In this section, the development of procedures to account for two-way action of the three wall types is presented. Also included is an interim, or preliminary, procedure for determining the effect of a window opening on the resistance function.

The extension of the models from one-way structural action to two-way action required that additional, and sometimes tenuous, assumptions be made, especially for the inelastic portions of the wall response. This resulted primarily from the lack of definitive experimental information or theoretical developments that adequately describe the load-response relationship of unreinforced walls after elastic cracking has occurred. The resistance functions presented should therefore be considered as interim developments, which can be modified when better information becomes available. On the other hand, as discussed in Section IV, the use of probability functions in the procedures for predicting the incipient collapse overpressure of a wall makes the use of precise resistance functions less critical than would otherwise be the case.

The general case considered is shown in Figure 4. Initial development of resistance functions for two-way action walls was restricted to the following four support conditions, which are illustrated in Figure 5.

Support Case 1--Simply supported on four edges.

Support Case 2--Fixed on four edges.

Support Case 3--Fixed on vertical edges; simply supported on horizontal edges.

Support Case 4--Simply supported on vertical edges; fixed on horizontal edges.

So that certain assumptions could be made regarding the location at which cracking of the wall initially occurs, the development of resistance functions was further restricted to walls in which the length was greater than, or equal to, the height. Most walls of practical interest are believed to fall within these limitations. In all cases the walls were assumed to be of uniform thickness.

Unreinforced Concrete or Masonry Unit Wall (Without Arching)

As was the case for one-way action walls, the resistance function for two-way unreinforced concrete or masonry unit walls without arching was assumed to consist of an elastic phase followed by a decaying phase. The elastic phase is controlled by the bending strength, the failure is assumed to occur when the extreme fiber stress reaches the modulus of rupture for concrete members or the tensile bond strength for brick or masonry unit walls. For a wall simply supported on four edges (Support Case 1), an elastic failure occurs at the center of the wall, while for a wall fixed on two or more edges (Support Cases 2, 3, and 4), an initial elastic failure occurs at the fixed edges, with a secondary elastic failure occurring at the center. Thus, as shown in Figures 6 and 7, the elastic phase of the resistance function for Support Case 1 is described

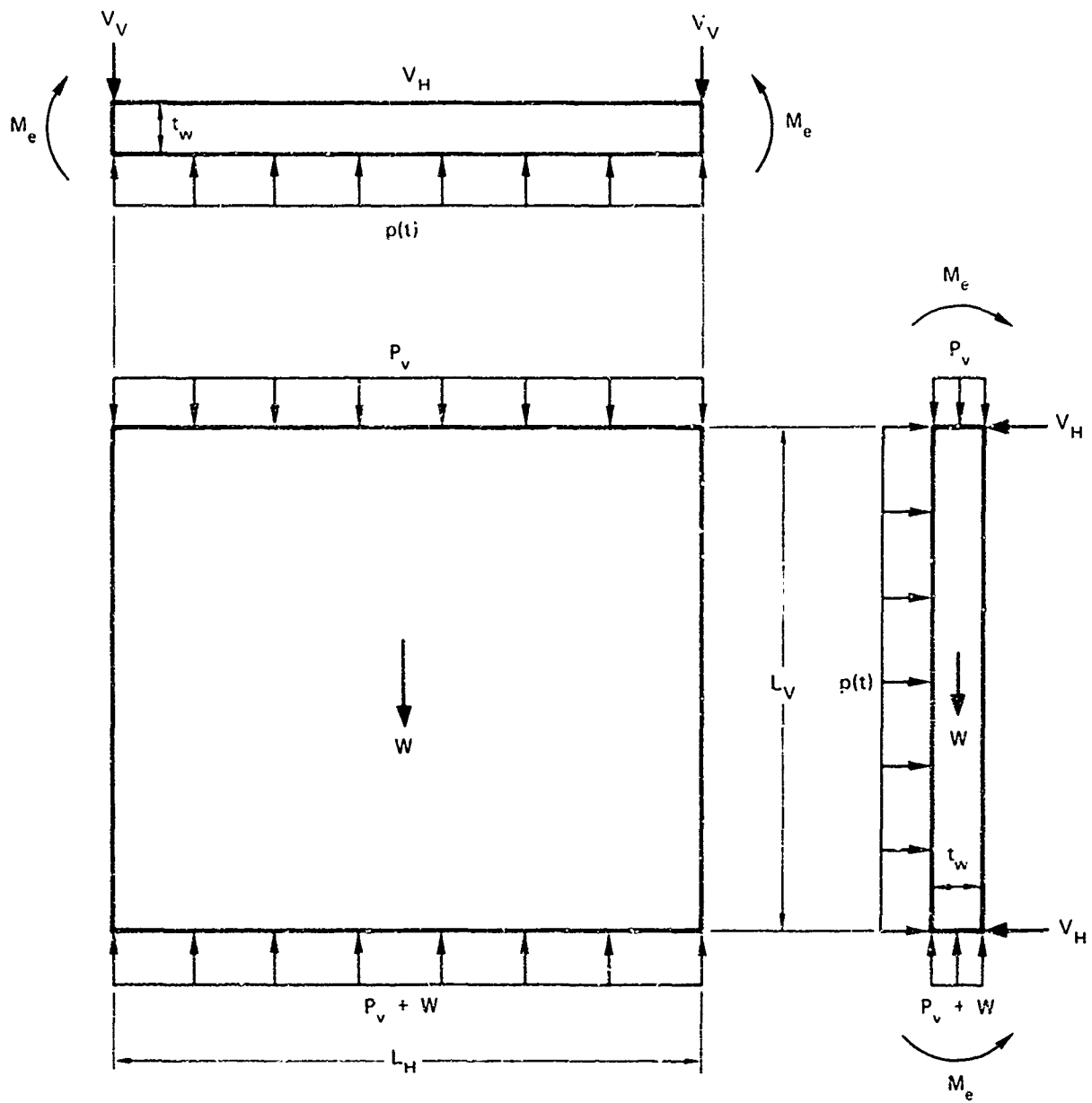
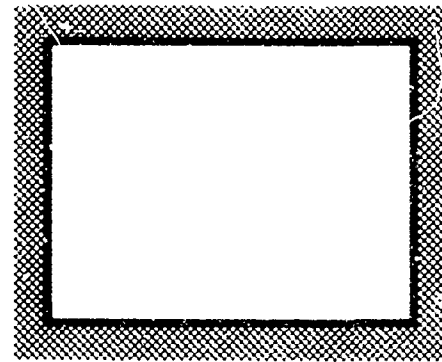


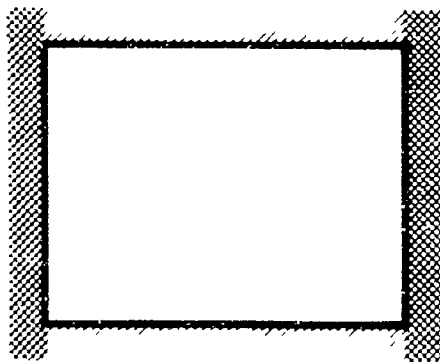
FIGURE 4 WALL ELEMENT ASSUMED FOR ANALYSIS



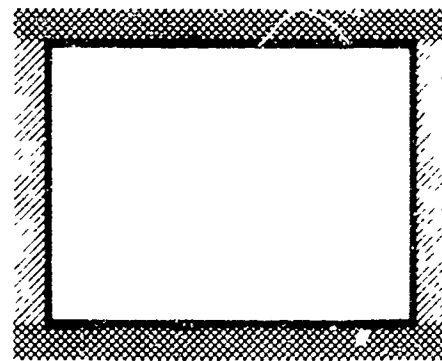
Support Case 1



Support Case 2



Support Case 3



Support Case 4

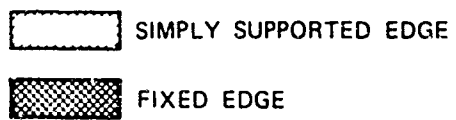


FIGURE 5 SUPPORT CASES

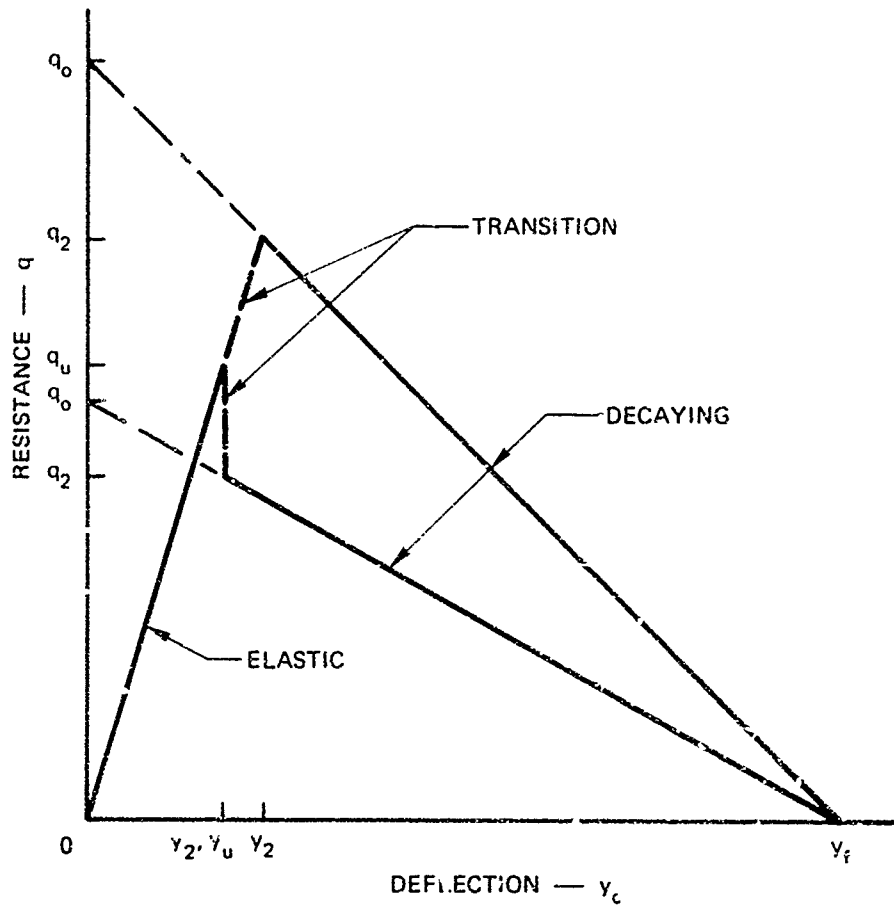


FIGURE 6 RESISTANCE FUNCTION FOR A TWO-WAY ACTION UNREINFORCED CONCRETE OR MASONRY UNIT WALL WITHOUT ARCHING SUPPORT CASE I

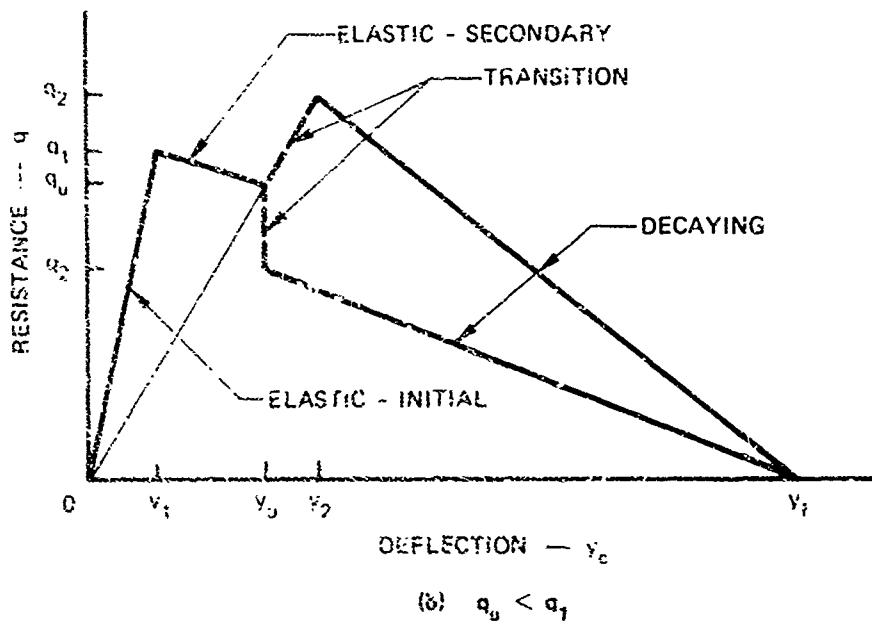
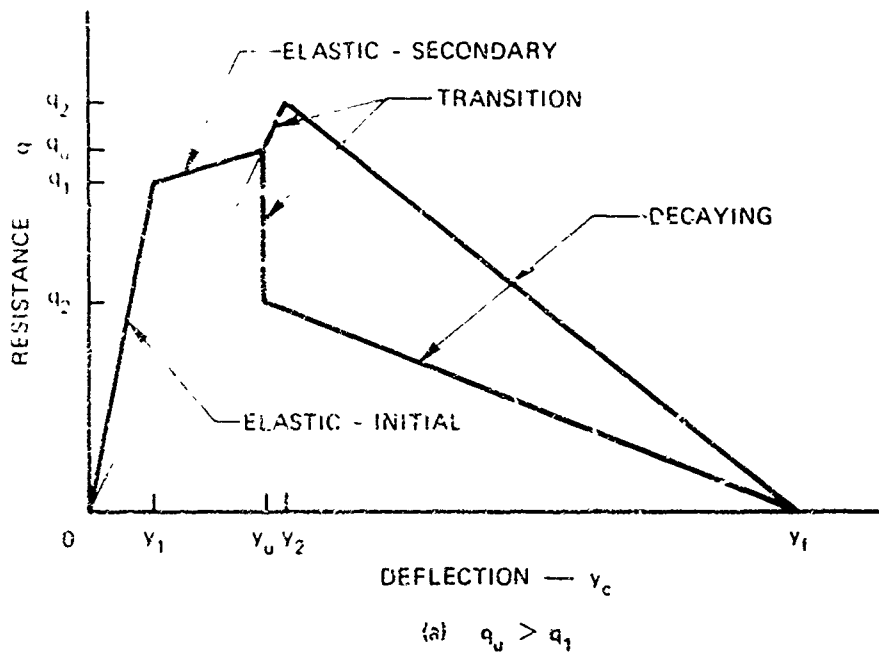


FIGURE 7 RESISTANCE FUNCTION FOR A TWO-WAY ACTION UNREINFORCED CONCRETE OR MASONRY UNIT WALL WITHOUT ARCHING SUPPORT CASES 2, 3, & 4

by a single elastic portion, whereas for Support Cases 2, 3, and 4, it is described by an initial and secondary elastic portion. Further, the elastic phase must be calculated separately for walls with and without vertical dead load (other than the wall's own weight). For the case of the wall with a vertical load, it was assumed that the vertical load was acting in the plane of the wall, as shown in Figure 4. The effect of any initial eccentricity of the vertical load thus was not considered in determining the resistance.

After the elastic phase, the wall resistance in the decaying phase is provided by the geometry of the wall and the magnitude of the vertical axial forces in the plane of the wall.

Resistance Function

Elastic Phase - Wall Without Vertical Axial Load. During the elastic phase the wall was assumed to behave as an elastic homogeneous plate. The maximum elastic resistance is therefore developed when the maximum moment occurring in the wall equals the ultimate moment capacity of the wall. For a wall simply supported on four sides (Support Case 1) with a uniform lateral load (i.e., a uniform load acting normal to the face of the wall), the maximum moment occurs at the center of the wall, and is found from Ref. 13 to have a value equal to

$$M_c = B_1 q L_v^2 \quad (2)$$

where B is a numerical factor depending on both the support conditions and the ratio L_u/L_v . The subscript 1 indicates Support Case 1. Values of B are plotted against the ratio L_u/L_v in Figure 8 for all support cases.

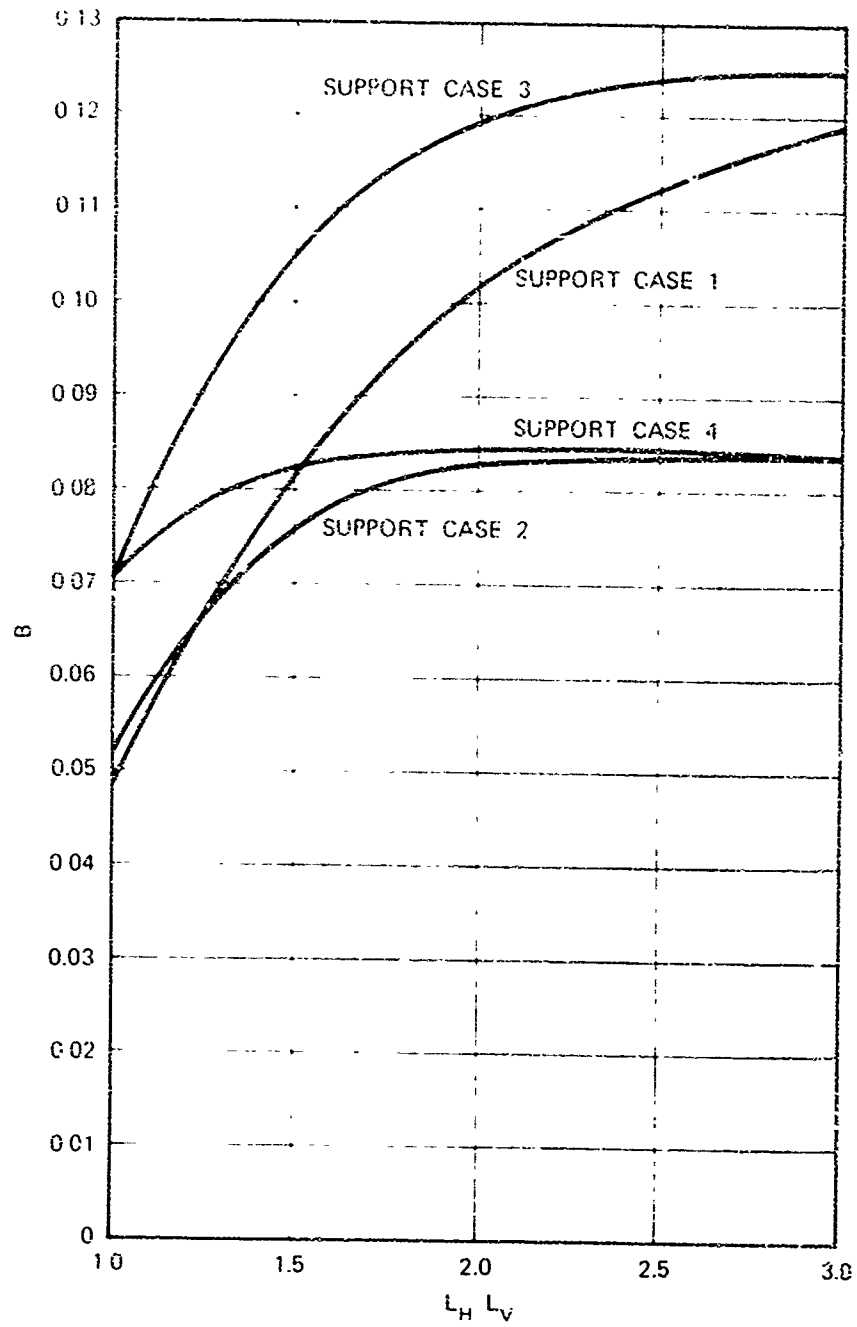


FIGURE 8 COEFFICIENTS FOR MAXIMUM ELASTIC MOMENT IN TWO-WAY ACTION WALLS WITHOUT VERTICAL LOAD

The corresponding ultimate moment capacity at the center of the wall is given by

$$M_{u,c} = \frac{I_g}{t_w/2} f + \frac{W/2}{t_w} \quad (3)$$

where, depending on the type of wall construction, the value of f may be the modulus of rupture or the tensile bond strength. The gross, or uncracked, moment of inertia per unit width is given by

$$I_g = t_w^3/12 \quad (4)$$

The ultimate elastic resistance for Support Case 1 is now obtained by equating the maximum moment developed at the center of the wall (Eq. 2) to the ultimate moment capacity at the center of the wall (Eq. 3). Substituting the value of I_g (Eq. 4) into the resulting expression and solving for q_u yields

$$q_u = \frac{t_w(2ft_w + W)}{12B_1 L_v^2} \quad (5)$$

For Support Case 1, the maximum center deflection is found from Ref. 13 to be

$$y_u = \frac{A_1 q_u L_v^4}{Et_w^3/12(1 - \nu^2)} \quad (6)$$

where A is a numerical factor, again dependent on the support conditions and the ratio L_w/L_f , and the subscript 1 again indicates Support Case 1. Values of A are plotted against the ratio L_w/L_f in Figure 9.

Noting from Eq. 4 that the uncracked moment of inertia per unit width is equal to $t_w^3/12$, Eq. 6 can be rewritten as

$$v_w = \frac{(1 - \nu^2) A_1 q_w L_f^3}{E I_s} \quad (7)$$

For Support Cases 2, 3, and 4, in which the wall is fixed on two or more edges, the maximum moment for a uniform lateral load initially occurs along the fixed edges. For Support Case 2, fixed on four edges, the maximum moment occurs along the horizontal edges, or for the case of a square wall, along all four edges. For Support Cases 3 and 4, the maximum moment occurs along the fixed edges. The value of this maximum moment is again found from Ref. 13 and is given by

$$M_w = B_i q L_f^2 \quad , \quad i = 2, 3, 4 \quad (8)$$

where the value of the subscript i corresponds to the support case. Values of B for Support Cases 2, 3, and 4 are given in Figure 8.

The ultimate moment capacity along the fixed edges is given by

$$M_{w,u} = \frac{I_s f}{t_w/2} \quad (9)$$

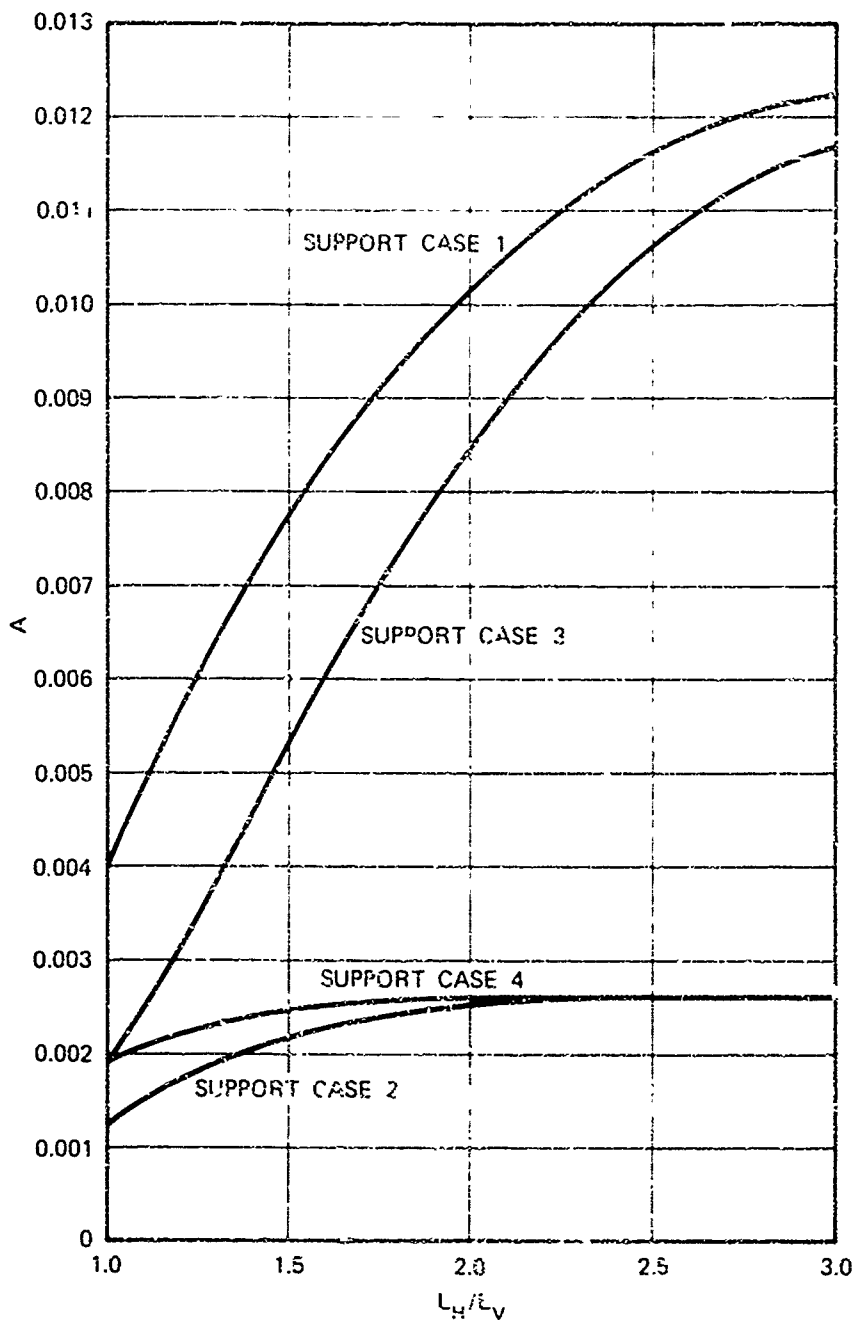


FIGURE 9 COEFFICIENTS FOR CENTER ELASTIC DEFLECTION OF TWO-WAY ACTION WALLS WITHOUT VERTICAL LOAD

Equating this ultimate moment capacity to the maximum moment along the fixed edges of the wall and substituting the value of I_g from Eq. 4, the maximum resistance for the initial portion of the elastic phase for Support Cases 2, 3, and 4 is

$$q_i = \frac{f t_w^2}{6B_i L_y^2} \quad (10)$$

The corresponding maximum deflection for the initial portion of the elastic phase of a wall fixed on two or more edges is

$$y_1 = \frac{(1 - \nu^2) A_i q_i L_y^4}{EI_g}, \quad i = 2, 3, 4 \quad (11)$$

where the subscript i corresponds to the support case. Values of A for Support Cases 2, 3, and 4 are given in Figure 9.

After cracking occurs at the fixed edges, the bending resistance at the edges is reduced to zero, and the wall responds as if it were simply supported on four edges. The maximum resistance and deflection during the secondary portion of the elastic phase may be determined from Eqs. 5 and 6, respectively. For the corresponding behavior of one-way action walls, the influence of this phase was not believed to be important since the maximum resistance for a simply supported element is only two-thirds that of the fixed-end element. Therefore it was neglected. For the two-way action wall, however, the maximum resistance for a wall simply supported on four sides may - for certain L_u/L_v ratios - be greater than the corresponding resistance for walls fixed on two or more edges. Even for situations where this is not the case, computed results have indicated

that for some dynamic loads the inclusion of a secondary portion of the elastic phase may have a significant effect. For this phase, it was assumed that a linear relationship existed between the maximum values of the fixed-edge and simply supported walls.

Elastic Phase - With Vertical Load. The case of an elastic plate simply supported on four edges (Support Case 1) with a combined uniform lateral load and uniform compressive axial forces along two opposite edges is discussed in Ref. 14. The resulting differential equations are solved in terms of an infinite series. By summing this series, the maximum elastic resistance and deflection can be expressed in an identical form to that used for the wall without vertical load. The resulting maximum elastic resistance for the case where the compressive load acts along the horizontal edges is given by

$$q_v = \frac{t_w(2f t_w + W)}{12B_{v1}L_v^2} \quad (12)$$

where B_{v1} is a numerical coefficient given by the infinite series

$$B_{v1} = \frac{4}{\pi} \left(\frac{L_H}{L_V} \right)^2 \sum_{n=1,3}^{\infty} \frac{(-1)^{(n-1)/2}}{m \left(\frac{m\pi}{L_V/L_H} \right)^2 \left[\left(\frac{m\pi}{L_V/L_H} \right)^2 - 4\pi \frac{P_V}{P_H} \right]} \left\{ \frac{(L_H \gamma_n)^2 \left[\nu(L_H \gamma_n)^2 - \left(\frac{m\pi}{L_V/L_H} \right)^2 \right]}{\frac{4m\pi^2}{L_V/L_H} \sqrt{\frac{P_V}{P_H}} \cosh \frac{L_H \gamma_n}{2}} - \frac{(L_H \gamma_n)^2 \left[\nu(L_H \gamma_n)^2 - \left(\frac{m\pi}{L_V/L_H} \right)^2 \right]}{\frac{4m\pi^2}{L_V/L_H} \sqrt{\frac{P_V}{P_H}} \cosh \frac{L_H \gamma_n}{2}} \right. \\ \left. + \left(\frac{m\pi}{L_V/L_H} \right)^6 \right\} \quad (13)$$

and

$$L_1 \eta_1^2 = \left(\frac{m\pi}{L_1/L_2} \right)^2 + \frac{2m^2}{L_1/L_2} \sqrt{\frac{P_1}{P_2}} \quad (13a)$$

$$(L_1 \eta_2)^2 = \left(\frac{m\pi}{L_1/L_2} \right)^2 - \frac{2m^2}{L_1/L_2} \sqrt{\frac{P_1}{P_2}} \quad (13b)$$

$$P_2 = \frac{1-\nu^2 E I_f}{I_s} \quad (13c)$$

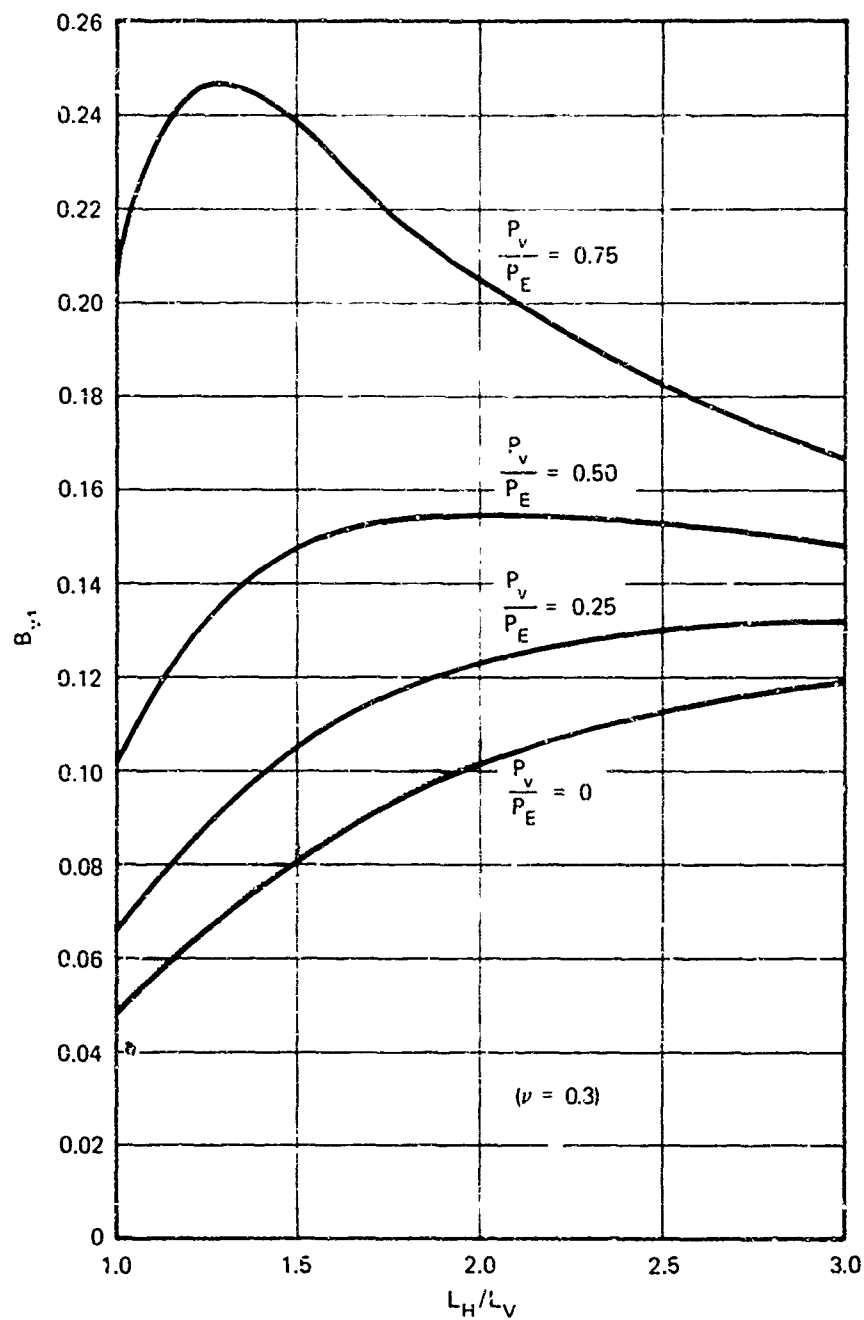
The value of B_{v1} may generally be obtained to sufficient accuracy by summing the first three or four terms of the series. Values of B_{v1} are plotted against L_1/L_2 ratios for various values of the nondimensional parameter P_1/P_2 in Figure 10.

The corresponding maximum elastic deflection for the wall with vertical load is given by

$$y_1 = \frac{A_{v1} L_1^3 q_1}{E I_f} \quad (14)$$

where A_{v1} is a numerical coefficient given by the infinite series

$$A_{v1} = \frac{4}{\pi} (1 - \nu^2) \left(\frac{L_1}{L_2} \right)^4 \sum_{n=1,3}^{\infty} \frac{(-1)^{(n-1)/2}}{m \left(\frac{m\pi}{L_1/L_2} \right)^2 \left[\left(\frac{m\pi}{L_1/L_2} \right)^2 - 4\pi^2 \frac{P_1}{P_2} \right]} \left\{ 1 + \frac{\left((L_1 \eta_1)^2 \cosh \frac{L_1 \eta_1}{2} - (L_1 \eta_2)^2 \cosh \frac{L_1 \eta_2}{2} \right)}{\frac{4m^2}{L_1/L_2} \sqrt{\frac{P_1}{P_2}} \cosh \frac{L_1 \eta_1}{2} \cosh \frac{L_1 \eta_2}{2}} \right\} \quad (15)$$



Notes: The shaded area indicates the range of values of primary interest for wall analysis.

FIGURE 10 COEFFICIENTS FOR MAXIMUM ELASTIC MOMENT IN TWO-WAY ACTION WALLS WITH VERTICAL LOAD SUPPORT CASE 1

Again sufficient accuracy may usually be obtained by summing the first three or four terms of the series. Values of A_{v1} are plotted for various values of the P/P_c in Figure 11.

For Support Cases 2, 3, and 4, no published information was found in the literature concerning walls with fixed edges subjected to a combined uniform lateral load and uniform compressive axial forces. In the absence of such information, the following approximate procedure was used to determine the maximum elastic resistance and deflection for these support cases.

The ratio of the moment coefficient for the wall with vertical load, B_v , to that for the wall without vertical load, B , was assumed to be the same for each of the four support cases considered. Therefore:

$$\frac{B_{v1}}{B_1} = \frac{B_{v2}}{B_2} = \frac{B_{v3}}{B_3} = \frac{B_{v4}}{B_4} \quad (16)$$

where the subscript numeral indicates the corresponding support case.

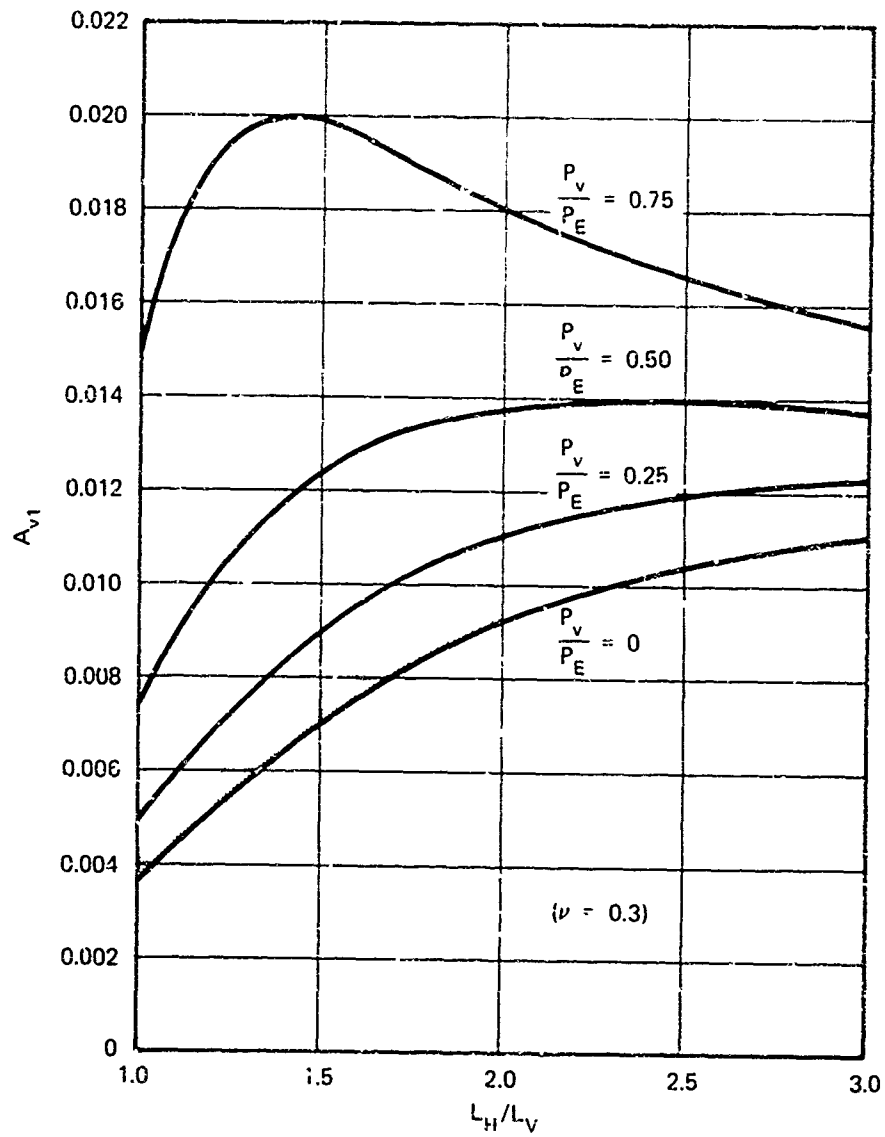
The moment coefficient for the wall with vertical load for Support Cases 2, 3, and 4 can thus be determined from the relationship

$$B_{vi} = \left(\frac{B_{v1}}{B_1} \right) B_i, \quad i = 2, 3, 4 \quad (17)$$

where the subscript i corresponds to the support case.

The maximum resistance in the initial portion of the elastic phase for a wall with vertical load can now be determined from

$$q_1 = \frac{M_{e1}}{B_{vi} L_v^2}, \quad i = 2, 3, 4 \quad (18)$$



Note: The shaded area indicates the range of values of primary interest for wall analysis

FIGURE 11 COEFFICIENTS FOR CENTER ELASTIC DEFLECTION OF TWO-WAY ACTION WALLS WITH VERTICAL LOAD SUPPORT CASE 1

Using the same assumption as was used for the moment coefficients, the deflection coefficient for the wall with vertical load may be determined from the relationship

$$A_{y,i} = \left(\frac{A_{y1}}{A_1} \right) A_i, \quad i = 2,3,4 \quad (19)$$

The maximum elastic deflection for the wall with vertical load can then be determined from

$$y_i = \frac{A_{y,i} L_v^3 q_i}{EI_s}, \quad i = 2,3,4 \quad (20)$$

After cracking occurs at the fixed edges, the wall again responds as if it were simply supported on four edges. The maximum resistance and deflection for the secondary portion of the elastic phase can be determined from Eqs. 12 and 14, respectively. It was again assumed that during this phase, a linear relationship exists between the maximum values of the fixed-edge and simply supported walls.

Decaying Phase. The determination of the actual resistance developed by a two-way action unreinforced concrete or masonry unit wall during the decaying phase is a complex problem for which no experimental data exist. However, limited experiments such as those conducted in the URS shock tunnel (Ref. 15) provide a qualitative picture of the crack patterns, although no mathematical description has been formulated. Because of the lack of information, it has been necessary to base the development of the resistance functions primarily on engineering judgment.

For unreinforced one-way action walls, the resistance function was developed by establishing the internal restoring moments resulting from the equilibrium of the wall system. For two-way action, the use of the

equilibrium of forces to develop the resistance function is less clear, especially for the determination of the restoring moment along a diagonal crack. As a cracked two-way action wall rotates during the decaying phase, slippage and shear forces of unknown magnitude occur between the various segments that cannot be rationally accounted for in the equilibrium equations. This necessitates gross simplifying assumptions that cannot be verified without additional experimental information.

The resistance of an unreinforced wall during the decaying phase results from the vertical forces that produce a restoring moment on the wall. For a wall cracked as indicated in Figure 12, the development of restoring forces on a vertical section through the horizontal line d-c is fairly straightforward. However for a vertical section such as A-A through both the trapezoidal and triangular portions, an accurate description of the restoring forces would include shear forces between segments and account for any change in relative position of the segments with increasing deflection. The effect of side, or lateral, restraint on a wall panel and the possible development of arching forces between adjacent panels complicate the problem further.

For this study, it was assumed that an unreinforced two-way action wall developed its resistance during the decaying phase in a manner analogous to the yield-line theory of reinforced concrete slabs. In the yield-line theory, it is assumed that the reinforcing steel yields where it intersects the line between segments. This provides the basis for determining the moment capacity for each yield line and permits a solution to be obtained for the load capacity of the slab. For a cracked unreinforced wall panel, the resistance or restoring moment results from the vertical forces on the segments, rather than from the moment resistance developed between segments. However, in this analysis, it was assumed that the effect of the restoring forces was the same as the development of a

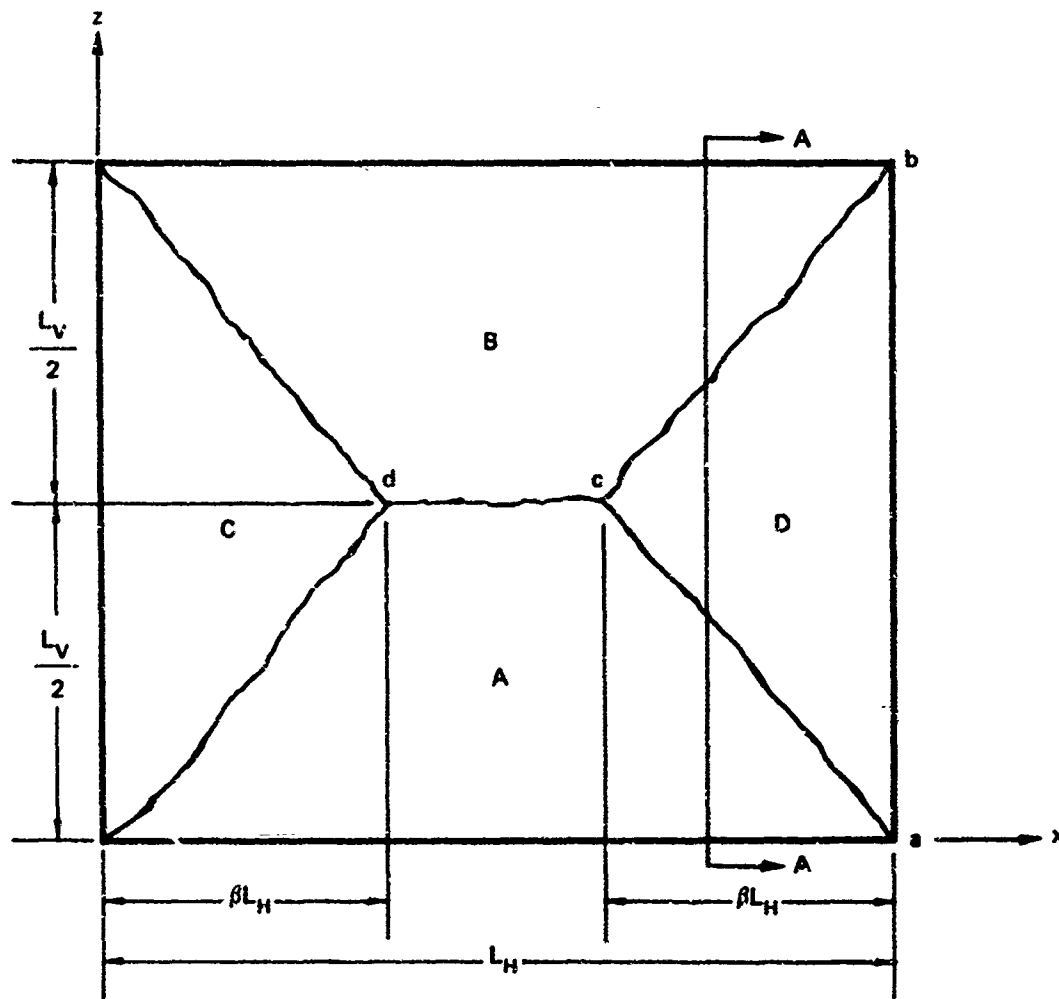


FIGURE 12 CRACK PATTERN ASSUMED FOR ANALYSIS OF TWO-WAY ACTION WALL

moment resistance across yield lines. This simplifying assumption leads to other necessary assumptions, which are mentioned during the development of the resistance function.

Because of the relative change in the position between segments during the deflection of the wall shown in Figure 12, a solution to the problem of the resistance function for the secondary phase is not tractable without considerable simplification of the actual situation. That is, as the wall panel deflects under blast loading, either the upper or lower trapezoidal segments lose contact at the horizontal line d-c in the figure, the triangular segments move laterally outward in the plane of the wall, crushing occurs along the diagonals similarly to that in arching walls, or some combination of these occurs. Therefore, since sufficient experimental information was not available, the resistance function for the secondary phase was determined for the deflection $y_c = 0$, and it was assumed that the resistance decayed linearly to zero at the maximum deflection $y_f = t_w$, where the wall segments become unstable and collapse occurs.

After a two-way action unreinforced concrete or masonry unit wall fails in the initial elastic phase, a crack pattern is developed in the wall similar to that shown in Figure 12.* To formulate the equations for the wall resistance in the secondary phase, it was assumed that the four wall segments remained in contact and rotated about the supports as rigid bodies. It was also assumed that the lateral restraint provided by the adjacent wall panels was sufficient to develop the restoring moment. Furthermore it was assumed that the shear forces at the cracked lines

* In a number of actual air blast tests on brick wall panels, simply supported on four sides, and at pressure levels well in excess of the incipient collapse pressure, the primary crack pattern included a rectangular segment near the center of the panel rather than a single horizontal crack as shown in Figure 12 (Ref. 15).

were internal forces that did not affect the restoring moment. Therefore, the resistance of a two-way action wall was related to the vertical axial load, the wall dead load, the wall dimensions, the deflection, and the crack pattern.

The approach used in this study was (1) to determine the restoring moment from the equilibrium of forces on each wall segment and (2) to use the restoring moment in the work equations developed from the concepts of the yield-line theory.

An examination of the vertical restoring forces on a section through the lower trapezoidal wall segment A on Figure 13(a) will show that the restoring moment is equal to

$$M = \left(\frac{t_w - y}{2} \right) [2P_v + (1 + \lambda)W] \quad (21)$$

where λ is the proportion of the wall panel height above the cracked section. Since along line d-c, λ is a constant equal to 0.5, and since only the maximum resistance at $y = 0$ is determined, Eq. 21 becomes

$$M_1 = \frac{t_w}{4} (4P_v + 3W) \quad (22)$$

which is assumed to be equivalent to the moment resistance for the lower segment along the horizontal cracked line d-c in Figure 12.

Along a diagonal crack, such as c-a in Figure 12, the value of λ increases linearly from point c to a. The restoring moment at c is equal to Eq. 22, and at a, for $\lambda = 1$, is equal to

$$M_a = t_w (P_v + W) \quad (23)$$

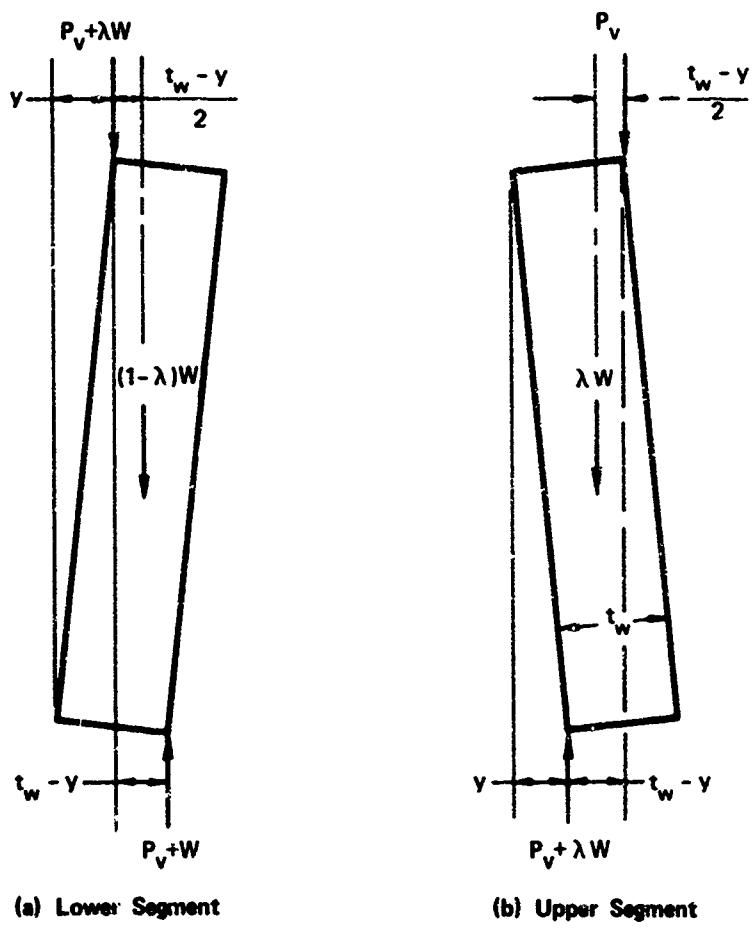


FIGURE 13 ASSUMED VERTICAL FORCES ON SEGMENTS OF TWO-WAY ACTION UNREINFORCED WALL

The average moment resistance, M_2 , along line c-a, would therefore be

$$M_2 = \frac{M_b + M_a}{2}$$

or

$$M_2 = \frac{t_w}{8} (8P_v + 7W) \quad . \quad (24)$$

In a similar manner the restoring moment for the upper segment B can be determined from Figure 13(b) to be equal to

$$M = \left(\frac{t_w - y}{2} \right) (2P_v + \lambda W) \quad (25)$$

which for line d-c, Figure 12, with $\lambda = 0.5$ and $y = 0$, becomes

$$M_3 = \frac{t_w}{4} (4P_v + W) \quad (26)$$

and for point b, with $\lambda = 0$, becomes

$$M_b = t_w P_v \quad . \quad (27)$$

The average moment resistance, M_4 , along the diagonal line c-b would therefore be

$$M_4 = \frac{t_w}{8} (8P_v + W) \quad . \quad (28)$$

To develop the resistance function for the secondary phase, the work-energy method from the yield-line theory for reinforced concrete slabs was used (e.g., Refs. 16 and 17). For rigid body rotation of the

segments, the work done can be found by multiplying the resisting moment per unit length normal to the axis of rotation by the angle of rotation, and summing over the length of the segment. The work done by the restoring moment acting on segment A is

$$W_A = M_1(L_H - 2\beta L_H)\theta_A + M_2(2\beta L_H)\theta_A$$

and on segment B is

$$W_B = M_3(L_H - 2\beta L_H)\theta_B + M_4(2\beta L_H)\theta_B$$

Since for small deflections

$$\theta_A = \theta_B = \frac{2y_c}{L_V}$$

then

$$W_A = \frac{2y_c L_H}{L_V} [M_1(1 - 2\beta) + 2M_2\beta] \quad (29)$$

and

$$W_B = \frac{2y_c L_H}{L_V} [M_3(1 - 2\beta) + 2M_4\beta] \quad (30)$$

Because of symmetry, the work done by the restoring moment acting on the triangular segments is equal, and since

$$\theta_c = \theta_d = \frac{y_c}{\beta L_H}$$

then

$$W_C = W_D = \frac{y_c L_v}{2\beta L_H} (M_2 + M_4) \quad (31)$$

The total work done on the wall would be

$$W_T = W_A + W_B + W_C + W_D$$

which, by substitution of Eqs. 29, 30, and 31 becomes

$$W_T = 2y_c \left\{ \frac{L_H}{L_v} [(M_1 + M_3)(1 - 2\beta) + 2\beta(M_2 + M_4)] + \frac{L_v}{2\beta L_H} (M_2 + M_4) \right\} \quad (32)$$

The energy input for a uniform load, q , can be determined by multiplying the total load acting on the segment by the deflection at the center of gravity of the load on the segment. The energy input for the various wall segments shown on Figure 12 is

$$E_A = E_B = q(L_H - 2\beta L_H) \left(\frac{L_v}{2} \right) \left(\frac{y_c}{2} \right) + 2q \left(\frac{\beta L_H}{2} \right) \left(\frac{L_v}{2} \right) \left(\frac{y_c}{3} \right)$$

or

$$E_A = E_B = \frac{q y_c L_v L_H}{12} (3 - 4\beta) \quad (33)$$

and

$$E_C = E_D = q \left(\frac{L_v}{2} \right) (\beta L_H) \left(\frac{y_c}{3} \right)$$

or

$$E_c = E_D = \frac{qy_c L_y L_H \beta}{6} \quad (34)$$

The total energy input of the load would be

$$E_T = E_A + E_B + E_C + E_D$$

which, by substitution of Eqs. 33 and 34 becomes

$$E_T = \frac{qy_c L_y L_H}{6} (3 - 2\beta) \quad (35)$$

Since the total work done equals the total energy input

$$W_T = E_T$$

which, by substitution of Eqs. 32 and 35 and solving for the wall resistance, yields

$$q = \frac{12}{L_y^2 (3 - 2\beta)} \left[(M_1 + M_3)(1 - 2\beta) + (M_2 + M_4) \left(2\beta + \frac{L_y^2}{2\beta L_H^2} \right) \right] \quad (36)$$

By substituting the various moments into Eq. 36, the maximum resistance (at $y_c = 0$) for the secondary phase for a two-way action unreinforced concrete or masonry unit wall is found to be

$$q_o = \frac{12t_w (2P_y + W)}{L_y^2 (3 - 2\beta)} \left(1 + \frac{L_y^2}{2\beta L_H^2} \right) \quad (37)$$

To obtain a solution to the above resistance function, the length coefficient, β , must be determined. However, the solution to the cubic equation for β , derived for the unreinforced wall without arching, depends on the ratio of the height to width of the wall, the deflection of the wall during the rotational phase, and the magnitude of the vertical in-plane forces.

The dependence of the coefficient β on the ratio L_v/L_H presents no special problem, since the cubic equation can readily be solved for $0 \leq L_v/L_H \leq 1$. The dependence of the coefficient β on the wall deflection implies that the length βL_H varies with the rotation of the wall segments, which, of course, cannot occur after formation of the initial crack in an unreinforced wall. The problem of defining the coefficient β is therefore a problem of determining the initial crack pattern at the end of the initial elastic phase of response. However, this is complicated by the influence of the vertical forces, which results in a unique solution of the coefficient for each value of the load P_v . Since there is no general solution for β in terms of the length ratio L_v/L_H , it was assumed in this study that the equation derived by the yield-line analysis for isotropic reinforced concrete slabs in Ref. 17 was applicable for unreinforced masonry or concrete walls without arching, i.e.:

$$\beta = \frac{1}{2} \left[\sqrt{3 \left(\frac{L_v}{L_H} \right)^3 + \left(\frac{L_v}{L_H} \right)^4} - \left(\frac{L_v}{L_H} \right)^3 \right] \quad (38)$$

For computational purposes, the maximum resistance q_0 during the decaying phase was determined for the case $y_c = 0$, and it was assumed that the resistance decayed linearly to zero at the maximum deflection $y_f = t_w$, as shown on Figures 6 and 7. However, for an actual wall, the decaying phase is not initiated until after the wall fails in the elastic phase, which occurs when the deflection reaches the maximum elastic

deflection y_u . The maximum resistance during the decaying phase is thus equal to

$$q_2 = q_0(1 - y_u/t_w) \quad (39)$$

where q_0 is given by Eq. 37.

Since the method of determining the resistance curves for the elastic and decaying phases generally results in a discontinuity, an assumption regarding the transition between the two phases was required. For the case where the maximum decaying resistance is less than the ultimate elastic resistance, the resistance function is assumed to decrease to the decaying resistance function, as shown by the vertical dashed transition line in Figures 6 and 7. For the case where the maximum decaying resistance is greater than the maximum elastic resistance, the elastic resistance is assumed to increase linearly until it intersects the decaying resistance function, as shown by the upper dashed transition line in Figures 6 and 7. In an actual case the resistance function would exhibit a smooth transition between the two phases, rather than as used in the mathematical models herein. The error is assumed to be minor, however.

Unreinforced Concrete or Masonry Unit Wall (With Arching)

In Ref. 1, the arching theory was developed for one-way behavior of walls constrained between rigid supports at top and bottom. This theory may be extended to include two-way arching of walls that are restrained between rigid supports on all four edges. Since the tensile strength of the masonry material is neglected, two-way arching, as was also the case for one-way arching, is independent of the type of support conditions, rather depending only on the rigidity of the supports against in-plane motion. For two-way arching, only the case of rigid supports is

considered, whereas for one-way arching the effect of elastic supports was also examined.

Resistance Function

In the development of one-way arching, the wall was assumed to crack at midspan, with the resulting two halves rotating as rigid bodies about their supports. However, two-way wall tests (Refs. 18 and 19) have shown that masonry walls restrained on four sides crack in a four-segment pattern similar to that shown in Figure 12. During subsequent motion each of two triangular and two trapezoidal segments thus formed is assumed to rotate as a rigid body about its support. These segments become wedged into the opening, and compressive or arching forces are developed in the vertical and horizontal directions as the wall deflects laterally. Because of the compressive forces, couples are developed that resist the rigid body rotation.

This behavior is similar to that previously assumed for the decaying phase of two-way unreinforced walls without arching. One primary difference, however, is that for the arching case the resistance is developed as a result of the in-plane compressive forces, whereas for the nonarching case it is due to the vertical load.

Because of the similarity between these two cases, the approach used to determine the decaying resistance for the two-way unreinforced wall without arching was extended to the arching case. This approach was (1) to determine the distribution of the resisting moment on each wall segment and (2) to use this resisting moment in the work equations developed from the concepts of yield-line theory of reinforced concrete slabs.

In yield-line theory, the resisting moment across the yield lines is developed as a result of yielding of the reinforcing steel. In the

case of arching walls, however, this resisting moment is a result of compressive forces being developed in the plane of the wall because of the resistance of the supports to outward motion. In the analysis in this study, it was assumed that the effect of the resisting moment resulting from the compressive forces was analogous to the development of a moment resistance across the yield lines.

The magnitude of the resisting moment acting on the segments can be determined from the corresponding resistance curves for one-way arching. These curves are shown in Figure 14 for the cases of a solid and a hollow unreinforced masonry wall with rigid supports at top and bottom. The corresponding expressions for the resisting moment are summarized from Ref. 1 as follows:

Solid wall:

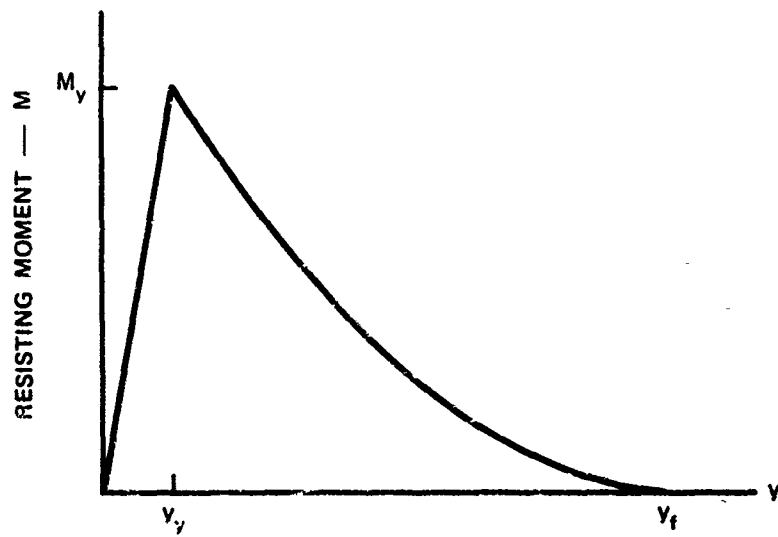
$$M = \left(\frac{M_y}{y_y} \right) y \quad 0 \leq y \leq y_y \quad (40)$$

$$M = \frac{1}{4} f'_m (t_w - y)^2 \quad y_y \leq y \leq y_f \quad (41)$$

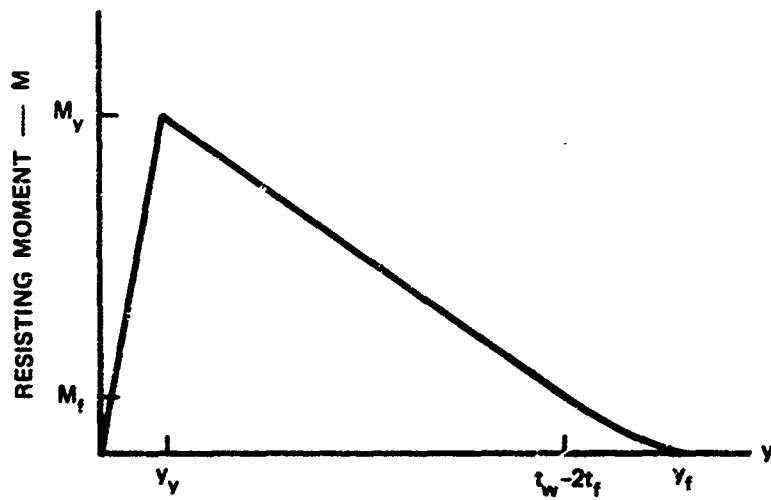
where

$$M_y = \frac{1}{4} f'_m (t_w - y_y)^2 \quad (42)$$

$$y_y = \frac{t_w f'_m}{E_s} \frac{\sqrt{(L_v/2)^2 + (t_w)^2}}{\sqrt{(L_v/2)^2 + (t_w)^2} - L_v/2} \quad (43)$$



(a) Solid Unreinforced Masonry Wall



(b) Hollow Unreinforced Masonry Wall

FIGURE 14 RESISTING MOMENT FOR ONE-WAY ARCHING OF UNREINFORCED MASONRY WALLS WITH RIGID SUPPORTS

Hollow wall:

$$M = \left(\frac{M_y}{y_y} \right) y \quad 0 \leq y \leq y_y \quad (44)$$

$$M = f'_m t_f (t_w - t_f - y) \quad y_y \leq y \leq (t_w - 2t_f) \quad (45)$$

$$M = \frac{1}{4} f'_m (t_w - y)^2 \quad (t_w - 2t_f) \leq y \leq t_f \quad (46)$$

where

$$M_y = f'_m t_f (t_w - y_y - t_f) \quad (47)$$

$$M_f = f'_m t_f^2 \quad (48)$$

Thus, along the horizontal cracked center line d-c, Figure 12, the resisting moment M_1 normal to the horizontal axis of rotation is given by Eqs. 40 to 48 with $y = y_c$.

Along the diagonal c-a, the resisting moment per unit width dx normal to the horizontal axis of rotation is $M dx$, where M is a function of the deflection along the diagonal. The average resisting moment, M_2 , along the diagonal can thus be obtained by integrating from 0 to βL_H and dividing by the total length βL_H , or

$$M_2 = \frac{1}{\beta L_H} \int_0^{\beta L_H} M dx \quad (49)$$

where M is given by Eqs. 40 to 48.

The deflection along the diagonal increases linearly from zero at point a to y_c at point c and is given by

$$y = \frac{y_c}{3L_d} x \quad . \quad (50)$$

Differentiating both sides of this equation yields

$$dy = \frac{y_c}{3L_d} dx \quad . \quad (51)$$

Substituting Eq. 51 into Eq. 49 and making the appropriate changes in the limits of integration, M_2 can be rewritten as

$$M_2 = \frac{1}{y_c} \int_0^{y_c} M dy \quad . \quad (52)$$

The integral in Eq. 52 is equal to the area under the resistance curve between $y = 0$ and $y = y_c$. Substituting the corresponding value of M from Eqs. 40 to 48 into Eq. 52, and performing the integration, the following expressions for M_2 are obtained:*

* In performing the integration, the resisting moment M was assumed to vary in proportion to the deflection along the diagonal. However, for deflections less than y_y , M will be slightly different since the value of y_y and therefore of M_y vary along the diagonal. This results in a nonlinear variation of M for $y < y_y$ rather than the linear variation assumed. Thus the value of M_2 will be slightly less than that given in Eqs. 53 and 57. The difference is believed to be minor, however.

Solid wall:

$$M_2 = \frac{M_y y_c}{2y_y} \quad 0 \leq y_c \leq y_y \quad (53)$$

$$M_2 = \frac{1}{y_c} \left\{ \frac{M_y y_y}{2} + \frac{f'_w}{12} [(t_w - y_y)^3 - (t_w - y_c)^3] \right\} \quad y_y \leq y_c \leq y_f \quad (54)$$

Hollow wall:

$$M_2 = \frac{M_y y_c}{2y_y} \quad 0 \leq y_c \leq y_y \quad (55)$$

$$M_2 = \frac{1}{y_c} \left\{ \frac{M_y y_y}{2} + \frac{f'_t t_f}{2} [(t_w - t_f - y_y)^2 - (t_w - t_f - y_c)^2] \right\} \quad y_y \leq y_c \leq t_w - 2t_f \quad (56)$$

$$M_2 = \frac{1}{y_c} \left\{ \frac{M_y y_y}{2} + \frac{f'_t}{2} \left[t_f (t_w - t_f - y_y)^2 + \frac{t_f^3}{3} - \frac{1}{6} (t_w - y_c)^3 \right] \right\} \quad t_w - 2t_f \leq y_c \leq t_w \quad (57)$$

Because of symmetry, the resisting moment acting on the trapezoidal segments is the same. Thus:

$$M_1 = M_3$$

and

$$M_2 = M_4 \quad (59)$$

Using the same procedure for the triangular segments as for the trapezoidal segments, it can be shown that along the diagonals c-a and c-b, Figure 12, the average resisting moment normal to the vertical axis of rotation is also equal to M_2 .

Substituting Eqs. 58 and 59 into Eq. 32, the total work done on the wall by the resisting moments is found to be

$$W_T = 2y_c \frac{L_H}{L_V} \left\{ 2M_1(1 - 2\beta) + \beta M_2 \left[4 + \left(\frac{L_V}{\beta L_H} \right)^2 \right] \right\} \quad (60)$$

The total energy input resulting from the uniform load q on the wall is again given by Eq. 35:

$$E_T = \frac{q y_c L_V L_H}{6} (3 - 2\beta) .$$

Equating the total work done to the total energy input and solving for the resistance of two-way walls with arching yields

$$q = \frac{12}{L_V^2 (3 - 2\beta)} \left\{ 2M_1(1 - 2\beta) + \beta M_2 \left[4 + \left(\frac{L_V}{\beta L_H} \right)^2 \right] \right\} \quad (61)$$

where the value of M_1 is given by Eqs. 40 to 48, using $y = y_c$, and the value of M_2 is given by Eqs. 53 to 57.

To obtain a solution to the above resistance function again requires the determination of the coefficient β . As discussed for the decaying phase of unreinforced masonry walls without arching, the problem of defining the coefficient β is actually a problem of determining the initial crack pattern that develops at the end of the elastic phase. The value of β thus depends on the distribution of the resisting moment during the elastic phase. If it is assumed that the resisting moment is uniformly

distributed along the diagonal, as is the case for isotropic reinforced concrete slabs, the value of β given by Eq. 38 is obtained as follows:

$$\beta = \frac{1}{2} \left[\sqrt{3 \left(\frac{I_V}{I_H} \right)^2 + \left(\frac{I_V}{I_H} \right)^4} - \left(\frac{I_V}{I_H} \right)^2 \right] \quad (38)$$

Because a sensitivity study using different assumptions for the distribution of the resisting moment showed little difference in the final results, it was assumed that the value of β given by Eq. 38 was applicable for unreinforced masonry walls with arching.

Using the above results, a typical resistance curve was determined for an unreinforced masonry wall rigidly supported against in-plane movement on four edges. This curve is shown in Figure 15. As can be seen, the two-way resistance function indicates substantial resistance remaining at a deflection equal to the thickness of the wall. Since at this point the segments no longer remain in contact along the central portion of the wall, it is believed that the wall would become unstable. This makes questionable the use of the indicated resistance for deflections greater than the wall thickness. Therefore, it was decided to disregard this portion of the resistance function and decrease the resistance abruptly to zero when the deflection reaches the wall thickness. This is indicated by the dashed line shown in Figure 15.

Reinforced Concrete Wall

In general, for reinforced concrete walls, the moment capacity is not constant throughout the wall. However, to simplify the determination of the resistance function, the study was restricted to walls in which the moment capacity is uniform along the vertical and horizontal directions, although not necessarily the same in both directions. This applies to both positive and negative moment capacity. It was further assumed

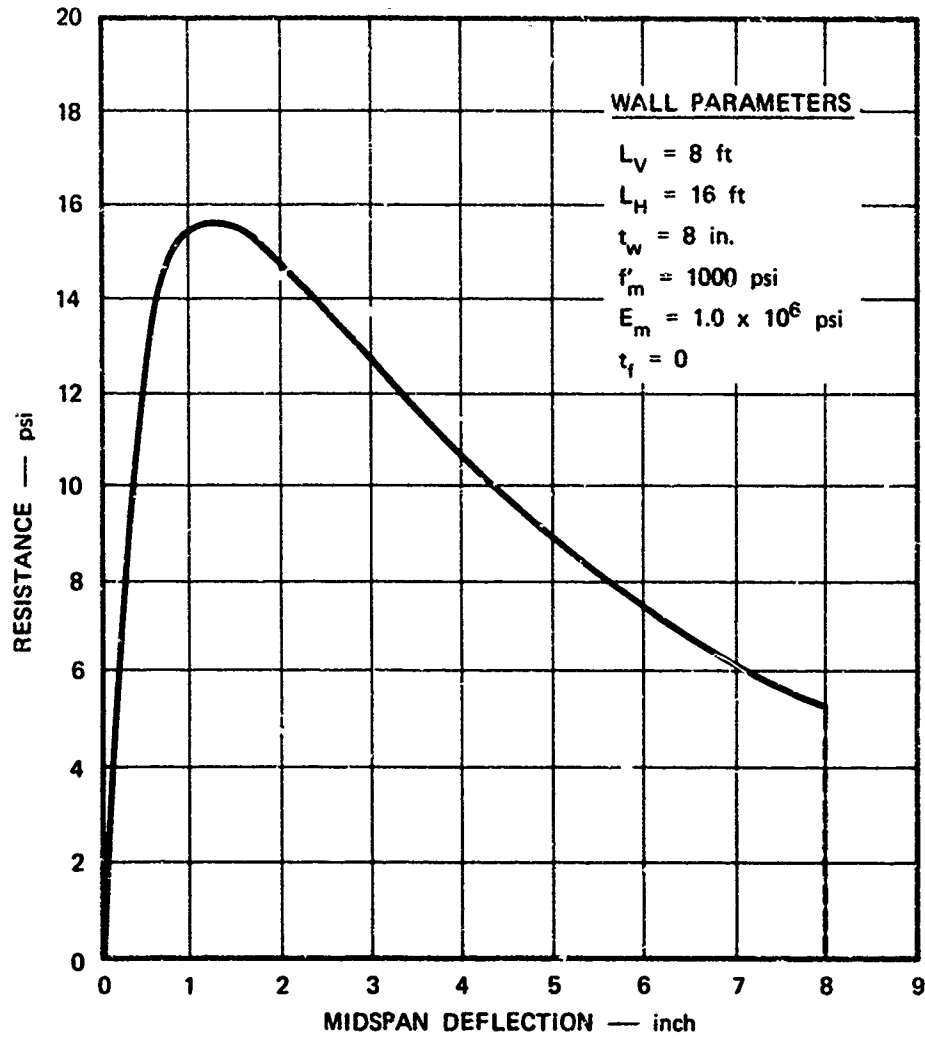


FIGURE 15 TYPICAL RESISTANCE FUNCTION FOR UNREINFORCED MASONRY WALL WITH TWO-WAY ARCHING

that the negative moment capacity along opposite edges of the wall is the same, which will generally be the case for the doubly symmetrical support conditions considered. Using these assumptions, the resistance of the wall can be fully defined by specifying the moment capacities at the following locations:

Section 1--Positive moment capacity per unit width at center of vertical span

Section 2--Positive moment capacity per unit width at center of horizontal span

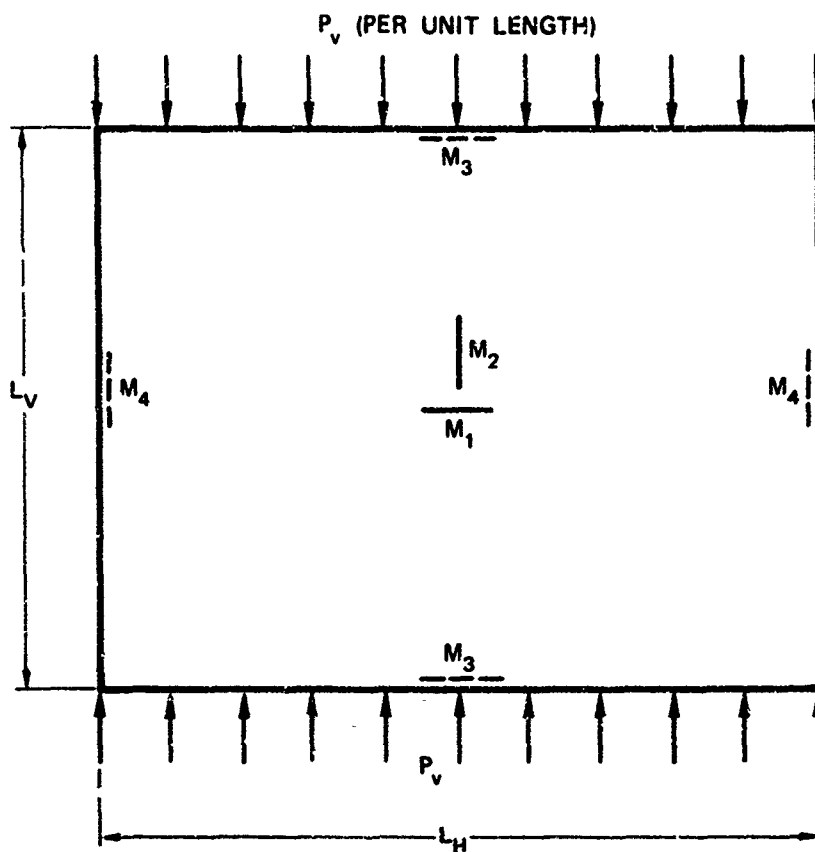
Section 3--Negative moment capacity per unit width along horizontal edges

Section 4--Negative moment capacity per unit width along vertical edges.

The method used in this study to identify the moment capacity at these locations includes moment key lines, as shown in Figure 16. These moment key lines indicate the moment per unit width perpendicular to the direction indicated by the line. The subscript number shown in Figure 16 corresponds to the appropriate section indicated above. The moment capacity corresponding to the uncracked or cracked section is indicated by an additional subscript m or u, respectively. Thus, the notation M_{12} indicates the positive moment capacity for the uncracked section at the center of the horizontal span. The moment capacities of the uncracked and cracked sections are determined using the equations previously developed for one-way walls in Appendix A of Ref. 1.

Resistance Function

Development of the two-way resistance function for reinforced concrete walls was restricted to the four support cases considered previously for the unreinforced walls. Note that each of these support cases is



Note: Moment key lines indicate the moment capacity per unit length perpendicular to these lines (solid—positive moment; dashed—negative moment)

FIGURE 16 WALL AND MOMENT KEYLINE NOTATION

symmetrical about the center line in both directions and that for a simply supported edge the moment capacity is zero.

As in the analysis of one-way reinforced concrete walls (Ref. 1), the resistance function is divided into the following four phases, as illustrated in Figures 17 and 18:

1. Elastic, uncracked phase
2. Elastic, cracked phase
3. Elasto-plastic phase*
4. Plastic phase.

For two-way walls, these phases are defined as follows.

The elastic, uncracked phase exists until formation of the first crack. This phase is included since, as discussed in Ref. 1, for lightly reinforced concrete walls, the uncracked section may provide a greater moment resistance than the cracked section, as noted by the dashed lines in Figures 17 and 18. The elastic, cracked phase exists from the first crack until development of the plastic moment at the location corresponding to the first crack. The elasto-plastic phase exists from the initial development of the plastic moment along the fixed edges until full development of the plastic moment along all yield lines, at which point the plastic phase is initiated.* The plastic phase exists until the wall collapses.

The procedures used to obtain the resistance function required the establishment of the maximum resistance and deflection for each of these phases. It was then assumed that a linear relationship existed between the maxima. During the elastic and elasto-plastic phases, the wall was assumed to behave as an elastic, homogeneous plate, the behavior of which

* No elasto-plastic phase exists for Support Case 1.

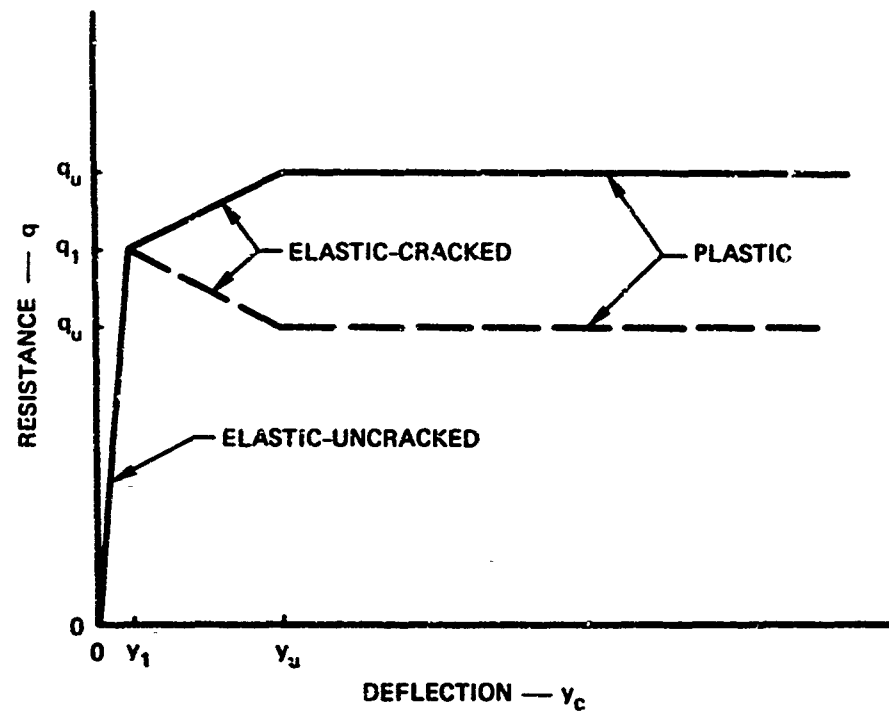


FIGURE 17 RESISTANCE FUNCTION FOR A TWO-WAY ACTION REINFORCED CONCRETE WALL SUPPORT CASE 1

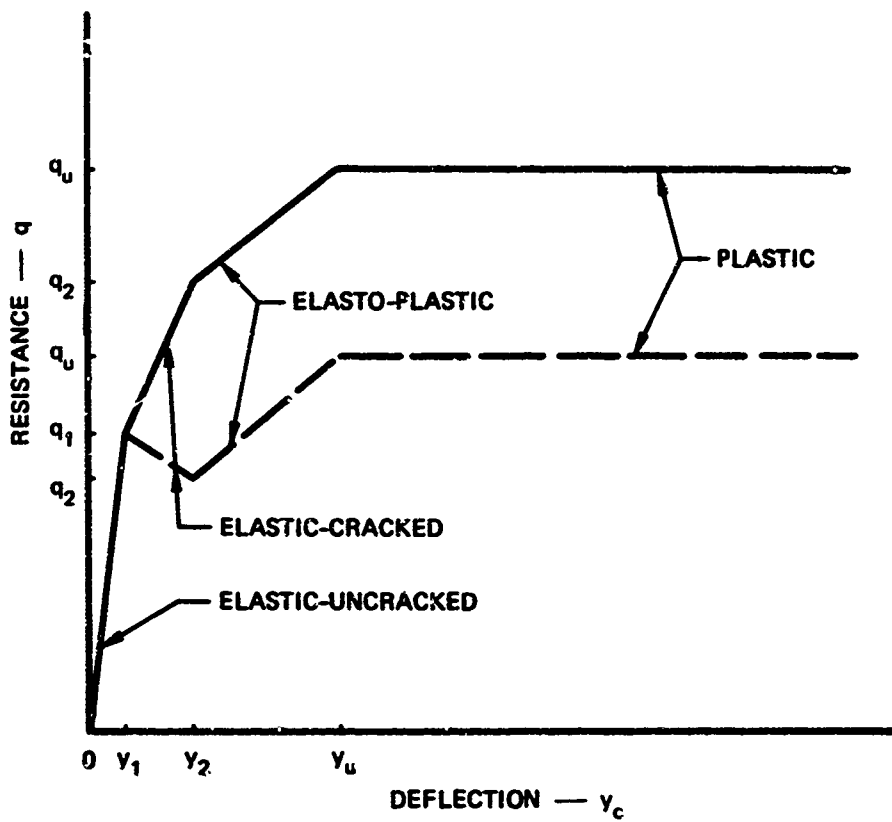


FIGURE 18 RESISTANCE FUNCTION FOR A TWO-WAY ACTION REINFORCED CONCRETE WALL SUPPORT CASES 2, 3, AND 4

has been discussed previously in the development of the resistance function for unreinforced masonry walls without arching. In determining the maximum deflection for the elastic, uncracked phase, the uncracked moment of inertia was used, while for the elastic, cracked phase, the cracked moment of inertia was used. In determining the cracked moment of inertia, it was assumed that the wall was uniformly cracked throughout. Although it is well known that tensile cracking in reinforced concrete members under flexural loads is not uniformly distributed, the error in the magnitude of the deflection resulting from this assumption is not too important for the prediction of wall collapse. The resistance during the plastic phase was determined through use of the yield-line theory.

The resistance functions for walls with and without a vertical load are presented separately.

Wall Without Vertical Axial Load. The four phases of the resistance function for reinforced concrete walls without vertical in-plane forces is as follows.

Elastic, Uncracked Phase

The maximum resistance in the initial, or uncracked, elastic phase is reached when the maximum moment in the wall reaches the ultimate uncracked moment capacity. For a uniformly distributed load, this maximum moment is given by Eqs. 2 and 8:

$$M_j = B_i q L_v^2, \quad i = 1, 2, 3, 4 \quad (62)$$

where the subscript i corresponds to the support case and the subscript j corresponds to the location at which the moment occurs. For the case where $L_u \geq L_v$, this location is as follows:

Support Case 1--Section 1

Support Case 2--Section 3

Support Case 3--Section 4

Support Case 4--Section 3

Values of the numerical factor B are plotted against the ratio L_H/L_V in Figure 8.

The ultimate moment capacity for the uncracked section is given by

$$M_u = \frac{f_r I_g}{t_w/2} \quad (63)$$

The value of I_g is essentially constant throughout the wall, varying only slightly because of differences in the amount and location of the steel reinforcement. Thus the value of M_u may be assumed to be the same throughout the wall.

Substituting M_u for M_i in Eq. 62, the maximum resistance during the elastic, uncracked phase is given by

$$q_i = \frac{M_u}{B_i L_v^2}, \quad i = 1, 2, 3, 4 \quad (64)$$

The maximum deflection for the elastic, uncracked phase is given by Eqs. 6 and 11:

$$y_i = \frac{(1 - \nu^2) A_i q_i L_v^4}{EI_c}, \quad i = 1, 2, 3, 4 \quad (65)$$

where values of the numerical factor A are plotted against the ratio L_H/L_V in Figure 9.

Elastic, Cracked Phase

For Support Case 1, the maximum resistance in the elastic, cracked phase is equal to the ultimate resistance of the wall. Thus, for Support Case 1

$$q_2 = q_u \quad (66)$$

where the value of q_u is determined in a later subsection.

The maximum resistance in the elastic, cracked phase for Support cases 2, 3, and 4 is reached when the ultimate cracked moment capacity is reached at the location corresponding to the first crack. Using Method 3 of the design of two-way slabs given in the ACI Building Code (Ref. 20) the maximum moment is given by

$$M_j = C_i q L_v^2, \quad i = 2,3,4 \quad (67)$$

where C is a numerical factor depending on the support conditions and the ratio L_x/L_y . Values of C are given in Figure 19.

The ultimate moment capacity for the cracked section, M_u , can be determined from the formulas presented in Appendix A of Ref. 1. Substituting the ultimate moment capacity at section j for M_j in Eq. 67, the maximum resistance for the elastic, cracked phase for Support Cases 2, 3, and 4 is

$$q_2 = \frac{M_{uj}}{C_i L_v^2}, \quad i = 2,3,4 \quad (68)$$

The maximum deflection for the elastic cracked phase is found from Eq. 65 by substituting q_2 for q_1 and using the moment of inertia for the cracked section, thus obtaining

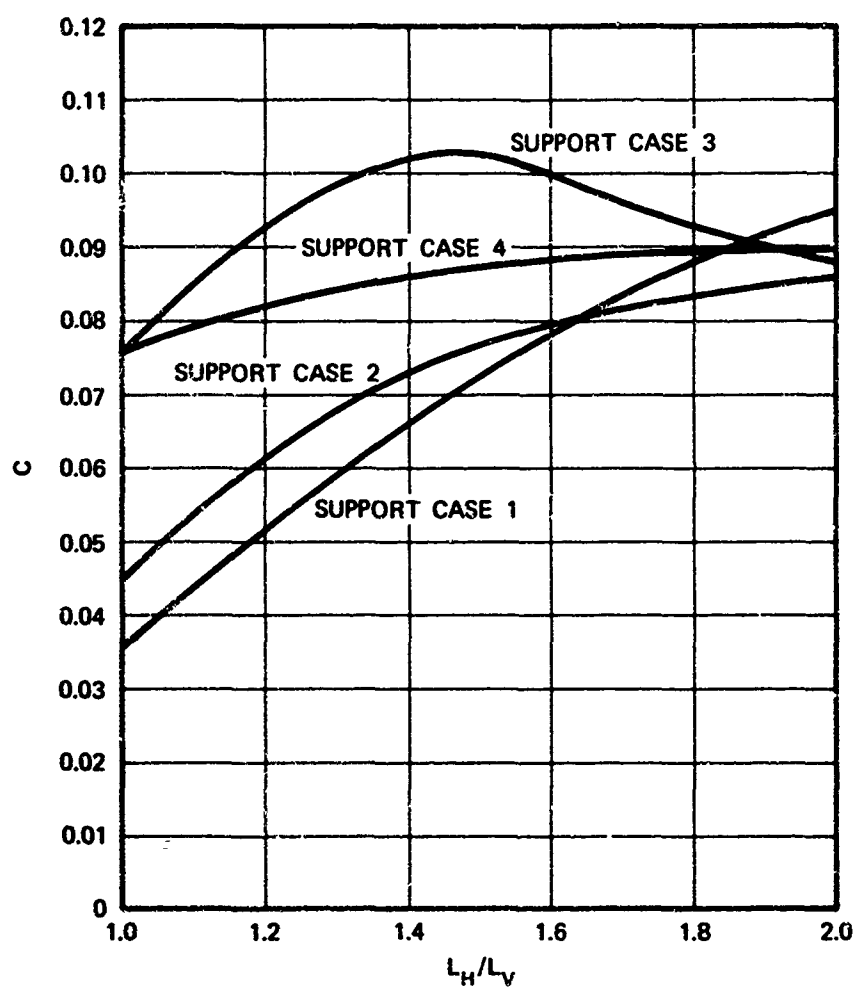


FIGURE 19 ACI MOMENT COEFFICIENTS FOR TWO-WAY ACTION WALLS

$$y_2 = \frac{(1 - \nu^2) A_1 L_w^4}{EI_c} q_2, \quad i = 1, 2, 3, 4 \quad (69)$$

The value of I_c was taken to be the average value throughout the wall.

Elasto-Plastic Phase

The elasto-plastic phase occurs for walls having one or more fixed edges, i.e., Support Cases 2, 3, and 4 in this study. After the ultimate cracked moment capacity is reached along the fixed edges, the wall continues to deflect, thus developing an additional resistance as a result of the simply supported wall action. The maximum elasto-plastic resistance is developed when the wall reaches its ultimate resistance, as determined in the following subsection. The additional resistance developed during the elasto-plastic phase is thus given by

$$\Delta q = q_u - q_2 \quad (70)$$

Since during the elasto-plastic phase the wall deflects as if it were simply supported on four sides,* the additional deflection can be determined from Eq. 69 by substituting $i = 1$ (corresponding to Support Case 1). The following equation is thus obtained for the deflection during this phase:

$$\Delta y = \frac{(1 - \nu^2) A_1 L_w^4}{EI_c} \Delta q \quad (71)$$

* Although yielding may not yet have occurred along all four edges for Support Case 2 (fixed on four edges) the additional deflection was determined as if all edges had yielded.

The deflection at ultimate resistance is thus given by the sum of the deflection during the elastic and elasto-plastic phases, or

$$y_u = y_2 + \Delta y \quad . \quad (72)$$

Substituting for y_2 and Δy from Eqs. 69 and 71, respectively, the deflection at ultimate resistance for Support Cases 2, 3, and 4 is

$$y_u = \frac{(1 - \nu^2) I_y^4}{EI_c} (A_1 q_2 + A_1 \Delta q) \quad , \quad i = 2, 3, 4 \quad . \quad (73)$$

For Support Case 1 no elasto-plastic phase exists, thus for this case the deflection at ultimate resistance is given by Eq. 69.

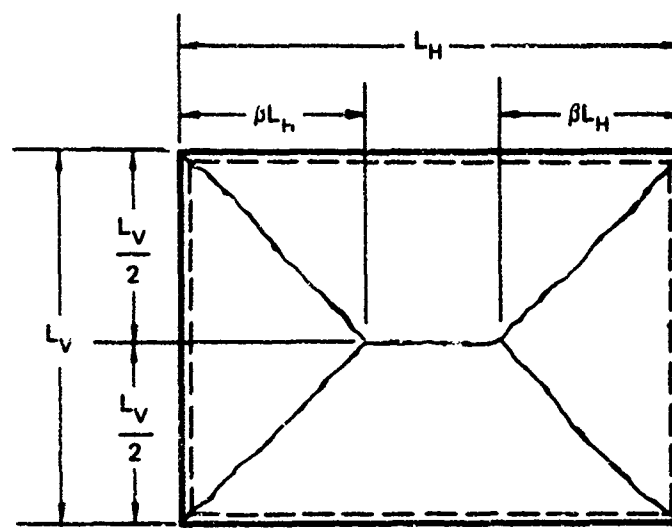
Plastic Phase

The plastic phase is initiated with the full development of the plastic, or ultimate cracked, moment along all assumed yield lines. Yield lines are assumed to form in one of the two collapse modes shown in Figure 20. In most cases of interest, collapse mode "a" will occur. Thus for the sake of clarity, it will be the only one discussed in this section. Collapse mode "b" is discussed in Appendix B.

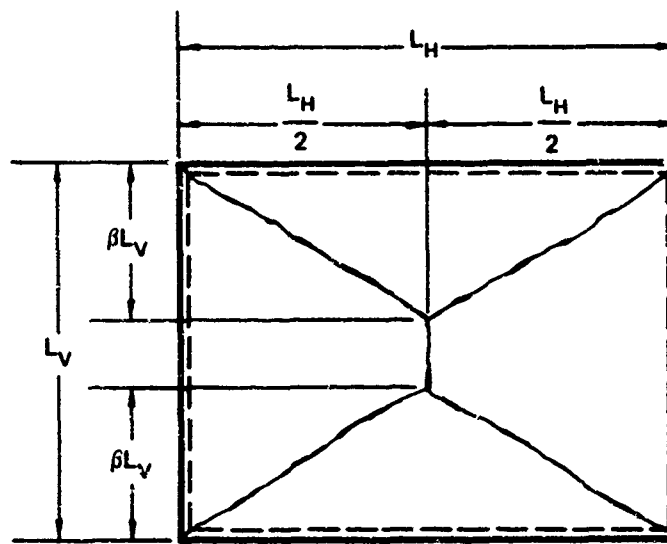
The ultimate resistance for a rectangular, orthogonally isotropic reinforced concrete wall subjected to a uniformly distributed lateral load can be determined from the following equation, given in Ref. 17:*

$$M_{u1} = \frac{qL_y^3}{6\gamma_1} \left\{ \sqrt{3 + \left(\frac{M_{u2}}{M_{u1}} \right) \left(\frac{L_y \gamma_2}{L_x \gamma_1} \right)^2} - \sqrt{\frac{M_{u2}}{M_{u1}} \left(\frac{L_y \gamma_2}{L_x \gamma_1} \right)^2} \right\} \quad (74)$$

* Notation changed to conform to that used in this study.



(a) Collapse Mode "a"



(b) Collapse Mode "b"

NOTATION:
 ——— Positive Yield Line
 - - - Negative Yield Line

FIGURE 20 ASSUMED COLLAPSE MODES (YIELD LINES) FOR REINFORCED CONCRETE WALL

where

$$\gamma_1 = 2\sqrt{1 + M_{u3}/M_{u1}} \quad (74a)$$

and

$$\gamma_2 = 2\sqrt{1 + M_{u4}/M_{u2}} \quad (74b)$$

This equation is valid for simply supported or fixed edges. A simply supported edge may be indicated by setting the value of the corresponding moment capacity to zero.

Solving Eq. 74 for the ultimate resistance, the following equation is obtained:

$$q_u = \frac{6\gamma_1^2 M_{u1}}{L_v^2 \left\{ \sqrt{3 + \left(\frac{M_{u2}}{M_{u1}} \right) \left(\frac{L_v \gamma_2}{L_H \gamma_1} \right)^2} - \sqrt{\frac{M_{u2}}{M_{u1}} \left(\frac{L_v \gamma_2}{L_H \gamma_1} \right)^2} \right\}^2} \quad (75)$$

The value of the numerical factor β , which defines the location of the yield lines, is given by

$$\beta = \frac{1}{2} \frac{M_{u2} \gamma_2 (L_v)}{M_{u1} \gamma_1 (L_H)} \left\{ \sqrt{\left(\frac{\gamma_2}{\gamma_1} \right)^2 + 3 \frac{M_{u1} (L_v)}{M_{u2} (L_H)}} - \frac{\gamma_2}{\gamma_1} \right\} \quad (76)$$

For the assumption of collapse mode "a" to be valid, β must be less than or equal to 0.5. If this is not the case, the preceding equations are invalid and the corresponding equations for q_u and β derived in Appendix B should be used in place of Eqs. 75 and 76.

Wall With Vertical Axial Load. The four phases of the resistance function for reinforced concrete walls with vertical load are presented below. The vertical load was assumed to act as an axial load in the

plane of the wall, and the effect of an initial eccentricity of the load was not considered in determining either the wall deflection or resistance.

Elastic, Uncracked Phase

The maximum resistance in the elastic, uncracked phase for a wall with vertical axial load can be obtained from Eq. 64, substituting B_{v1} for B_1 ,

$$q_1 = \frac{M_u}{B_{v1} L_v} \quad , \quad i = 1,2,3,4 \quad . \quad (77)$$

The numerical factor B_v is given by Eq. 13 for Support Case 1 and by Eq. 17 for Support Cases 2, 3, and 4. Values of B_{v1} are also plotted in Figure 10. The ultimate uncracked moment capacity is given by

$$M_u = \frac{I_g}{t_w/2} \left(f_r + \frac{P_v}{t_w} \right) \quad . \quad (78)$$

The corresponding maximum deflection for the elastic, uncracked phase is obtained from Eq. 65 by substituting A_{v1} for A_1

$$y_1 = \frac{(1 - \nu^2) A_{v1} q_1 L_v^4}{EI_g} \quad , \quad i = 1,2,3,4 \quad . \quad (79)$$

The numerical factor A_v is given by Eq. 15 for Support Case 1 and by Eq. 19 for Support Cases 2, 3, and 4. Values of A_{v1} are also plotted in Figure 11.

Elastic, Cracked Phase

For Support Case 1, the maximum resistance for the elastic, cracked phase of the wall with vertical load is again given by Eq. 66. However, in determining the ultimate resistance, q_u , the vertical axial load must be taken into consideration. This effect is discussed in a later subsection.

For Support Cases 2, 3, and 4, as was the case for the elastic, uncracked phase, no information was found concerning walls with fixed edges subjected to combined uniform lateral load and uniform compressive axial forces. Therefore, the approximate procedure used to determine B_v for Support Cases 2, 3, and 4 was extended to determine the numerical factor C_v . That is, it was assumed that the ratio of the moment coefficients for the wall with and without vertical axial load was the same for both the elastic, uncracked and elastic, cracked phases. Therefore:

$$\frac{C_{vi}}{C_i} = \frac{B_{vi}}{B_i}$$

or

$$C_{vi} = \left(\frac{B_{vi}}{B_i} \right) C_i \quad . \quad (80)$$

Since the ratio B_{vi}/B_i was assumed to be the same for each of the four support cases, as expressed by Eq. 16, this equation can be rewritten as

$$C_{vi} = \left(\frac{B_{vi}}{B_i} \right) C_i \quad , \quad i = 2,3,4 \quad (81)$$

where values of the numerical coefficients B_i and B_{vi} are given in Figure 19.

The maximum resistance in the elastic, cracked phase for Support Cases 2, 3, and 4 can now be determined by substituting $C_{v,i}$ for C_i in Eq. 68, thus obtaining

$$q_2 = \frac{M_{u,i}}{C_{v,i} L_i^2} \quad , \quad i = 2,3,4 \quad . \quad (82)$$

The maximum deflection during the elastic, cracked phase is given by Eq. 69, substituting $A_{v,i}$ for A_i :

$$y_2 = \frac{(1 - \nu^2) A_{v,i} L_i^4}{EI_c} q_2 \quad , \quad i = 2,3,4 \quad . \quad (83)$$

Elasto-Plastic Phase

The maximum elasto-plastic resistance for a wall with vertical axial load is developed when the wall reaches its ultimate resistance. Thus, the additional resistance developed during the elasto-plastic phase for Support Cases 2, 3, and 4 is equal to the ultimate resistance minus the maximum resistance during the elastic, cracked phase, or

$$\Delta q = q_u - q_2 \quad .$$

The value of q_u is discussed in the following subsection.

As for the wall without vertical load, the maximum deflection at the development of the ultimate resistance is the sum of the deflection during the elastic and elasto-plastic phases. Since, during the elasto-plastic phase, the wall is again assumed to deflect as a wall simply supported on four sides, the additional deflection is equal to that given by Eq. 83 with subscript $i = 1$

$$\Delta y = \frac{(1 - \nu^2) A_{v1} L_v^4}{EI_e} \Delta q \quad . \quad (84)$$

Substituting Eqs. 83 and 84 into Eq. 72, the deflection at development of the ultimate resistance for Support Cases 2, 3, and 4 is given by

$$y_u = \frac{(1 - \nu^2) L_v^4}{EI_e} (A_{v1} q_2 + A_{v1} \Delta q) \quad , \quad i = 2, 3, 4 \quad . \quad (85)$$

Since no elasto-plastic phase occurs for Support Case 1, the deflection at ultimate resistance can be obtained from Eq. 83 by substituting q_u and y_u for q_2 and y_2 , respectively.

Plastic Phase

The resistance during the plastic phase for walls with vertical load was determined using yield-line theory. It was assumed that the vertical load had no effect on the location at which the yield lines formed; therefore, the two collapse modes previously assumed for the wall without vertical load are the same for the wall with vertical load. These two collapse modes are shown on Figure 20. Again, since collapse mode "a" is the one that usually occurs, it will be the only one discussed in this section. For the cases where collapse mode "b" does occur, the equations derived in Appendix B for q_u and β may be substituted in the following equations.

Although the vertical load is assumed not to affect the location of the yield lines, its influence must be considered in determining the value of the corresponding resistance. The effect of the vertical load can be interpreted as resulting in two compensating effects: (1) the resistance is increased because the ultimate moment capacity along the yield lines is increased and (2) the resistance is decreased because

the moment acting along the yield line is increased as a result of the wall deflecting. The first of these effects, the increase in the ultimate moment capacity, is taken into consideration in the formulas presented in Appendix A of Ref. 1. The second effect, the increase in the moment acting along the yield line, is given by

$$M_v = P_v y_{avg} \quad (86)$$

where M_v is the average moment as a result of P_v acting along the yield line and y_{avg} is the average deflection along the yield line.

At the initial development of the yield lines, the deflection of the wall is still predominantly elastic. Thus, the deflection along the yield lines is assumed to vary parabolically from the supports to the center of the wall.* The average deflection along the yield line at the beginning of the plastic phase can thus be related to the center deflection by the following equation:

$$y_{avg} = 0.66 y_c \quad (87)$$

Substituting Eq. 87 into Eq. 86, the following equation for M_v at the beginning of the plastic phase is obtained:

$$M_v = 0.66 P_v y_c \quad (88)$$

* A limited study based on the deflected shape given in Ref. 14 for a plate simply supported on four edges and subjected to a combined uniform lateral load and uniform compressive axial forces along the horizontal edges indicated values for the ratio y_{avg}/y_c to be somewhat less than that obtained using the assumption of a parabolic distribution. The difference is believed to be minor, however, in view of the other assumptions concerned.

The effect of this moment on the ultimate resistance can be determined by noting that M_v acts directly opposite to the resisting moment, thereby reducing the ultimate resistance. This effect is taken into consideration by subtracting M_v from M_{u1} in Eq. 74 and solving for q_u , which yields

$$q_u = \frac{6\gamma_1^2 (M_{u1} - M_v)}{L_v^2 \left\{ \sqrt{3 + \left(\frac{M_{u2}}{M_{u1}}\right) \left(\frac{L_v \gamma_2}{L_H \gamma_1}\right)^2} - \sqrt{\frac{M_{u2}}{M_{u1}} \left(\frac{L_v \gamma_2}{L_H \gamma_1}\right)} \right\}^2} \quad (89)$$

Introducing the coefficient C_u , this equation can be rewritten as

$$q_u = C_u (M_{u1} - M_v) \quad (90)$$

where

$$C_u = \frac{6\gamma_1^2}{L_v^2 \left\{ \sqrt{3 + \left(\frac{M_{u2}}{M_{u1}}\right) \left(\frac{L_v \gamma_2}{L_H \gamma_1}\right)^2} - \sqrt{\frac{M_{u2}}{M_{u1}} \left(\frac{L_v \gamma_2}{L_H \gamma_1}\right)} \right\}^2} \quad (91)$$

Substituting the value of M_v from Eq. 88 into Eq. 90 and noting that at the beginning of the plastic phase $y_c = y_u$, the following equation is obtained:

$$q_u = C_u (M_{u1} - 0.66 P_v y_u) \quad (92)$$

This equation cannot be solved explicitly for q_u since y_u is dependent on q_u . For Support Case 1, the relationship between y_u and q_u is given by Eq. 83, with $y_2 = y_u$ and $y_2 = q_u$. Substituting Eq. 83 into Eq. 92 and solving for q_u , the following equation is obtained for the ultimate plastic resistance for Support Case 1:

$$q_u = \frac{C_u M_{u1}}{1 + \frac{0.66 P_v C_u A_{v1} L^4}{EI_c}} \quad (93)$$

For Support Cases 2, 3, and 4, the relationship between y_u and q_u is given by Eqs. 70, 83, and 85. Substituting these equations into Eq. 92 and solving for q_u , the following equation is obtained for the ultimate plastic resistance for Support Cases 2, 3, and 4:

$$q_u = \frac{C_u [M_{u1} - 0.66 P_v (1 - \nu^2) L_v^4 q_u (A_{v1} - A_{vi}) / EI_c]}{1 + 0.66 C_u P_v (1 - \nu^2) L_v^4 A_{v1} / EI_c}, \quad (94)$$

$$i = 2, 3, 4$$

As the deflection increases, the value of M_v increases, thus causing the resistance to lateral load to decrease. At some value of the deflection, M_v will equal M_{u1} and there will be no further resistance to lateral load. This deflection is the collapse or failure deflection resulting from the vertical load. Its value is obtained by substituting M_v for M_{u1} in Eq. 86 and solving for the center deflection. The value of the average deflection along the yield lines will be different from that given by Eq. 87, however, since the deflected shape of the wall is no longer elastic, as assumed for the beginning of the plastic phase. Instead the deflected shape of the wall is assumed to be a rigid body rotation of the segments about their supports. The average value of the deflection along the yield lines thus depends on the location of the yield lines and is given by

$$y_{avg} = (1 - \theta) y_c \quad (95)$$

Substituting this value into Eq. 86, the value of the collapse deflection resulting from the vertical load is given by

$$y_{fv} = \frac{M_{u1}}{P_v(1 - \beta)} \quad (96)$$

The resistance during the plastic phase is assumed to vary linearly between the initial and final points.

Failure Criteria

As was found to be the case for one-way reinforced concrete walls, there is little information available on which to base a failure, or collapse, criterion, particularly for the small amounts of reinforcement usually found in walls.

Because of this lack of information it was decided to adapt the collapse criteria that were arbitrarily established for one-way reinforced concrete walls to two-way walls. These criteria are summarized as follows:

1. Limiting steel strain criterion: During the plastic phase, the sections bounded by the yield lines rotate essentially as rigid bodies. The deflection at collapse is determined by assuming that the elongation of the yielding steel occurs over a length, l , sufficient to develop the ultimate tensile strength of the reinforcing steel in bond to the concrete

$$l = \frac{A_s f_u}{U_u} \quad (97)$$

The deflection at collapse is thus given by

$$y_f = (l \epsilon_{su})^2 + L_v l \epsilon_{su} \quad (98)$$

2. Instability criterion: This criterion applies only to walls with vertical load and is the deflection at which the moment

caused by the vertical load is equal to the ultimate moment capacity. This deflection is given by Eq. 96

$$y_f = \frac{M_{u1}}{P_v(1 - \beta)}$$

3. Ductility criterion: Collapse of the wall is predicted when the ductility ratio (ratio of the maximum deflection to the deflection at the beginning of the plastic phase) is equal to

$$\mu = \frac{0.10}{p_1} \quad (99)$$

up to a maximum value of $\mu = 30$. Thus

$$y_f = \frac{0.10}{p_1} y_u \quad (100)$$

Collapse of the wall is assumed to occur when the center deflection of the wall reaches the minimum of the three values of y_f given above.

Window Openings

Since the wall resistance and loading are modified by the presence of an opening, it is apparent that window openings can affect the incipient collapse overpressure of reinforced and unreinforced walls. The determination of both a realistic net load and a resistance function for a wall with openings are exceedingly complex problems for which no solution is currently available. However, to predict the incipient collapse pressure of walls with openings for this study, it was necessary to develop an interim procedure for modifying the method of calculating the resistance function. This was accomplished by making certain simplifications of the actual wall.

It is obvious that both the elastic and decaying phase resistances of two-way unreinforced walls and all phases of reinforced concrete will be influenced by the presence of window openings. Since no solutions

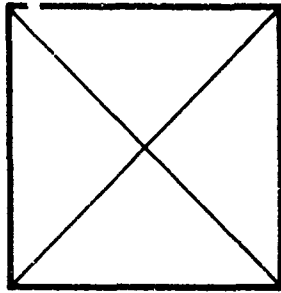
were readily available for determining the elastic phase resistance, it was assumed in the current study that the elastic phase resistance could be determined by the methods presented herein. The magnitude of the error in the predicted incipient collapse pressure resulting from this assumption was not investigated during the current effort. In a subsequent study, the influence of window openings on the elastic phase resistance of two-way action wall elements will be examined with an available finite element computer program.

For other than the elastic phase, the modification of the resistance for the various types of walls with openings was based on the assumption that the crack patterns in the walls were similar to the yield-line patterns in reinforced concrete slabs. It was also assumed that the ratio of the resistance of a wall with windows to that of a wall without windows was the same for unreinforced as for reinforced concrete walls.

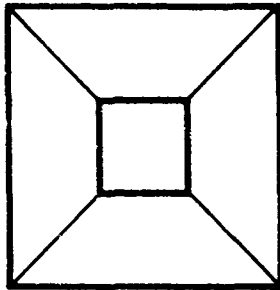
The yield-line analysis of reinforced concrete slabs provides a convenient method of determining the minimum resistance function for a wall with various openings. For a square wall panel without windows, and with isotropic reinforcement, the primary yield-line pattern would consist of diagonal yield lines between the corners, as noted on Figure 21(a). If the wall has a centrally located window, the yield lines will form along the wall diagonals between the window and the wall corner as noted on Figure 21(b). However, for some window geometries* of a square wall, the yield lines can form between the wall corners and one edge of the window opening as indicated on Figure 21(c).

For a rectangular wall panel, without windows and with isotropic reinforcement, the yield lines will form as noted on Figure 22(a). A

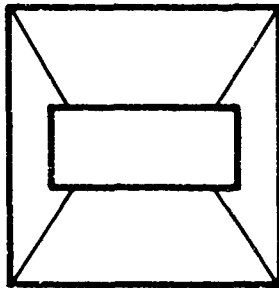
* For example, a 21 percent window opening with the window height equal to 0.3 times the wall height and the window width equal to 0.7 times the wall width.



(a) Wall Without Window

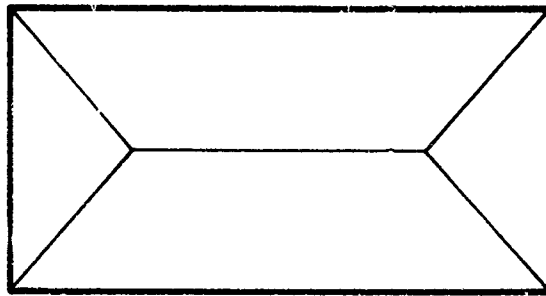


(b) Wall With Square Window

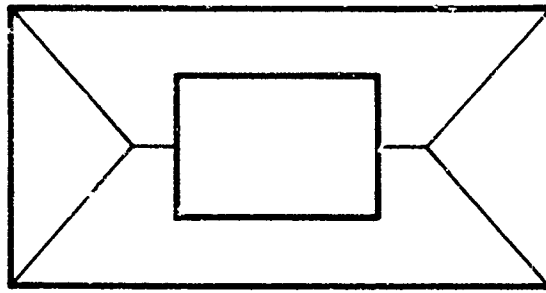


(c) Wall With Long Rectangular Window

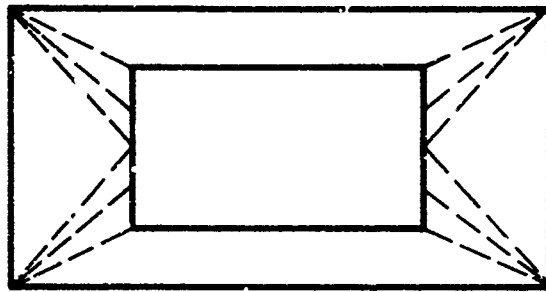
FIGURE 21 YIELD-LINE PATTERNS FOR SQUARE WALL PANEL WITH ISOTROPIC REINFORCEMENT



(a) Wall Without Window



(b) Typical Yield Line For Wall With Window



(c) Yield Line For Wall With Wide Window

FIGURE 22 YIELD-LINE PATTERNS FOR RECTANGULAR WALL PANEL WITH ISOTROPIC REINFORCEMENT

centrally located window in such a wall will result in one of two general types of yield-line patterns. First, the typical yield line may form between the wall corners and a horizontal line through the window, as noted on Figure 22(b). Second, the yield lines may form between the wall corner and some point on the vertical edge of the window, as illustrated on Figure 22(c).

Since a generalized expression is not available from yield-line analysis, it is necessary to use a trial-and-error procedure to obtain the minimum resistance value for each window size and shape. Also, for square, or nearly square walls, it is necessary to examine crack patterns that intersect either the horizontal or vertical window edges.

Using the yield-line analysis and assuming that the yield lines intersect the vertical edge of the window, an expression can be formulated for the resistance of a simply supported wall panel with isotropic reinforcement. The total energy input of a uniform static load for the various wall segments shown on Figure 23 is

$$\begin{aligned}
 E_T = 2q_w & \left[(L_{VW} - \alpha) \left(\frac{L_H - L_{HK}}{2} \right) \times \frac{1}{2} + 2 \left(\frac{L_V - L_{VW} + \alpha}{2} \right) \left(\frac{L_H - L_{HK}}{2} \right) \right. \\
 & \times \frac{1}{2} \times \frac{1}{3} + (L_{HK}) \left(\frac{L_V - L_{VW}}{2} \right) \times \frac{1}{2} \left(\frac{L_V - L_{VW}}{L_V - L_{VW} + \alpha} \right) \\
 & \left. + 2 \left(\frac{L_H - L_{HK}}{2} \right) \left(\frac{L_V - L_{VW} + \alpha}{2} \right) \times \frac{1}{2} \times \frac{1}{3} \right]
 \end{aligned}$$

or

$$E_T = \frac{q_w}{6} \left[(L_H - L_{HK})(L_{VW} + 2L_V - \alpha) + 3L_{HK} \frac{(L_V - L_{VW})^2}{(L_V - L_{VW} + \alpha)} \right] \quad (101)$$

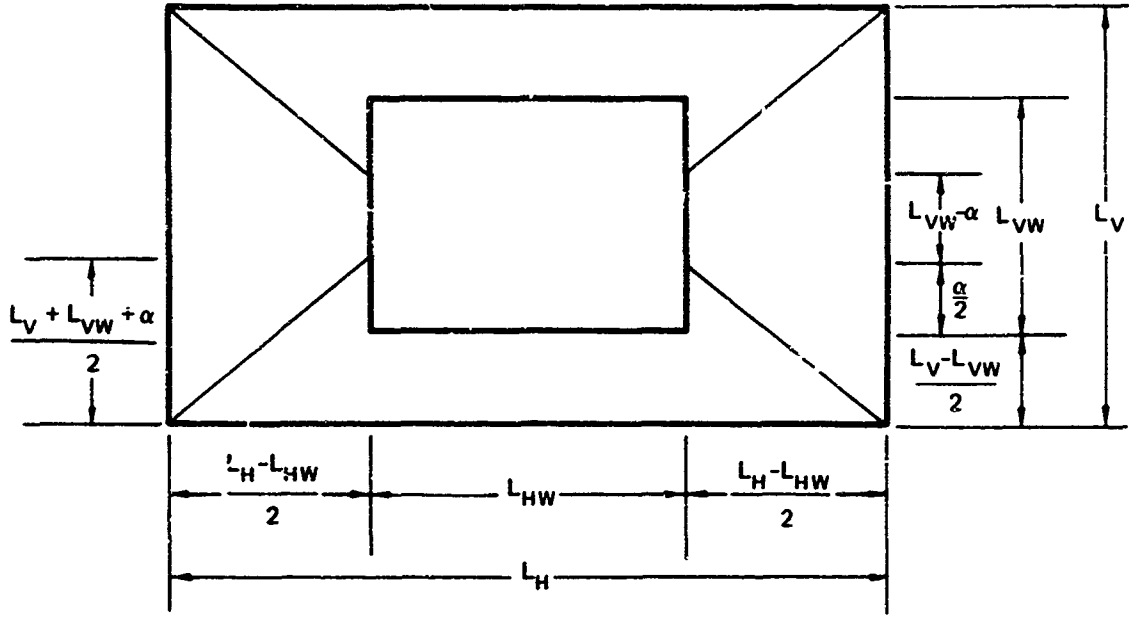


FIGURE 23 WALL WITH YIELD-LINE PATTERN INTERSECTING VERTICAL EDGE OF WINDOW

The total work done by the moment acting on each segment is

$$W_T = \left[2 \frac{(L_V - L_{VM} + \alpha)}{2} \times \frac{2}{(L_H - L_{HM})} + 2 \frac{(L_H - L_{HM})}{2} \right. \\ \left. \times \frac{2}{(L_V - L_{VM} + \alpha)} \right] 2M$$

or

$$W_T = 4M \left[\frac{(L_V - L_{VM} + \alpha)}{(L_H - L_{HM})} + \frac{(L_H - L_{HM})}{(L_V - L_{VM} + \alpha)} \right] \quad (102)$$

Since the total energy input equals the total work done

$$E_T = W_T$$

and by substituting Eqs. 101 and 102 in the preceding equation, the unit resistance is

$$q_w = 24M \left[\frac{(L_V - L_{VM} + \alpha)}{L_H - L_{HM}} + \frac{(L_H - L_{HM})}{L_V - L_{VM} + \alpha} \right] \\ \left[(L_H - L_{HM})(L_{VM} + 2L_V - \alpha) + 3L_{HM} \frac{(L_V - L_{VM})^2}{(L_V - L_{VM} + \alpha)} \right]^{-1} \quad (103)$$

For the case where the yield lines from the wall corners intersect at a common point before intersecting a centrally located window, as noted in Figure 24, the expression for the unit resistance can be shown to be equal to

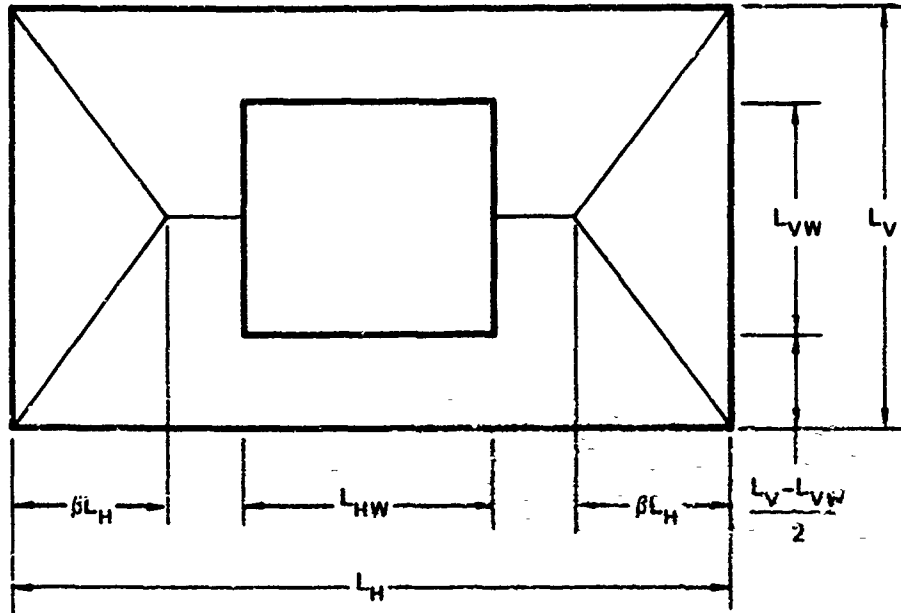


FIGURE 24 WALL WITH YIELD-LINE PATTERN INTERSECTING AT COMMON POINT AND WINDOW EDGE

$$q_w = \frac{12M}{3L_x} \left[\frac{L_y^2 + 2\beta L_x (L_x - L_{xw})}{L_y^2 L_x (3 - 2\beta) + 3L_{xw} L_{yw} (L_{yw} - 2L_y)} \right] \quad (104)$$

where β for isotropic reinforcement is

$$\beta = \frac{1}{2} \left[\sqrt{3 \left(\frac{L_y}{L_x} \right)^2 + \left(\frac{L_y}{L_x} \right)^4} - \left(\frac{L_y}{L_x} \right)^2 \right] \quad (105)$$

To obtain the minimum unit resistance for a square wall panel, it is necessary to investigate Eq. 103 for yield lines intersecting either the horizontal or the vertical window edges. For rectangular wall panels, it is necessary to examine both Eqs. 103 and 104 to obtain the minimum resistance value. However, the effect of either in-plane forces or anisotropic reinforcement on the crack pattern are not accounted for in the above formulations.

Since Eqs. 103 and 104 were developed for a wall with isotropic reinforcement, the resistance values are not directly applicable to an unreinforced masonry or concrete wall. To apply the results to unreinforced walls, it was assumed that the crack pattern in the unreinforced wall was identical to that in the isotropically reinforced wall. Also, it was assumed that the ratio of the resistance function for a reinforced wall with windows to one without windows (q_w/q) was applicable to an unreinforced wall with the same geometry. That is, to determine the decaying phase resistance function for an unreinforced wall with window openings, the resistance is calculated for a wall without windows, and then multiplied by the resistance function ratio q_w/q obtained for an isotropically reinforced wall. The resistance function ratio was used in a like manner for reinforced concrete walls with openings, regardless of whether the reinforcement was isotropic or anisotropic.

Although Eqs. 103 and 104 could be programmed directly to determine the resistance function ratio for the many conceivable wall and window geometries, the approach used in this study was, first, to generate numerical values for a series of walls with ratios of wall length to height (L_w/L_v) between 1 and 3 and ratios of window to wall length (L_{wM}/L_w) and window to wall height (L_{vM}/L_v) between 0.1 and 0.8 and second to fit the data with a multiple regression analysis to obtain an equation relating the resistance function ratio to various wall parameters, for any wall within the specified limits.

From the multiple regression analysis, the best fit was found to be

$$\begin{aligned} \frac{q_w}{q} = & 0.62022 - 2.23415 \left(\frac{A_w}{A_T} \right)^{(L_{wM}/L_w)^4} - 0.79451 \left(\frac{L_{wM}}{L_w} \right)^2 \\ & - 2.27663 \frac{L_{vM}}{L_v} + 0.62522 \left(\frac{L_{vM}}{L_v} \right) \left(\frac{A_T}{A_w} \right)^{0.3} \\ & + 2.63043e^{(A_w/A_T)} - 0.09268 \frac{L_{vM}}{L_v} \end{aligned} \quad (106)$$

Although the above expression was applicable for most wall and window sizes, for certain conditions, i.e.:

where

$$\frac{L_w}{L_v} > 1.5 \quad ,$$

and

$$\frac{L_{vM}}{L_v} \leq 0.7 \quad ,$$

and

$$\frac{L_{wH}}{L_v} > 0.5 \quad ,$$

but

$$\frac{L_{vH}}{L_v} \neq \frac{L_{wH}}{L_v}$$

the best fit was found to be

$$\begin{aligned} \frac{q_w}{q} = & -5.85461 - 12.66440 \left(\frac{A_w}{A_T} \right) + 4.39662 \frac{L_{vH}}{L_v} + 0.84843 \frac{L_{wH}}{L_v} \\ & - 0.22300 \frac{L_{vH}}{L_v} - 1.07269 \left(\frac{L_{vH}}{L_{wH}} \right)^{0.8} + 6.59942 e^{(A_w/A_T)} \quad . \end{aligned} \quad (107)$$

The maximum error entailed in the use of Eqs. 106 and 107 to determine the resistance function ratio is less than 15 percent, generally much less than 10 percent, when compared with Eqs. 103 and 104, for any of the wall and window geometries discussed previously. This error was felt to be compatible with the assumptions made in the analysis and adequate for an interim procedure.

It should be noted that Eqs. 106 and 107 were used in this study even though a particular wall contained multiple or asymmetrical window openings. For such cases, e.g., two adjacent windows, the resistance function ratio was determined for a single window configuration by assuming that the width of the single window was equal to the total width of all the windows and that the window was symmetrically located in the wall panel.

IV PROBABILITY CONSIDERATIONS

Introduction

The approach used in this study has been to develop resistance functions for the types of exterior walls of interest and to use these resistance functions to obtain a deterministic solution for the response of a wall when subjected to a dynamic load. In the initial report (Ref. 1), the methods developed for one-way action walls were used in this manner to calculate the response of a specific wall for comparison with experimental data and to examine the sensitivity of the incipient collapse overpressure for various selected wall elements and load-time functions.

Although useful information can be obtained by a sensitivity analysis, such an analysis has two major shortcomings for the evaluation of existing structures. First, the relationship between the response of a wall subjected to an arbitrarily selected load function and the response during the passage of a blast wave is not obvious. Some of the problems associated with determining the net blast load on an exterior wall are discussed in Section II. Second, although a sensitivity analysis indicates the relative importance of the parameters, it does not provide adequate information for predicting the most probable collapse overpressure of a wall where actual values for many of the parameters are not known. This is especially true for the case when a number of parameters, say 5 or 6, are concerned. This can be illustrated by the discussion and example below.

Even under the most ideal conditions, i.e., laboratory tests, the physical properties of a prototype wall are known only within certain limits, since the properties are usually determined from small specimens,

which are constructed separately from the prototype, and the in-place conditions of the prototype are not known precisely. Generally, for laboratory tests of structural elements, such discrepancies are minor since the properties are usually obtained from a number of specimens and past experience provides guidance for relating the specimen data to the prototype performance. For an actual wall in a building, however, the physical properties are at best ill-defined if not likely unknown, the support conditions are often obscure, and information is lacking for relating laboratory test data to the performance of full-scale structures.

Therefore, when the response of a wall is examined analytically, it is useful to vary each parameter to determine the parameters that have an important influence on the wall response and to assist in estimating the predicted incipient collapse overpressure. For example, consider an unreinforced arching masonry wall that was included in a nuclear field test.* The wall was constructed of a 4 in. wythe of brick backed by an 8 in. wythe of cinder block and contained two 5 ft-5 in. high by 3 ft-3 in. wide centrally located windows that equalled 19 percent of the wall area. The wall was mounted in a nonfailing reinforced concrete support structure that formed a 16-ft by 18-ft by 10-ft room behind the wall. Figure 25 shows the variation of the predicted incipient collapse overpressure when the ultimate compressive strength of the mortar is varied between 1000 and 2500 psi. Even though the ultimate compressive strength is not known exactly, if the range of strengths examined is reasonable for the particular mortar, the collapse pressure for the wall would be expected to fall between 14.5 and 24.3 psi. Furthermore, since the ultimate compressive strength can be assumed as normally distributed for a series of similar mortar

* The correlation of the predicted collapse overpressure for this wall with the results from the nuclear field test reported in Ref. 19 is presented in Section VI and Appendix C.

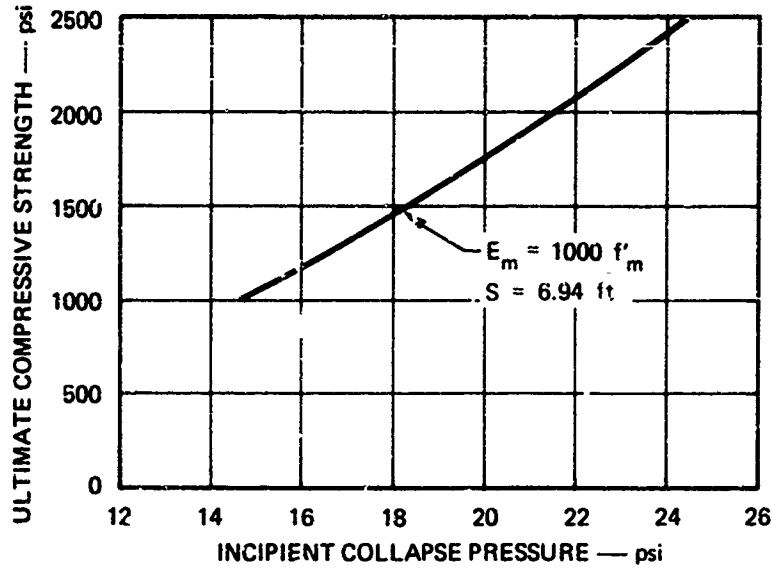


FIGURE 25 PEAK INCIDENT OVERPRESSURE AT INCIPIENT COLLAPSE VERSUS ULTIMATE COMPRESSIVE STRENGTH
Two-Way Unreinforced Wall With Arching

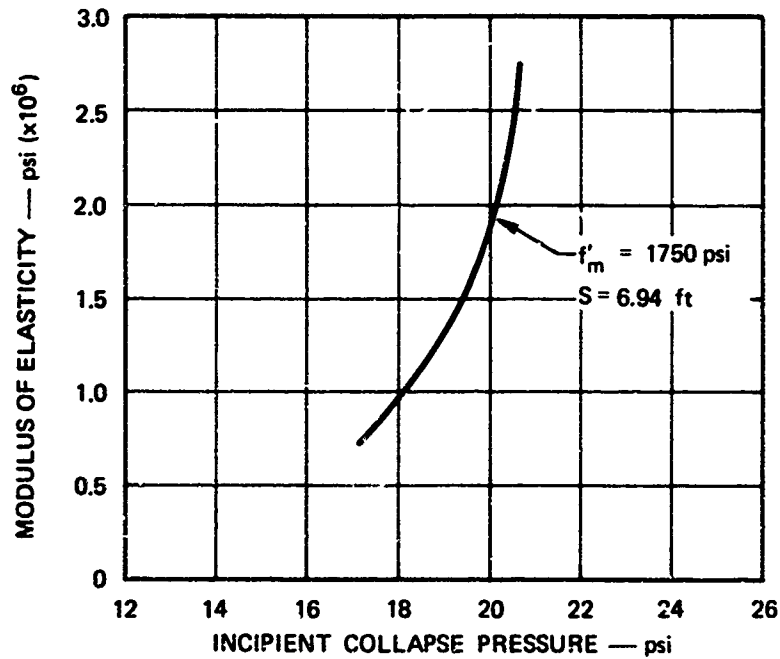


FIGURE 26 PEAK INCIDENT OVERPRESSURE AT INCIPIENT COLLAPSE VERSUS MODULUS OF ELASTICITY
Two-Way Unreinforced Wall With Arching

specimens, a first order estimate, when only a variation in mortar strength is considered, would be a 50 percent probability of collapse occurring at about 20 psi.

In addition to the mortar strength, the modulus of elasticity of the mortar might be included in the analysis of the wall, because it also has an important influence on the collapse strength of an unreinforced arching masonry wall. Since no test information was available from Ref. 19, the modulus of elasticity of the mortar was assumed to follow the relationship, $E_m = \alpha f'_m$. For a mortar strength of 1750 psi, Figure 26 shows the variation in the predicted incipient collapse overpressure when α is varied between 500 and 1500. If the influences of the two parameters are considered together for the ranges discussed, then the predicted collapse pressure would be within the shaded area on Figure 27 between 13.2 and 25.4 psi. Again, for a normal distribution of both the compressive strength and the modulus of elasticity, an estimate of the 50 percent probability of collapse would be about 19 psi.

If there are no other parameters that influence the wall behavior significantly, it would only be necessary to calculate the collapse pressure deterministically to provide an acceptable estimate of the wall collapse. However, as noted in Ref. 1 and Section II of this report, there are a number of other parameters that also affect the collapse of unreinforced arching walls. For example, the presence of a window affects both the net wall loading and the wall resistance, as discussed in Sections II and III, respectively. The effect of the window on the exterior load function and the sensitivity of the incipient collapse pressure of the wall to the variation in load can be illustrated by varying the clearing time of the blast wave. Figure 28 shows the variation of the predicted incipient collapse overpressure when the clearing time of the reflected overpressure, expressed as a function of the clearing distance S , is varied between 2.7 and 11.2 ft. As mentioned previously, if only

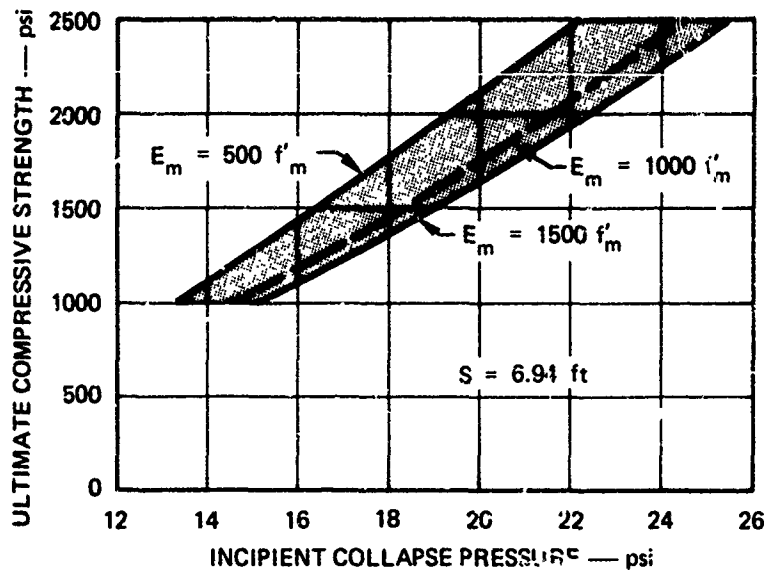


FIGURE 27 PEAK INCIDENT OVERPRESSURE AT INCIPIENT COLLAPSE VERSUS ULTIMATE COMPRESSIVE STRENGTH AND MODULUS OF ELASTICITY
Two-Way Unreinforced Wall With Arching

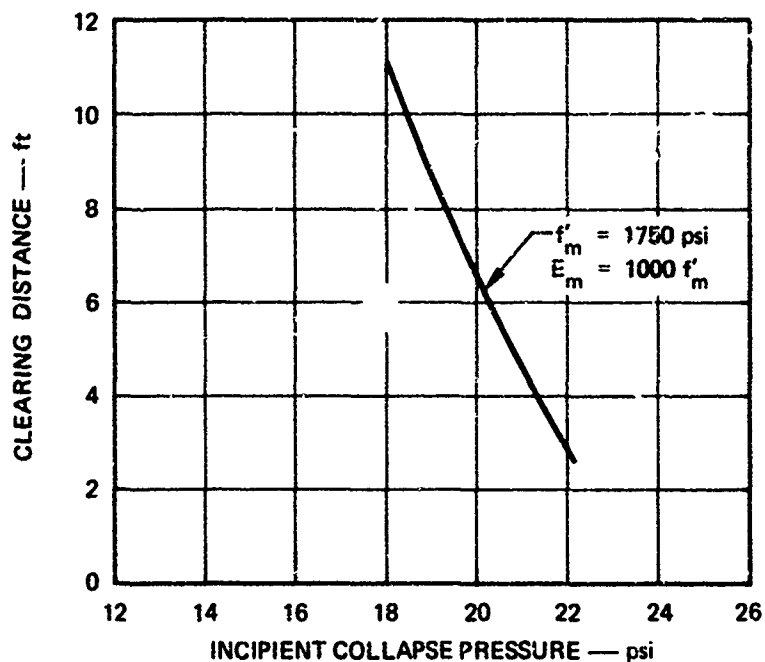


FIGURE 28 PEAK INCIDENT OVERPRESSURE AT INCIPIENT COLLAPSE VERSUS CLEARING DISTANCE
Two-Way Unreinforced Wall With Arching

one parameter affected the wall behavior significantly, an acceptable estimate of the predicted incipient collapse overpressure can be made even if the precise clearing distance is not known. However, for the example wall under discussion it has been shown that at least two other parameters, namely the ultimate compressive strength and modulus of elasticity of the mortar, also have a significant effect on the wall collapse pressure. If the influence of all three parameters is treated, a complex three-dimensional plot would be required to visualize the variation in the incipient collapse pressure, and an estimate of the most probable value would no longer be a relatively simple procedure. As described in the following subsections, for this program a probability function was included in the analytical procedure to permit a rational prediction of the incipient collapse pressure to be made regardless of the number of parameters. For comparative purposes, the results of such an analysis are shown in Figure 29 for a variation of the three parameters as previously illustrated.

Statistical Analysis

Monte Carlo

It is apparent that the determination of the incipient collapse overpressure for a given wall, or type of wall, depends on a number of variables, at least some of which must be considered to be randomly distributed. Although the probability distribution of these random variables may be determined fairly easily, at least in an approximate manner, the extension of this step to determining the probability distribution of the resulting collapse overpressure is not so easy.

It is not possible to obtain an exact distribution because an explicit relationship between the incipient collapse overpressure and the wall properties is not available. Even if such a relationship were

WALL PARAMETERS

$L_V = 120$ in.
 $L_H = 192$ in.
 $t_w = 12$ in.
 $t_f = 1.5$ in.
 $\gamma = 105$ pcf
 2-5'-5" x 3'-3" windows

LOAD PARAMETERS

$W = 27$ kt
 $P_o = 13.2$ psi
 $c_o = 1104$ fps

ROOM SIZE

$f'_m = 1000-2500$ psi
 $E_m = 500-1500 f'_m$ psi
 $S = 2.71-11.17$ ft

HEIGHT = 10 ft
 WIDTH = 16 ft
 DEPTH = 18 ft

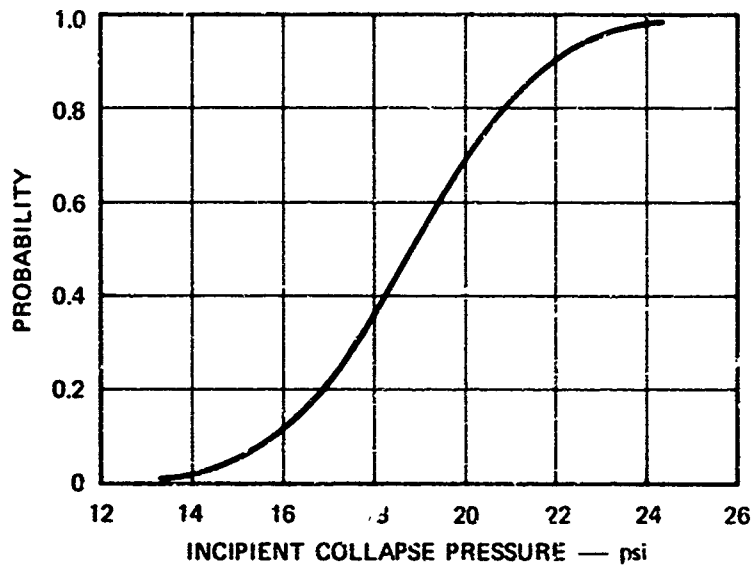


FIGURE 29 PROBABILITY OF OCCURRENCE OF PEAK INCIDENT OVERPRESSURE AT INCIPIENT COLLAPSE
 Two-Way Unreinforced : all With Arching

available, it would be so complicated as to make intractable the calculus needed to evaluate the integrals required for determining the probability distribution. Thus it was decided to use Monte Carlo, or simulation, techniques to determine the probability distribution for the incipient collapse overpressure.

The technique uses a set of mathematically simulated walls, each of which possesses the characteristics of some actual wall, to determine an approximate distribution of the incipient collapse overpressure. This set of simulated walls is prepared by selecting the parameters to be varied and determining the values of these parameters by randomly sampling their corresponding probability distribution functions. Each simulated wall is then analyzed using the deterministic equations developed previously in the wall study. The results of these analyses provide a probability distribution of the incipient collapse overpressure.

Two problems were encountered in using this method of approach. The first of these entailed determination of the probability distribution for each of the random variables under consideration. No restriction is placed on this determination by the Monte Carlo method, therefore, the problem is only concerned with using the distribution best describing the actual world. This problem will not be discussed further here since the determination is entirely dependent on the variable concerned. The second problem was determining the number of simulated walls that need to be analyzed to represent the infinite number of real cases adequately. It is a complicated problem, because of the probability distributions used and the degree of accuracy that is acceptable, and is discussed further in the following subsection.

Sampling Distribution of the Mean and Variance

Two statistical measures that are often used to describe the probability distribution of a random variable are the mean and standard deviation (square root of the variance). These two measures describe completely the probability distribution of a normal, or Gaussian, distributed random variable and give considerable information essential in describing other types of distributions. Thus, the mean and standard deviation of the results obtained from the Monte Carlo technique can be used to describe the probability distribution of the incipient collapse overpressure for a given wall or wall type. The problem still remains, however, regarding the number of simulated walls that need to be analyzed for the mean and standard deviation of the finite sample \bar{x} and s , to represent the mean and standard deviation of the total population, ξ and σ , adequately.

The solution to this problem can be approached by establishing confidence limits for the sample mean and standard deviation. These limits establish confidence intervals that, to any desired degree of confidence less than 1, contain the mean and standard deviation of the total population. The width of these confidence intervals depends on three factors: (1) the degree of confidence desired, (2) the dispersion of the incipient collapse overpressure; and (3) the sample size n . The degree of confidence chosen for use in this study was the 95 percent confidence interval. The dispersion of the incipient collapse overpressure depends on the individual wall properties. Thus, for any given sample size, the width of the confidence intervals for the mean and standard deviation of the incipient collapse overpressure will increase as the dispersion of the individual wall properties increases. It is important to observe that the confidence limits depend on the sample size n , thus, for a fixed confidence level, the interval can be made as short as desired by increasing the number of simulated walls analyzed.

Through the study of several cases, details of which are given in Appendix C, confidence limits of plus or minus 10 percent of the sample mean were chosen as the values to be used in determining when a sufficient number of simulated walls had been analyzed. It was further judged that at least 20 simulated walls were required for the sample mean and standard deviation to represent adequately the mean and standard deviation of the total population. These guidelines are summarized as follows:

1. Minimum sample size, $n = 20$.
2. The 95 percent confidence for the sample mean, \bar{x} , should be within ± 10 percent of \bar{x} .
3. The 95 percent confidence limits for the sample standard deviation, s , should be within $\pm 0.10 \bar{x}$ (10 percent of the sample mean) of s (the upper confidence limit is the critical one).

For the cases studied, where the above criteria were met, the sample mean and standard deviation were within 10 and 20 percent, respectively, of the values obtained when the sample size was doubled. This accuracy was felt to be adequate in view of the many other unknown variables present.

The question still arises as to how the 95 percent confidence limits for the sample mean and standard deviation are determined. For the case where the random variable is normally distributed, the following theorem regarding the sample mean can be derived: The mean \bar{x} of n stochastically independent observations from a normally distributed population with mean ξ and variance σ^2 is normally distributed with mean ξ and variance σ^2/n . In other words, the distribution of the sample mean depends on the distribution of the individual random variables constituting the sample mean. The standard deviation of the mean, also called the standard error of the mean, is equal to the square root of the variance, or σ/\sqrt{n} .

This theorem may be used in determining the probability distribution of the incipient collapse overpressure (even though in this case the exact distribution is not known) since for large sample size n the central limit theorem* can be applied. This permits considering the sample mean and variance as being approximately normally distributed.

Rewriting the distribution of the sample mean in terms of the standardized normal distribution u , the following expression is obtained:

$$u = \frac{\bar{x} - \xi}{\sigma/\sqrt{n}} \quad (108)$$

This relation, in conjunction with standard tables for the u -distribution, could be used to determine the confidence limits for ξ , provided that σ was known. However, σ is unknown in this case, and an alternative approach must be taken. Replacing σ by s , the standard deviation estimated from the sample observations and multiplying the denominator by σ/s , the right side of Eq. 108 becomes

$$\frac{\bar{x} - \xi}{s/\sqrt{n}} = \frac{\bar{x} - \xi}{\frac{s}{\sqrt{n}} \frac{\sigma}{\sigma}} = \frac{\bar{x} - \xi}{\frac{\sigma}{\sqrt{n}} \frac{s}{\sigma}} = \frac{u}{s/\sigma} \quad (109)$$

The value of s may be obtained from the expression

$$s = \frac{1}{n-1} \sqrt{\sum_{i=1}^n (x_i - \bar{x})^2} \quad (110)$$

* The central limit theorem states that the distribution of the sum of n independent random variables tends to the normal distribution for $n \rightarrow \infty$ under fairly general conditions, two of which are that the variance of the sums tends to infinity and the variance of each variable divided by the variance of the sum tends to zero.

Dividing both sides of this equation by σ , the following result is obtained:

$$\frac{s}{\sigma} = \frac{1}{\sqrt{n-1}} \sqrt{\sum_{i=1}^n \left(\frac{x_i - \bar{x}}{\sigma} \right)^2} . \quad (111)$$

The expression under the radical, $\sum_{i=1}^n \left(\frac{x_i - \bar{x}}{\sigma} \right)^2$, has a chi-square distribution. Thus replacing this expression by χ^2 and letting $f = n - 1$, Eq. 111 can be rewritten as

$$\frac{s}{\sigma} = \sqrt{\frac{\chi^2}{f}} . \quad (112)$$

Equating Eqs. 109 and 112 yields

$$\frac{\bar{x} - \xi}{s/\sqrt{n}} = \frac{u}{\sqrt{\chi^2/f}} . \quad (113)$$

It can further be shown (Ref. 21) that the random variable $u/\sqrt{\chi^2/f}$ has a t-distribution with f degrees of freedom. Thus the lefthand side of Eq. 113 must also have a t-distribution with $f = n - 1$ degrees of freedom. This is indicated by writing

$$t = \frac{\bar{x} - \xi}{s/\sqrt{n}} . \quad (114)$$

This test statistic is independent of both ξ and σ , being a function only of the sample mean \bar{x} , the sample standard deviation s , and the sample size n . Like the u-distribution, the t-distribution is symmetrical about

zero, and for $f \rightarrow \infty$, it tends to the normal distribution as s converges to σ . Confidence limits for the mean ξ can now be determined from the relationship

$$P \left\{ \bar{x} - t_{p_2} \frac{s}{\sqrt{n}} < \xi < \bar{x} - t_{p_1} \frac{s}{\sqrt{n}} \right\} = P_2 - P_1 \tag{115}$$

where t_{p_1} and t_{p_2} are available from tables of the t-distribution for various values of the cumulative probability P and the number of degrees of freedom f . Thus, for a 95 percent confidence interval, this relationship becomes

$$P \left\{ \bar{x} - t_{0.975} \frac{s}{\sqrt{n}} < \xi < \bar{x} - t_{0.025} \frac{s}{\sqrt{n}} \right\} = 0.95 \tag{116}$$

It is expected, with 95 percent confidence, that the population mean, ξ , will fall in the above interval. Given values of s and \bar{x} , n can be chosen so that the interval of uncertainty about ξ falls within tolerable limits.

A similar approach can be used to determine confidence limits for the standard deviation s . Squaring both sides of Eq. 112 yields

$$s^2 = \sigma^2 \frac{\chi^2}{f} \tag{117}$$

Values of χ^2/f are available from tables of the chi-square distribution for various values of P and f . Confidence limits for the standard deviation are easily derived from the above since

$$s = \sigma \sqrt{\frac{\chi^2}{f}} = \frac{\sigma \chi}{\sqrt{f}} \tag{118}$$

The confidence limits for s are thus given by

$$P \left\{ \frac{s}{\chi_{p_2} \sqrt{T}} < \sigma < \frac{s}{\chi_{p_1} \sqrt{T}} \right\} = P_2 - P_1 \quad (119)$$

which for a 95 percent confidence interval reduces to

$$P \left\{ \frac{s}{\chi_{0.975} \sqrt{n-1}} < \sigma < \frac{s}{\chi_{0.025} \sqrt{n-1}} \right\} = 0.95 \quad (120)$$

since $f = n - 1$. Again it can be expected, with 95 percent confidence, that the population variance, σ , will fall within the above interval.

Given values of x and s , the 95 percent confidence limits for the sample mean and standard deviation can now be obtained from Eqs. 116 and 119, respectively. These values, along with the previously established guidelines, may now be used to determine the number of simulated walls that needs to be analyzed.

10 Percent and 90 Percent Probability Values

The mean value of the incipient collapse overpressure may be taken as the overpressure at or below which failure will occur 50 percent of the time. Also of interest in this study are the values for which failure will occur 10 and 90 percent of the time. These values will be referred to as the 10 percent probability value and the 90 percent probability value.

For the case where the incipient collapse overpressure is normally distributed, these values are easily obtained from the following:

$$10 \text{ percent probability value} = \bar{x} - 1.282 s$$

$$90 \text{ percent probability value} = \bar{x} + 1.282 s$$

The accuracy of these relations depends on how closely the probability distribution for the incipient collapse overpressure is approximated by a normal distribution. This can be investigated by plotting the cumulative probability distribution on probability paper. When plotted in this manner a normal distribution will plot as a straight line. Thus, a visual approximation of how close the actual distribution is to the normal distribution can be obtained by seeing how closely the data approximate a straight line. For the cases studied in Appendix C, the probability distribution of the data was sufficiently close to the normal distribution so that the 10 and 90 percent probability values can be obtained from the above equations with little error.

In determining the confidence limits for the 10 and 90 percent probability values, one might be inclined to use the individual confidence limits for the sample mean and standard deviation given by the t and the χ^2 distributions, assuming that the probability of both occurrences is the product of the separate probabilities. This is incorrect, however, because t and u (from which the χ^2 distribution is derived) are not independent. Therefore the joint probability that the two intervals cover the true parameter values is not equal to the product of the separate probabilities. Methods are available to determine the confidence region for these two parameter values; however, these were believed to be beyond the scope of this study.

An approximate method was developed that assumes that the mean value obtained from the sample is the true mean value for the entire distribution. This is at best only approximately true; however, it permits confidence intervals to be obtained for the 10 and 90 percent probability values by merely using the 95 percent confidence limits for the standard deviation along with the sample mean. The confidence in this value will be somewhat less than 95 percent, although exactly how much less is not known.

These methods enable values to be determined for the mean, standard deviation, 10 percent probability value, and 90 percent probability value of the incipient collapse overpressure. Confidence intervals of 95 percent may also be obtained for the mean and standard deviation, along with limits of a somewhat smaller, but unknown, confidence for the 10 and 90 percent probability values. These techniques were used in investigating the incipient collapse overpressure for several masonry walls with arching, and a detailed statistical analysis of one of these walls is presented in Appendix C.

V WALL REACTIONS

Introduction

The response of a dynamically loaded wall element is influenced by the elements' structural characteristics, as well as by those of the supporting structure. In this study, however, it has been assumed that the natural frequencies of the wall and its supporting structure are so related that the wall may be considered to act independently of the supports, thus permitting the wall to be analyzed as a separate single-degree-of-freedom system, rather than as part of a coupled multidegree system.

The reaction of the equivalent single-degree-of-freedom system used to determine the wall response is equal to the spring resistance; however, for the actual wall, the reaction is also a function of the distributed inertia forces. To account for these forces, it was assumed that the distribution of the inertia forces is the same as the curve of the static deflected shape of the wall. Although this assumed distribution of the inertia forces does not take into account the higher response modes, the error is felt to be minor, especially when reactions for a failing member are being predicted.

Dynamic Reactions

The method used to calculate the dynamic reactions of two-way action walls was essentially the same as that used in Ref. 1 for one-way action walls. In a similar manner to that outlined for the one-way walls, the dynamic reactions for two-way walls are determined by assuming that the

distribution of the inertia forces along a vertical or horizontal strip is the same as the deflected shape of a beam with the same support conditions. The total reaction along each edge was determined in accordance with the assumed crack, or yield line, pattern shown in Figure 12 (Section III), with only the adjacent segment contributing to the reaction along each edge. The corresponding reactions for collapse mode "b" shown in Figure 20(b) (Section III) for the reinforced concrete wall are discussed in Appendix B.

The dynamic reaction along the horizontal edges of the wall can thus be determined by considering the equilibrium of forces on segment A, shown in Figure 30. Since these forces are in dynamic equilibrium, the sum of the moments about the line of action of the resultant of the inertia forces yields

$$V_A \bar{z} - P_A (\bar{z} - z') - M_A - M'_A = 0 \quad (121)$$

where \bar{z} and z' are the distances to the centroids of the inertia force and the lateral load, respectively. The moments M_A and M'_A , which are assumed to be uniformly distributed, are related to the total resistance of the segment, Q_A , by

$$M_A + M'_A = z' Q_A \quad (122)$$

which by substituting in Eq. 121 yields

$$V_A = \left(1 - \frac{z'}{\bar{z}}\right) P_A + \frac{z'}{\bar{z}} Q_A \quad (123)$$

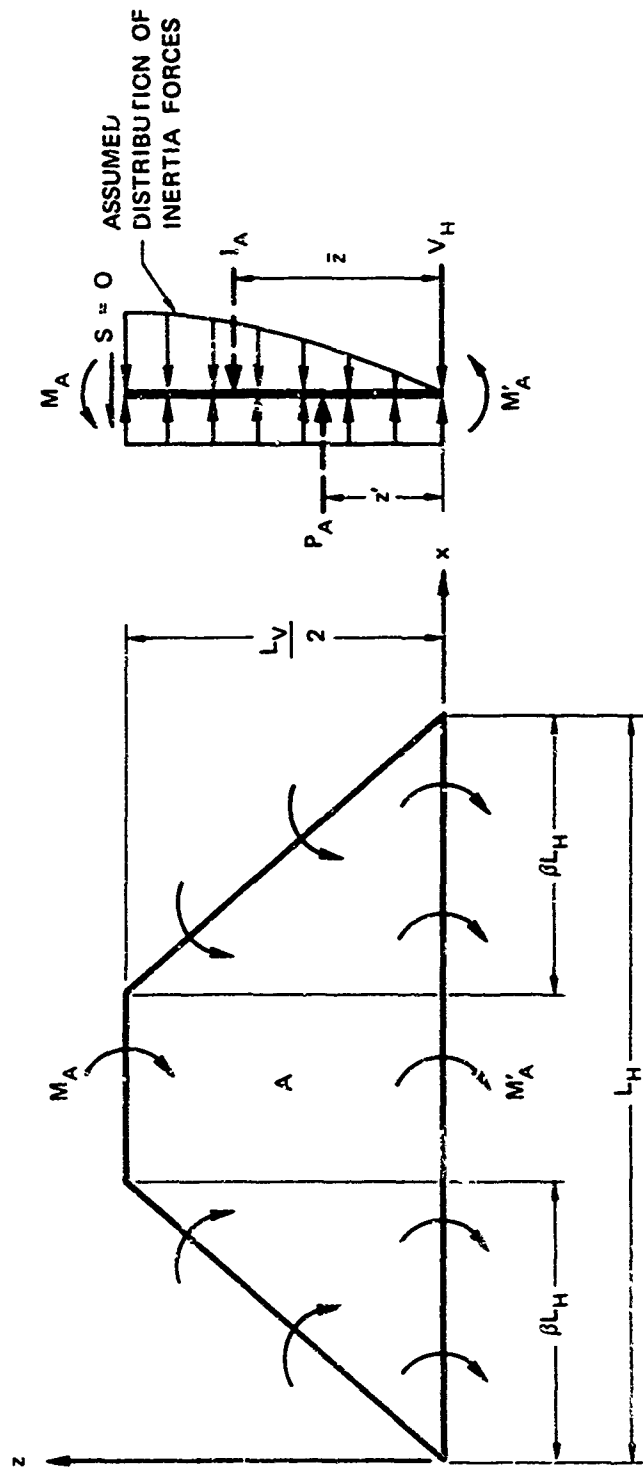


FIGURE 30 DYNAMIC FORCES ACTING ON SEGMENT A

For a uniformly distributed lateral load, the distance z' to the centroid of the load acting on the trapezoidal segment is given by

$$z' = \frac{1 - \frac{4}{3}\beta}{4(1 - \beta)} L_v \quad (124)$$

where the value of β is obtained from Eq. 38 for unreinforced masonry or concrete walls and from Eq. 76 for reinforced concrete walls. The distance \bar{z} to the centroid of the inertia forces depends on the assumed deflected shape of the segment and is discussed in the following subsections.

In a similar manner, the dynamic reaction along the vertical edges of the wall can be determined by considering the equilibrium of the forces acting on segment C, shown in Figure 31. Taking moments about the line of action of the resultant of the inertia forces yields

$$V_v \bar{x} - P_c(\bar{x} - x') - M_c - M'_c = 0 \quad (125)$$

where \bar{x} and x' are the distances to the centroids of the inertia force and the lateral load, respectively. The moments M_c and M'_c , which are again assumed to be uniformly distributed, are related to the static resistance Q_c by

$$M_c + M'_c = x' Q_c \quad (126)$$

which by substituting in Eq. 125 yields

$$V_v = \left(1 - \frac{x'}{\bar{x}}\right) P_c + \frac{x'}{\bar{x}} Q_c \quad (127)$$

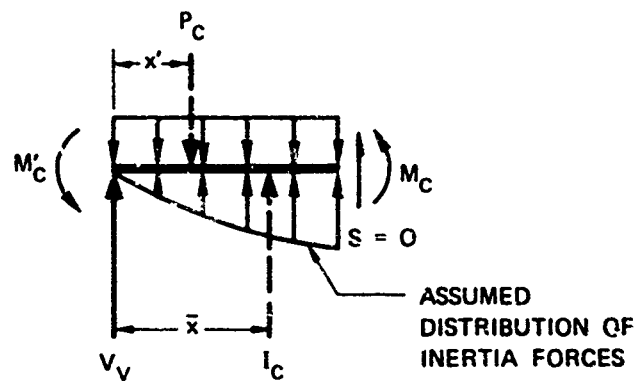
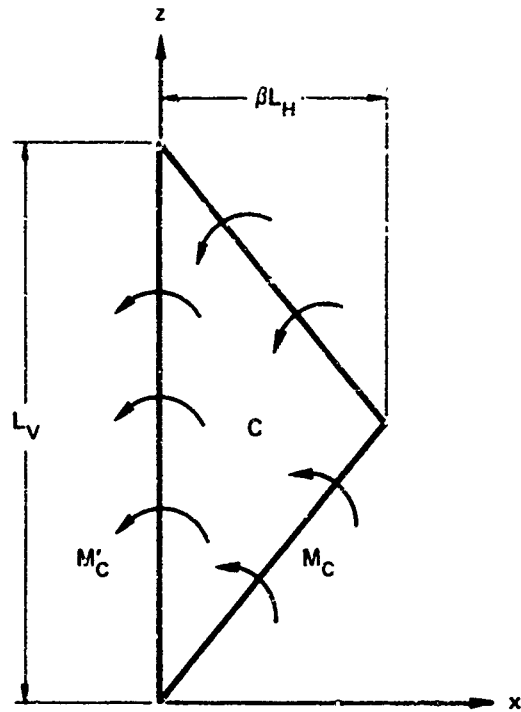


FIGURE 31 DYNAMIC FORCES ACTING ON SEGMENT C

For a uniformly distributed lateral load, the distance x' to the centroid of the load on the triangular segment is given by

$$x' = \frac{1}{3} \beta L_w \quad . \quad (128)$$

The distance \bar{x} to the centroid of the inertia force depends on the assumed deflected shape of the segment and is discussed further in the following subsections.

As a result of symmetry, the total load on the wall is equal to

$$P_T = 2P_A + 2P_C \quad . \quad (129)$$

The load acting on each of the segments is thus related to the total load in proportion to their areas, or

$$\frac{P_C}{P_T} = \frac{\beta L_w L_y / 2}{L_w L_y} = \frac{1}{2} \beta \quad (130)$$

$$\frac{P_A}{P_T} = \frac{1}{2} \left(1 - 2 \frac{P_C}{P_T} \right) = \frac{1}{2} (1 - \beta) \quad . \quad (131)$$

Similarly, the total resistance of the wall is equal to

$$Q_T = 2Q_A + 2Q_C \quad . \quad (132)$$

By assuming the total resistance to be uniformly distributed, the resistance provided by each of the segments is also related to the total resistance in proportion to their areas, or

$$\frac{e_c}{e_T} = \frac{1}{2} \beta \quad (133)$$

$$\frac{e_A}{e_T} = \frac{1}{2} (1 - \beta) \quad (134)$$

Substituting Eqs. 130, 131, 133, and 134 into Eqs. 123 and 127 yields the following expressions for the dynamic reactions along the horizontal and vertical edges:

$$V_H = \frac{1}{2} (1 - \beta) \left[\left(1 - \frac{z'}{z}\right) P_T + \frac{z'}{z} Q_T \right] \quad (135)$$

$$V_V = \frac{1}{2} \beta \left[\left(1 - \frac{x'}{x}\right) P_T + \frac{x'}{x} Q_T \right] \quad (136)$$

where z' and x' are given by Eqs. 124 and 128, respectively.

These reaction equations are applicable to all of the types of walls considered in this study.* The magnitudes will be different, however, since the reactive forces at any particular time depend on both the load and the resistance function. Differences will also result from the variation in the assumed deflection shape for the different support conditions and the resistance phases, since both \bar{z} and \bar{x}

* For reinforced concrete walls in which collapse mode "b" [Figure 20(b), Section III] occurs, the above equations are not applicable. This case is discussed in Appendix B.

are a function of the deflection shape. The values of \bar{z} and \bar{x} for walls with the four support conditions considered are as follows.

Support Case 1

During the elastic phase, the equation for the deflection of a simply supported, one-way wall of length L_w with a uniformly distributed load is

$$y = \frac{qz}{24EI}(L_w^3 - 2L_w z^2 + z^3) \quad (137)$$

Since it was assumed that the distribution of the inertia forces along a vertical strip of the two-way wall is the same as the deflection shape of a one-way wall with the same simple support conditions, the distance \bar{z} to the centroid of the inertia forces on segment A is given by

$$\bar{z} = \frac{\int yz \, dA}{\int y \, dA} \quad (138)$$

where the integration is carried out over the area of segment A. Substituting Eq. 137 into Eq. 138 and integrating gives

$$\bar{z} = \frac{(0.127 - 0.185\beta)}{(0.400 - 0.508\beta)} L_w \quad (139)$$

Similarly, the distance \bar{x} to the centroid of the inertia forces on segment C is given by

$$\bar{x} = \frac{\int yx \, dA}{\int y \, dA} \quad (140)$$

where the integration is carried out over the area of segment C. The elastic deflection along a horizontal strip is given by

$$y = \frac{qx}{24EI}(L_H^3 - 2L_Hx^2 + x^3) \quad (141)$$

Substituting this expression into Eq. 140 and integrating gives

$$\bar{x} = \frac{\left(\frac{1}{12} + \frac{1}{15}\beta^2 + \frac{1}{42}\beta^3\right)}{\left(\frac{1}{6} - \frac{1}{10}\beta^2 + \frac{1}{30}\beta^3\right)} \quad (142)$$

Substituting these expressions for \bar{z} and \bar{x} in Eqs. 135 and 136 yields the equations for the dynamic reactions along the horizontal and vertical edges during the elastic phase for unreinforced walls without arching and reinforced concrete walls. For Support Case 1, the resisting moments along the edges, M_A' and M_C' , are zero.

After cracking of the wall in the elastic phase, both the resistance and the deflection are altered as noted in Section III. Since it was assumed that the motion of the wall after cracking is a rigid body rotation of the segments about their supports, the deflection along a vertical strip is given by

$$y = \frac{2z}{L_w} y_c \quad (143)$$

Similarly, the deflection along a horizontal strip is given by

$$x = \frac{x}{\beta L_H} y_c \quad (144)$$

Substituting Eqs. 143 and 144 into Eqs. 138 and 140, respectively, yields the following expressions for \bar{z} and \bar{x} :

$$\bar{z} = \frac{\left(\frac{1}{24} - \frac{1}{16} \beta\right)}{\left(\frac{1}{8} - \frac{1}{6} \beta\right)} L_v \quad (145)$$

$$\bar{x} = \frac{1}{2} \beta L_v \quad (146)$$

These values are substituted into Eqs. 135 and 136 to determine the reactions along the horizontal and vertical edges for unreinforced walls with arching and during the decaying phase of unreinforced walls without arching and the plastic phase of reinforced concrete walls.

Support Case 2

The reaction for two-way walls fixed on four edges is determined in a manner similar to that in the previous subsection. The distribution of the inertia forces along a vertical strip is assumed to be the same as the deflected shape of a uniformly loaded, one-way, fixed edge wall of length L_v , or

$$y = \frac{qz^2}{24EI} (L_v - z)^2 \quad (147)$$

Similarly, the deflected shape along a horizontal strip is given by

$$y = \frac{qx^2}{24EI} (L_H - x)^2 \quad (148)$$

Substituting Eqs. 147 and 148 into Eqs. 138 and 140, respectively, results in the following values for \bar{z} and \bar{x} :

$$\bar{z} = \frac{(0.092 - 0.130\beta)}{(0.237 - 0.367\beta)} L_v \tag{149}$$

$$\bar{x} = \frac{(1/20 - \beta/15 + \beta^2/42)}{(1/12 - \beta/10 + \beta^2/30)} \beta L_H \tag{150}$$

These values are substituted into Eqs. 135 and 136 to determine the reactions along the horizontal and vertical edges during the initial portion of the elastic phase of unreinforced walls without arching and the elastic, uncracked phase and elastic, cracked phase of reinforced concrete walls.

After cracking (or yielding of the steel in a reinforced concrete wall) along the fixed edges, the wall is assumed to respond as if it were simply supported on four edges. Thus, the resulting values of \bar{z} and \bar{x} during the secondary portion of the elastic phase of unreinforced walls without arching and the elasto-plastic phase of reinforced concrete walls are given by Eqs. 139 and 142. During the decaying phase of unreinforced walls without arching and the plastic phase of reinforced concrete walls, the values of \bar{z} and \bar{x} are again given by Eqs. 145 and 146.

Support Case 3

For Support Case 3, the distribution of the inertia forces along a vertical strip is assumed to be the same as the deflected shape of a uniformly loaded, simply supported one-way wall of length L_v , as expressed by Eq. 137. The distribution of the inertia forces along a horizontal

strip, however, is assumed to be the same as for a one-way, fixed-edge wall of length L_w , as expressed by Eq. 148. The resulting values of \bar{z} and \bar{x} for the initial portion of the elastic phase of unreinforced walls without arching and the elastic, uncracked phase and the elastic, cracked phase of reinforced concrete walls are thus given by Eqs. 139 and 150.

After cracking (or yielding of the steel in a reinforced concrete wall) along the fixed edges, the wall is again assumed to respond as if it were simply supported on four edges. The resulting values of \bar{z} and \bar{x} during the secondary portion of the elastic phase of unreinforced walls without arching and the elasto-plastic phase of reinforced concrete are therefore again given by Eqs. 139 and 142. During the decaying phase of unreinforced walls without arching and the plastic phase of reinforced concrete walls the values of \bar{z} and \bar{x} are given by Eqs. 145 and 146.

Support Case 4

For Support Case 4, the values of \bar{z} and \bar{x} during the initial portion of the elastic phase of unreinforced walls without arching and the elastic, uncracked phase and elastic, cracked phase of reinforced concrete walls correspond to those given by Eqs. 149 and 142, respectively. Again, after cracking (or yielding for a reinforced wall) occurs along the fixed edges, the values of \bar{z} and \bar{x} during the secondary portion of the elastic phase of unreinforced walls without arching and the elasto-phase of reinforced concrete walls are given by Eqs. 139 and 142. During the decaying phase of unreinforced walls without arching and the plastic phase of reinforced concrete walls, the values of \bar{z} and \bar{x} are again given by Eqs. 145 and 146.

The values of x and z for each of the four support cases, along with the values of x' and z' , are summarized for unreinforced concrete or masonry unit walls and reinforced concrete walls in Tables 1 and 2.

Table 1

DYNAMIC REACTIONS FOR TWO-WAY UNREINFORCED CONCRETE OR MASONRY UNIT WALLS

$$V_y = \frac{\beta}{2} \left[\left(1 - \frac{x'}{\bar{x}}\right) P_T + \frac{x'}{\bar{x}} Q_T \right] \quad V_H = \frac{(1 - \beta)}{2} \left[\left(1 - \frac{z'}{\bar{z}}\right) P_T + \frac{z'}{\bar{z}} Q_T \right]$$

Support Case	Elastic - Initial Phase	Elastic - Secondary Phase	Decaying Phase
1	$\bar{x} = \frac{(1/12 + \beta^2/15 + \beta^3/42) \beta L_H}{(1/6 - \beta^3/10 + \beta^3/30)}$	No elastic - secondary phase	
	$\bar{z} = \frac{(0.127 - 0.185\beta) L_y}{(0.400 - 0.508\beta)}$		
2	$\bar{x} = \frac{(1/20 - \beta/15 + \beta^2/42) \beta L_H}{(1/12 - \beta/10 + \beta^2/30)}$		$\bar{x} = \frac{1}{2} \beta L_H$
	$\bar{z} = \frac{(0.092 - 0.138\beta) L_y}{(0.267 - 0.367\beta)}$		
3	$\bar{x} = \frac{(1/20 - \beta/15 + \beta^2/42) \beta L_H}{(1/12 - \beta/10 + \beta^2/30)}$		$\bar{z} = \frac{(1/24 - \beta/16) L_y}{(1/8 - \beta/6)}$
	$\bar{z} = \frac{(0.127 - 0.185\beta) L_y}{(0.400 - 0.508\beta)}$		
4	$\bar{x} = \frac{(1/12 + \beta^2/15 + \beta^3/42) \beta L_H}{(1/6 - \beta^3/10 + \beta^3/30)}$		
	$\bar{z} = \frac{(0.092 - 0.138\beta) L_y}{(0.267 - 0.367\beta)}$		
1,2,3,4	$x' = \frac{1}{3} \beta L_H$	$z' = \frac{(1 - 4\beta/3) L_y}{4(1 - \beta)}$	

Note: Reactions for unreinforced walls with arching correspond to those given above for decaying phase.

Table 2

DYNAMIC REACTIONS FOR TWO-WAY REINFORCED CONCRETE WALLS
(Collapse Mode "a")

$$V_v = \frac{\beta}{2} \left[\left(1 - \frac{x'}{\bar{x}}\right) P_T + \frac{x'}{\bar{x}} Q_T \right] \quad V_H = \frac{(1 - \beta)}{2} \left[\left(1 - \frac{z'}{\bar{z}}\right) P_T + \frac{z'}{\bar{z}} Q_T \right]$$

Support Case	Elastic Phase	Elasto-Plastic Phase	Plastic Phase
1	$\bar{x} = \frac{(1/12 + \beta^2/15 + \beta^3/42)}{(1/6 - \beta^2/10 + \beta^3/30)} \beta L_H$	No elasto-plastic phase	
	$\bar{z} = \frac{(0.127 - 0.185\beta)}{(0.400 - 0.508\beta)} L_W$		
2	$\bar{x} = \frac{(1/20 - \beta/15 + \beta^2/42)}{(1/12 - \beta/10 + \beta^2/30)} \beta L_H$		$\bar{x} = \frac{1}{2} \beta L_H$
	$\bar{z} = \frac{(0.092 - 0.138\beta)}{(0.267 - 0.367\beta)} L_W$		
3	$\bar{x} = \frac{(1/20 - \beta/15 + \beta^2/42)}{(1/12 - \beta/10 + \beta^2/30)} \beta L_H$		$\bar{z} = \frac{(1/24 - \beta/16)}{(1/8 - \beta/6)} L_W$
	$\bar{z} = \frac{(0.127 - 0.185\beta)}{(0.400 - 0.508\beta)} L_W$		
4	$\bar{x} = \frac{(1/12 + \beta^2/15 + \beta^3/42)}{(1/6 - \beta^2/10 + \beta^3/30)} \beta L_H$		
1, 2, 3, 4	$x' = \frac{1}{3} \beta L_H$	$z' = \frac{(1 - 4\beta/3)}{4(1 - \beta)} L_W$	

VI DISCUSSION

Introduction

As discussed in Ref. 1, to determine the dynamic response of the various walls, computer programs were developed using the Newmark β method (Ref. 4) for analyzing the walls with the resistance functions previously determined in Section III. The transformation factors, as developed in Appendix A for two-way action walls, were used to reduce the wall from a distributed mass system to an equivalent single-degree-of-freedom system. The input data required in the programs consist of the wall and load properties, including probability distributions where needed, and the output can be either a complete time-history of the response of the wall up to collapse, or a prediction of the probability of occurrence of the incipient collapse overpressure, as presented in Section IV. The computer flow charts for the analysis of the three types of walls are presented in Appendix D.

To provide insight into the parameters that significantly influence the collapse of two-way action exterior walls, a limited sensitivity analysis was performed. Also, a comparison was made of the available experimental information on dynamically loaded wall elements and the theoretical predictions. The findings from these studies are presented in the following subsections.

Variation of Parameters

To determine the individual effects of a few of the more important parameters in the behavior of dynamically loaded walls, the incipient collapse overpressure was calculated for various values of the parameters.

The parameters investigated for each of the three wall types were the ratio of the height to the width of the wall, the area of the window opening, and the volume of the room. Based on engineering judgment, a two-way action wall with the following properties, except where noted otherwise on the graphs, was selected as the standard from which all variations were made:

- Height, L_v 8 ft
- Width, L_h 12 ft
- Thickness, t_w 8 in.
- Modulus of elasticity
 - Masonry, E_m 1,000,000 psi
 - Concrete, E_c 3,000,000 psi
 - Reinforcing steel, E_s 30,000,000 psi
- Modulus of rupture, f_r 100 psi
- Unit weight, γ
 - Masonry 120 pcf
 - Concrete 145 pcf
- Vertical load, P_v 0
- Window area, A_w 0

In addition, for walls with windows, the window was centrally located in the wall, and the window height was maintained at 4 ft, while the width was varied to obtain the desired window area. The edge support for all walls was Support 2 (fixed on all four edges).

A value for the clearing distance of $S = 10$ ft and weapon yield of $W = 1$ Mt were chosen as the standard values for the study of the other parameters. This eliminated the effect of a variable clearing time and yield on the behavior of the walls.

Unreinforced Concrete or Masonry Unit Wall (Without Arching)

Figure 32 illustrates the effect of the width-to-height ratio on the peak incident overpressure at incipient collapse for an unreinforced, two-way action, fixed-edge wall without arching. The two curves are for a vertical load in the plane of the wall of $P_v = 0$, and $P_v = 100$ lb/in. of wall, which is equivalent to about two story heights above the wall. For values of $L_u/L_v > 3$, the wall was assumed to respond primarily as a one-way rather than a two-way wall. For comparative purposes, the collapse pressure for a one-way action wall is also indicated in Figure 32.

The effect on the incipient collapse overpressure of the percentage of window opening in a two-way action wall, which is face-on to the blast wave, is shown in Figure 33 for three different room volumes. To calculate these values, it was assumed that the interior walls of the room did not fail during the collapse of the exterior wall. As can be seen, an increase in the window area from 15 to 35 percent of the wall area resulted in an increase in the incipient collapse overpressure of about 50 to 60 percent for the room volumes investigated.

Figure 34 shows the effect of the room volume on the incipient collapse overpressure of a two-way action, fixed edge wall for window openings of 15, 25 and 35 percent. For all three window areas, if the volume of the room is doubled from 1000 to 2000 cu ft, the incipient collapse overpressure is decreased by about one-third.

WALL PARAMETERS

$L_V = 8$ ft
 $L_H = 12$ ft
 $t_w = 8$ in.
 $f_r = 100$ psi
 $E = 1.0 \times 10^6$ psi
 $\gamma = 120$ pcf
 $L_{VW} = 0$
 $L_{HW} = 0$
 Support Case 2

LOAD PARAMETERS

$W = 1$ Mt
 $S = 10$ ft

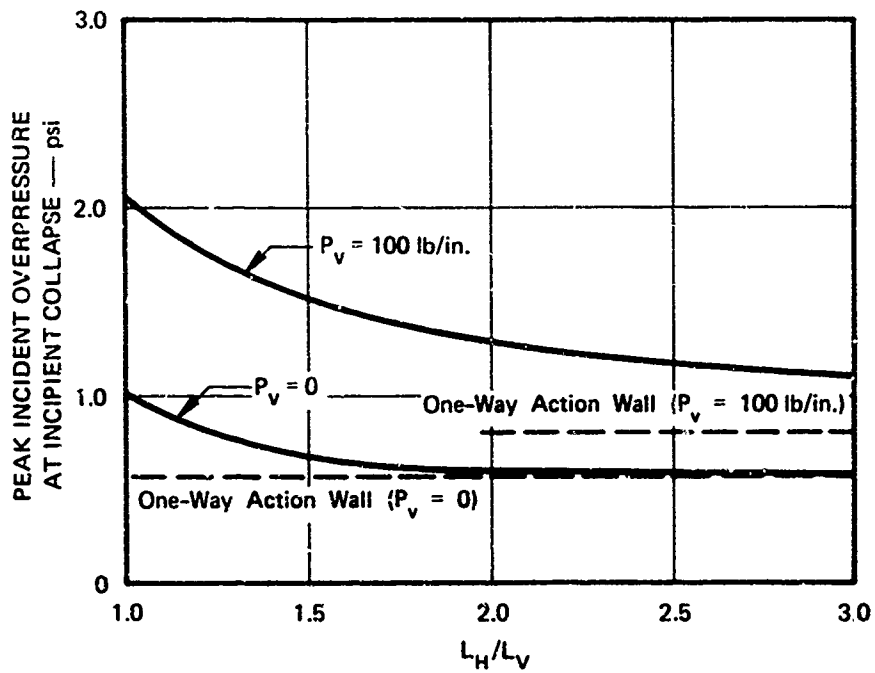
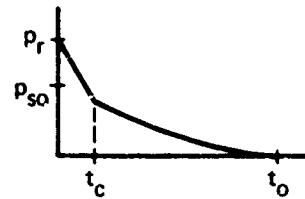


FIGURE 32 PEAK INCIDENT OVERPRESSURE AT INCIPIENT COLLAPSE VERSUS L_H/L_V RATIO

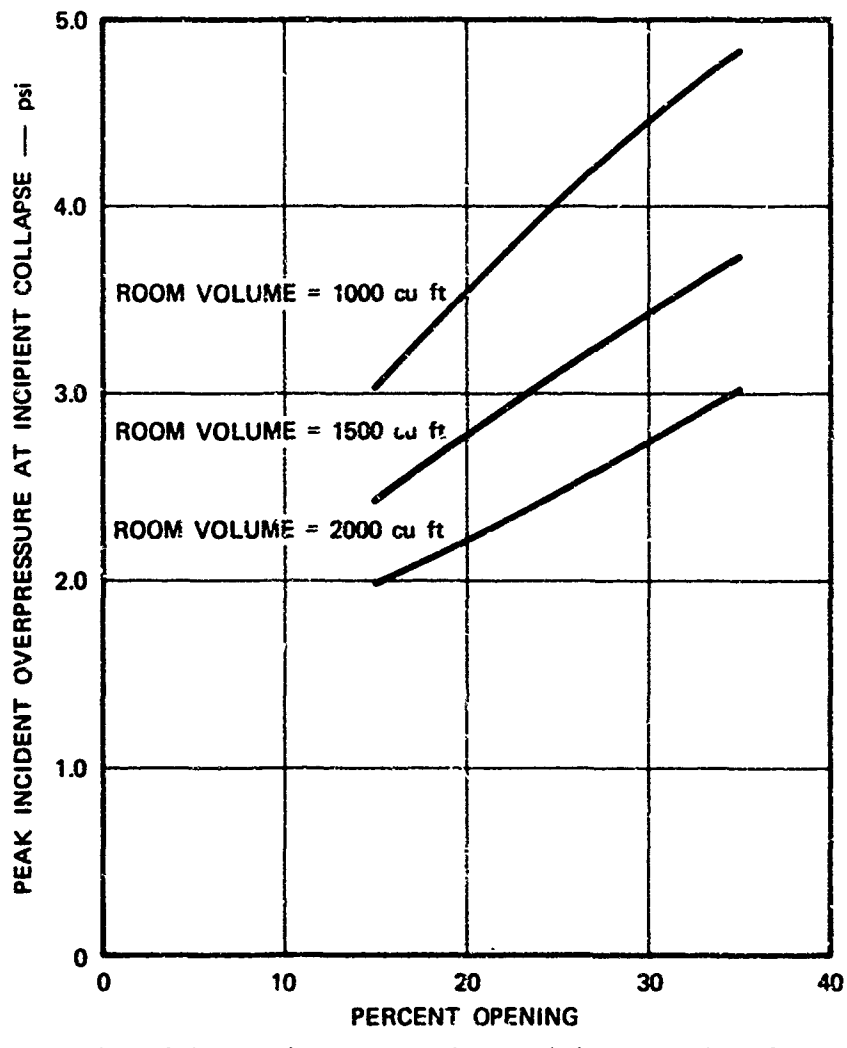
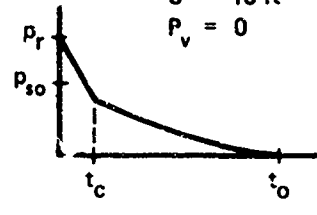
Two-Way Unreinforced Wall Without Arching

WALL PARAMETERS

- $L_V = 8$ ft
 - $L_H = 12$ ft
 - $t_w = 8$ in.
 - $f_r = 100$ psi
 - $E = 1.0 \times 10^6$ psi
 - $\gamma = 120$ pcf
 - $L_{V,\gamma} = 48$ in.
- Support Case 2

LOAD PARAMETERS

- $W = 1$ Mt
- $S = 10$ ft
- $P_v = 0$



(One window opening symmetrically located about centerlines of front wall. 3 msec delay in breaking.)

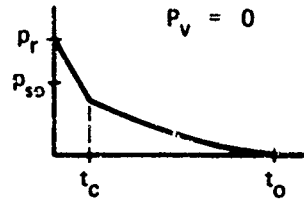
FIGURE 33 PEAK INCIDENT OVERPRESSURE AT INCIPENT COLLAPSE VERSUS PERCENT WINDOW OPENING Two-Way Unreinforced Wall Without Arching

WALL PARAMETERS

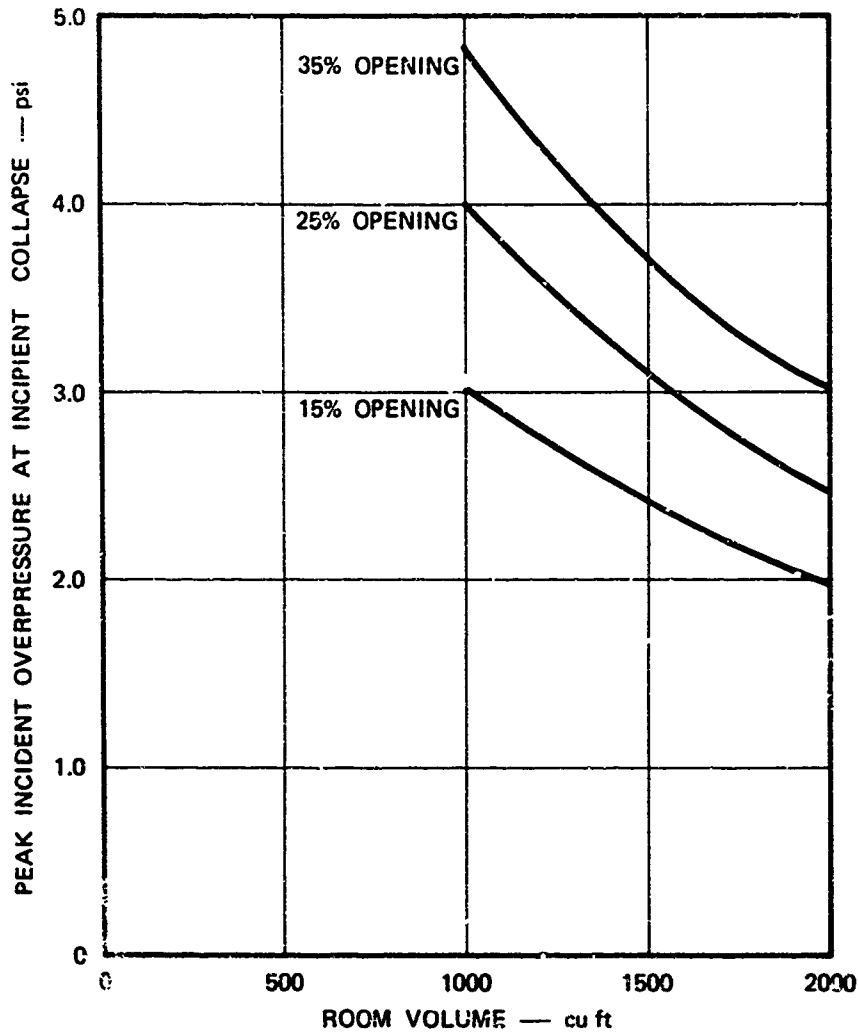
$L_V = 8 \text{ ft}$
 $L_H = 12 \text{ ft}$
 $t_w = 8 \text{ in.}$
 $f_r = 100 \text{ psi}$
 $E = 1.0 \times 10^6 \text{ psi}$
 $\gamma = 120 \text{ pcf}$
 $L_{VW} = 48 \text{ in.}$

LOAD PARAMETERS

$W = 1 \text{ Mt}$
 $S = 10 \text{ ft}$
 $P_V = 0$



Support Case 2



One window opening symmetrically located about centerlines of front wall. 3 msec delay in breaking.

FIGURE 34 PEAK INCIDENT OVERPRESSURE AT INCIPIENT COLLAPSE VERSUS ROOM VOLUME
 Two-Way Unreinforced Wall Without Arching

Unreinforced Concrete or Masonry Unit Wall (With Arching)

Figure 35 illustrates the effect of the width-to-height ratio on the incipient collapse overpressure for an unreinforced, two-way action, fixed-edge wall with arching. For an increase in the L_H/L_V ratio from 1 to 3, there is a decrease in the incipient collapse pressure of about 40 percent.

Figures 36 and 37 show the effect on the incipient collapse overpressure of the percent of window opening and the room volume, respectively. The effect of these parameters is much less for unreinforced two-way walls with arching than without arching.

Reinforced Concrete Wall

Figure 38 illustrates the effect of the width-to-height ratio on the incipient collapse overpressure for a two-way reinforced concrete wall. For an increase in the L_H/L_V ratio from 1 to 3, there is a corresponding decrease in the incipient collapse overpressure of about 40 percent; this is about the same as for the unreinforced masonry wall with arching.

Figures 39 and 40 show the effect on the incipient collapse overpressure of the percent of window opening and the room volume, respectively. This is about the same relative effect as was found for the unreinforced wall with arching.

Experimental Correlation

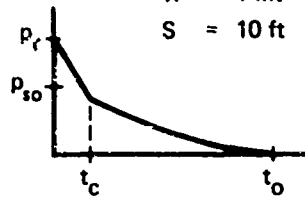
The approach used in this study for predicting the behavior of wall elements has been to develop rational analytical procedures that are consistent with the available experimental response observations. Wherever possible the test data are then used to provide a correlation with the analytical predictions.

WALL PARAMETERS

$L_V = 8$ ft
 $L_H = 12$ ft
 $t_w = 8$ in.
 $f'_m = 1000$ psi
 $E_m = 1.0 \times 10^6$ psi
 $\gamma = 120$ pcf

LOAD PARAMETERS

$W = 1$ Mt
 $S = 10$ ft



Rigid Supports

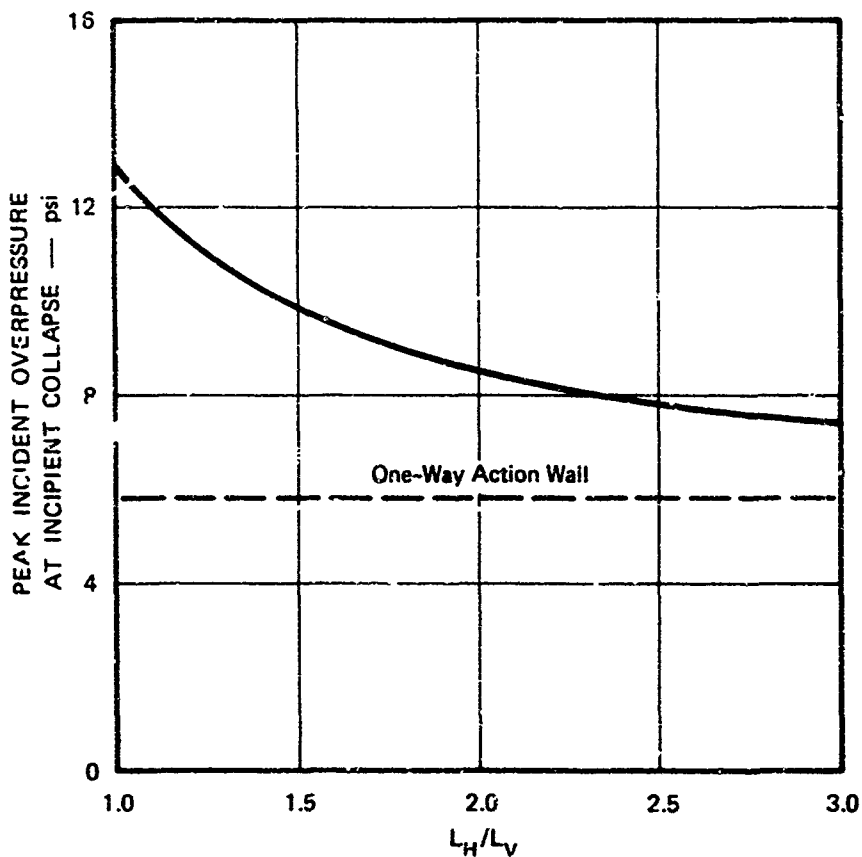


FIGURE 35 PEAK INCIDENT OVERPRESSURE AT INCIPIENT COLLAPSE VERSUS L_H/L_V RATIO

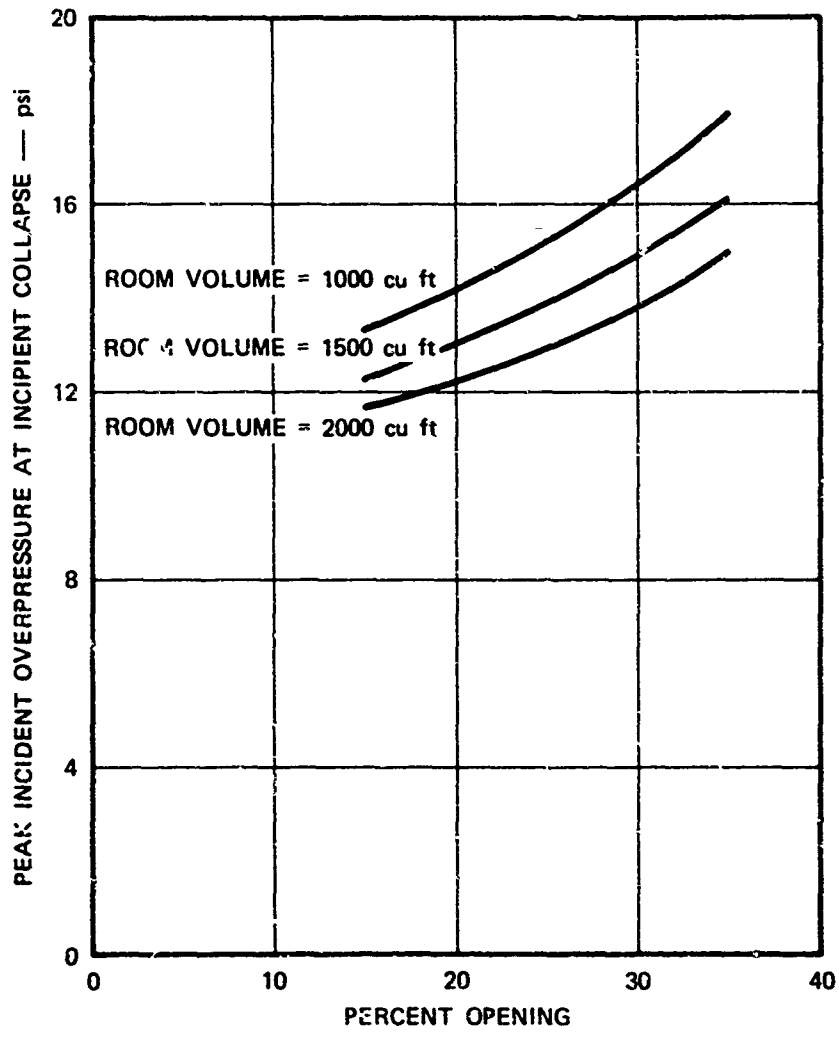
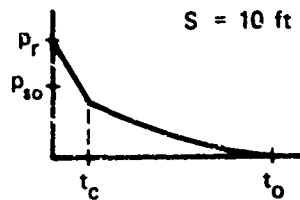
Two-Way Unreinforced Wall With Arching

WALL PARAMETERS

$L_V = 8 \text{ ft}$
 $L_H = 12 \text{ ft}$
 $t_w = 8 \text{ in.}$
 $f'_m = 1600 \text{ psi}$
 $E_m = 1.0 \times 10^6 \text{ psi}$
 $\gamma = 120 \text{ pcf}$
 Rigid Supports

LOAD PARAMETERS

$W = 1 \text{ Mt}$
 $S = 10 \text{ ft}$



One window opening symmetrically located about centerlines of front wall. 3 msec delay in breaking.

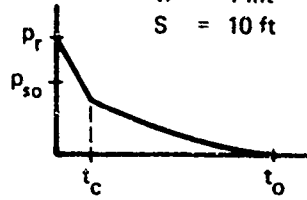
FIGURE 36 PEAK INCIDENT OVERPRESSURE AT INCIPIENT COLLAPSE VERSUS PERCENT WINDOW OPENING
Two-Way Unreinforced Wall With Arching

WALL PARAMETERS

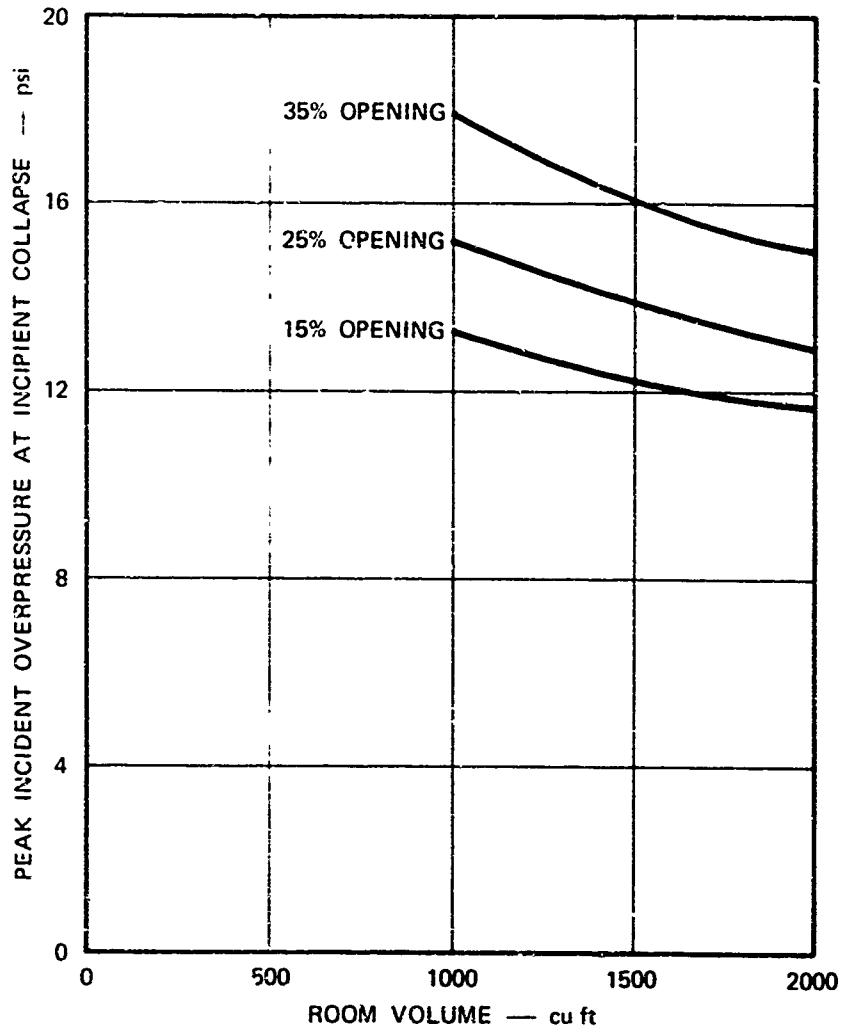
$L_V = 8 \text{ ft}$
 $L_H = 12 \text{ ft}$
 $t_w = 8 \text{ in.}$
 $f'_m = 1900 \text{ psi}$
 $E_m = 1.0 \times 10^6 \text{ psi}$
 $\gamma = 120 \text{ pcf}$

LOAD PARAMETERS

$W = 1 \text{ Mt}$
 $S = 10 \text{ ft}$



Rigid Supports



One window opening symmetrically located about centerlines of front wall. 3 msec delay in breaking.

**FIGURE 37 PEAK INCIDENT OVERPRESSURE AT INCIPIENT COLLAPSE
 VERSUS ROOM VOLUME
 Two-Way Unreinforced Wall With Arching**

WALL PARAMETERS

$L_V = 8 \text{ ft}$
 $t_w = 8 \text{ in.}$
 $f'_{dc} = 3750 \text{ psi}$
 $f_{dy} = 42,000 \text{ psi}$
 $\rho = 0.0025 \text{ (d = 7 in.)}$
 $\rho' = 0.0025 \text{ (d' = 1 in.)}$
 $L_{VW} = 0$
 $L_{HW} = 0$
 Support Case 2

LOAD PARAMETERS

$W = 1 \text{ Mt}$
 $S = 10 \text{ ft}$
 $P_V = 0$

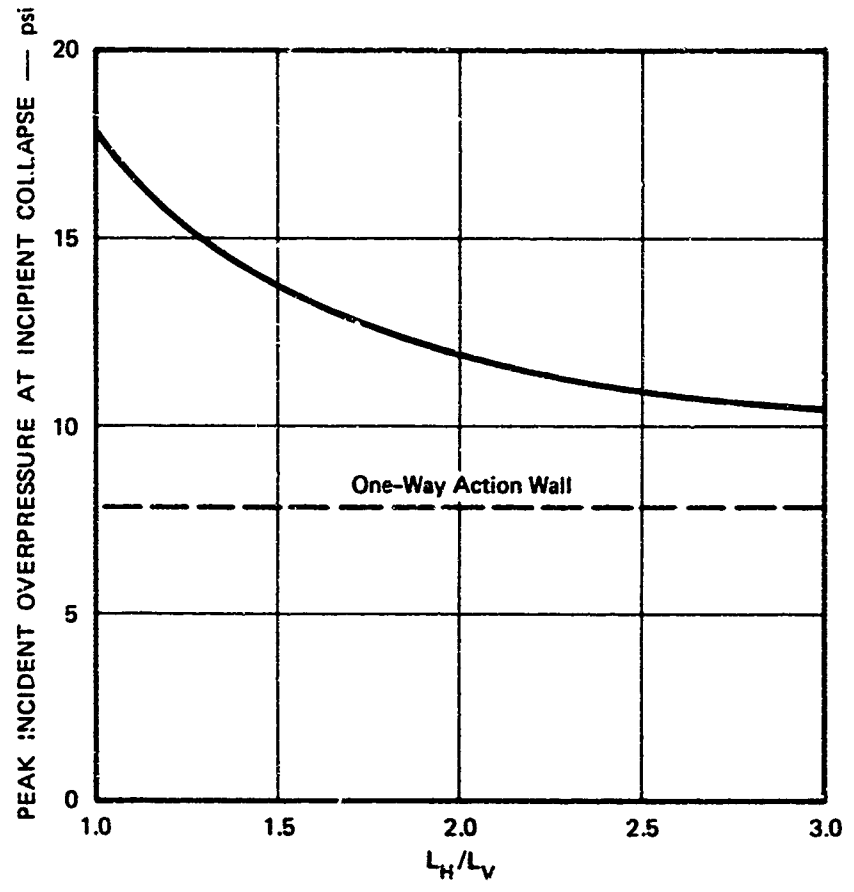
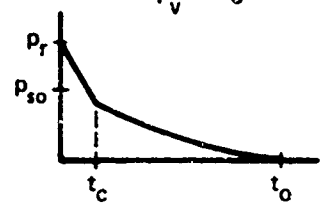


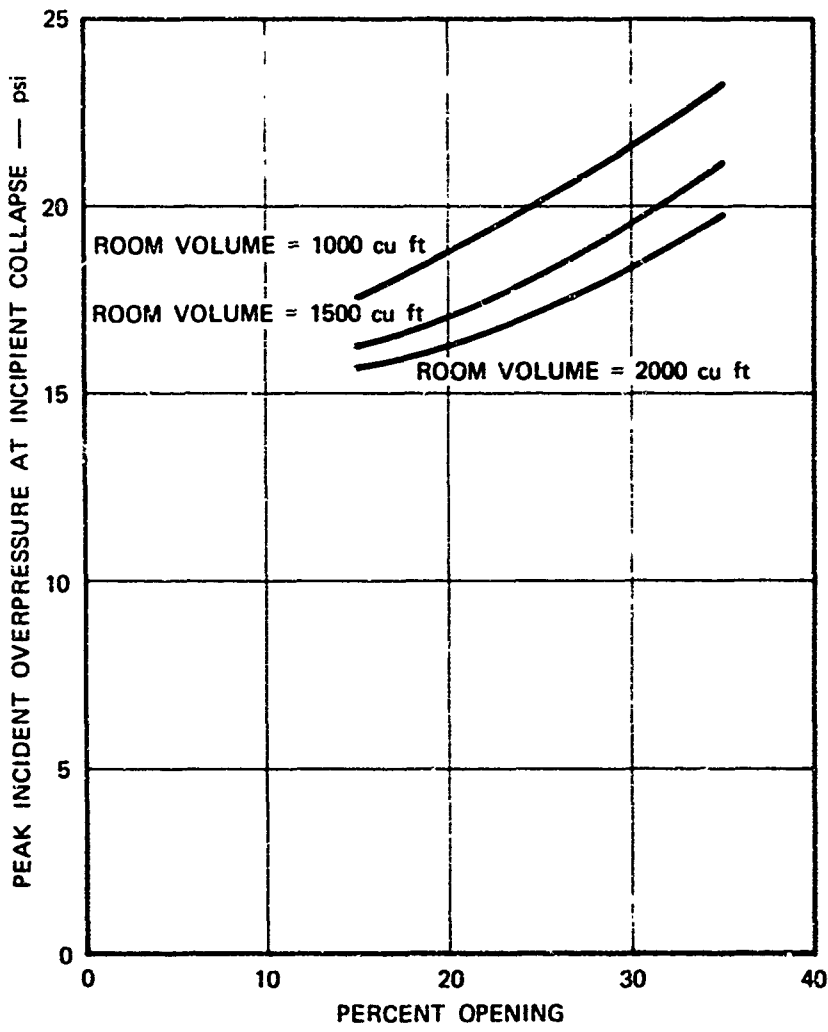
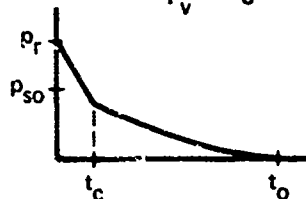
FIGURE 38 PEAK INCIDENT OVERPRESSURE AT
 INCIPIENT COLLAPSE VERSUS L_H/L_V
 RATIO
 Two-Way Reinforced Concrete Wall

WALL PARAMETERS

$L_V = 8$ ft
 $L_H = 12$ ft
 $t_w = 8$ in.
 $f'_{dc} = 3750$ psi
 $f_{dy} = 42,000$ psi
 $\rho = 0.0025$ ($d = 7$ in.)
 $\rho' = 0.0025$ ($d' = 1$ in.)
 $L_{VW} = 48$ in.
 Support Case 2

LOAD PARAMETERS

$W = 1$ Mt
 $S = 10$ ft
 $P_V = 0$



One window opening symmetrically located about centerlines of front wall. 3 msec delay in breaking.

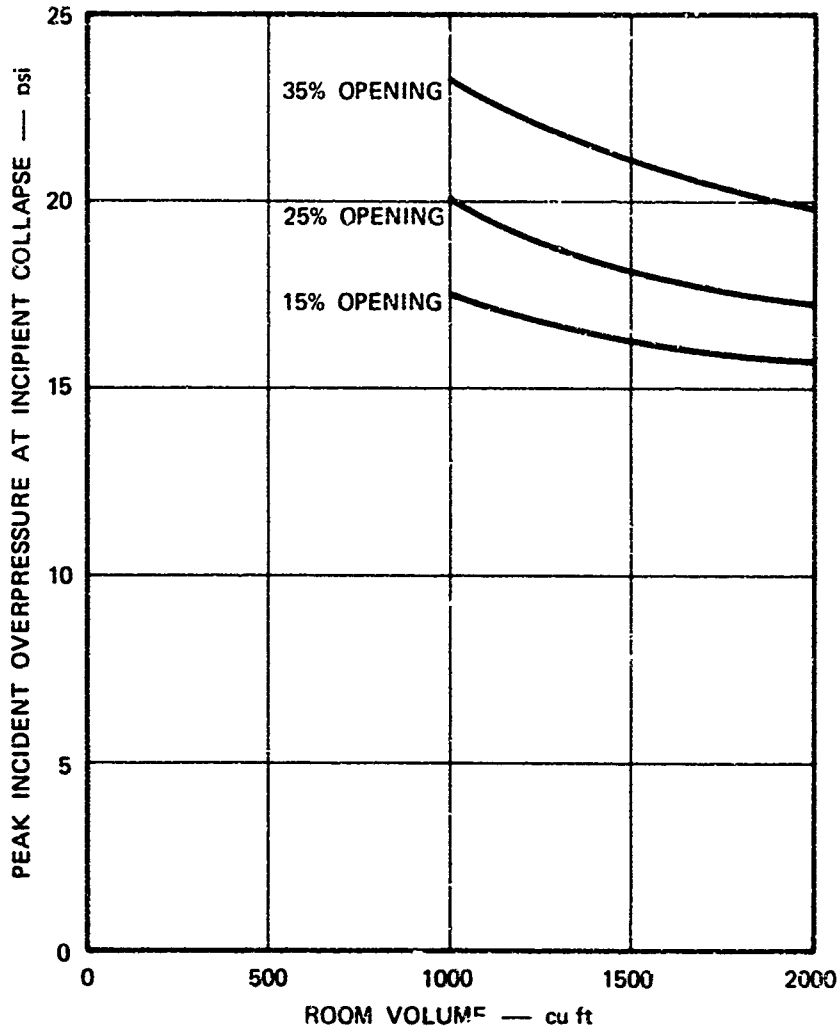
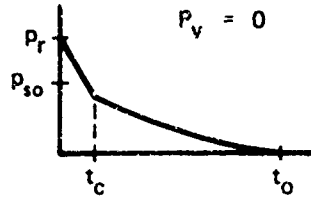
FIGURE 39 PEAK INCIDENT OVERPRESSURE AT INCIPIENT COLLAPSE VERSUS PERCENT WINDOW OPENING Two-Way Reinforced Concrete Wall

WALL PARAMETERS

LOAD PARAMETERS

$L_V = 8$ ft
 $L_H = 12$ ft
 $t_w = 8$ in.
 $f'_{dc} = 3750$ psi
 $f_{dy} = 42,000$ psi
 $\rho = 0.0025$ ($d = 7$ in.)
 $\rho' = 0.0025$ ($d' = 1$ in.)
 $L_{VW} = 48$ in.
 Support Case 2

$W = 1$ Mt
 $S = 10$ ft
 $P_V = 0$



One window opening symmetrically located about centerlines of front wall. 3 msec delay in breaking.

**FIGURE 40 PEAK INCIDENT OVERPRESSURE AT INCIPIENT COLLAPSE VERSUS ROOM VOLUME
Two-Way Reinforced Concrete Wall**

As discussed in Section IV, it is desirable that experimental data from controlled tests be used to verify a mathematical model. Unfortunately, for the dynamically loaded walls examined in this study, it was possible to provide such a correlation for only one case where response-time data were available. In general, however, even with experimental information available, certain data such as physical properties and precise load-time functions are either lacking or ill-defined. Therefore, a deterministic description of behavior cannot be generated for correlation with the experimental data. This is the primary problem with using the data obtained from nuclear field tests. For such cases, it was necessary to provide a probability distribution for the values of the unknown parameters. This meant that only the probability of occurrence of the incipient collapse pressure, rather than a specific deterministic value, could be compared with the experimental results.

During this program, it was possible to compare analytical predictions with experimental data obtained from a wall tested in the URS shock tunnel and with test walls and houses in nuclear field tests. The results of these comparisons are presented in the following subsections.

Laboratory Wall Test

The dynamic response data from a test of a 12-in. thick brick wall was obtained from URS Research Company for comparison with the theoretically predicted response prepared during this study. The 8-ft high by 12-ft wide wall was located in the URS shock tunnel and mounted in a steel frame that provided simple support at the top and bottom edges while permitting the side edges to move freely. Since the wall blocked the cross section of the tunnel, it was subjected to the full reflected overpressure on the front face, while a back face loading was prevented until the wall collapsed. The load applied to the wall by the blast wave

approximated a step pulse of 4 psi, which decayed linearly to 3.3 psi at 69 msec and to zero at 102 msec.

For this analysis, the most useful test information was the velocity-time data measured at the horizontal centerline of the wall; the velocity gage recorded only during the first 4 in. of wall movement. The experimental and theoretical velocity-time data are reproduced in Figure 41. During the early times, e. g., at 20 msec, there is a difference of about 100 percent between the experimental and predicted velocity. However, at 90 msec, the predicted velocity is only about 15 percent higher than the measured velocity.

Although the correlation between the theoretical and experimental is excellent at the higher wall deflections (theoretical wall deflection equals 8.5 in. at 90 msec), the reason for the large discrepancy during the early times is not actually known, but it could be the result of several factors. Since the analysis was simplified to treat the wall as a single-degree-of-freedom system, the higher response modes were not included. This could result in relatively large differences in response during the early portion of the elastic phase, where the maximum deflection before cracking of an unreinforced masonry wall is less than 0.1 in. If the model correctly predicts the wall response during the decaying phase, the effect of the differences in velocity during the early times would become relatively less significant as the wall deflection increased - this is shown in Figure 41 to be the case. On the other hand, the supports for the test wall and the velocity gage mount were independent of each other. Therefore, it is possible that a small differential motion between gage and wall supports would result in a pseudo-wall velocity. For example, the experimental velocity trace shows a change in slope at about 18 msec, which could be related to the formation of the primary horizontal crack in the test wall. This

WALL PARAMETERS

Simple One-Way Support

- $L_v = 8 \text{ ft}$
- $r_w = 12 \text{ in.}$
- $f_r = 200 \text{ psi}$
- $E_m = 0.5 \times 10^6 \text{ psi}$
- $\gamma = 120 \text{ pcf}$

LOAD PARAMETERS

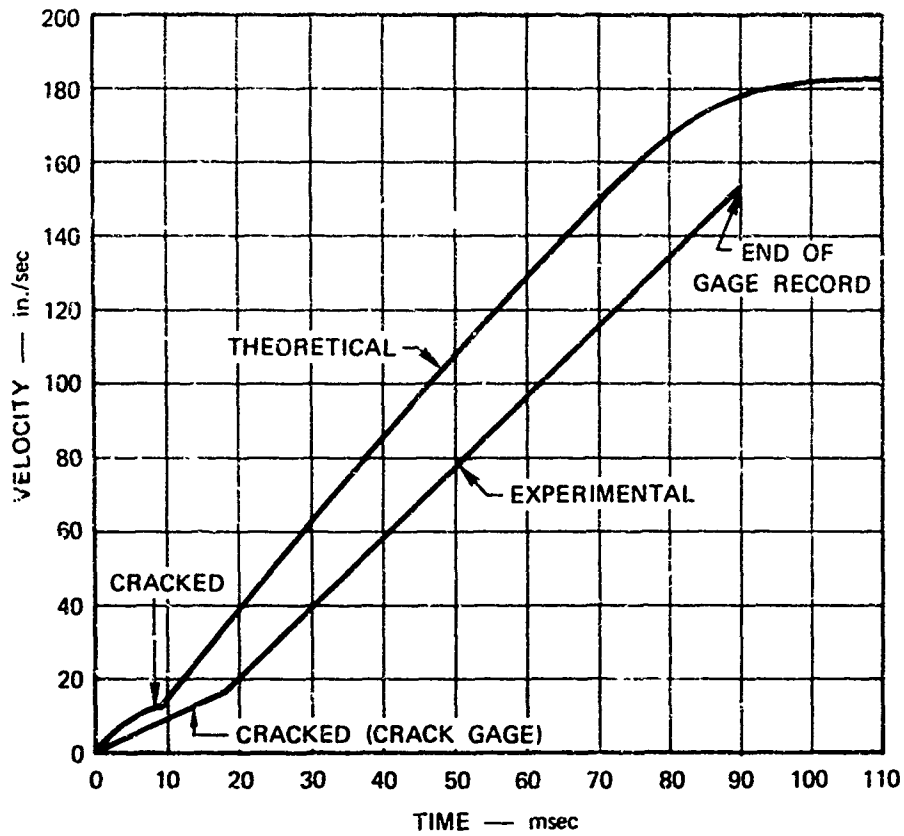
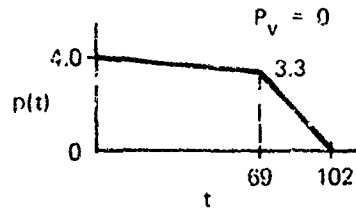


FIGURE 41 VELOCITY VERSUS TIME FOR ONE-WAY SIMPLY SUPPORTED BRICK WALL

6

corresponds to a time to first crack of 14 msec, as measured experimentally by an independent crack gage, and a time of 8.5 msec as indicated by the analytical prediction. If the velocity gage time scale were arbitrarily corrected by the difference between the theoretical time to cracking and the experimental time indicated by the velocity gage, the predicted velocity at 20 msec would be about 30 percent greater than the measured velocity, rather than the 100 percent mentioned previously.

Field Test Wall Panels

References 18 and 19 contain the most comprehensive field test data available for correlation with the analytical prediction method developed in this study. The test set-up consisted of a series of reinforced concrete support structures, constructed of cells into which various types of walls were built (Figure 42). The test structures resembled long, low, narrow buildings, although the design permitted failure of individual test wall panels without interference with adjacent panels or failure of the support structure. Because of the method of constructing the wall panels, and the stiffness of the support structure, one- or two-way arching action was induced in all walls.

The results of the test for eight types of concrete block or brick masonry walls were used for comparison with the analytical predictions made in this study. The probability of occurrence of the incipient collapse overpressure of each wall was calculated by the method outlined in Section IV, the details of which are presented in Appendix C.

A summary of the eight walls analyzed and their physical properties is given in Table 3. The results of the statistical analyses are summarized in Table 4 and also shown graphically in Figure 43. A brief discussion of the predictions for each wall type, together with a comparison to the field test results, follows:



SOURCE: Ref. 18

FIGURE 42 VIEW OF ARCHING WALL PANEL TEST STRUCTURES

Table 3

PHYSICAL PROPERTIES OF TEST WALLS

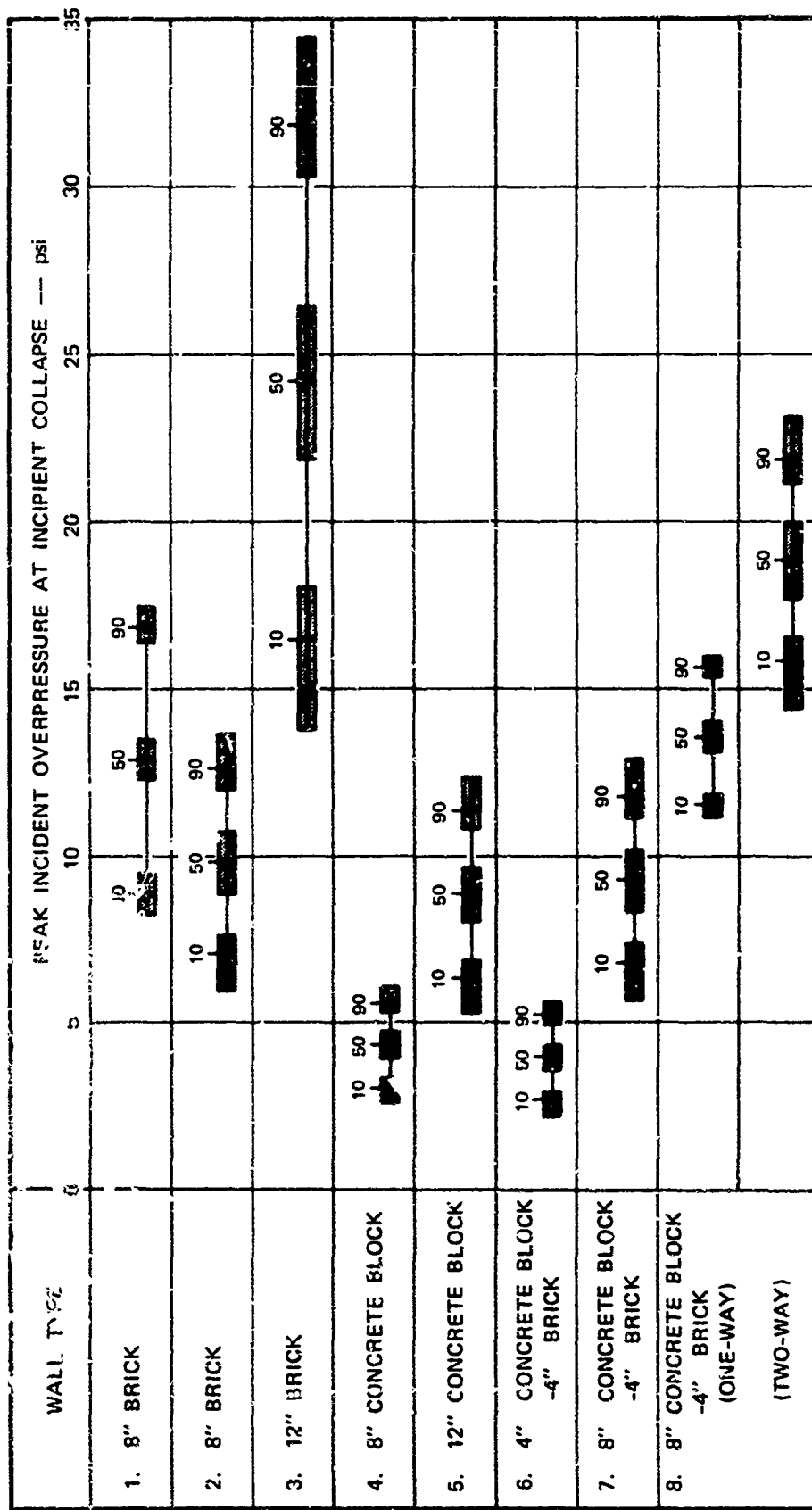
Wall Type	Description	t_w (in.)	L_y (in.)	L_x (in.)	γ (pcf)	t_f (in.)	f_c (psi)		α		Percent Opening	S (ft)		Remarks
							Mean	Std. Dev.	Mean	Std. Dev.		Mean	Std. Dev.	
1	8 in. brick	8	105	165	120	--	2000	600	1000	300	0	10	--	Ref. 18--walls 3.5 ac, 3.5 bf, 3.5 ce
2	8 in. brick	8	120	192	120	--	2000	600	1000	300	0	11	--	Ref. 19--wall 6 (a,c)
3	12 in. brick	12	120	192	120	--	2000	600	1000	300	0	11	--	Ref. 19--wall 3 (a,c)
4	8 in. concrete block	8	120	192	80	1.5	1200	350	1000	300	0	11	--	Ref. 19--wall 2 (a,c)
5	12 in. concrete block	12	120	192	80	1.75	1200	350	1000	300	0	11	--	Ref. 19--wall 7 (a,c)
6	4 in. concrete block --4 in. brick	8	120	192	100	1.375	1200	350	1000	300	0	11	--	Ref. 19--walls 5, 8, 11 (a,c)
7	8 in. concrete block --4 in. brick	12	120	192	100	1.5	1750	450	1000	300	0	11	--	Ref. 19--walls 3, 4, 10 (a,c)
8	8 in. concrete block --4 in. brick	12	120	192	100	1.5	1750	450	1000	300	19	7.0	2.1	Ref. 19--walls 1, 4-9, 11-14, 16 (b,d)

Table 4

SUMMARY OF STATISTICAL ANALYSES OF ARCHING WALLS
(Overpressure, psi)

Wall Type	Description	Mean		Standard Deviation		95 Percent		10 Percent		90 Percent		Remarks	
		Value	Confidence Interval	Value	Confidence Interval	Value	Confidence Interval	Value	Confidence Interval	Value	Confidence Interval		
1	8 in. brick (105 in. x 165 in.)	12.91	12.30	13.52	3.07	2.70	3.57	8.93	8.33	9.15	16.85	17.19	0 of 7 failed at 1.2 and 7.3 psi; 1 of 1 failed at 12 psi.
2	8 in. brick (120 in. x 192 in.)	9.84	8.93	10.75	2.16	1.69	3.01	7.07	5.98	7.67	12.61	13.69	0 of 1 failed at 1.5 psi; 1 of 1 failed at 8.1 psi
3	12 in. brick	24.20	21.91	26.48	6.01	1.79	8.08	16.19	13.83	18.06	31.93	31.76	0 of 1 failed at 1.5 psi; 1 of 1 failed at 8.1 psi
4	8 in. concrete block	4.37	3.96	4.77	0.96	0.75	1.81	3.13	2.65	3.10	5.60	5.33	0 of 1 failed at 4.5 psi
5	12 in. concrete block	8.88	8.05	9.71	1.97	1.51	2.74	6.35	5.36	6.90	11.10	12.35	1 of 3 failed at 4.5 psi
6	4 in. concrete block --4 in. brick	3.97	3.60	4.35	0.99	0.79	1.33	2.70	2.26	2.96	5.25	5.68	2 of 2 failed at 1.5 psi
7	8 in. concrete block --4 in. brick	9.30	8.38	10.23	1.92	1.46	2.81	6.81	5.71	7.13	11.77	11.18	0 of 3 failed at 4.5 psi; 3 of 3 failed at 8.1 psi
8	8 in. concrete block --4 in. brick (One-way) (Two-way)	13.57	13.11	14.03	1.59	1.40	1.85	11.53	11.20	11.78	15.61	15.91	0 of 12 failed at 4.5 psi; 0 of 12 failed at 8.1 psi
		18.81	17.69	19.94	2.35	1.78	3.13	15.81	14.42	16.53	21.82	23.21	

* Confidence limits for the 10 and 90 percent probability values are somewhat less than 95 percent.



NOTE: Values shown above are peak incident overpressures for 10, 50, and 90 percent probabilities of collapse. Blocked areas represent confidence limits for the above values.

FIGURE 43 STATISTICAL ANALYSIS OF INCIPIENT COLLAPSE OVERPRESSURE FOR ARCHING WALLS

Wall Type 1 - 8 in. Brick Wall. Only the results of the analysis of this 105 in. high by 165 in. wide wall will be summarized here, since a detailed analysis is contained in Appendix C. The values obtained for the 10, 50, and 90 percent probabilities of collapse were 8.9, 12.9, and 16.8 psi, respectively. These compare fairly well, although perhaps somewhat on the high side, with the field test results (Ref. 18), which showed slight damage occurring at 7.1 psi and collapse at 12 psi.

Wall Type 2 - 8 in. Brick Wall. This wall is similar to wall type 1, except that the dimensions are 120 in. high by 192 in. wide. The results obtained for the 10, 50, and 90 percent probability values were 7.1, 9.8, and 12.6 psi, somewhat lower than the corresponding values for the first wall type. The field test results (Ref. 19) showed that the wall tested at 4.5 psi did not fail, while the wall tested at 8.4 psi collapsed. The predicted results again agree fairly well with the test results, although possibly on the high side.

Wall Type 3 - 12 in. Brick Wall. The results obtained for the 10, 50, and 90 percent probability values were 16.5, 24.2, and 31.9 psi, respectively. These values are substantially different than the field test results (Ref. 19), where the wall tested at the 8.4 psi overpressure level collapsed. A possible explanation of this rather wide difference between the predicted and test results is indicated by an examination of the field test results. Pictures, such as Figure 44, show that a failure occurred on a nearly vertical plane normal to the wall near the center of the horizontal span. This indicates that arching did not develop in the vertical direction, and, therefore, the primary resistance of the wall was caused by one-way horizontal arching. If the wall is analyzed using the mean values of f'_m and E_m and assuming that the wall arches in the horizontal direction, the predicted incipient collapse



SOURCE: Ref. 19
FIGURE 44 PICTURE OF 12 IN. BRICK WALL PANEL TEST

overpressure is 6.2 psi. This is in much closer agreement with the field test results. It was also noted in the test report that failure occurred, at least partially, along a diagonal plane, which indicates the possibility of a shear failure. This mode of failure was not investigated in the study herein.

Wall Type 4 - 8 in. Concrete Block Wall. The predictions for the 10, 50, and 90 percent probability values were 3.1, 4.4, and 5.6 psi. Field test results (Ref. 19) showed failure at the 4.5 psi overpressure level, indicating a good agreement between the analytical and test results.

Wall Type 5 - 12 in. Concrete Block Wall. The results obtained for the 10, 50 and 90 percent probability values were 6.4, 8.9, and 10.4 psi. These values disagree with the field test results (Ref. 19) where the wall failed when subjected to 4.5 psi overpressure. The reason for the disagreement is not known although it may possibly have resulted from the assumed resistance function, which is only approximate for arching walls constructed of hollow block masonry.

Wall Type 6 - 4 in. Concrete Block - 4 in. Brick Wall. The results obtained for the 10, 50, and 90 percent probability values were 2.7, 4.0, and 5.2 psi, which are in good agreement with the field test results (Ref. 19) in which two walls of the same type failed when subjected to 4.5 psi overpressure.

Wall Type 7 - 8 in. Concrete Block - 4 in. Brick Wall. The height of the wall was 120 in. with a length of 192 in., resulting in a height-to-length ratio of 0.625. The values used for the compressive strength were obtained from materials strength field data, which showed a compressive strength for the 8 x 8 x 16 in. hollow masonry units of 1050 psi

based on the gross section. Since the net area is approximately 60 percent of the gross section, this results in a value of 1750 psi for the compressive strength of the material. Assuming a further 30 percent reduction in strength as a result of the effects of workmanship, a final value of 1200 psi was used for the mean compressive strength. A standard deviation of 350 psi was obtained by assuming the 5 and 95 percent probability values to be 600 and 1800 psi, respectively. The results obtained for the 10, 50, and 90 percent probability values were 6.8, 9.3, and 11.8 psi, respectively. These correspond to the field test results (Ref. 19), in which none of the three walls tested at 4.5 psi failed, while all three walls tested at 8.4 psi failed. Again, this indicates fair agreement, although slightly on the high side.

Wall Type 8 - 8 in. Concrete Block - 4 in. Brick Wall (19 percent openings). This type of wall was identical to the preceding wall type, except that it contained 19 percent window openings. Because of these openings, it was not known whether the wall would be able to develop two-way structural action. Therefore, in addition to the analysis for two-way arching, the wall was analyzed for one-way arching action between the top and bottom supports. The results obtained for the 10, 50, and 90 percent probability values were 11.5, 13.6, and 15.6 psi for one-way arching and 15.8, 18.8, and 21.8 psi for two-way arching. These results indicate a substantial increase in the incipient collapse overpressure of the wall (for either one-way or two-way arching) as a result of the presence of window opening. The field test results (Ref. 19), although substantiating the results of both these analyses to some extent, do not indicate whether two-way arching was developed, since none of the 12 walls tested at 8.4 psi failed.

Overall, the results obtained from the statistical analysis of the eight wall types agree fairly well with the results of the field tests, although the predictions were generally somewhat on the high side. The discrepancies noted could be because of the lack of valid material property data for the test walls. Also, the variation may be related to the effect of two-way arching action, since little experimental information was available for the development of the resistance function. As noted for the 12 in. concrete block wall, there is also the possibility of a wall failing in a different mode than assumed in the analysis. For arching walls, this would result in lower incipient collapse pressures than those predicted.

Field Test Brick Houses

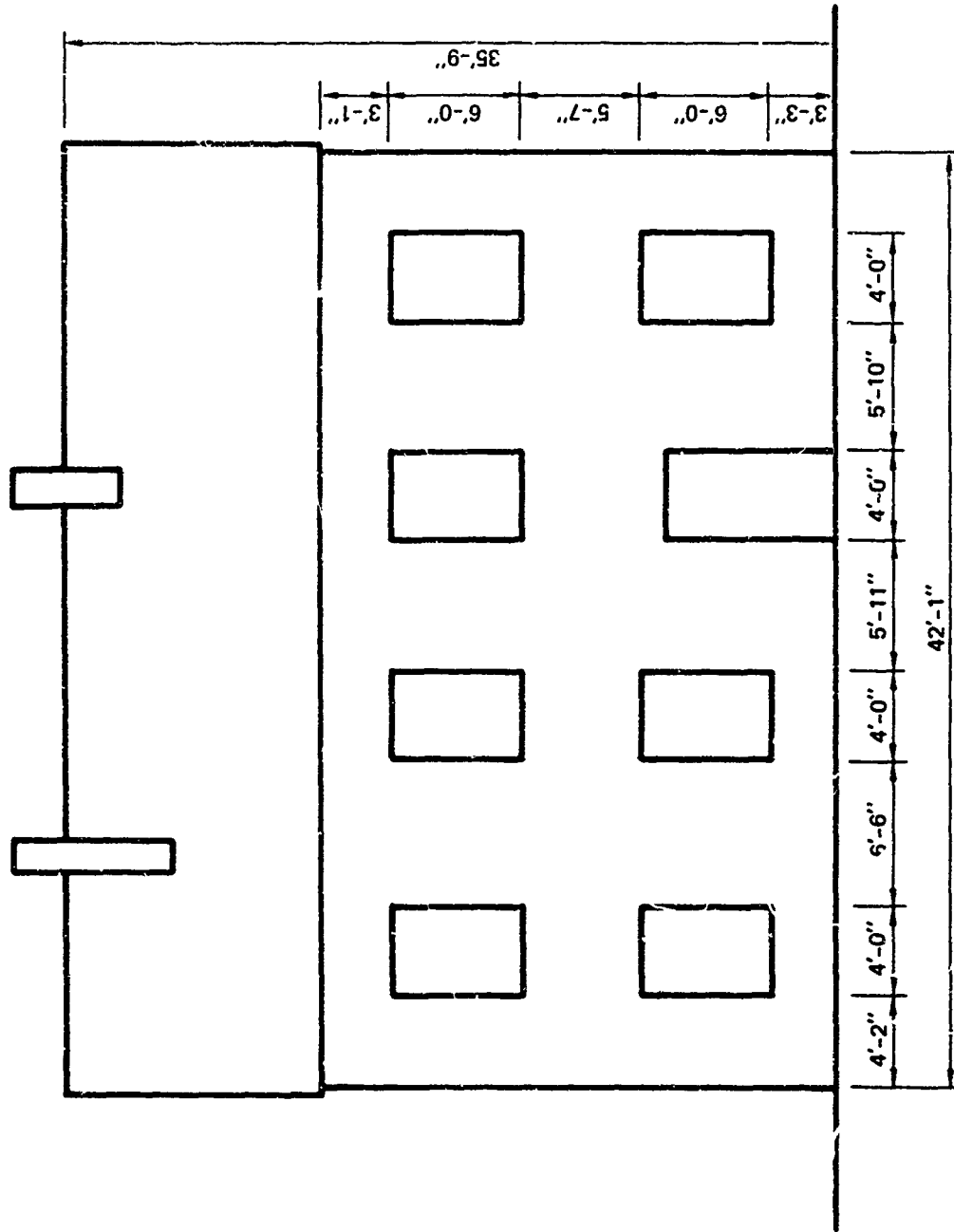
The results of nuclear field tests of two types of brick load-bearing wall houses were available for comparison with the predictions from the analytical two-way action models developed for unreinforced masonry walls without arching. The first type was a two-story house representing typical European construction. Two identical houses of this type were tested during Operation GREENHOUSE, one at an overpressure level of 3.4 psi and the other at an overpressure of 8.7 psi (Ref. 22). The second type was a two-story house representing typical U.S. construction practice. Two of these houses were tested during Operation TEAPOT, at overpressure levels of 1.7 and 5.1 psi (Ref. 23).

The masonry walls of the houses with the European type of construction were generally much thicker than in U.S. practice. Also, an abundance of lumber was used in the floors and roofs, and the use of sand as insulation in ceilings was markedly different from U.S. construction. These differences result in the European house being significantly stronger than its U.S. counterpart, as indicated both by the test results

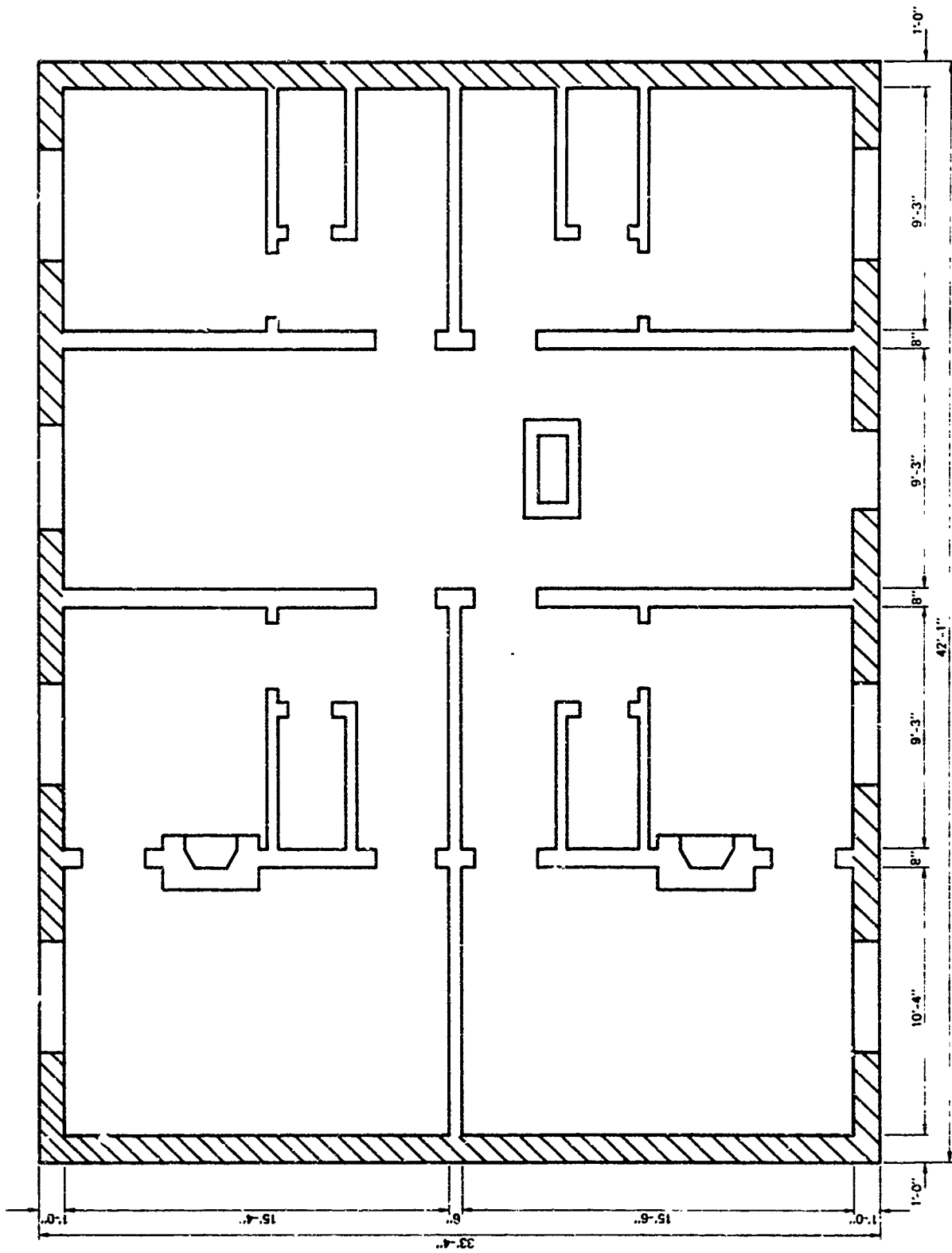
and the analyses. Predicted incipient collapse overpressures were 6.2 and 2.4 psi, respectively. Other differences between the two types of houses that tended to make the European house stronger included the use in the latter of 8-in. thick brick interior load-bearing walls, which served as shear walls dividing the front wall into essentially four continuous segments over rigid supports in both the upper and lower stories. Finally, the ceiling and floor joists in the European house were supported by the front and rear walls, compared with the side walls in the U.S. house, which placed a larger vertical load on the front walls of the European house.

In subsequent subsections, a deterministic analysis of each type of house is presented, and the results are compared with the field test data. Following this, the results of a statistical analysis to determine the probability of occurrence of the incipient collapse overpressure of the houses are described.

Brick Houses (GREENHOUSE). Front elevation and plan views of the brick load-bearing wall houses, representative of European construction, are shown in Figures 45 and 46. The houses are approximately 42 ft by 33 ft in plan and 36 ft high. The exterior walls are 12-in. thick brick. Three 8 in. brick interior partitions run transversely to the side walls, and a load-bearing partition, constructed of 2 x 6 in. studs on 12 in. centers covered by 1/2 in. of plaster on metal lath, runs longitudinally along the center of the house. Roof rafters (2 x 8 in. on 12 in. centers) and ceiling joists (2 x 10 in. on 12 in. centers) run parallel to the side walls and are supported by the front and rear walls and the longitudinal load-bearing partition.



SOURCE: Ref. 22
 FIGURE 45 FRONT ELEVATION OF TWO-STORY BRICK HOUSE
 (GREENHOUSE)



SOURCE: Rpt 22

FIGURE 46 PLAN VIEW OF TWO-STORY BRICK HOUSE (GREENHOUSE)

Test Results

The two houses were tested at overpressure levels of 3.4 and 8.7 psi. The house located at the 3.4 psi overpressure level was about 10 percent damaged (100 percent damage taken as complete collapse) with the main damage consisting of the windows being blown out, some spalling of interior partitions, and stripping of the roof. With the exception of cracks in about 80 percent of the fill-in brickwork under the eaves and a horizontal crack in the gable of the right wall, there was no damage to any of the brick walls.

The house at 8.7 psi overpressure was about 40 percent damaged. Figures 47 and 48 show front and left-side views of the post-test damage. The front and rear walls were relatively undamaged, remaining in place with the exception of the upper left corner of the front wall. The front wall cracked vertically along the 8 in. brick shear walls at either side of the lower hall. In contrast, the side walls were almost completely demolished, both failing outward. The difference in damage was stated to be "... probably due to the fact that the front walls receive additional support from the first and second floor ceiling joists, whereas the side walls are comparatively free standing against inside loads. The pressure inside the front rooms could have reached a level higher than side-on due to reflection of the blast wave entering the front window, thus probably causing the net loading on the side walls to be outward."

Analysis

Front Wall. The complexity of these brick load-bearing wall structures makes a precise analysis impossible. However, by making certain assumptions, an estimate of the incipient collapse overpressure



SOURCE: Ref. 22

FIGURE 47 POST-SHOT PICTURE OF FRONT OF BRICK HOUSE LOCATED AT
8.7 PSI OVERPRESSURE (GREENHOUSE)

NOT REPRODUCIBLE



COURCE: Ref. 22

FIGURE 48 POST-SHOT PICTURE OF LEFT SIDE OF BRICK HOUSE LOCATED AT 8.7 PSI OVERPRESSURE (GREENHOUSE)

can be made with the procedures developed in this study. The presence of the 8 in. brick interior partitions and first floor ceiling divide the front wall into eight continuous panels over essentially rigid supports. Since these panels are of approximately equal dimensions, with each containing an opening, they are believed to be about the same strength. An approximation of the strength of the front wall may therefore be obtained by analyzing any of the panels. The panels analyzed herein were the upper and lower panels adjacent to the left edge of the house. These panels were selected because the interior rooms behind the panels were not complicated by the presence of closets or other obstructions, thus giving more credence to the values obtained from the interior room pressure calculations.

The panels were assumed to behave as two-way walls fixed on four edges. The properties of the wall are summarized as follows:

L_v	=	126 in.
L_H	=	126 in.
t_w	=	12 in.
γ	=	120 pcf
E_m	=	1,000,000 psi
f_r	=	100 psi
P_v	=	31.4 lb/in. (upper story); 111.3 lb/in. (lower story)
L_{vH}	=	72 in.
L_{HH}	=	48 in.

Since information regarding the modulus of elasticity, E_m , and the modulus of rupture, f_r , was not available for the two houses tested, the values above were chosen from studies of other tests as being "typical" values of brick structures employing good construction practice.

The exterior loading was assumed to result from an idealized nuclear blast wave, as shown in Figure 1. The parameters required to define the loading are summarized as follows:

$$W = 47 \text{ kt}$$

$$P_0 = 14.7 \text{ psi}$$

$$c_0 = 1120 \text{ fps}$$

$$S = 7.1 \text{ ft (upper story); } 7.3 \text{ ft (lower story)}$$

The clearing distance, S , was determined by the procedure outlined in Section II. The weighted average clearing distance, which was considered to be a minimum, was calculated to be 2.78 ft for the upper panel and 3.16 ft for the lower panel. The maximum clearing distance, assumed to be equal to the greatest distance from any point of the panel to the nearest edge of the building where clearing could occur, was determined to be 11.42 ft for both panels. The maximum and minimum values of S were then averaged to obtain the values used in the analysis.

The interior wall loading was determined using the room-filling process described in Section II. A failure time of 3 msec was assumed for the front windows, during which time the interior pressures remained at zero (Refs. 2 and 24). The load-bearing partition along the center of the house was assumed to remain standing during the time of collapse of the front wall. This assumption was made since it was felt that even if the partition failed at the pressure corresponding to the incipient collapse overpressure of the front wall, the time required for failure would be such that the effect of the resulting change in the interior pressure on the behavior of the front wall would be insignificant. The net load on the front wall was then obtained by subtracting the interior load from the exterior load.

The upper and lower panels were analyzed with the net load obtained as noted above and with the two-way action model developed in Section III to determine the resistance function for unreinforced masonry walls without arching. The peak incident overpressures at incipient collapse were found to be 6.2 psi for the upper panel and 7.8 psi for the lower panel. These values agree fairly well with the test results, although they may be slightly low since the front wall of the test house remained standing at 8.7 psi, except for the upper lefthand corner, as shown in Figure 47. Possible reasons for this discrepancy may be differences between the actual and assumed values for the modulus of rupture or clearing distance, the unknown effect of failure of the side walls on the interior pressure build-up, or some other factor.

Side Wall. The test results for the house tested at 8.7 psi showed that the side walls failed outward. To determine whether the model developed herein would indicate such behavior, an analysis of one side wall was made. To make this analysis, several assumptions were required in addition to those made for the front wall. Since the computer program used for the analysis was not developed to solve for the incipient collapse overpressure for a side wall, only its behavior at specific overpressure levels of interest was determined.

The net load on the side wall was determined by calculating the exterior pressure-time function using the procedure given in Ref. 12 and subtracting the interior pressure found from the room-filling process discussed in Section II. The determination of the interior pressure was complicated, since the load-bearing partition failed during the loading process, thus changing the size of the room in which room filling takes place. Since the method used to calculate the interior pressure was unable to account for a change in room volume during the analysis (even if it could account for such a change, the exact time of failure

of the partition was unknown), the interior pressure was determined for two cases; one in which the interior partition did not fail and the other as if the partition was nonexistent (thus creating a larger volume room). The resulting analytical net load functions for these two cases are shown in Figures 49 and 50. The analytical results from these two extremes are felt to bracket the actual net load on the sidewall.

The manner in which the side wall responds to this net load is extremely complicated. Although the net load on the wall is seen to be initially inward, the interior pressure soon becomes greater than the exterior pressure, resulting in a net outward load. This outward load continues for the duration of the blast wave, although decreasing in magnitude. This results in a similar behavior of the side wall, i.e., it initially deflects inward and at some later time changes direction and deflects outward. Depending on the magnitude and duration of the inward and outward portions of the net load, failure may occur in either direction. To use the previously developed computer program for analyzing the behavior of the side wall under such a loading, it was necessary to treat the inward and outward portions of the net load as if they acted separately on the wall.*

The support conditions during this behavior vary, depending on the direction in which the wall is responding. During inward motion of the wall the floors, because of their axial stiffness, act essentially as rigid supports. Thus, for this phase, the walls were analyzed as being fixed at the ground level and at the first and second floor ceilings.

* The computer program used in the analysis has not yet been developed sufficiently to analyze a wall that deflects initially in one direction and, if failure does not occur in that direction, subsequently deflects in the other direction. Therefore, the results from an analysis, in which the two portions are treated separately, must be considered as merely a first approximation of the actual behavior.

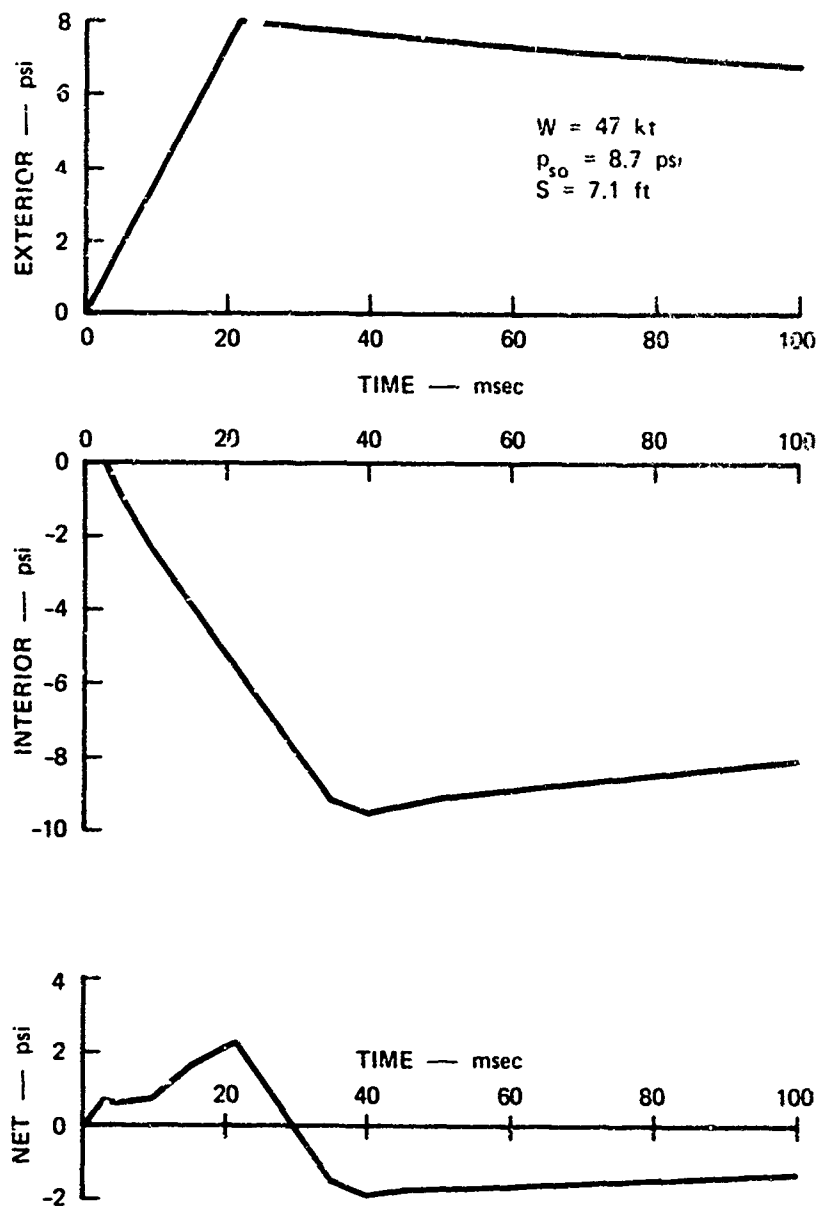


FIGURE 49 CALCULATED LOAD-TIME ON SIDE WALL OF BRICK HOUSE (GREENHOUSE)
Room Volume = 1660 cu ft

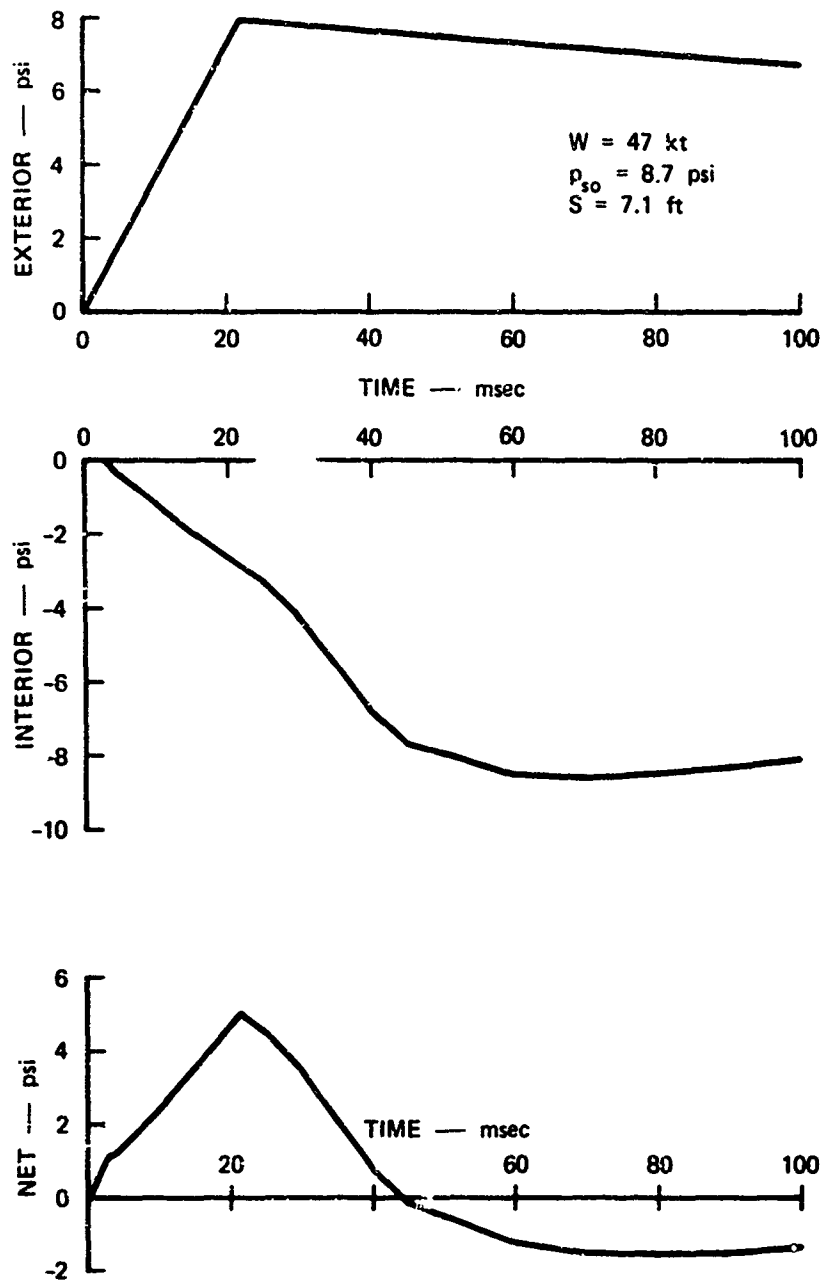


FIGURE 50 CALCULATED LOAD-TIME ON SIDE WALL
 OF BRICK HOUSE (GREENHOUSE)
 Room Volume = 3320 cu ft

However, during outward motion of the wall, the amount of restraint provided by the floors depends on the strength of the connections between the floors and wall. For many cases, this restraint may be very small, which leaves the wall nearly free-standing against interior loads. Since the amount of restraint provided by the connections between the floor and wall was not known, the behavior of the side wall during outward motion was analyzed for each of the following three support conditions:

1. Fixed at ground level and first and second floor ceilings.
2. Fixed at ground level and second floor ceiling; no restraint provided by first floor ceiling.
3. Simply supported at ground level and first and second floor ceilings.

Initially, i.e., when the net pressure was inward, the behavior of the wall was felt to correspond to the first support condition. However, if the reaction at the first floor ceiling exceeds the restraint provided by the connections, subsequent behavior would correspond more closely to the second support condition. Since the computer program has not been sufficiently developed to account for a change in the support conditions during the response of the wall, the third support condition was introduced to act as a comparison with the first two conditions.

For the case where the load-bearing partition remained standing, it was assumed to provide the same restraint as that provided by the first floor ceiling. For the case where the partition was taken to be nonexistent, no restraint was provided.

The results of the analysis were essentially the same for the two assumptions regarding the interior loading, indicating that the effect of these assumptions is inconsequential for the analysis. For each of the three support conditions considered, the analyses predicted no

failure during the inward motion of the wall. During the outward motion, however, failure was predicted to occur for the cases where the first floor ceiling was assumed to provide no restraint (Case 2,), or only restraint equivalent to a simply supported edge (Case 3). For Case 1, where the wall was assumed to be fixed at all levels, no failure was predicted. Since the field test wall failed during the outward motion, it is probable that the condition of fully fixed edges at all floor levels was incorrect.

A similar analysis performed for the house tested at 3.4 psi overpressure indicated failure would occur during the outward motion for Case 2, but that no failure would occur for Cases 1 and 3, where the first floor was assumed to provide either a fixed or simply supported edge. Since no failure of the side wall occurred in the test house located at 3.4 psi overpressure, the analyses indicate that the floors do provide some restraint. However, the restraint is not enough to provide a fully fixed condition during the entire behavior of the wall; this was the behavior expected.

At the incipient collapse overpressure of 5.2 psi for the upper front wall, the analysis predicts a failure of the side wall also. However, for a 10 percent increase in the modulus of rupture, no failure is predicted, indicating that incipient collapse of both the front and side walls occurs at approximately the same overpressure. Therefore, the predicted incipient collapse overpressure for the house is 6.2 psi.

Brick Houses (TEAPOT). Figure 51 shows the front view of the two-story and basement brick houses, typical of U.S. construction, that were tested during Operation TEAPOT. The houses were approximately 25 ft by 33 ft in plan and 22 ft in height. The first floor plan view is shown in Figure 52. The 8-in. thick exterior load-bearing walls

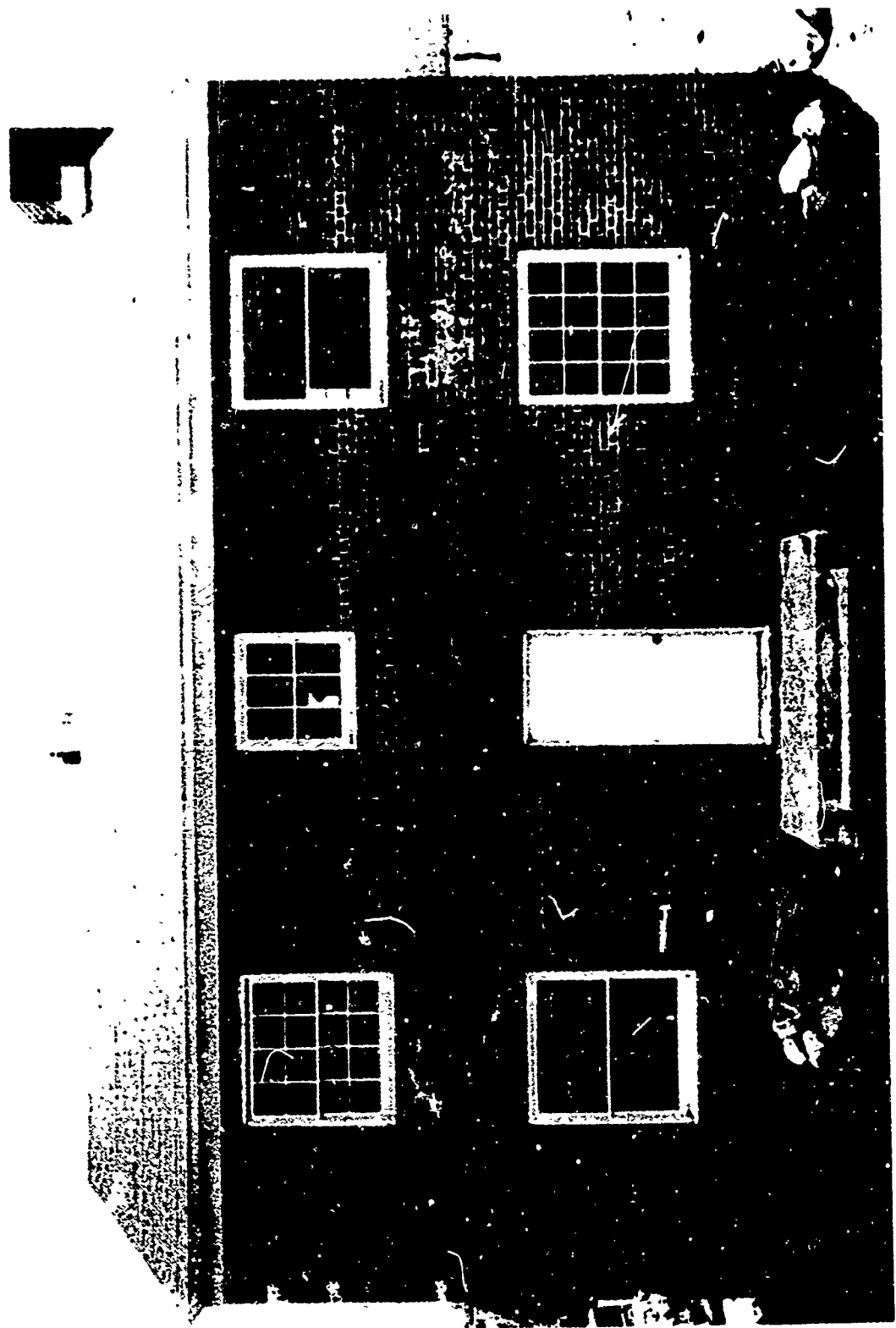
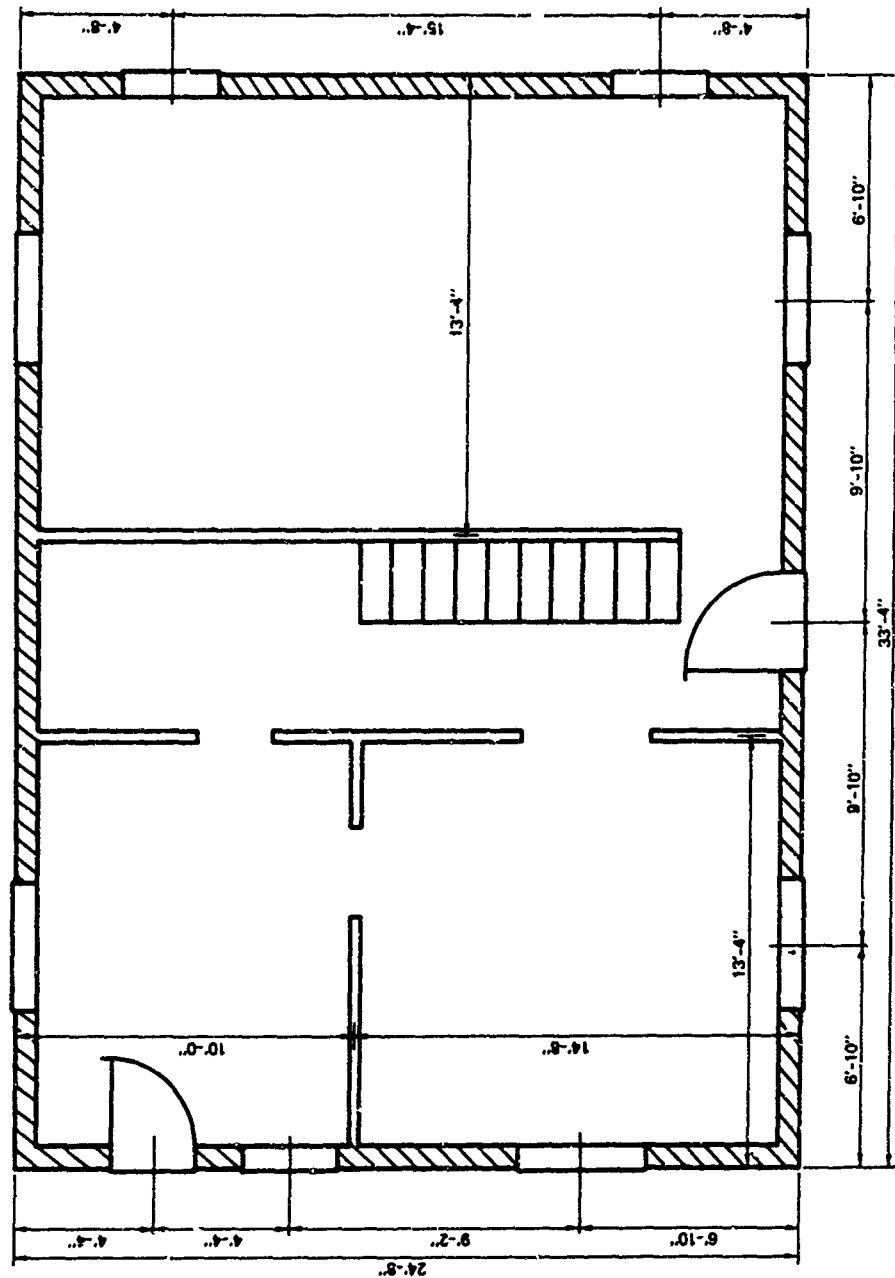


FIGURE 51 FRONT VIEW OF TWO-STORY BRICK HOUSE (TEAPOT)

SOURCE: Ref. 23



SOURCE: Ref. 23

FIGURE 52 PLAN VIEW OF TWO-STORY BRICK HOUSE (TEAPOT)

were constructed of an outer wythe of brick and a back-up wythe of cinder block. The basement walls were 12-in. thick cinder block. The gable roof was of typical frame construction with 2 x 4 in. joists at 16 in. centers running parallel to the side walls of the house. First and second floor joists were 2 x 8 in. at 16 in. centers, and ran parallel to the front wall, with a 4 in. bearing on the cinder block wythe. The construction was conventional, with no special attempts made to strengthen the house.

Test Results

The two houses were tested at overpressure levels of 1.7 and 5.1 psi. The house located at 1.7 psi suffered relatively heavy damage, although there was no apparent damage to the exterior masonry walls. The windows and doors were blown in, and there was considerable damage to the roof and second-floor framing. Interior plastered wall and ceiling finishes were badly damaged.

The aboveground portion of the house at the 5.1 psi overpressure level was demolished beyond repair. Exterior walls had collapsed outward, with little wall debris falling on the floor framing. Some of the load-bearing partitions around the staircase remained standing, but were badly racked. The 12-in. thick cinder block basement walls below the ground surface suffered little damage. In regard to the outward failure of the exterior walls, Ref. 23 states:

The second-floor system offered considerable resistance to the external pressure of the blast; it appears the blast wave, as it enveloped the house, blew in the windows and doors and built up a high overpressure inside the house, at the same time weakening the front wall and probably the others. As the pressure outside dropped off in intensity, the high-pressure volume of air inside the house expanded and forced the walls outward, collapsing

the structure. The second-floor system as designed offered very little resistance to internal lateral pressure since the fire-cut joists were designed to bear on, but were not secured to, the cinder-block wythe of the exterior wall.

Analysis

Front Wall. As was the case with the brick houses tested during Operation GREENHOUSE, several assumptions were required to reduce the complex structural action of the brick houses tested during Operation TEAPOT to cases that could be analyzed using the mathematical models developed in this study.

To simplify the determination of the interior load, only the righthand portion of the house was considered. The room-filling process thus involved only one room, rather than a series of rooms. This room, as shown in Figure 52, has four openings; one in the front wall, two in the side wall, and one in the rear wall. The interior partitions were assumed to survive for a sufficient time so that the room-filling process was not affected by their failure.

The properties of the front wall are summarized as follows:

- L_v = 100 in. (upper story); 98 in. (lower story)
- L_w = 150 in.
- t_w = 8 in.
- γ = 105 pcf
- E_s = 1,000,000 psi
- f_r = 100 psi
- P_v = 10 lb/in. (upper story); 60 lb/in. (lower story)
- $L_{v,n}$ = 48 in.
- $L_{w,n}$ = 8 in.

The composite wall was assumed to act as a solid wall having material properties equal to the average of the brick and cinder block. Again, since information regarding the modulus of elasticity and the modulus of rupture was not available, the "typical" values given above were used.

The exterior loading for this case was also assumed to result from an idealized nuclear blast wave, as shown in Figure 1. The parameters required to define the loading are summarized as follows:

$$\begin{aligned} W &= 30 \text{ kt} \\ P_0 &= 13.0 \text{ psi} \\ c_0 &= 1104 \text{ fps} \\ S &= 5.8 \text{ ft (upper story); } 8.2 \text{ ft (lower story)} \end{aligned}$$

The values for S were determined by the procedure outlined in Section II, with the minimum value of the clearing distance being approximately 3.3 ft for both the upper and lower stories and the maximum values being 8.3 ft for the upper story and 13.1 ft for the lower story. The average of the maximum and minimum values results in the clearing distances shown above. For determining the interior pressure build-up, the windows were assumed to break in 3 msec.

The incipient collapse overpressure for the front wall, using the values indicated above, was calculated to be 2.4 and 3.2 psi for the upper and lower stories, respectively. These compare favorably with the test results, which showed no failure of the front wall at 1.7 psi and collapse at 5.1 psi.

Side Wall. The side wall was analyzed using the same three support conditions discussed for the brick houses tested during Operation GREENHOUSE. Analyses of the wall for each of these three support conditions predicted no failure of the wall at the 1.7 psi test location and

failure in an outward direction of the wall at the 5.1 psi test location. Although these agree with the test results, there is no indication as to which of the support conditions describes the actual wall more accurately. At the predicted incipient collapse overpressure of 2.4 psi for the front wall upper story, no failure was predicted for the side wall for any of the three support conditions. This indicates that the front wall is predicted to fail at a lower overpressure level than the side wall.

Rear Wall. The rear wall was also analyzed for each of the three support conditions considered for the side wall. The procedure outlined in Ref. 12 was used to determine the average pressure-time function for the exterior face of the rear wall. The clearing distance, S , used to determine the time to maximum load was taken to be the greatest distance from any point on the panel under consideration to the nearest edge of the building where clearing could occur. Any exterior loading resulting from outward flow through the windows in the rear wall was ignored. The interior pressure used for the rear wall was the same as that for the front and side walls. However, the interior load on the rear wall was assumed to remain at zero until a time equal to the time required for the failure of the front window, taken as 3 msec, plus the time required for the interior shock front to travel across the room. The calculated exterior and interior pressures, together with the net load on the rear wall, are shown in Figure 53 for the case of the house located at the 5.1 overpressure level. The small net load acting inward was ignored in the analysis. The analysis indicated that the rear wall failed outward at the 5.1 psi overpressure range for all three support conditions.

For the house located at 1.7 psi, no failure was predicted for the rear wall for any of the three support conditions. These results correspond to the field test results. At the incipient collapse

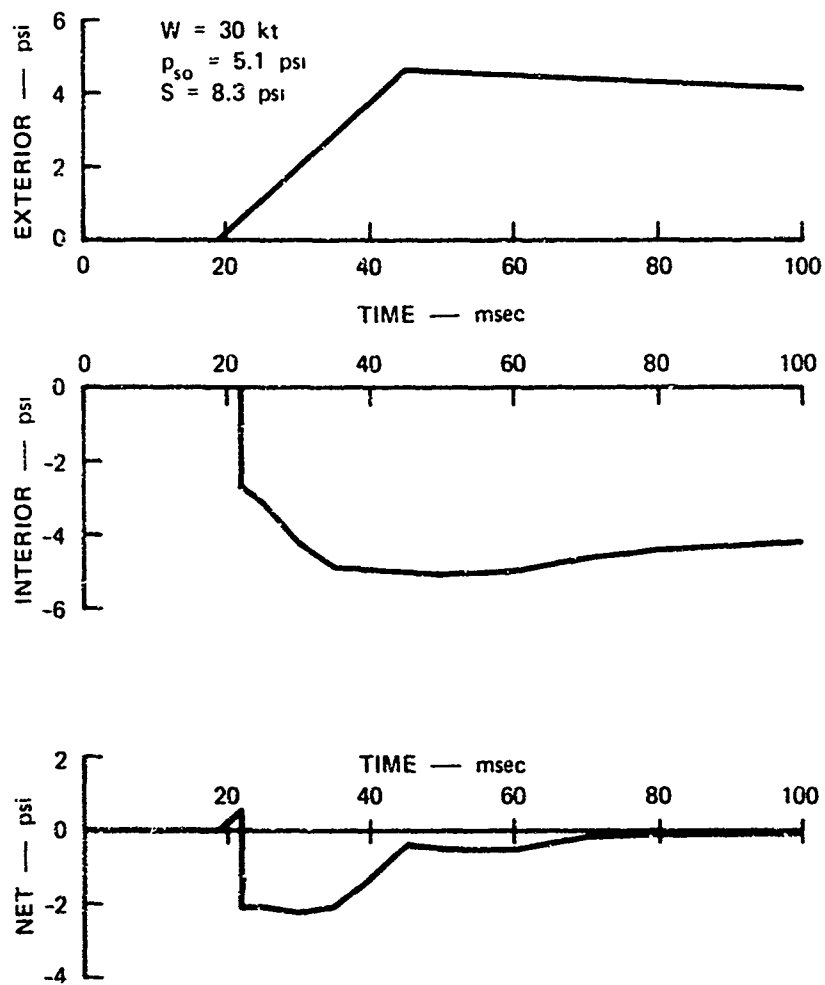


FIGURE 53 CALCULATED LOAD-TIME ON REAR WALL OF BRICK HOUSE (TEAPOT)

overpressure of 2.4 psi predicted for the front wall, no failure is predicted for the rear wall. Thus, for this house, the front wall is predicted to be the initial wall element to fail and the incipient collapse overpressure for the house may be taken as the value corresponding to the incipient collapse of the front wall.

Summary The two-way action model developed in this study for unreinforced masonry walls without arching gave results that were in reasonable agreement with the test data obtained from the two-story brick houses included in Operations GREENHOUSE and TEAPOT. However, to analyze the actual structure, it was necessary to make assumptions regarding the material properties, wall support conditions, and loading. Therefore, even though the predictions gave a good indication of the behavior of complex brick structures, the analytical procedures should be considered as interim techniques until additional correlation with experimental results can be obtained.

It also should be remembered that at the present time there are very few experimental results available on which to base the formulation of analytical procedures for predicting collapse of structural elements, and that virtually all experimental information that do exist are for high explosive or low kiloton yield tests. One question that must be raised for the larger weapon yields is concerned with the effect of the long duration dynamic pressure phase on structural collapse. For instance, it is possible that a structure or element could be weakened during the relatively short diffraction phase, but not collapse unless it was subjected to the long duration drag forces from a megaton yield weapon.

Statistical Analysis. In the previous deterministic analyses of the brick houses, specific values for the modulus of elasticity,

modulus of rupture, and clearing distance were assumed. In reality, however, precise values for these parameters were not known, and the best that they could be known is to some degree of statistical accuracy. To take into account the uncertainty in the values of the physical parameters for the actual brick houses, statistical analyses were made using the Monte Carlo method discussed in Section IV.

With the present computer program, the incipient collapse overpressure may be determined only for the front wall without repeated cut-and-trial program runs. Therefore, the statistical analysis was restricted to the upper story panels of the front wall of each of the two types of houses. It was believed that this restriction was not too important, however, since the results from the previous deterministic analyses indicated that this panel was the weakest, or at least close to the weakest, wall element.

For the statistical analysis, the modulus of rupture and the clearing distance were treated probabilistically. Since previous sensitivity studies (Ref. 1) indicated that the incipient collapse overpressure for reinforced masonry walls without arching is relatively insensitive to the modulus of elasticity, this parameter was not varied in the statistical analysis. The values of the other parameters required in the analysis were the same as used in the deterministic analysis.

The normal distribution may be described completely by specifying the mean and standard deviation. For the modulus of rupture, the mean value was assumed to be equal to the "typical" value of 100 psi used in the previous analyses. Next, 30 and 170 psi were selected as having a 5 and 95 percent probability of occurrence, respectively (values that will exceed 5 and 95 percent of the occurrences); this resulted in a standard deviation of 42.5 psi. These values were used for both of the brick houses.

The mean value for the clearing distance was taken to be the average values used for the panels in the deterministic analyses. The weighted average clearing distance,* previously considered to be a minimum, was selected as having a 5 percent probability of occurrence. The maximum clearing distance,* previously assumed to be equal to the greatest distance from any point on the panel to the nearest edge of the building where clearing could occur, was selected as having a 95 percent probability of occurrence. This procedure resulted in a mean clearing distance of 7.1 ft and a standard deviation of 2.63 ft for the houses tested during Operation GREENHOUSE and a mean clearing distance of 5.8 ft and a standard deviation of 1.62 ft for the houses tested during Operation TEAPOT.

The results obtained from the statistical analyses using the above values are summarized as follows:

<u>Brick House (GREENHOUSE)</u>		<u>Brick House (TEAPOT)</u>	
Mean	6.36 psi	Mean	2.50 psi
Standard Deviation	0.36 psi	Standard Deviation	0.18 psi
10% Probability Value	5.90 psi	10% Probability Value	2.27 psi
90% Probability Value	6.82 psi	90% Probability Value	2.73 psi

The 10 and 90 percent probability values indicate overpressures for which collapse will occur 10 and 90 percent of the time, respectively. The mean value may be taken as the overpressure at, or below which, collapse will occur half of the time.

The above values are in fairly good agreement with the test results, where the upper left front wall of the house in Operation GREENHOUSE failed at 8.7 psi and the exterior wall of the house in Operation

* For the Operation GREENHOUSE houses $S' = 2.8$ ft and $S = 11.4$ ft, and for the Operation TEAPOT houses $S' = 3.3$ ft and $S = 8.3$ ft.

TEAPOT experienced no apparent damage at 1.7 psi and complete collapse at 5.1 psi. It is not surprising that the mean values of 6.36 and 2.5 psi obtained for the incipient collapse overpressure by the statistical procedure are approximately the same as the values of 6.2 and 2.4 psi obtained from the deterministic analysis when the mean values for the modulus of rupture and clearing distance are used. However, the statistical results provide further information by indicating that collapse may be expected to occur approximately 10 percent of the time at overpressures of 5.90 and 2.27 psi for the GREENHOUSE and TEAPOT houses, respectively. Similarly, collapse may be expected to occur approximately 90 percent of the time at overpressures of 6.82 and 2.73 psi, respectively.

VII SUMMARY AND RECOMMENDATIONS

Summary

During this phase of the effort to develop a procedure for the evaluation of existing structures, computer programs were completed for predicting the collapse of two-way structural action walls of the three basic types considered in Ref. 1, i.e., unreinforced concrete or masonry unit walls with arching, unreinforced concrete or masonry unit walls without arching, and reinforced concrete walls. This required the formulation of the resistance function for two-way walls and the development of procedures for determining both the resistance and net load-time functions for walls with window openings. In addition, the evaluation procedure was extended to include a probability distribution to handle various "unknown" wall and load parameters.

At the present time, there are insufficient experimental data available from controlled tests to provide the definitive information needed to check, verify, or modify the various mathematical wall response models developed in this study. Therefore, the approach adopted was first to use the limited laboratory data to check deterministically the predicted wall response-time history and then to use the nuclear field test data to check the predicted probability of occurrence of the incipient collapse overpressure.

As noted in Section VI of this report, it was possible to correlate the theoretical predictions with laboratory tests of one unreinforced brick wall without arching and with nuclear field tests of eight types of unreinforced brick or concrete masonry wall panels with arching and two types of brick houses with unreinforced load-bearing brick exterior

walls. Although the experimental information was insufficient for a correlation to be made for all of the types of walls and support conditions of interest, the wall response models generally provided an adequate prediction of the experimental behavior. However, in the case where the correlation was poor, the experimental information was inadequate for establishing the relative importance of the parameters related to the response and collapse of walls under dynamic loading.

Recommendations

This investigation has emphasized the need for a balanced analytical and experimental program to develop an evaluation procedure for existing structures that meets the requirements of OCD. From the standpoint of predicting the collapse of exterior walls, it is recommended that the following research be conducted in the next phase of the effort:

- A sensitivity analysis should be conducted to investigate the effect on the incipient collapse overpressure of varying the probability distribution of the important load and wall parameters. In this study, sensitivity analyses have been used to assist in identifying the wall and load parameters that have an important influence on the incipient collapse overpressure of specific walls. In addition, since the evaluation of actual structures includes physical parameters that cannot readily be measured or determined precisely, the analytical procedure was modified to include a probability distribution for the important parameters rather than a single value. This, of course, lessens the requirement for preciseness in some or all of the parameters. However, some parameters may have such a large effect on the predicted collapse of a specific wall that their degree of uncertainty may mask the uncertainty in any or all of the other unknown parameters. A sensitivity study will indicate the parameters that must be determined accurately and also will provide guidance in selecting the more important areas for experimental research.

- A literature search should be conducted to gather basic information on material properties for use in this project. The analyses of wall elements in this study emphasized the need for readily available statistical data on the material properties of exterior walls, and information should be obtained for all materials needed in the evaluation of existing structures.
- Static and dynamic tests of typical exterior walls should be conducted to permit an examination of the validity of the mathematical models presented in this report or to establish the basis for additional or substitute procedures. As noted in Section III, the establishment of the resistance functions for two-way action walls with windows required that various assumptions be made in addition to those outlined in Ref. 1. To support the analytical work, the specific areas for which experimental information is needed include the resistance function for various types of walls and support conditions; the effect of two-way action for walls with and without windows; the effect of shear and connections on wall failure; the reaction of walls throughout their response history, including collapse; and the effect of vertical in-plane forces on the resistance of wall elements. The emphasis in any test program should be to establish the primary collapse mechanism of two-way action walls with and without windows and to determine the effect of variation of the important parameters on the incipient collapse overpressure of walls.
- Air blast interaction studies should be continued to establish more definitive blast load prediction techniques than are now available. In Section II, a method is presented for calculating the net load-time function resulting from the interaction of an air blast wave with a structure with openings. The method evolved from the available schemes for determining the blast loading on the exterior surface of a building with openings and the interior pressure build-up caused by a blast wave entering a room. However, since the net load-time function is an important factor in predicting the collapse of walls in actual buildings, better information is needed to develop a more accurate procedure than used in this study. Although a number of parameters influence the blast wave interaction process, the primary areas where information is needed for determining the collapse of exterior walls are the clearing

time of the reflected overpressure on the front face of any wall in a building with openings, the effect of window openings on the back-face loading of an exterior wall, and the adequacy of using the average room pressure calculated from the room-filling procedure as the loading on the interior surface of exterior walls located on any side of a building.

Appendix A

TRANSFORMATION FACTORS

Appendix A

TRANSFORMATION FACTORS

Introduction

Because of the complex behavior of two-way action walls, it was convenient to reduce the real system to an equivalent single-degree-of-freedom system. This was done through the use of transformation factors that, when multiplied by the total load, mass, and resistance of the real structure, gave the corresponding parameters for the equivalent single-degree-of-freedom system. For one-way action walls treated in Ref. 1, the transformation factors from Ref. 25 for beams and one-way slabs were used directly. However, because of the difference in the method of calculating β ,* the transformation factors for two-way slabs from Ref. 25 could not be used for two-way action walls, and it was therefore necessary to develop these factors.

The transformation factors were developed on the basis of an assumed deflection shape for the real structure. For the two-way action wall the deflected shape along a vertical or horizontal strip was assumed to be the same as that of a beam with the same load distribution and the same support conditions. The deflection of the equivalent system was taken to be the same as that of the center of the wall. Since the time scale was not altered, the deflection-time response of the equivalent system was the same as that for the center of the actual wall.

* The coefficient β is used to indicate the position of the crack, or yield lines, as shown in Figures 12 and 20 of Section III.

From these assumptions, the mass factor can be determined by equating the kinetic energies of the real and equivalent systems, the load factor by equating the work, and the resistance factor by equating the strain energy. Comparison of the resistance and load factors show that these two factors are the same, therefore only the load and mass factors are derived in the following subsections. The transformation factors are the same for the three types of walls considered in this study. However, because of variations in the assumed deflection shapes, they are different for the various support conditions and resistance phases considered. Also, for reinforced concrete walls, the transformation factors will be different for the two collapse modes considered in Section III (Figure 20). For the sake of clarity, only collapse mode "a" will be considered in this appendix, while collapse mode "b" will be discussed in Appendix B.

Mass Factor

The mass factor for the two-way action wall can be determined by dividing the total kinetic energy of the actual wall by the kinetic energy of the equivalent system. The two-way wall is assumed to be divided into four segments by the crack, or yield, lines, as shown in Figure A-1. The kinetic energy for each of these segments is given by

$$(KE) = \int \frac{1}{2} m \dot{y}^2 dA \quad (A-1)$$

where m is the mass per unit area and \dot{y} is the velocity along the element. The integration is carried out over the area of the segment. The total kinetic energy of the wall is equal to the sum of the kinetic energies of the individual segments. Since segment B is the same as segment A and D is the same as C, the total kinetic energy of the actual wall is given by

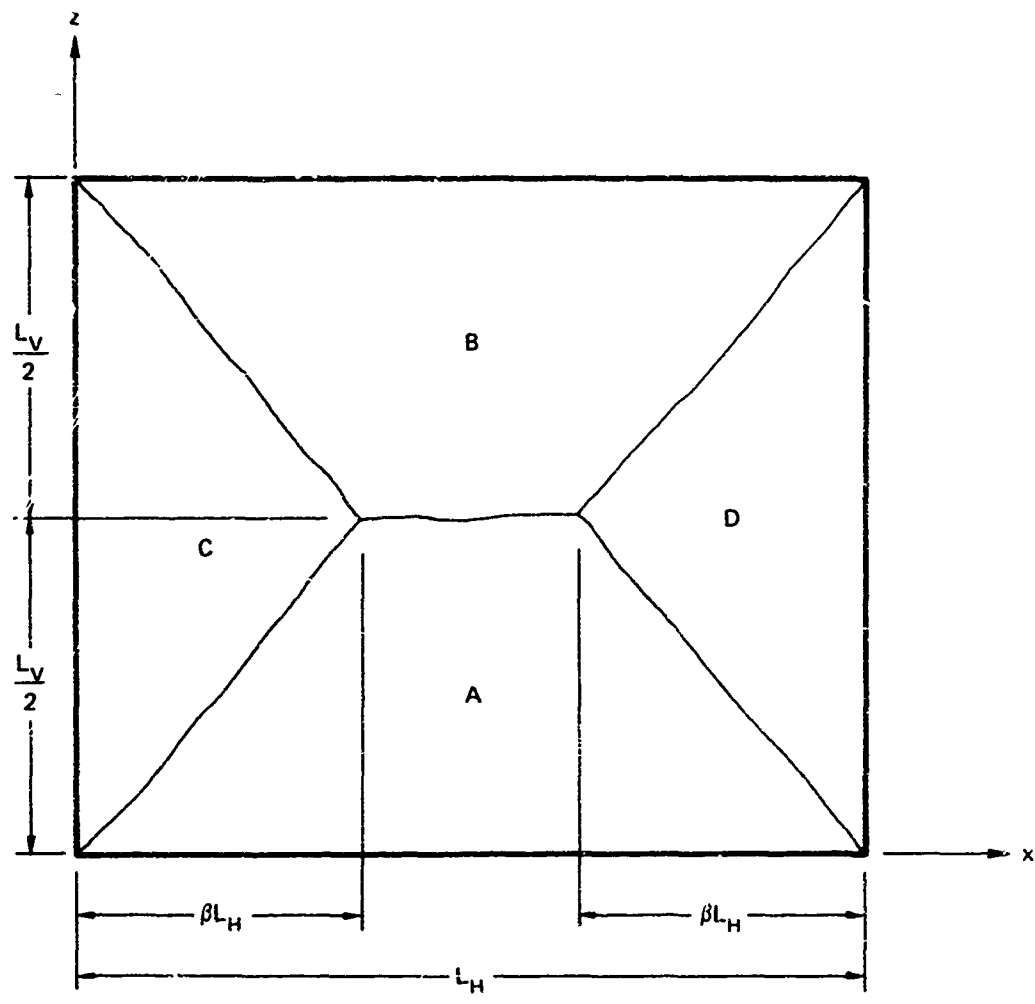


FIGURE A-1 ASSUMED CRACK, OR YIELD-LINE PATTERN FOR TWO-WAY ACTION WALL

$$(KE)_T = 2'(KE)_A + 2(KE)_C \quad . \quad (A-2)$$

The kinetic energy of the equivalent system is given by

$$(KE)_e = \frac{1}{2} M_T \dot{y}_e^2 \quad (A-3)$$

where

$$M_T = mL_V L_M \quad . \quad (A-4)$$

Dividing Eq. A-2 by Eq. A-3, the mass factor is given by

$$K_M = \frac{2 \left[\int \frac{1}{2} m \dot{y}^2 dA \right]_A + 2 \left[\int \frac{1}{2} m \dot{y}^2 dA \right]_C}{\frac{1}{2} mL_V L_M \dot{y}_e^2} \quad . \quad (A-5)$$

It can be shown that

$$\frac{\dot{y}}{\dot{y}_e} = \frac{y}{y_e} \quad . \quad (A-6)$$

Therefore, since by definition $y_e = y_c$, the following relationship is obtained:

$$\frac{\dot{y}}{\dot{y}_e} = \frac{y}{y_c} \quad (A-7)$$

which, when substituted into Eq. A-5, yields

$$K_v = \frac{2}{L_v L_w} \left\{ \left[\int \left(\frac{y}{y_c} \right)^2 dA \right]_A + \left[\int \left(\frac{y}{y_c} \right)^2 dA \right]_C \right\} \quad (A-8)$$

where the quantity y/y_c depends on the support conditions and resistance phase of the wall. The mass factor is evaluated for each of the four support conditions considered in Section III as follows.

Support Case 1

During the elastic phase, the deflection along a vertical strip of segments A-B is assumed to be the same as that of a simply supported beam of length L_v with a uniformly distributed lateral load, or

$$y = \frac{16z}{5L_v^4} (L_v^3 - 2L_v z^2 + z^3) y_c \quad (A-9)$$

Similarly, the elastic deflection along a horizontal strip of segments C-D is

$$y = \frac{16x}{5L_w^4} (L_w^3 - 2L_w x^2 + x^3) y_c \quad (A-10)$$

Substituting these values into Eq. A-8 and integrating gives the following expression for the mass factor during the elastic phase of unreinforced walls without arching and reinforced concrete walls:

$$K_M = 20.48 \beta^3 \left(\frac{1}{12} - \frac{\beta^2}{7.5} + \frac{\beta^3}{21} + \frac{\beta^4}{14} - \frac{\beta^5}{18} + \frac{\beta^6}{90} \right) + 0.5038 - 0.7056 \beta \quad (A-11)$$

After cracking of the wall in the elastic phase, the motion of the wall is assumed to be a rigid body rotation of the segments about their supports. Thus, for segment A the deflection along a vertical strip is

$$y = \frac{2z}{L_v} y_c \quad . \quad (A-12)$$

Similarly, for segment C the deflection along a horizontal strip is

$$y = \frac{x}{\beta L_h} y_c \quad . \quad (A-13)$$

Substituting these values into Eq. A-8 and integrating gives the following expression for the mass factor for unreinforced walls with arching and for the decaying phase of unreinforced walls without arching and the plastic phase of reinforced concrete walls:

$$K_u = \frac{1}{3} (1 - \beta) \quad . \quad (A-14)$$

Support Case 2

During the elastic phase, the deflection along a vertical strip of segments A-B is initially assumed to be the same as that for a fixed-edge beam of length L_v with a uniformly distributed lateral load, or

$$y = \frac{16z^2}{L_v^4} (L_v - z)^2 y_c \quad . \quad (A-15)$$

Similarly the elastic deflection along a horizontal strip of segments C-D is

$$y = \frac{16x^2}{L_h^4} (L_h - x)^2 y_c \quad . \quad (A-16)$$

Substituting these values into Eq. A-8 and integrating gives the following expression for the mass factor during the initial portion of the elastic phase of unreinforced walls without arching and the elastic, uncracked phase and elastic, cracked phase of reinforced concrete walls:

$$K_M = 512\beta^5 \left(\frac{1}{30} - \frac{\beta}{10.5} + \frac{3\beta^2}{28} - \frac{\beta^3}{18} + \frac{\beta^4}{90} \right) + 0.4065 - 0.6144\beta \quad (A-17)$$

After cracking (or yielding of the steel in a reinforced concrete wall) occurs along the edges, the wall is assumed to deflect as if it were simply supported on four edges. The mass factor during the secondary portion of the elastic phase of unreinforced walls without arching and the elasto-plastic phase of reinforced concrete walls are thus given by Eq. A-11. During the decaying phase of unreinforced walls without arching and the plastic phase of reinforced concrete walls, the mass factor is given by Eq. A-14.

Support Case 3

During the elastic phase, the deflection along a vertical strip of segments A-B is given by Eq. A-9 and along a horizontal strip of segments C-D by Eq. A-16. Substituting these values into Eq. A-8 and integrating results in the following expression for the mass factor during the initial portion of the elastic phase of unreinforced walls without arching and the elastic, uncracked phase and elastic, cracked phase of reinforced concrete walls:

$$K_M = 512\beta^3 \left(\frac{1}{30} - \frac{\beta}{10.5} + \frac{3\beta^2}{28} - \frac{\beta^3}{18} + \frac{\beta^4}{90} \right) + 0.5033 - 0.7066\beta \quad (A-18)$$

After cracking (or yielding of the steel in a reinforced concrete wall) occurs along the fixed edges, the wall is again assumed to deflect as if it were simply supported on four edges, with the mass factor for the secondary portion of the elastic phase of unreinforced walls without arching and the elasto-plastic phase of reinforced concrete walls corresponding to that given by Eq. A-11. During the decaying phase of unreinforced walls without arching and the plastic phase of reinforced concrete walls, the mass factor is again given by Eq. A-14.

Support Case 4

During the elastic phase, the deflection along a vertical strip of segments A-B is given by Eq. A-15 and along a horizontal strip of segments C-D by Eq. A-10. Substituting these values into Eq. A-3 and integrating results in the following expression for the mass factor during the initial portion of the elastic phase of unreinforced walls without arching and the elastic, uncracked phase and elastic, cracked phase of reinforced concrete walls:

$$K_w = 20.48 f^3 \left(\frac{1}{12} - \frac{f^2}{7.5} + \frac{f^3}{21} + \frac{f^4}{14} - \frac{f^5}{18} + \frac{f^6}{90} \right) + 9.4065 - 0.6144f \quad (A-19)$$

After cracking (or yielding of the steel in a reinforced concrete wall) occurs along the fixed edges, the wall is again assumed to deflect as if it were simply supported, with the resulting mass factor for the secondary portion of the elastic phase of unreinforced walls without arching and the elasto-plastic phase of reinforced concrete walls being given by Eq. A-11. During the decaying phase of unreinforced walls without arching and the plastic phase of reinforced concrete walls, the mass factor is again given by Eq. A-14.

Load Factor

The load factor for two-way walls can be determined by dividing the total work done by the load on the actual wall by the work done by the load on the equivalent system. The work done on each of the segments shown in Figure A-1 is given by

$$W = \int qy dA \quad (A-20)$$

where the integration is carried out over the area of the segment. The total work done on the wall is equal to the sum of the work done on the individual segments. Because of symmetry of the segments, the total work done is therefore given by

$$W_T = 2 \left[\int qy dA \right]_A + 2 \left[\int qy dA \right]_C \quad (A-21)$$

The work done on the equivalent system is given by

$$W_e = P_T y_e \quad (A-22)$$

where

$$P_T = qL_v L_h \quad (A-23)$$

and by definition $y_e = y_c$.

Dividing Eq. A-21 by Eq. A-22, the load factor is given by

$$K_L = \frac{2}{L_v L_h} \left\{ \left[\int \frac{y}{y_c} dA \right]_A + \left[\int \frac{y}{y_c} dA \right]_C \right\} \quad (A-24)$$

where the quantity y/y_c again depends on the support conditions and resistance phase of the wall. The load factor is evaluated for each of the four support conditions considered in this study as follows.

Support Case 1

During the elastic phase, the deflection along a vertical strip of segments A-B is given by Eq. A-9 and along a horizontal strip of segments C-D by Eq. A-10. Substituting these values into Eq. A-24 and integrating results in the following expression for the load factor during the elastic phase of unreinforced walls without arching and reinforced concrete walls:

$$K_t = 6.4\beta^2 \left(\frac{1}{6} - \frac{\beta^2}{10} + \frac{\beta^3}{30} \right) + 0.6400 - 0.8134\beta \quad . \quad (A-25)$$

After cracking of the wall in the elastic phase, the motion of the wall is again assumed to be a rigid body rotation of the segments about their supports. Thus, for segments A-B the deflection along a vertical strip is given by Eq. A-12 and for segments C-D the deflection along a horizontal strip is given by Eq. A-13. Substituting these values into Eq. A-24 and integrating gives the following expression for the load factor for unreinforced walls with arching and during the decaying phase of unreinforced walls without arching and the plastic phase of reinforced concrete walls:

$$K_t = \frac{1}{2} - \frac{1}{3} \beta \quad . \quad (A-26)$$

Support Case 2

During the elastic phase, the deflection along a vertical strip of segments A-B is given by Eq. A-15, and along a horizontal strip of segments C-D by Eq. A-16. Substituting these values into Eq. A-24 and integrating gives the following expression for the load factor during the initial

portion of the elastic phase of unreinforced walls without arching and the elastic, uncracked phase and elastic, cracked phase of reinforced concrete walls:

$$K_L = 32\beta^3 \left(\frac{1}{12} - \frac{\beta}{10} + \frac{\beta^2}{30} \right) + 0.5344 - 0.7328\beta \quad . \quad (A-27)$$

After cracking (or yielding for a reinforced concrete wall) occurs along the edges, the wall is assumed to deflect as a simply supported wall and the load factor for the secondary portion of the elastic phase of unreinforced walls without arching and the elasto-plastic phase of reinforced concrete walls is given by Eq. A-25. The load factor during the decaying phase of unreinforced walls without arching and the plastic phase of reinforced concrete walls is given by Eq. A-26.

Support Case 3

During the elastic phase, the deflection along a vertical strip of segments A-B is given by Eq. A-9 and along a horizontal strip of segments C-D by Eq. A-16. Substituting these values into Eq. A-24 and integrating gives the following expression for the load factor during the initial portion of the elastic phase of unreinforced walls without arching and the elastic, uncracked phase and elastic, cracked phase of reinforced concrete walls:

$$K_L = 32\beta^3 \left(\frac{1}{12} - \frac{\beta}{10} + \frac{\beta^2}{30} \right) + 0.6400 - 0.8134\beta \quad . \quad (A-28)$$

After cracking (or yielding for a reinforced concrete wall) occurs along the fixed edges, the wall is again assumed to deflect as a wall simply supported on four edges, with the load factor during the secondary

portion of the elastic phase of unreinforced walls without arching and the elasto-plastic phase of reinforced concrete walls given by Eq. A-25. The load factor during the decaying phase of unreinforced walls without arching and the plastic phase of reinforced concrete walls is again given by Eq. A-26.

Support Case 4

During the elastic phase, the deflection along a vertical strip of segments A-B is given by Eq. A-15 and along a horizontal strip of segments C-D by Eq. A-10. Substituting these values into Eq. A-24 and integrating gives the following expression for the load factor for the initial portion of the elastic phase of unreinforced walls without arching and the elastic, uncracked phase and elastic, cracked phase of reinforced concrete walls:

$$K_L = 6.4\beta^2 \left(\frac{1}{6} - \frac{\beta^2}{10} + \frac{\beta^2}{30} \right) + 0.5344 - 0.7328\beta \quad . \quad (A-29)$$

After cracking (or yielding for a reinforced concrete wall) occurs along the fixed edges, the wall is again assumed to deflect as if it were simply supported on four edges, with the resulting load factor for the secondary portion of the elastic phase of unreinforced walls without arching and the elasto-plastic phase of reinforced concrete walls given by Eq. A-25. The load factor during the decaying phase of unreinforced walls without arching and the plastic phase of reinforced concrete walls is given by Eq. A-26.

Load-Mass Factor

For use in the numerical integration of the equation of motion for the single-degree-of-freedom system, the load and mass factors can be combined into a single factor, the load-mass factor, K_{LM} , where

$$K_{LM} = \frac{K_M}{K_L} \quad (A-30)$$

As previously noted, the factors for the various support conditions and the resistance phases are different, varying discontinuously as the deflection increases. In the numerical integration analysis, the different load-mass factors are used for the appropriate support conditions and resistance phases.

The values of the load and mass factors for each of the four support cases are summarized in Tables A-1 and A-2 for unreinforced concrete or masonry unit walls and reinforced concrete walls.

Table A-1

TRANSFORMATION FACTORS FOR TWO-WAY UNREINFORCED CONCRETE
OR MASONRY UNIT WALLS

Phase	Support Case	Transformation Factors
Elastic-Initial	1	$K_v = 20.48 \beta^2 \left(\frac{1}{12} - \frac{\beta^2}{7.5} + \frac{\beta^3}{21} + \frac{\beta^4}{14} - \frac{\beta^5}{18} + \frac{\beta^6}{90} \right) + 0.5038 - 0.7066 \beta$ $K_t = 6.4 \beta^2 \left(\frac{1}{6} - \frac{\beta^2}{10} + \frac{\beta^3}{30} \right) + 0.6400 - 0.8134 \beta$
	2	$K_v = 512.0 \beta^5 \left(\frac{1}{30} - \frac{\beta}{10.5} + \frac{3\beta^2}{28} - \frac{\beta^3}{18} + \frac{\beta^4}{90} \right) + 0.4065 - 0.6144 \beta$ $K_t = 32.0 \beta^2 \left(\frac{1}{12} - \frac{\beta}{10} + \frac{\beta^2}{30} \right) + 0.5344 - 0.7328 \beta$
	3	$K_v = 512.0 \beta^3 \left(\frac{1}{30} - \frac{\beta}{10.5} + \frac{3\beta^2}{28} - \frac{\beta^3}{18} + \frac{\beta^4}{90} \right) + 0.5038 - 0.7066 \beta$ $K_t = 32.0 \beta^2 \left(\frac{1}{12} - \frac{\beta}{10} + \frac{\beta^2}{30} \right) + 0.6400 - 0.8134 \beta$
	4	$K_v = 20.48 \beta^2 \left(\frac{1}{12} - \frac{\beta^2}{7.5} + \frac{\beta^3}{21} + \frac{\beta^4}{14} - \frac{\beta^5}{18} + \frac{\beta^6}{90} \right) + 0.4065 - 0.6144 \beta$ $K_t = 6.4 \beta^2 \left(\frac{1}{6} - \frac{\beta^2}{10} + \frac{\beta^3}{30} \right) + 0.5344 - 0.7328 \beta$
Elastic-Secondary	1	No elastic - secondary phase
	2,3,4	$K_v = 20.48 \beta^2 \left(\frac{1}{12} - \frac{\beta^2}{7.5} + \frac{\beta^3}{21} + \frac{\beta^4}{14} - \frac{\beta^5}{18} + \frac{\beta^6}{90} \right) + 0.5038 - 0.7066 \beta$ $K_t = 6.4 \beta^2 \left(\frac{1}{6} - \frac{\beta^2}{10} + \frac{\beta^3}{30} \right) + 0.6400 - 0.8134 \beta$
Decaying	1,2,3,4	$K_M = \frac{(1 - \beta)}{3}$ $K_t = \frac{1}{2} - \frac{1}{3} \beta$

Note: Transformation factors for unreinforced walls with arching correspond to those given above for decaying phase.

Table A-2

TRANSFORMATION FACTORS FOR TWO-WAY REINFORCED CONCRETE WALLS
(Collapse Mode "a")

Phase	Support Case	Transformation Factors
Elastic	1	$K_v = 20.48\beta^3 \left(\frac{1}{12} - \frac{\beta^2}{7.5} + \frac{\beta^3}{21} + \frac{\beta^4}{14} - \frac{\beta^5}{18} + \frac{\beta^6}{90} \right) + 0.5038 - 0.7066\beta$ $K_L = 6.4\beta^2 \left(\frac{1}{6} - \frac{\beta^2}{10} + \frac{\beta^3}{30} \right) + 0.6400 - 0.8134\beta$
	2	$K_v = 512.0\beta^5 \left(\frac{1}{30} - \frac{\beta}{10.5} + \frac{3\beta^2}{28} - \frac{\beta^3}{18} + \frac{\beta^4}{90} \right) + 0.4065 - 0.6144\beta$ $K_L = 32.0\beta^3 \left(\frac{1}{12} - \frac{\beta}{10} + \frac{\beta^2}{30} \right) + 0.5344 - 0.7328\beta$
	3	$K_v = 512.0\beta^3 \left(\frac{1}{30} - \frac{\beta}{10.5} + \frac{3\beta^2}{28} - \frac{\beta^3}{18} + \frac{\beta^4}{90} \right) + 0.5038 - 0.7066\beta$ $K_L = 32.0\beta^3 \left(\frac{1}{12} - \frac{\beta}{10} + \frac{\beta^2}{30} \right) + 0.6400 - 0.8134\beta$
	4	$K_v = 20.48\beta^3 \left(\frac{1}{12} - \frac{\beta^2}{7.5} + \frac{\beta^3}{21} + \frac{\beta^4}{14} - \frac{\beta^5}{18} + \frac{\beta^6}{90} \right) + 0.4065 - 0.6144\beta$ $K_L = 6.4\beta^2 \left(\frac{1}{6} - \frac{\beta^2}{10} + \frac{\beta^3}{30} \right) + 0.5344 - 0.7328\beta$
Elasto-plastic	1	No elasto-plastic phase
	2,3,4	$K_v = 20.48\beta^3 \left(\frac{1}{12} - \frac{\beta^2}{7.5} + \frac{\beta^3}{21} + \frac{\beta^4}{14} - \frac{\beta^5}{18} + \frac{\beta^6}{90} \right) + 0.5038 - 0.7066\beta$ $K_L = 6.4\beta^2 \left(\frac{1}{6} - \frac{\beta^2}{10} + \frac{\beta^3}{30} \right) + 0.6400 - 0.8134\beta$
Plastic	1,2,3,4	$K_v = \frac{(1 - \beta)}{3}$ $K_L = \frac{1}{2} - \frac{1}{3}\beta$

Appendix B

COLLAPSE MODE "b" FOR REINFORCED CONCRETE WALLS

Appendix B

COLLAPSE MODE "b" FOR REINFORCED CONCRETE WALLS

Introduction

In Section III, the ultimate resistance of a reinforced concrete wall was determined by yield-line analysis. The yield lines were assumed to form in one of the two patterns shown in Figure 20. In most cases of interest, the yield lines will form in a pattern similar to that shown as collapse mode "a." Equations for the ultimate resistance and the coefficient $\hat{\beta}$, which defines the location of the yield lines, were presented. In some situations, however, the yield lines will form in the pattern shown as collapse mode "b", for which the equations for the ultimate resistance derived in this appendix are provided. Similarly, the equations for the dynamic reactions and transformation factors corresponding to collapse mode "b" replace those in Section V and Appendix A, respectively, which were for collapse mode "a."

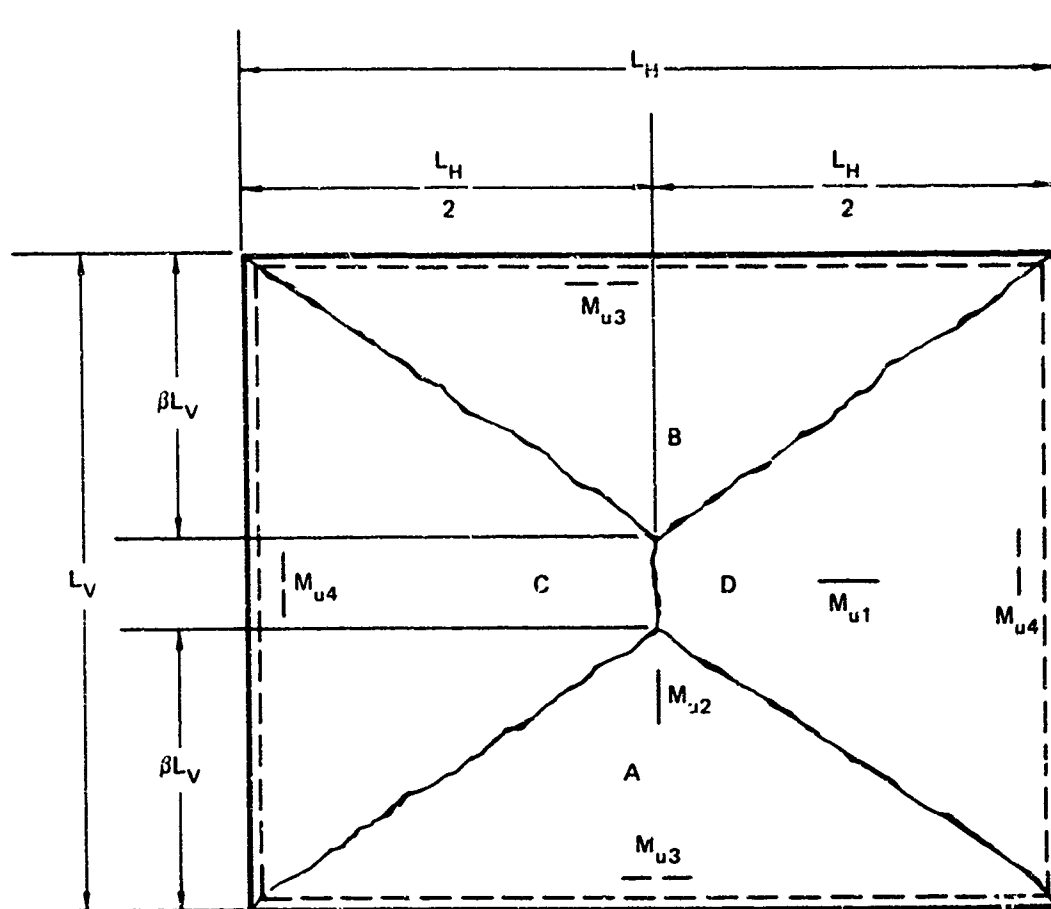
Ultimate Resistance

The general case for collapse mode "b" is shown in Figure B-1. To determine the ultimate resistance the work-energy method, as described in Ref. 17, was used.

The work done by the resisting moment acting on segment A is

$$W_A = M_{u1}L_M\theta_A + M_{u3}L_M\theta_A \quad (B-1)$$

Preceding page blank



NOTATION:
 ——— Positive Yield Line
 - - - Negative Yield Line

FIGURE B-1 COLLAPSE MODE "b" FOR REINFORCED CONCRETE WALL

where for small deflections,

$$\theta_A = \frac{y_c}{\beta L} \quad . \quad (B-2)$$

Similarly, the work done on segment C is

$$W_C = M_{u2} L_V \theta_C + M_{u4} L_V \theta_C \quad (B-3)$$

where for small deflections,

$$\theta_C = \frac{y_c}{L_H/2} \quad . \quad (B-4)$$

The total work done on the wall is equal to the sum of the work done on the individual segments. Since segment B is identical to segment A, and D identical to C, the total work done is given by

$$W_T = 2y_c \left[\frac{L_H}{\beta L_V} (M_{u1} + M_{u3}) + \frac{2L_V}{L_H} (M_{u2} + M_{u4}) \right] \quad . \quad (B-5)$$

The energy input for a uniform load q on the various wall segments in Figure B-1 is

$$E_A = E_B = q \left(\frac{L_H}{2} \right) (\beta L_V) \left(\frac{y_c}{3} \right) = \frac{1}{6} q \beta L_V L_H y_c \quad (B-6)$$

and

$$E_C = E_D = q (L_V - 2\beta L_V) \left(\frac{L_H}{2} \right) \left(\frac{y_c}{2} \right) + 2q \left(\frac{\beta L_V}{2} \right) \left(\frac{L_V}{2} \right) \left(\frac{y_c}{3} \right) \quad (B-7)$$

$$= \frac{1}{12} q L_V L_H y_c (3 - 4\beta) \quad .$$

The total energy input of the load is equal to the sum of the energy inputs to the various segments, or

$$E_T = \frac{1}{6} q L_V L_H Y_c (3 - 2\beta) \quad (B-8)$$

Since the total work done equals the total energy input:

$$W_T = E_T$$

which, by substituting Eqs. B-5 and B-8 into the above equation and solving for the wall resistance, yields

$$q = \frac{3M_{u1}}{L_V^2 \beta (3 - 2\beta)} \left[\gamma_1^2 + 2\beta \gamma_2^2 \left(\frac{M_{u2}}{M_{u1}} \right) \left(\frac{L_V}{L_H} \right)^2 \right] \quad (B-10)$$

where

$$\gamma_1 = 2 \sqrt{1 + M_{u3}/M_{u1}} \quad (B-11)$$

$$\gamma_2 = 2 \sqrt{1 + M_{u4}/M_{u2}} \quad (B-12)$$

The critical value for collapse mode "b" can be found by differentiating the above equation with respect to β and setting the result equal to zero, obtaining

$$\frac{dq}{d\beta} = \frac{12M_{u2} \gamma_2^2}{L_H^2 \beta^2 (3 - 2\beta)^2} \left[\beta^2 + \left(\frac{M_{u1}}{M_{u2}} \right) \left(\frac{L_H \gamma_1}{L_V \gamma_2} \right)^2 \left(\beta - \frac{3}{4} \right) \right] = 0 \quad (B-13)$$

Solving this equation for β yields

$$\beta = \frac{1}{2} \frac{M_{u1}}{M_{u2}} \frac{\gamma_1}{\gamma_2} \left(\frac{L_H}{L_V} \right)^2 \left[\sqrt{\left(\frac{\gamma_1}{\gamma_2} \right)^2 + 3 \left(\frac{M_{u2}}{M_{u1}} \right) \left(\frac{L_V}{L_H} \right)^2} - \frac{\gamma_1}{\gamma_2} \right] \quad (B-14)$$

Substituting the above value of β in Eq. B-10 gives the following equation for the ultimate resistance for collapse mode "b":

$$q_u = \frac{6M_{u2}\gamma_2^2}{L_H^2} \left[\sqrt{3 + \left(\frac{M_{u1}}{M_{u2}} \right) \left(\frac{L_H\gamma_1}{L_V\gamma_2} \right)^2} - \sqrt{\left(\frac{M_{u2}}{M_{u1}} \right) \left(\frac{L_H\gamma_1}{L_V\gamma_2} \right)^2} \right]^{-2} \quad (B-15)$$

For the assumption of collapse mode "b" to be valid, the value of β given by Eq. B-14 must be less than, or equal to, 0.5.

Dynamic Reactions

The dynamic reaction equations for collapse mode "b" can be obtained from those previously developed in Section V by noting that for collapse mode "b", the segments adjacent to the horizontal edges are triangular, while the segments adjacent to the vertical edges are trapezoidal, exactly opposite that for collapse mode "a." Since the portion of the total load acting on each of the segments and similarly the portion of the total resistance provided by each of the segments is assumed to be proportional to its area, the equations for the dynamic reactions along the horizontal and vertical edges can be obtained for collapse mode "b"

by interchanging the factors $(1 - \bar{\rho})/2$ and $\bar{\rho}/2$ in Eqs. 135 and 136, thus obtaining

$$V_u = \frac{c}{2} \left[\left(1 - \frac{z'}{z}\right) P_T + \frac{z'}{z} Q_T \right] \quad (\text{B-16})$$

$$V_v = \frac{(1 - \bar{\rho})}{2} \left[\left(1 - \frac{x'}{\bar{x}}\right) P_T + \frac{x'}{\bar{x}} Q_T \right] \quad (\text{B-17})$$

Since the deflected shape of the wall is assumed to remain the same, the values of x' , z' , \bar{x} , and \bar{z} can also be obtained from the expressions previously developed in Section V. Changing the limits of integration to conform to the areas of the segments formed in collapse mode "b," the expressions given in Table B-1 were obtained.

Transformation Factors

Since the deflected shape of the wall is assumed to be the same for both collapse modes, the load and mass factors for collapse mode "b" can be obtained from the corresponding equations developed for collapse mode "a" in Appendix A by merely changing the limits of integration to conform to the areas of the segments formed in collapse mode "b". The resulting expressions are found to be the same as given in Table A-1, with the exception that the transformation factors during the elastic phase for Support Cases 3 and 4 must be interchanged.

Table B-1

DYNAMIC REACTIONS FOR TWO-WAY REINFORCED CONCRETE WALLS (Collapse Mode "b")

$$V_v = \frac{(1 - \beta)}{2} \left[\left(1 - \frac{z'}{\bar{x}}\right) P_T + \frac{x'}{\bar{x}} Q_T \right] \quad V_n = \frac{P}{2} \left[\left(1 - \frac{z'}{\bar{z}}\right) P_T + \frac{z'}{\bar{z}} Q_T \right]$$

Support Case	Elastic Phase	Elasto-Plastic Phase	Plastic Phase
1	$\bar{x} = \frac{(0.127 - 0.185\beta)}{(0.400 - 0.508\beta)} l_w$	No Elasto-plastic Phase	
	$\bar{z} = \frac{(1/12 + \beta^2/15 + \beta^3/42)}{(1/6 - \beta^3/10 + \beta^3/30)} \beta l_w$		
2	$\bar{x} = \frac{(0.092 - 0.138\beta)}{(0.267 - 0.367\beta)} l_w$		$\bar{x} = \frac{(1/24 - \beta/16)}{(1/8 - \beta/6)} l_w$
	$\bar{z} = \frac{(1/20 - \beta/15 + \beta^2/42)}{(1/12 - \beta/10 + \beta^2/30)} \beta l_w$		
3	$\bar{x} = \frac{(0.092 - 0.138\beta)}{(0.267 - 0.367\beta)} l_w$		$\bar{z} = \frac{1}{2} \beta l_w$
	$\bar{z} = \frac{(1/12 + \beta^2/15 + \beta^3/42)}{(1/6 - \beta^3/10 + \beta^3/30)} \beta l_w$		
4	$\bar{x} = \frac{(0.127 - 0.185\beta)}{(0.400 - 0.508\beta)} l_w$		
	$\bar{z} = \frac{(1/20 - \beta/15 + \beta^2/42)}{(1/12 - \beta/10 + \beta^2/30)} \beta l_w$		
1,2,3,4	$x' = \frac{(1 - 4\beta/3)}{4(1 - \beta)} l_w$	$z' = \frac{1}{3} \beta l_w$	

Appendix C

STATISTICAL STUDY OF MASONRY WALLS WITH ARCHING

Appendix C

STATISTICAL STUDY OF MASONRY WALLS WITH ARCHING

References 18 and 19 present the results of the test of a number of unreinforced masonry unit walls exposed to a nuclear blast. To analyze the behavior of these walls in a more rational manner than by merely assuming the properties of the wall and loading are known with certainty the statistical methods developed in Section IV were applied. To demonstrate the method for calculating the probability of occurrence of the incipient collapse overpressure, the details of the analysis are given for an 8-in. thick brick wall reported in Ref. 18.

Three walls of the same type were tested at overpressure levels of 4.2, 7.1, and 12 psi. The wall located at the 4.2 psi level was almost free of damage, the wall at 7.1 psi had slight damage although it remained in place, and the wall at 12 psi was blown out with only fringes of the brick remaining. The dimensions of the test walls were as follows:

$$t_w = 8 \text{ in.}$$

$$L_v = 105 \text{ in.}$$

$$L_h = 165 \text{ in.}$$

The procedure developed in Section III for two-way action of unreinforced walls with arching was used to determine the incipient collapse overpressure. In determining the values to use for the physical properties of the wall, it was assumed that the compressive strength, f'_m , and the modulus of elasticity, E_m , were normally distributed. The mean value for f'_m was taken as 2000 psi, and the standard deviation as 600 psi. These values were obtained by first assuming that the value most likely to occur was equal to the mean. Next, upper and lower values were

established by estimating the limits that would contain 90 percent of the actual values. These limiting values would necessarily be symmetrical about the mean for a normal distribution. Using these limits, the standard deviation was determined using the properties of the normal distribution. For this case, the limits were taken as 1000 and 3000 psi, thus resulting in a standard deviation of 600 psi. It should be noted that the assumption of a normal distribution for f'_c and its accompanying values was arbitrarily made. This was necessary due to the lack of information concerning the actual distribution of the compressive strengths of brick walls. To obtain such information would have required an extensive literature search, which was beyond the scope of this study. This type of information, however, would be desirable for future studies, since the accuracy of the statistical study is directly dependent upon the material properties used.

A similar procedure was used to determine the modulus of elasticity, E_c . The modulus of elasticity was taken as equal to $\alpha f'_c$, where α was assumed to be normally distributed with a mean of 1000 and a standard deviation of 300 (the 5 and 95 percent values were assumed to be 500 and 1500, respectively).

The value of the unit weight, γ , was taken as 120 pcf. It was not necessary to assume a probability distribution for the unit weight, since previous studies reported in Ref. 1 showed that variations in the value have little effect on the predicted collapse overpressure.

The results obtained in the Monte Carlo study (described in Section IV) using these values are shown in Table C-1. Mean values and confidence limits are given for the mean, standard deviation, and the 10 and 90 percent probability values for various values of n , the number of "samples" (random values) taken. The values for the mean and standard deviation obtained from 100 samples are 12.91 psi and 3.07 psi, respectively. In contrast, the values obtained from 25 samples are 12.64 and

Table C-1
 SUMMARY OF STATISTICAL ANALYSIS OF 8 IN. BRICK WALL.
 (Overpressure, psi, except for Percentages Columns)

n	Mean	95 Percent Confidence Interval		Percent Difference From Mean	Standard Deviation	95 Percent Confidence Interval		Maximum Difference From Standard Deviation		10 Percent Probability Value		90 Percent Probability Value		Confidence Interval	
		Lower	Upper			Lower	Upper	Value	Percent of Mean	Value	Percent of Mean	Value	Percent of Mean	Lower	Upper
10	13.91	12.09	15.73	13.1%	2.38	1.64	3.35	1.97	14.2%	10.86	8.33	11.81	16.96	16.01	19.45
20	12.87	11.32	14.42	12.3	3.23	2.46	4.72	1.49	11.6	8.73	6.82	9.72	17.01	16.02	18.92
25	12.64	11.38	13.90	10.0	3.00	2.34	4.17	1.17	9.3	8.80	7.30	9.61	16.48	15.1	17.98
30	12.62	11.54	13.70	8.6	2.83	2.25	3.80	0.93	7.7	8.39	7.75	9.71	16.25	15.50	17.49
40	12.16	11.19	13.13	8.0	2.97	2.43	3.81	0.84	6.9	8.35	7.28	9.01	15.97	15.28	17.04
50	12.44	11.58	13.30	6.9	3.03	2.53	3.78	0.75	6.0	8.56	7.59	9.20	16.32	15.68	17.29
100	12.91	12.29	13.53	4.8	3.07	2.70	3.57	0.50	3.9	8.97	8.33	9.15	16.85	16.37	17.49

* Confidence limits for the 10 and 90 percent probability values are somewhat less than 95 percent.

3.00 psi, which are within 2.1 and 2.3 percent, respectively, of the values from the 100 samples. The corresponding values of the 10 and 90 percent probability values are 8.97 and 16.85 psi for the 100 samples, and 8.80 and 16.48 psi for the 25 samples, differences of 1.9 and 2.2 percent. As can be seen, these differences are relatively small.

It remains to investigate how close the distribution of the incipient collapse overpressure is to a normal distribution. To do this, the cumulative probability distributions for both the 100 samples and 25 samples were plotted on probability paper; these plots are shown in Figures C-1 and C-2, respectively. Since the plots are reasonably close to a straight line, the incipient collapse overpressure approximates a normal distribution. Also shown in the plots are the 95 percent confidence limits for the mean and for the 10 and 90 percent probability values.*

In a manner similar to that just described for the 8-in. thick brick wall, an analysis was performed on seven additional types of walls that were included in the field tests reported in Ref. 19. However, based on the small differences in the values shown in Table C-1 for 25 or more samples, only 50 samples rather than 100 were used in the analysis of the seven walls.

A summary of all eight wall types analyzed and their physical properties is given in Table C-2. Included are the values used in the analysis for the mean and standard deviation of the compressive strength, f'_m , and the modulus of elasticity, E_m . Also, for case 8, which had a 19 percent window opening in the front wall, mean and standard deviation values are given for the clearing distance, S , which is assumed to be normally distributed.

The results of the statistical analyses are summarized in Table C-3, and also shown graphically in Figure C-3. Values are given for the 10,

* As discussed in Section IV, the confidence limits for the 10 and 90 percent probability values are somewhat less than 95 percent.

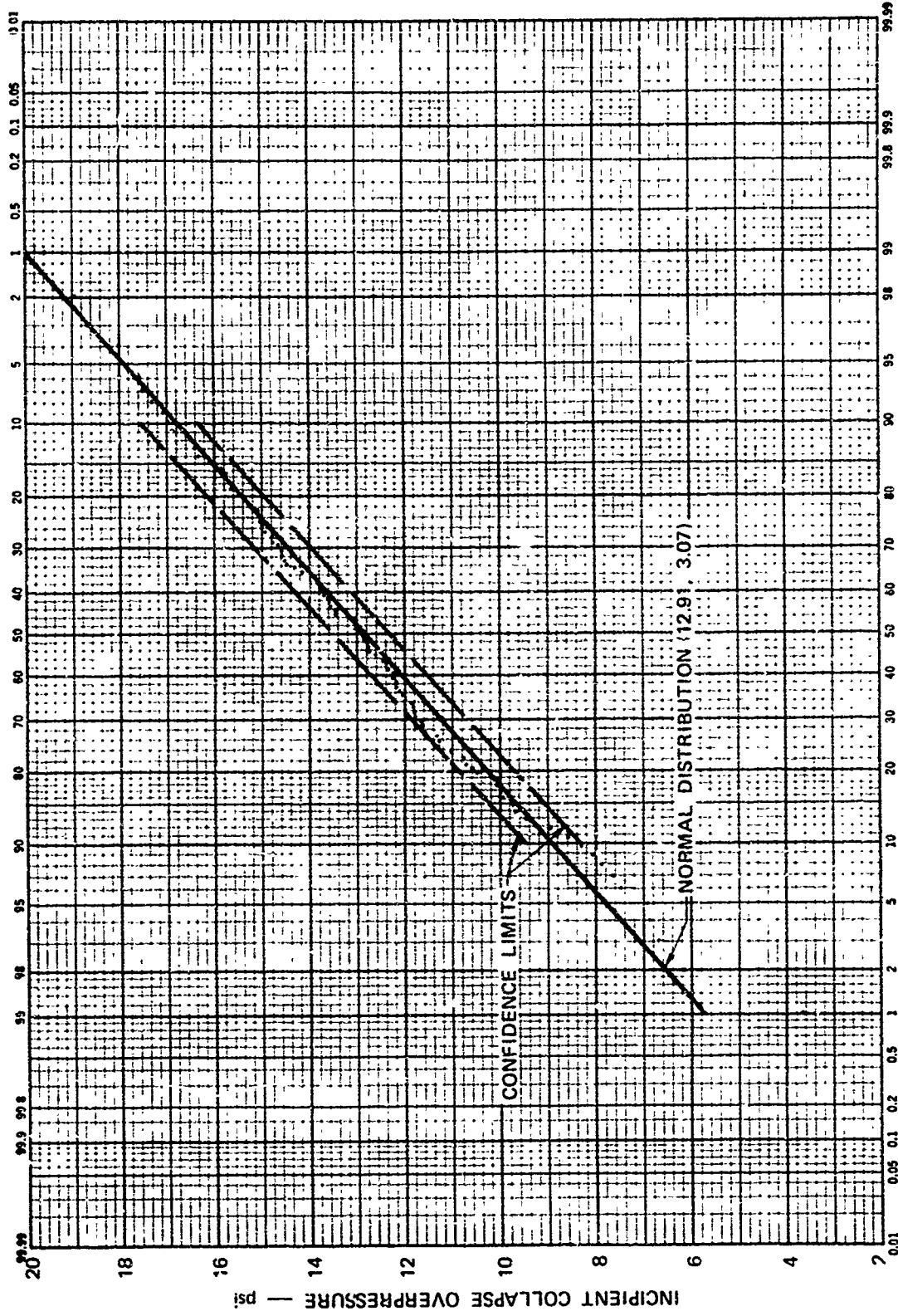


FIGURE C-1 INCIDENT COLLAPSE OVERPRESSURE OF 8 IN. BRICK WALL
 PANEL ON NORMAL PROBABILITY PAPER (n = 100)

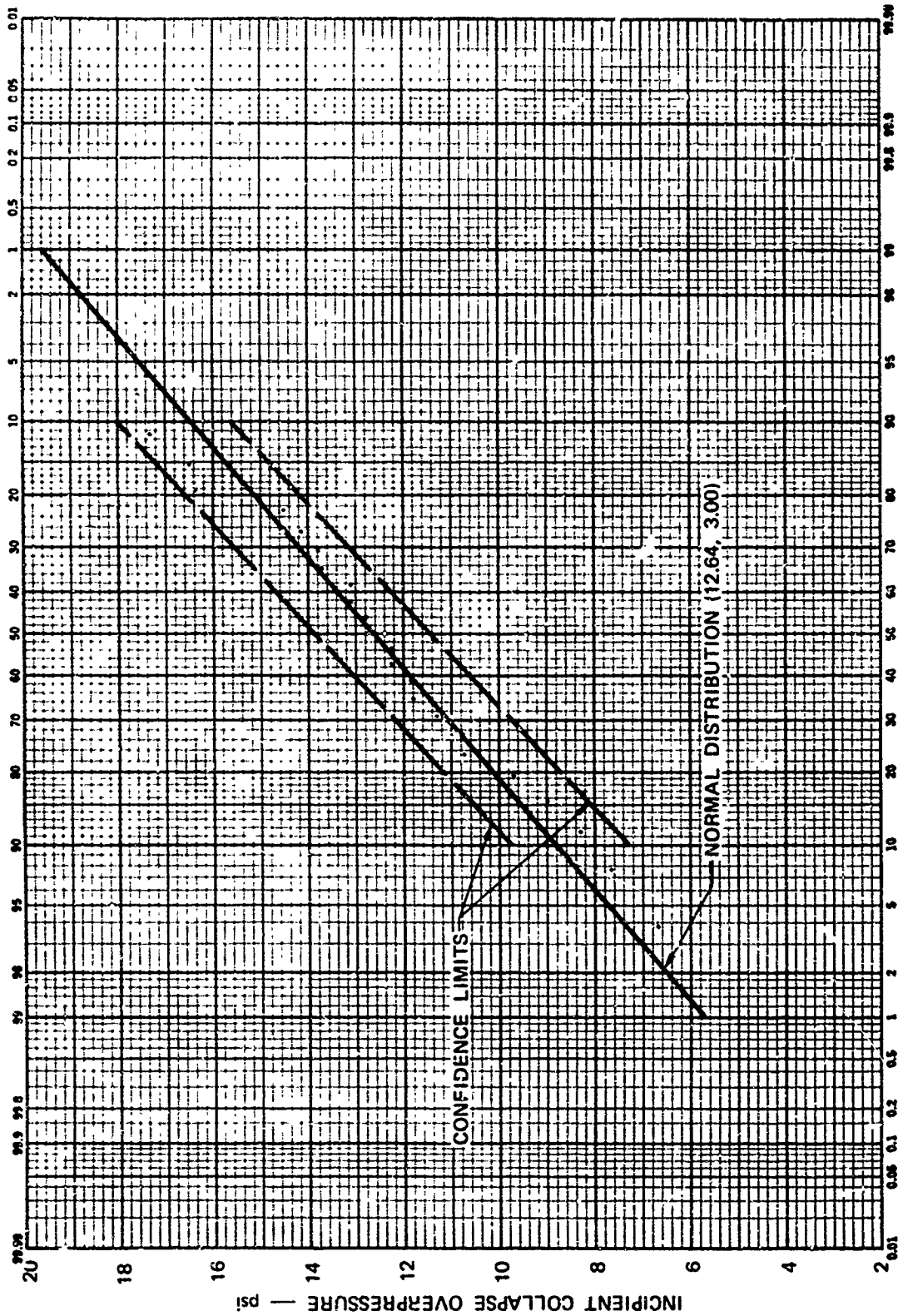


FIGURE C-2 INCIPIENT COLLAPSE OVERPRESSURE OF 8 IN. BRICK WALL
 PANEL ON NORMAL PROBABILITY PAPER (n = 25)

Table C-2

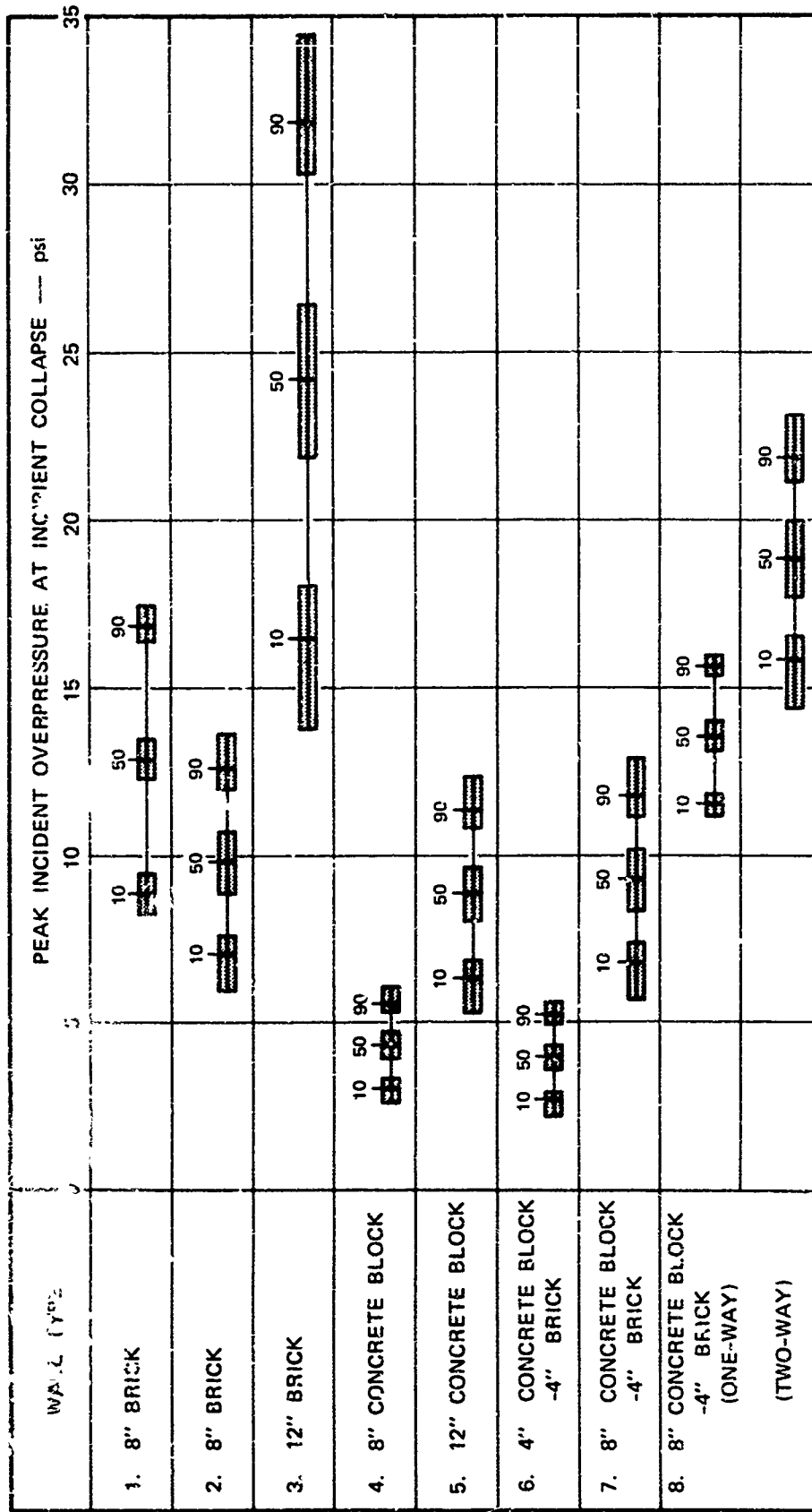
PHYSICAL PROPERTIES OF TEST WALLS

Wall Type	Description	t_w (in.)	l_v (in.)	l_h (in.)	γ (pcf)	t_f (in.)	f'_c (psi)		α		Percent Openings	S (ft)		Remarks
							Mean	Std. Dev.	Mean	Std. Dev.		Mean	Std. Dev.	
1	8 in. brick	8	105	165	120	--	2000	600	1000	300	0	10	--	Ref. 18--walls 3.5 av, 3.5 bf, 3.5 ce
2	8 in. brick	8	120	192	120	--	2000	600	1000	300	0	11	--	Ref. 19--wall 6 (a,c)
3	12 in. brick	12	120	192	120	--	2000	600	1000	300	0	11	--	Ref. 19--wall 3 (a,c)
4	8 in. concrete block	8	120	192	80	1.5	1200	350	1000	300	0	11	--	Ref. 19--wall 2 (a,c)
5	12 in. concrete block	12	120	192	80	1.75	1200	350	1000	300	0	11	--	Ref. 19--wall 7 (a,c)
6	4 in. concrete block --1 in. brick	8	120	192	100	1.375	1200	350	1300	300	0	11	--	Ref. 19--walls 5, 8, 11 (a,c)
7	8 in. concrete block --1 in. brick	12	120	192	100	1.5	1750	150	1000	300	0	11	--	Ref. 19--walls 3, 4, 10 (a,c)
8	8 in. concrete block --1 in. brick	12	120	192	100	1.5	1750	150	1000	300	19	7.0	2.1	Ref. 19--walls 1, 4-9, 11-14, 16 (b,d)

Table C-3
SUMMARY OF STATISTICAL ANALYSES OF ARCHING WALLS
(Overpressure, psi)

Wall Type	Description	Mean		Standard Deviation		95 Percent Confidence Interval		10 Percent Probability Value		90 Percent Probability Value		Remarks		
		Value	Confidence Interval	Value	Confidence Interval	Value	Confidence Interval	Value	Confidence Interval	Value	Confidence Interval			
1	8 in. brick (105 in. X 165 in.)	12.91	12.30	13.52	3.07	2.70	3.57	8.93	8.33	9.45	16.95	16.37	17.19	0 of 1 failed at 1.2 and 7.1 psi; 1 of 1 failed at 12 psi
2	8 in. brick (120 in. X 192 in.)	9.84	8.93	10.75	2.16	1.69	3.01	7.07	5.98	7.67	12.61	12.00	13.69	0 of 1 failed at 4.5 psi; 1 of 1 failed at 8.1 psi
3	12 in. brick	24.20	21.91	26.48	6.01	4.79	8.08	15.19	13.83	18.06	31.91	30.31	31.56	0 of 1 failed at 4.5 psi; 1 of 1 failed at 8.1 psi
4	8 in. concrete block	4.37	3.96	4.77	0.96	0.75	1.84	3.13	2.65	3.10	5.60	5.33	6.09	1 of 1 failed at 1.5 psi
5	12 in. concrete block	8.88	8.05	9.71	1.97	1.54	2.74	6.35	5.36	6.90	11.10	10.85	12.39	1 of 1 failed at 4.5 psi
6	4 in. concrete block --4 in. brick	3.97	3.60	4.35	0.99	0.79	1.33	2.70	2.26	2.96	5.35	4.99	5.69	2 of 2 failed at 4.5 psi
7	8 in. concrete block --4 in. brick	9.30	8.38	10.23	1.92	1.46	2.81	6.84	5.71	7.43	11.77	11.18	12.90	0 of 3 failed at 4.5 psi; 3 of 3 failed at 8.4 psi
8	8 in. concrete block --4 in. brick (One-way) (Two-way)	13.57	13.11	14.03	1.59	1.40	1.85	11.53	11.20	11.78	15.61	15.36	15.94	0 of 12 failed at 4.5 psi; 0 of 12 failed at 8.4 psi
		18.81	17.69	19.94	2.35	1.78	3.43	15.81	14.42	16.53	21.82	21.10	23.21	

* Confidence limits for the 10 and 90 percent probability values are somewhat less than 95 percent.



NOTE: Values shown above are peak incident overpressures for 10, 50, and 90 percent probabilities of collapse. Blocked areas represent confidence limits for the above values.

FIGURE C-3 STATISTICAL ANALYSIS OF INCIPIENT COLLAPSE OVERPRESSURE FOR ARCHING WALLS

50, and 90 percent probability of occurrence of the incipient collapse overpressure of each of the eight walls. Also given are the confidence intervals for each of these values. The corresponding values for the standard deviation are also listed in Table C-3.

Based on the above analysis of eight walls, the following guidelines were established to determine the number of samples required to describe the parameters of the assumed normal distribution of the incipient collapse overpressure within the desired degree of accuracy:

1. Minimum sample size, $n = 20$.
2. The 95 percent confidence limits for the sample mean, \bar{x} , should be within ± 10 percent of \bar{x} .
3. The 95 percent confidence limits for the sample standard deviation, s , should be within $\pm 0.10 \bar{x}$ (10 percent of the sample mean) of s (the upper confidence limit is the critical value).

Appendix D

COMPUTER PROGRAMS

Appendix D

COMPUTER PROGRAMS

The computer programs used in the dynamic analysis of the various two-way action wall types considered in this study consist of several routines common to each program, linked with other segments pertaining to each specific wall type. These parts are organized into the overall system illustrated in Figure D-1. Flow charts of each of these subroutines are given in Figures D-2 through D-8. The dashed boxes in these figures indicate that the enclosed operation is optional and is executed only if certain requirements are met, e.g., if the wall contains windows. The computer program is composed of the main routine, subroutines TRANS, LOAD, and FILL, and the appropriate RESIST subroutine corresponding to the particular wall type being analyzed.

The main routine, shown in Figure D-2, controls the execution sequence of the program, numerically integrates the equations of motion, and performs an interval halving procedure to determine the incipient collapse load. Subroutine RESIST, which is peculiar to each wall type, handles input and output of the wall data and calculates the appropriate resistance curve values. It also provides the resistance-displacement values required in the numerical integration routine. The corresponding flow charts for each of the three wall types in this study are shown in Figures D-3 through D-5. Subroutine TRANS (Figure D-6) calculates the load and mass transformation factors required to reduce the distributed mass system to an equivalent single-degree-of-freedom system. It also calculates the coefficients necessary to determine the dynamic reactions. Subroutine LOAD (Figure D-7) handles input and output of the exterior

load data, calculates the values of any parameters required, and provides the load-time values used in the numerical integration routine. The four loading cases discussed in Ref. 1, plus an arbitrary loading function, are available. Subroutine FILL (Figure D-8) calculates the interior load for the case of a wall containing openings.

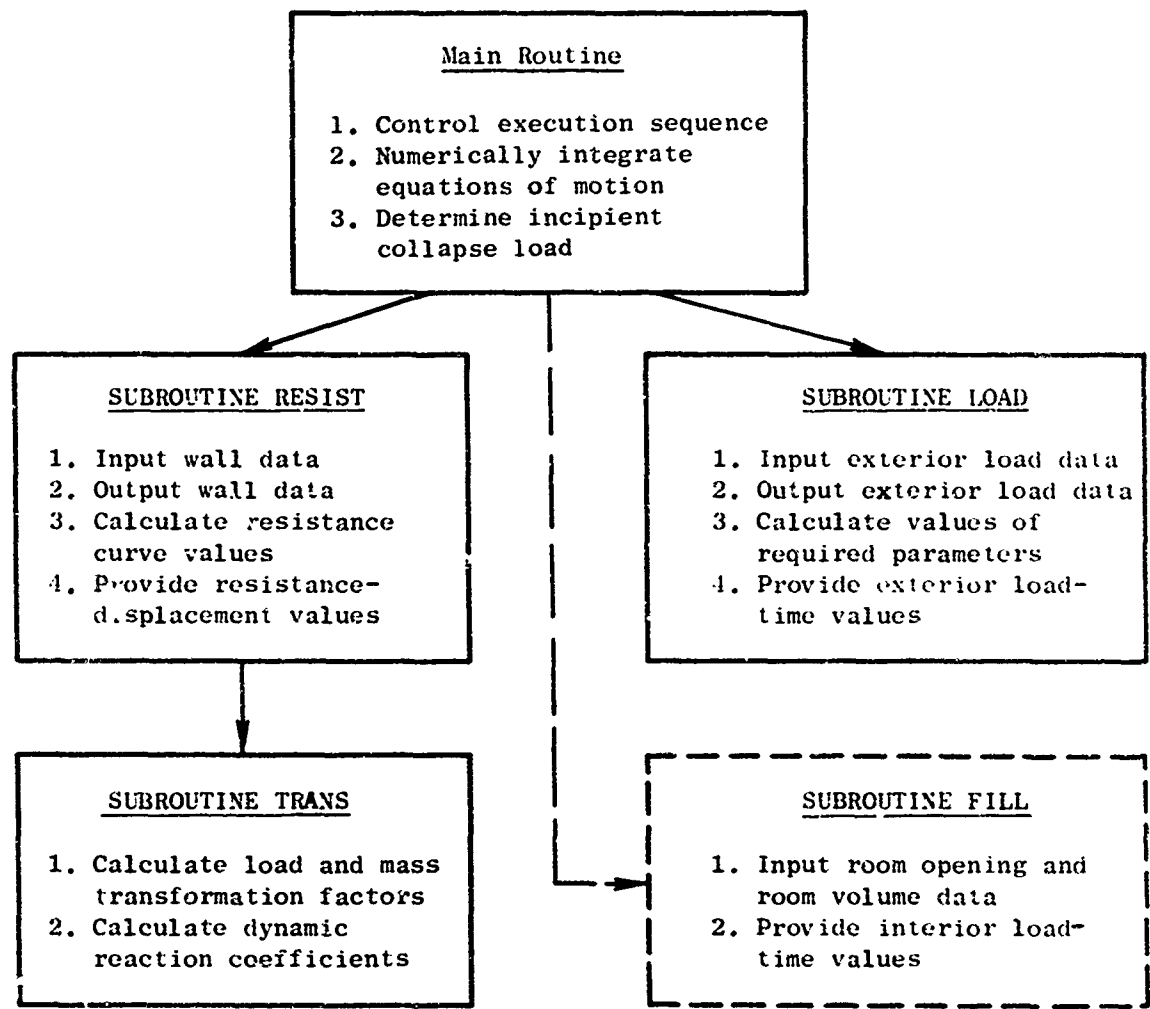


FIGURE D-1 OVERALL ORGANIZATION OF COMPUTER PROGRAMS

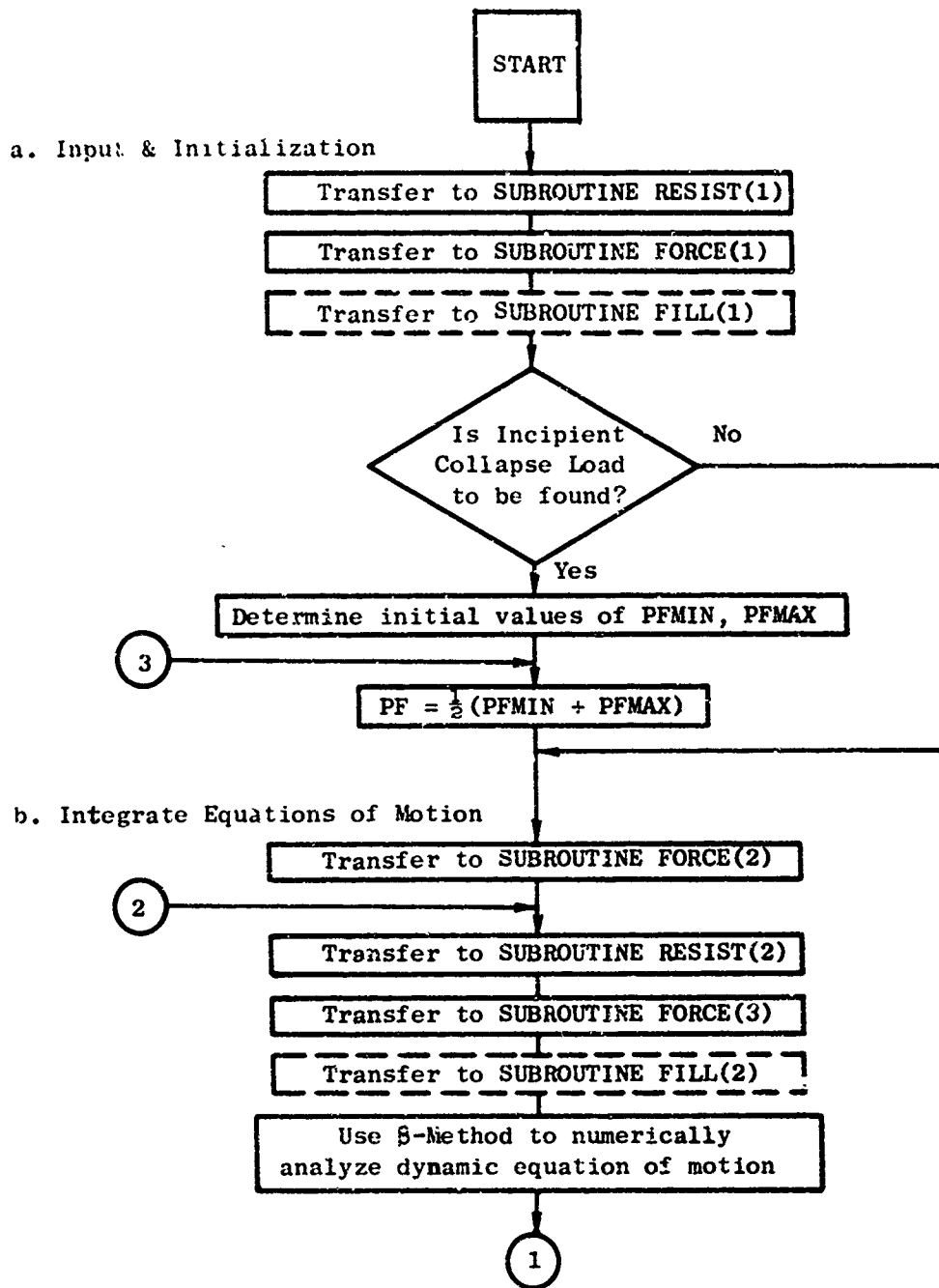
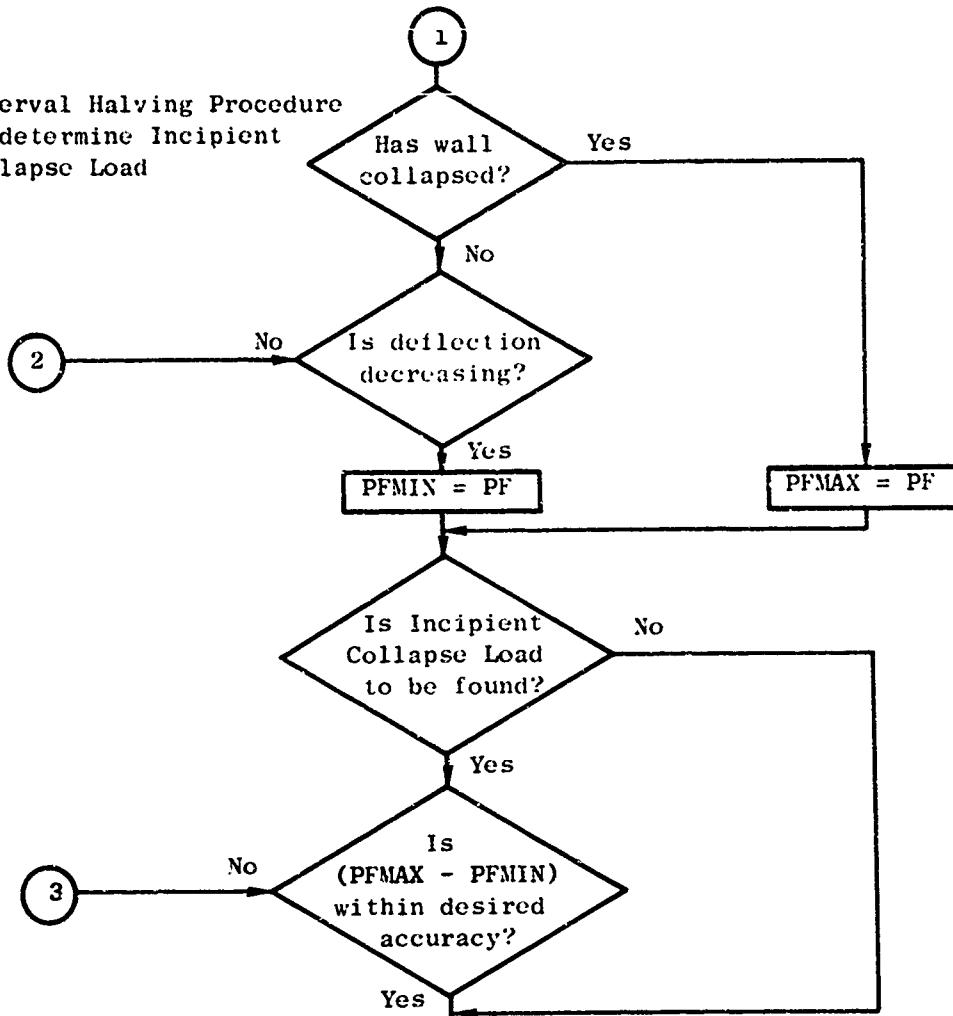


FIGURE D-2 FLOW CHART OF MAIN ROUTINE

c. Interval Halving Procedure to determine Incipient Collapse Load



d. Output Results

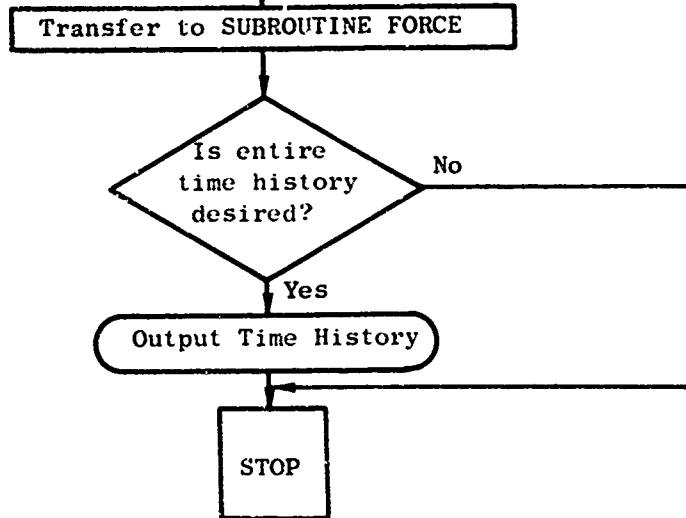


FIGURE D-2 (Concluded)

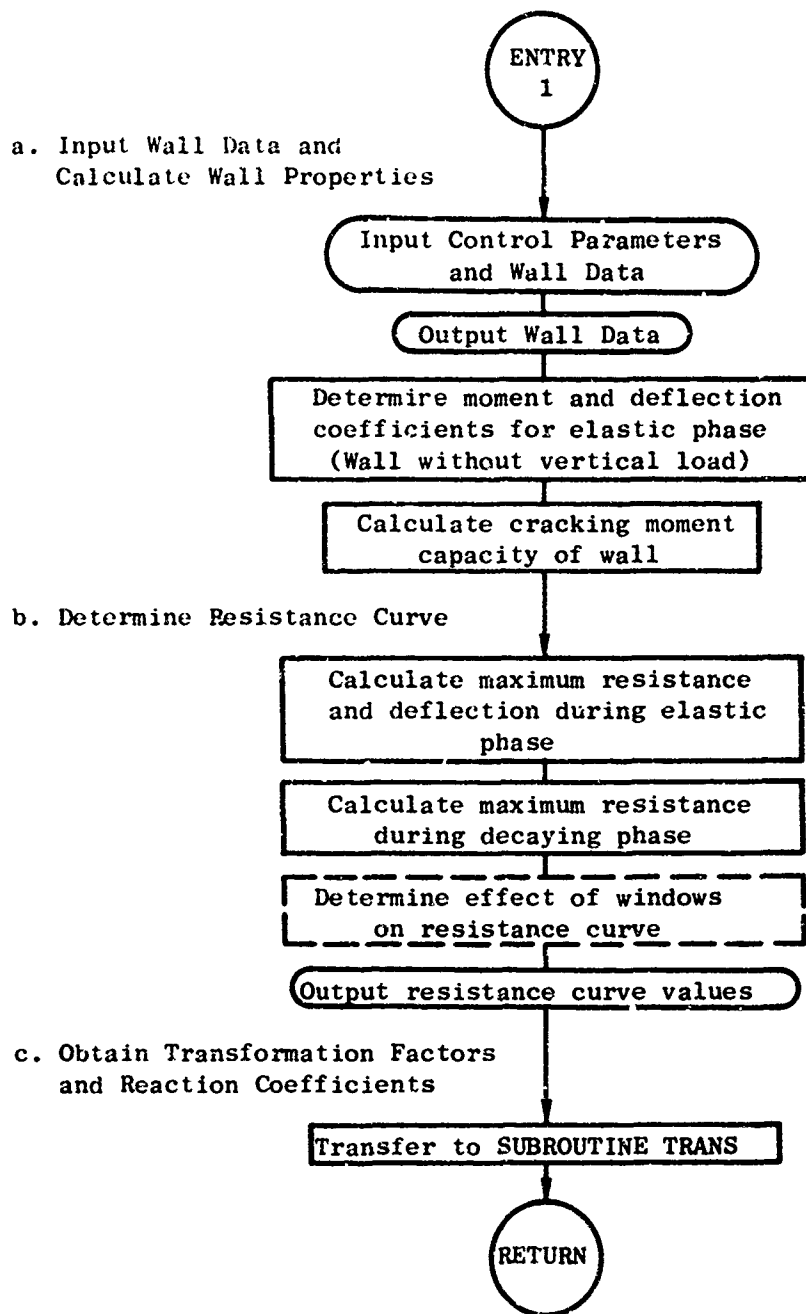


FIGURE D-3 FLOW CHART OF SUBROUTINE RESIST
Two-Way Unreinforced Wall Without Arching

a. Determine Resistance, Load-Mass Factor, and Reaction Coefficients for Y(I)

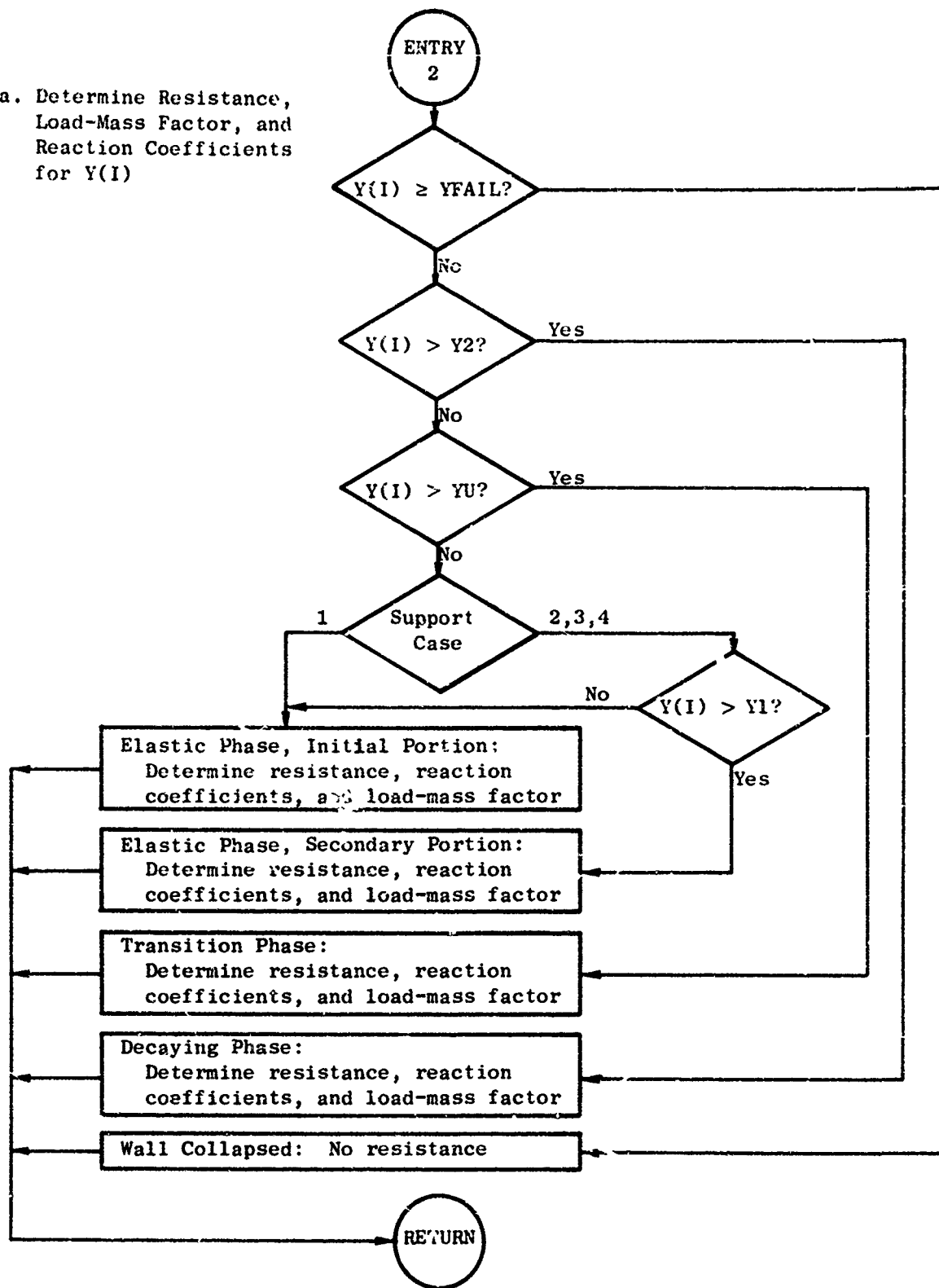


FIGURE D-3 (Concluded)

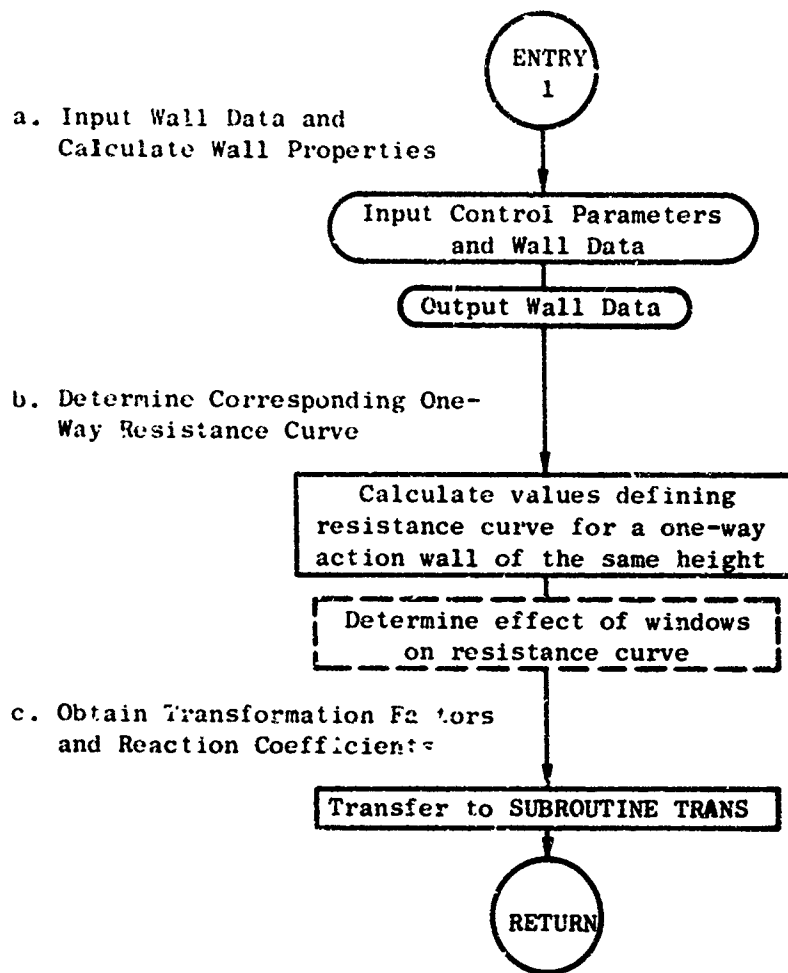


FIGURE D-4 FLOW CHART OF SUBROUTINE RESIST
Two-Way Unreinforced Wall Without Arching

d. Determine Resistance, Load-Mass Factor, and Reaction Coefficients for Y(I)

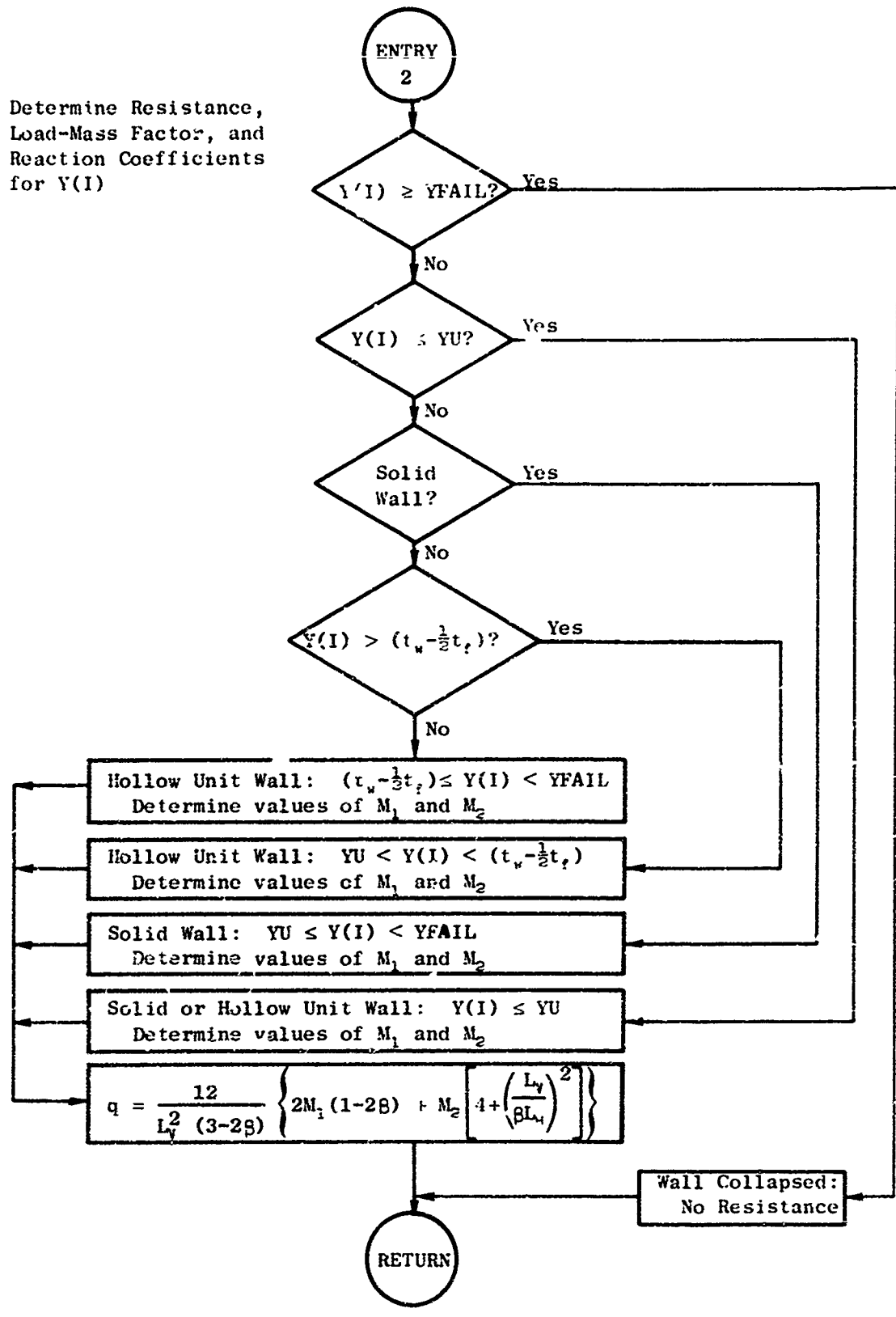


FIGURE D-4 (Concluded)

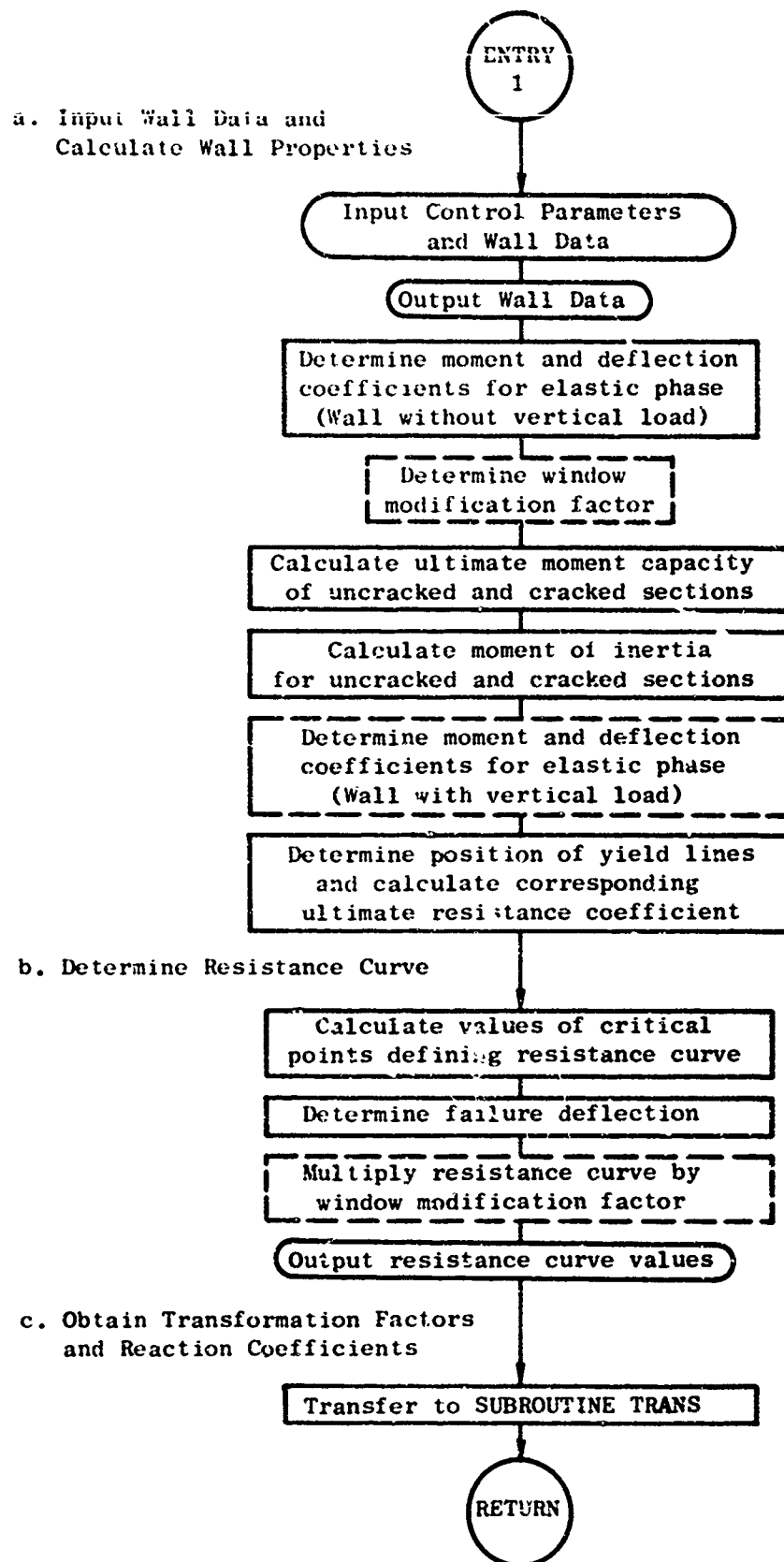


FIGURE D-5 FLOW CHART OF SUBROUTINE RESIST
Two-Way Reinforced Concrete Wall

d. Determine resistance, load-mass factor, and reaction coefficients for Y(I)

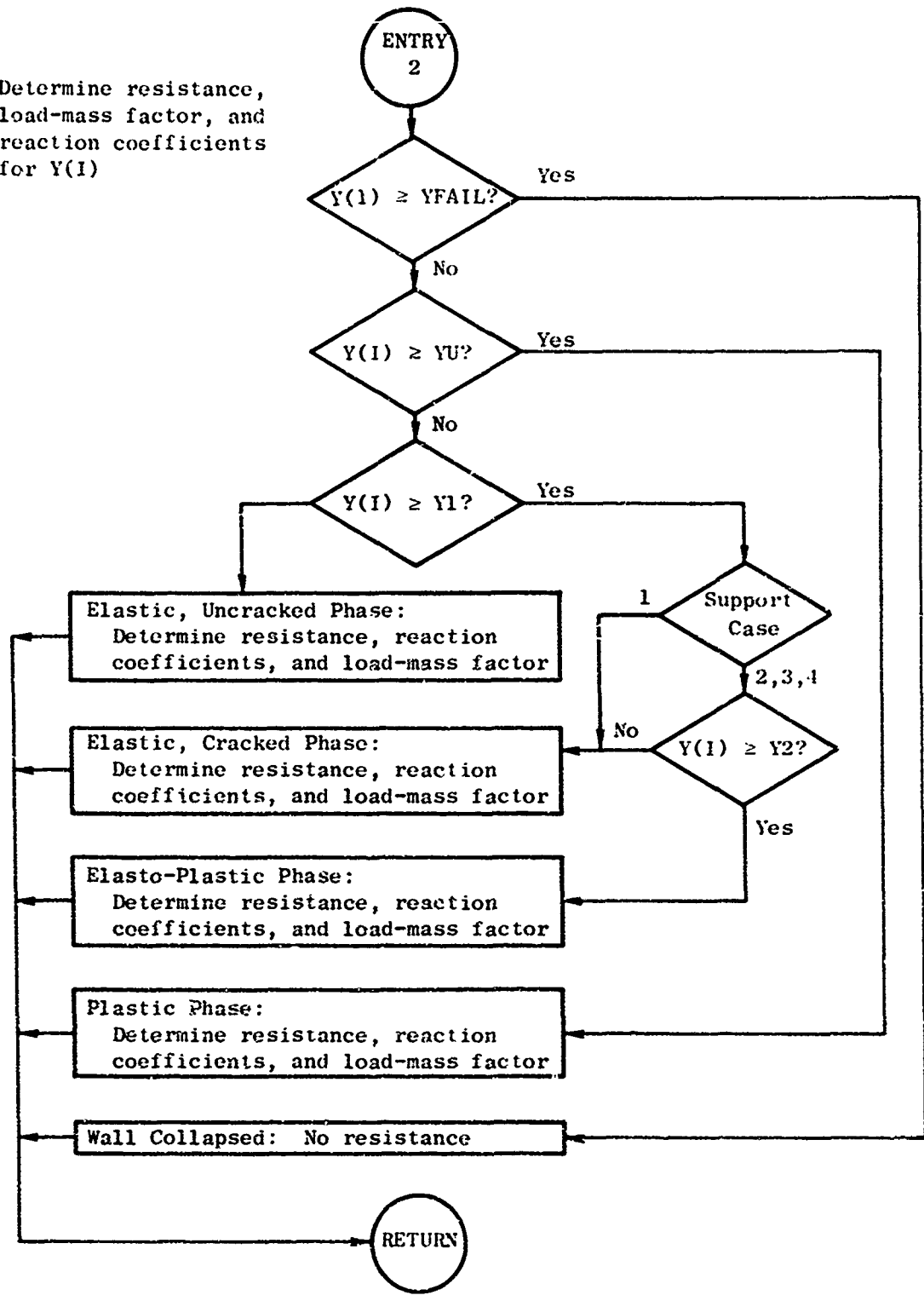


FIGURE D-5 (Concluded)

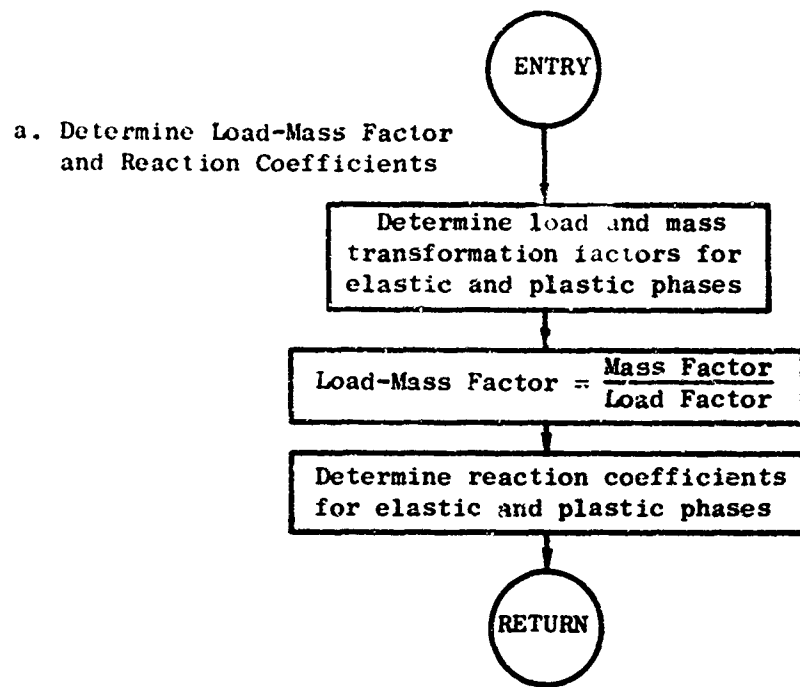


FIGURE D-6 FLOW CHART OF SUBROUTINE TRANS

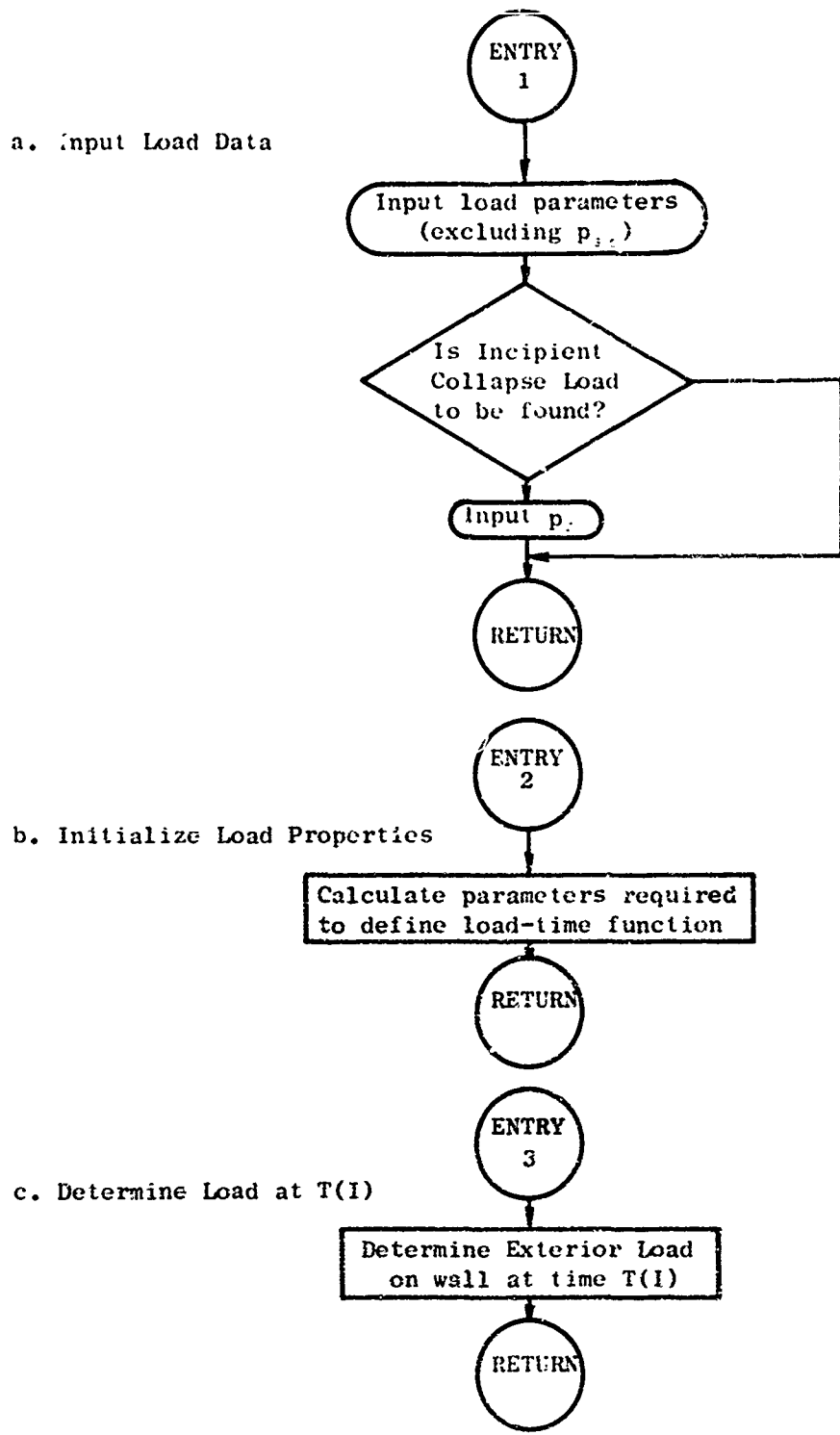


FIGURE D-7 FLOW CHART OF SUBROUTINE LOAD

d. Output Load Data

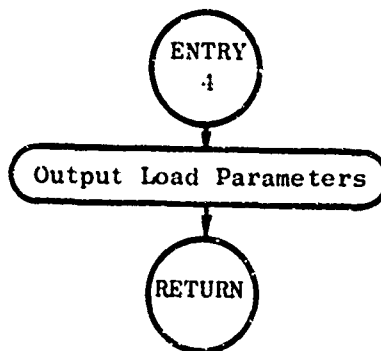
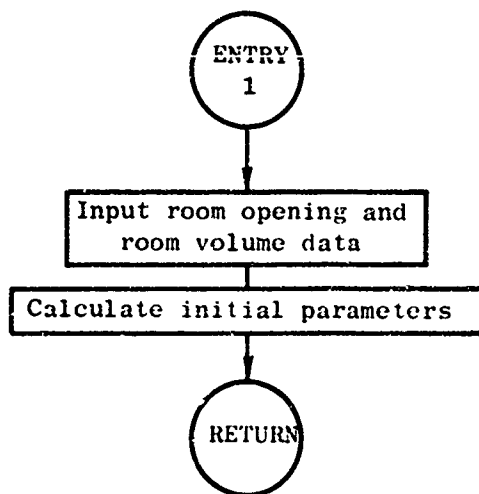


FIGURE D-7 (Concluded)

a. Input Room and Opening Data



b. Calculate Interior Pressure

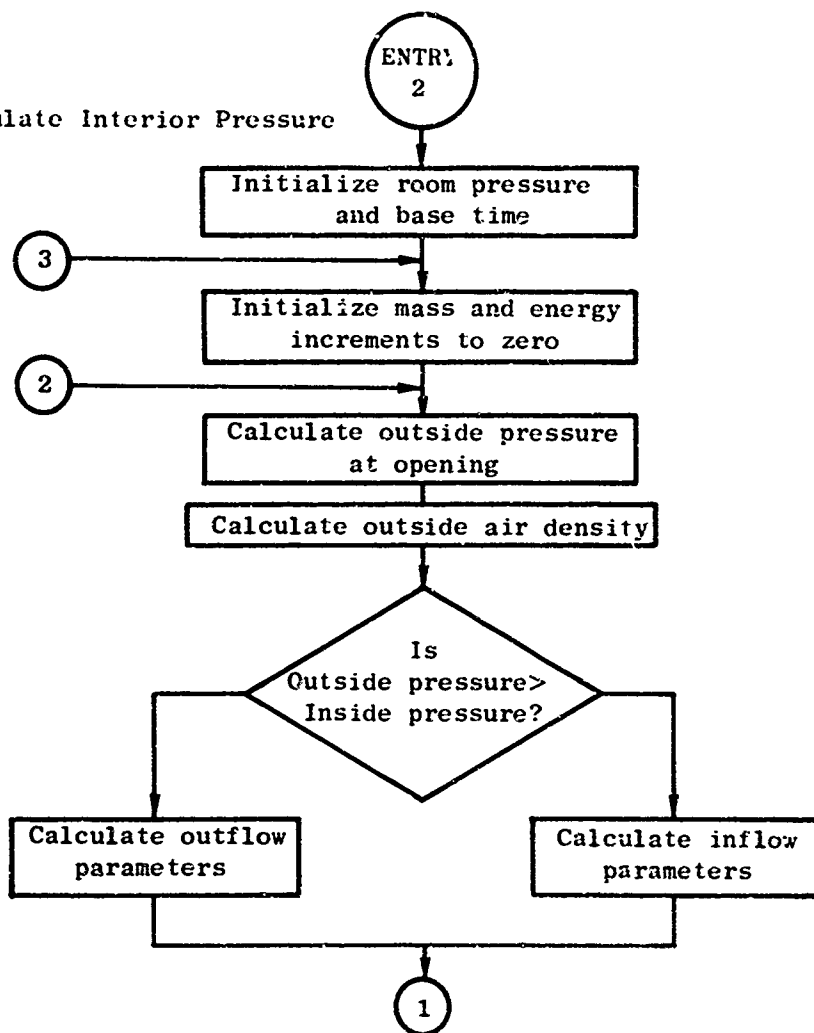


FIGURE D-8 FLOW CHART OF SUBROUTINE FILL

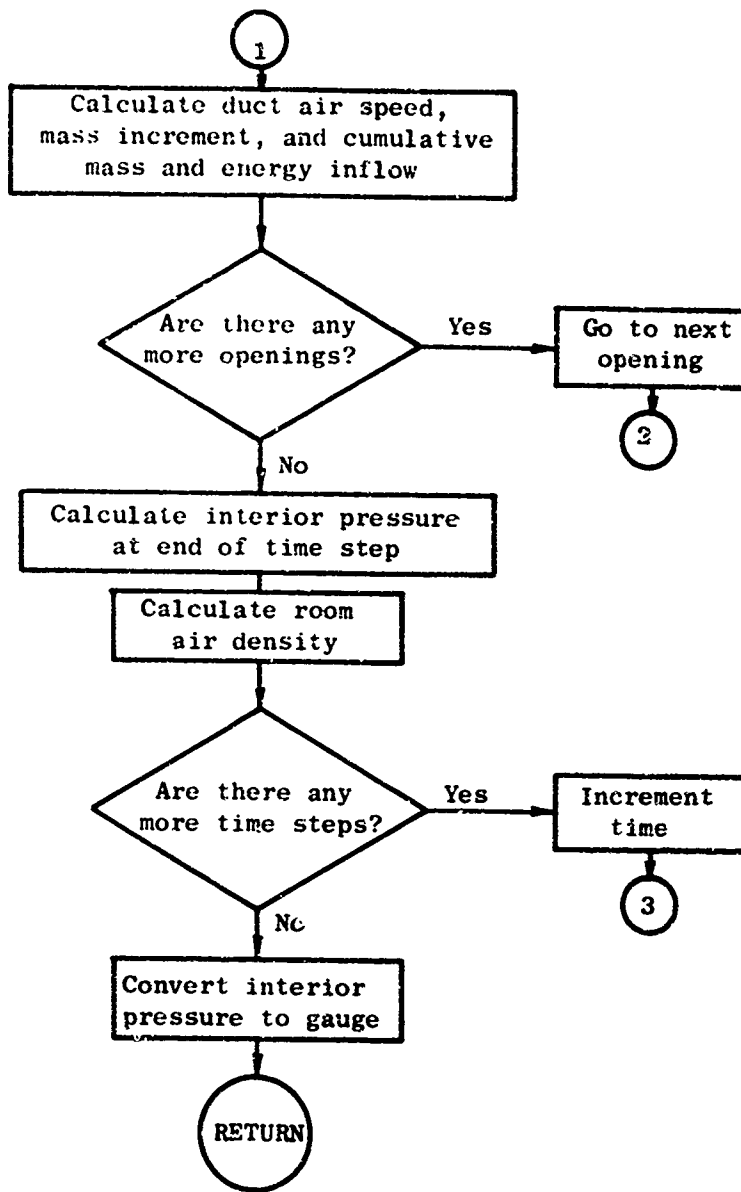


FIGURE D-8 (Concluded)

REFERENCES

1. Wiehle, C. K. and J. L. Bockholt, Existing Structures Evaluation, Part I: Walls, Stanford Research Institute (for Office of Civil Defense), Menlo Park, California, November 1968 (AD-687 293).
2. Iverson, J. H., Existing Structures Evaluation, Part II: Window Glass and Applications, Stanford Research Institute (for Office of Civil Defense), Menlo Park, California, December 1968 (AD-687 294).
3. Jensen, G. F., Existing Structures Evaluation, Part III: Structural Steel Connections, Stanford Research Institute (for Office of Civil Defense), Menlo Park, California, December 1969 (AD-701 088).
4. Newmark, N. M., "A Method of Computation for Structural Dynamics," ASCE Transactions, Paper No. 3384, Vol. 127, 1962, Part I.
5. Willoughby, A. B., C. Wilton, and B. Gabrielsen, Development and Evaluation of a Shock Tunnel Facility for Conducting Full Scale Tests of Loading, Response, and Debris Characteristics of Structural Elements, URS 680-2, URS Corporation (for Office of Civil Defense and Stanford Research Institute), Burlingame, California, December 1967 (AD-674 256).
6. "Weapons Effects Data", EM 1110-345-413, The Design of Structures to Resist the Effects of Atomic Weapons, Massachusetts Institute of Technology for the Office of Chief of Engineers, U. S. Army, Washington, D. C., 1957.
7. Rempel, J. R., "Room Filling From Air Blast," Appendix E of Final Report by H. L. Murphy, Feasibility Study of Slanting for Combined Nuclear Weapons Effects, Stanford Research Institute (for Office of Civil Defense), Menlo Park, California, June 1969 (AD-692 312).
8. Melichar, J. F., The Air-Blast-Induced Environment Within Civil Defense Blast-Slanted Shelters, URS 755-3, URS Research Company (for Office of Civil Defense and Stanford Research Institute), Burlingame, California, November 1969 (AD-708 564).
9. Ballistic Research Laboratories, Information Summary of Blast Patterns In Tunnels and Chambers, BRL MR 1390, DASA 1273, Aberdeen Proving Ground, Maryland, March 1962 (AD-274 228).

10. Childers, H. M., C. A. Vansant, and D. F. Mokrauer, Open Shelter Feasibility Study, The Vertex Corporation (for Office of Civil Defense), Kensington, Maryland, October 1968 (Ad-688 659).
11. Melichar, J. F., The Propagation of Blast Waves Into Chambers, BRL MR 1920, Ballistic Research Laboratories, Aberdeen Proving Ground, Maryland, March 1968 (Ad-672 476).
12. Glasstone, S., ed., The Effects of Nuclear Weapons, Department of Defense and Atomic Energy Commission, Washington, D.C., February 1964.
13. Timoshenko, S. and S. Woinowsky-Krieger, Theory of Plates and Shells, McGraw-Hill Book Company, Inc., New York, 1959.
14. Conway, H. D., "Bending of Rectangular Plates Subjected to a Uniformly Distributed Lateral Load and to Tensile or Compressive Forces in the Plane of the Plate," Journal of Applied Mechanics, September 1949, pp. 301-9.
15. Willoughby, A. B., et al., A Study of Loading, Structural Response, and Debris Characteristics of Wall Panels, URS 680-5, URS Research Company (for the Office of Civil Defense), Burlingame, California, July 1969 (AD-693 792).
16. Dunham, Clarence W., Advanced Reinforced Concrete, McGraw-Hill Book Company, New York, 1964.
17. Jones, L. L. and R. H. Wood, Yield-Line Analysis of Slabs, American Elsevier Publishing Company, Inc., New York, 1967.
18. Sevin, E., Tests on the Response of Wall and Roof Panels and the Transmission of Load to Supporting Structure, WT-724, Armed Forces Special Weapons Project, Sandia Base, Albuquerque, N. M. (for Air Material Command, Wright-Patterson A.F. Base), May 1955.
19. Taylor, B. C., Blast Effects of Atomic Weapons Upon Curtain Walls and Partitions of Masonry and other Materials, WT-741, Federal Civil Defense Administration, Battle Creek, Michigan, August 1956 (AD-636 766).
20. American Concrete Institute, Building Code Requirements for Reinforced Concrete, ACI 318-63, Detroit, Michigan, June 1963.

21. Hald, A., Statistical Theory with Engineering Applications, John Wiley and Sons, Inc., New York, 1952.
22. Pettitt, B. E., Air Force Structures Test, Volume I, Scientific Director's Report, Annex 3.3, Air Installations Division, Headquarters, Air Materiel Command, Wright-Patterson Air Force Base, Dayton, Ohio, August 1951 (AD-486 593I).
23. Randall, Phillip A., Damage to Conventional and Special Types of Residences Exposed to Nuclear Effects, WT-1194, Civil Effects Test Group, Atomic Energy Commission, Washington, D.C., March 1961 (AD-611 160).
24. Private Communication with J. F. Halsey, URS Research Company.
25. "Structural Elements Subjected to Dynamic Loads", EM 1110-345-416, The Design of Structures to Resist the Effects of Atomic Weapons, Massachusetts Institute of Technology for the Office of Chief of Engineers, U.S. Army, Washington, D.C., 1957 (AD-419 935).

NOMENCLATURE

A	Net area of wall with openings, sq ft	h_n	Clearing dimension subdivided wall w
A, A_v	Deflection coefficient for elastic phase of two-way wall for Support Case i; subscript v denotes wall with vertical load	i	Subscript denoting wall
A	Area of each portion of subdivided wall with openings, sq ft	I_A, I_C	Inertia force of wall, lb
A	Total gross area of wall, sq ft	I_C	Moment of inertia section, in ⁴ /in.
A_w	Area of window, sq ft	I_K	Moment of inertia section, in ⁴ /in.
B_i, B_v	Moment coefficient for elastic, uncracked phase of two-way wall for Support Case i; subscript v denotes wall with vertical load	j	Subscript denoting reinforced concrete
c	Ambient sound velocity ahead of shock, fps	K_L	Load factor
C_f	Pressure coefficient, front face	K_{LM}	Load-mass factor
C_i, C_v	Moment coefficient for elastic, cracked phase of two-way wall for Support Case i; subscript v denotes wall with vertical load	K_M	Mass factor
C	Coefficient defined by Eq. 91	KE	Kinetic energy, in
d	Distance from compression face to centroid of tension steel, in.	l	Length to develop of reinforcing steel
d'	Distance from compression face to centroid of compression steel, in.	L_H	Horizontal length
E	Modulus of elasticity, psi	L_{HW}	Horizontal length
$E_1 \dots E_3$	Energy input of the lateral load for wall segments A, B, C, and D, in.-lb	L_V	Vertical length
E_c	Modulus of elasticity of concrete, psi	L_{VW}	Vertical length
E_m	Modulus of elasticity of masonry, psi	m	Mass per unit area
E_s	Modulus of elasticity of steel, psi	M	Bending moment per
E_T	Total energy input of lateral load acting on wall, in.-lb	M_A, M_b	Bending moment per and b (Figure 12) way unreinforced
f	Unit stress, psi Degrees of freedom for χ^2 distribution	M_A, M_C	Component of total along the assumed A and C which is anterior edge of the
f'_c	Dynamic compressive strength of concrete, psi	M'_A, M'_C	Total negative bending moment per anterior edge of section
f'_s	Dynamic yield strength of reinforcing steel, psi	M_c	Bending moment per vertical span, in
f'_m	Ultimate compressive strength of masonry unit wall, psi	M_e	Bending moment per wall, in.-lb/in.
f_r	Modulus of rupture of concrete, psi	M_f	Arching moment per of $t_w - 2t_f$ for hole
f_s	Ultimate strength of reinforcing steel, psi	M_j	Bending moment per section j of two-way wall, in.-lb/in.

Clearing dimension for each portion of the subdivided wall with openings, ft.	M_u	Ultimate moment capacity per unit width of uncracked section, in.-lb/in.
Subscript denoting support case of two-way wall	M_{uc}	Ultimate moment capacity per unit width of uncracked center section, in.-lb/in.
Inertia force of segments A and C of two-way wall, lb	M_{uc}	Ultimate moment capacity per unit width of cracked section, in.-lb/in.
Moment of inertia per unit width of cracked section, in ⁴ /in.	M_T	Total mass of wall, lb-sec ² /in.
Moment of inertia per unit width of uncracked section, in ⁴ /in.	M_u	Ultimate moment capacity per unit width of cracked section, in.-lb/in.
Subscript denoting cross section of two-way reinforced concrete wall	$M_{u,j}$	Ultimate moment capacity per unit width of cracked section at cross section j of two-way reinforced concrete wall, in.-lb/in.
Load factor	M_y	Arching moment per unit width corresponding to yielding of masonry, in.-lb/in.
Load-mass factor	M_1	Average moment resistance per unit width along horizontal cracked line d-c of segment A (Figure 12) for two-way unreinforced masonry wall, in.-lb/in.
Mass factor	M_2	Average moment resistance per unit width along diagonal cracks of segment A (Figure 12) for two-way unreinforced masonry wall, in.-lb/in.
Kinetic energy, in.-lb	M_3	Average moment resistance per unit width along horizontal cracked line d-c of segment B (Figure 12) for two-way unreinforced masonry wall, in.-lb/in.
Length to develop ultimate tensile strength of reinforcing steel in bond to concrete, in.	M_4	Average moment resistance per unit width along diagonal cracks of segment B (Figure 12) for two-way unreinforced masonry wall, in.-lb/in.
Horizontal length (width) of wall, in.	n	Number of observations
Horizontal length (width) of window, in.	p	Steel ratio, tension steel
Vertical length (height) of wall, in.	p'	Steel ratio, compression steel
Vertical length (height) of window, in.	p ₁	Steel ratio at cross section 1, tension steel
Mass per unit area of wall, lb-sec ² /in ³	p(t)	Unit pressure exerted against any surface varying with time, psi
Bending moment per unit width, in.-lb/in.	p _c	Pressure exerted at time t _c , psi
Bending moment per unit width at corners a and b (Figure 12) of decaying phase of two-way unreinforced masonry wall, in.-lb/in.	p _d	Dynamic pressure varying with time, psi
Component of total positive bending moment along the assumed failure lines of segments A and C which is perpendicular to the exterior edge of the segment, in.-lb/in.	p _r	Reflected overpressure, psi
Total negative bending moment along the exterior edge of segments A and C, in.-lb/in.	p _s	Incident overpressure varying with time, psi
Bending moment per unit width at center of vertical span, in.-lb/in.	p _{s,o}	Peak incident overpressure, psi
Bending moment per unit width along edge of wall, in.-lb/in.	P	Probability of occurrence
Arching moment per unit width at a deflection of t _v -2t _v for hollow masonry wall, in.-lb/in.	P _A , P _C	Total lateral load on segments A and C, lb
Bending moment per unit width at cross section j of two-way reinforced concrete wall, in.-lb/in.	P _f	Parameter defined by Eq. 13c, lb/in.

P	Ambient atmospheric pressure, psi	u	Standardized norm defined by Eq. 11
P_L	Total lateral load acting on wall, lb	U_u'	Ultimate average length of reinfo
P_v	Total vertical force per unit width, lb/in.	V_w	Total reaction at way wall, lb
q	Unit resistance for uniformly loaded two-way wall, psi	V_v	Total reaction at way wall, lb
q_0	Additional resistance per unit area developed during elasto-plastic phase of two-way reinforced concrete wall, psi	W	Weapon yield, kt Weight of wall per
q_1	Resistance per unit area corresponding to zero deflection for decaying phase of two-way unreinforced masonry wall without arching, psi	$W_A \dots W_D$	Work done by resi segments A, B, C,
q_2	Ultimate resistance per unit area for elastic phase of two-way unreinforced masonry wall without arching, psi	W_T	Total work done by the wall, in.-lb
	Ultimate resistance per unit area for plastic phase of two-way reinforced concrete wall, psi	x	Horizontal distan
q_3	Resistance per unit area for two-way wall with windows, psi	\bar{x}	Mean value of sam Horizontal distan center of gravity segment, in.
q_4	Maximum resistance per unit area for initial portion of elastic phase of two-way unreinforced masonry wall without arching fixed on two or more edges, psi	x'	Horizontal distan centroid of later
	Maximum resistance per unit area for elastic, uncracked phase of two-way reinforced concrete wall, psi	y	Lateral deflectio
q_5	Maximum resistance per unit area for decaying phase of two-way unreinforced masonry wall without arching, psi	Δy	Additional deflec during elasto-pla concrete wall, in
	Maximum resistance per unit area for elastic, cracked phase of two-way reinforced concrete wall, psi	\dot{y}	Velocity, in./sec
Q_A, Q_C	Total resistance of segments A and C, lb	y_{ave}	Average deflectio
Q_u	Total resistance of uniformly loaded wall, lb	y_c	Lateral deflectio
s	Standard deviation of sample	y_e	Deflection of equ freedom system, 1
S	Clearing distance, ft Total shear along edge of segment, lb	\dot{y}_e	Velocity of equi freedom system, 1
S'	Weighted average clearing distance of front face of wall with openings, ft	y_f	Lateral deflectio
t	Time, sec Statistical quantity defined by Eq. 114	y_{fv}	Lateral deflectio inforced concrete bility resulting
t_c	Clearing time, front face, sec	y_u	Maximum deflectio way unreinforced arching, in. Deflection at ult reinforced concre
t_f	Flange thickness of hollow masonry block, in.	y_y	Lateral deflectio of masonry during
t_p	Duration of positive overpressure, sec		
t_d	Duration of positive dynamic pressure, sec		
t_w	Thickness of wall, in.		

Standardized normal distribution variable defined by Eq. 108	y_1	Maximum deflection for initial portion of elastic phase of two-way unreinforced masonry wall without arching fixed on two or more edges, in. Maximum deflection for elastic, uncracked phase of two-way reinforced concrete wall, in.
Ultimate average bond strength per in. of length of reinforcing bar, lb/in.		
Total reaction along horizontal edge of two-way wall, lb	y_2	Deflection at maximum resistance in decaying phase of two-way unreinforced masonry wall without arching in. Maximum deflection for elastic, cracked phase of two-way reinforced concrete wall fixed on two or more edges, in.
Total reaction along vertical edge of two-way wall, lb		
Weapon yield, kt	z	Vertical distance along wall, in.
Weight of wall per unit width, lb/in.	\bar{z}	Vertical distance from edge of wall to center of gravity of inertia force on segment, in.
Work done by resisting moment on wall segments A, B, C, and D, in.-lb	z'	Vertical distance from edge of wall to centroid of lateral load on segment, in.
Total work done by the resisting moment on the wall, in.-lb	α	Distance defining location of yield lines for two-way wall with windows (Figure 23), in. Coefficient relating compressive strength and modulus of elasticity of masonry
Horizontal distance along wall, in.	β	Coefficient defining location of yield lines
Mean value of sample	γ	Unit weight, pcf
Horizontal distance from edge of wall to center of gravity of inertia force on segment, in.	γ_n	Parameter defined by Eq. 13a
Horizontal distance from edge of wall to centroid of lateral load on segment, in.	γ_1, γ_2	Parameters defined by Eqs. 74a and 74b
Lateral deflection of wall, in.	δ_n	Sub-area clearing factor for wall with openings
Additional deflection at center of wall during elasto-plastic phase of reinforced concrete wall, in.	ϵ_{su}	Ultimate strain in tension steel, in./in.
Velocity, in./sec	η_n	Parameter defined by Eq. 13b
Average deflection along yield lines, in.	$\theta_A \dots \theta_D$	Angle of rotation of wall segments A, B, C, and D, radians
Lateral deflection at center of wall, in.	λ	Portion of wall height above the cracked section for two-way wall
Deflection of equivalent single degree-of-freedom system, in.	μ	Ductility factor, ratio of maximum deflection to deflection at yield
Velocity of equivalent single degree-of-freedom system, in./sec	ν	Poisson's ratio
Lateral deflection at collapse of wall, in.	ξ	Mean value of total population
Lateral deflection at which collapse of reinforced concrete wall occurs due to instability resulting from vertical load, in.	σ	Standard deviation of total population
Maximum deflection for elastic phase of two-way unreinforced masonry wall without arching, in.	χ^2	Statistical distribution function
Deflection at ultimate resistance of two-way reinforced concrete wall, in.		
Lateral deflection corresponding to yielding of masonry during arching, in.		

Unclassified
Security Classification

DOCUMENT CONTROL DATA - R & D

Security classification of title, body of abstract and indexing annotation must be entered when the overall report is classified

1. ORIGINATING ACTIVITY (Corporate author)		2a. REPORT SECURITY CLASSIFICATION	
STANFORD RESEARCH INSTITUTE Menlo Park, California 94025		Unclassified	
		2b. GROUP	
		Not applicable	
3. REPORT TITLE			
EXISTING STRUCTURES EVALUATION, Part IV: Two-Way Action Walls			
4. DESCRIPTIVE NOTES (Type of report and inclusive dates)			
Technical Report			
5. AUTHOR(S) (First name, middle initial, last name)			
Carl K. Wiehle James L. Bockholt			
6. REPORT DATE		7a. TOTAL NO OF PAGES	7b. NO OF REFS
September 1970		276	25
8a. CONTRACT OR GRANT NO		9a. ORIGINATOR'S REPORT NUMBER(S)	
OCD-DAHC20-67-C-0136			
b. PROJECT NO			
Work Unit No. 1154F			
c.		9b. OTHER REPORT NO(S) (Any other numbers that may be assigned this report)	
d.			
10. DISTRIBUTION STATEMENT			
Approved for public release; distribution unlimited.			
11. SUPPLEMENTARY NOTES		12. SPONSORING MILITARY ACTIVITY	
		Office of Civil Defense Office of the Secretary of the Army Washington, D.C. 20310	
13. ABSTRACT			
<p>The objective of this investigation was to develop an evaluation procedure applicable to existing NFSS-type structures and private homes for determining the blast protection afforded and the cost of structure modifications to improve the blast protection. The approach adopted was to formulate a procedure that would permit examining the response of a structure over a range of incident overpressure levels to determine the pressure at which failure of the various elements occurs.</p> <p>Past efforts in this program have been concerned with examining exterior walls, window glass, and steel frame connections. The phase of the work presented in this report extended the exterior wall response models previously developed by including exterior walls with two-way action and window openings. The evaluation procedure was also extended to include a probability distribution for each of the various "unknown" wall and load parameters. Using the wall evaluation procedure, a limited sensitivity analysis was performed and a comparison was made of the available experimental information on dynamically loaded wall elements with theoretical predictions.</p>			

Unclassified

Security Classification

KEY WORDS	LINK A		LINK B		LINK C	
	ROLE	WT	ROLE	WT	ROLE	WT
Walls Structures Blast Shelters Analysis Blast Mechanics						